SYNERGISTIC SYNTHETIC LETHAL DRUG COMBINATIONS FOR E-CADHERIN-DEFICIENT CANCERS

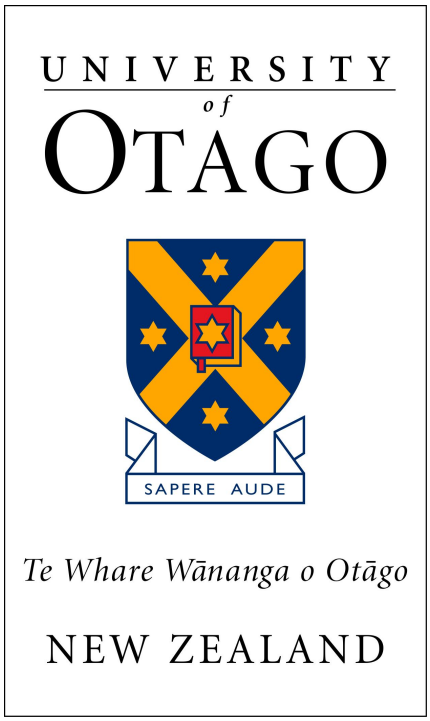

Andrew Single

A thesis submitted for the degree of
Doctor of Philosophy

University of Otago,
Dunedin, New Zealand
August 2017

ABSTRACT

E-cadherin is a cell-to-cell adhesion protein encoded by the gene *CDH1*. Germline inactivating mutations in *CDH1* underpin hereditary diffuse gastric cancer (HDGC), an autosomal dominant disease that strongly increases an individual's likelihood of developing diffuse gastric cancer (DGC) and invasive lobular breast cancer (ILBC). Current clinical intervention strategies for *CDH1* mutation carriers are limited, with the only available approaches being endoscopic surveillance or prophylactic gastrectomy. There is a pressing need to develop chemoprevention strategies to supplement the current approaches.

As E-cadherin is a tumour suppressor protein and lost from the cancer cell, it is not a conventional drug target. This issue can, however, be circumvented using a synthetic lethal approach. Synthetic lethality is defined as a genetic interaction in which a combination of mutations in two or more genes leads to cell death but no death with either mutation alone. Therapeutically, this approach allows for the specific targeting of cells harbouring tumour suppressor gene mutations.

We have previously applied a synthetic lethal strategy to identify candidate therapeutic drugs in a non-malignant isogenic pair of MCF10A cell lines, one with and one without *CDH1* expression (MCF10A *CDH1*$^{-/-}$). From this testing, a panel of lead drugs were identified, however, the synthetic lethal effects were relatively modest and also reduced the viability of E-cadherin-expressing MCF10A cells. This led to our interest in developing synergistic, synthetic lethal drug combinations, where co-treatment of an

additional drug may increase the synthetic lethal response whilst minimising toxicity to wild-type MCF10A cells.

Prior to drug testing, a range of endpoint (CellTiter-Glo, resazurin reduction, and nuclei counting) and real-time (IncuCyte and xCELLigence) cell viability assays were compared to develop an optimum drug screening platform for the MCF10A isogenic cells. We identified nuclei counting and IncuCyte assays as the most cost-effective and accurate approaches. These assay methodologies were used alongside the Chou-Talalay median effect analysis to assess drug synergy at 50% viability loss (ED50) via a combination index (CI), whereby a CI score below 0.9 represents a synergistic interaction.

A range of drugs were delivered simultaneously to the MCF10A isogenic pair in order to discover synergistic combinations that were synthetic lethal with *CDH1*. The lipid-lowering agents statins were identified as a drug class that specifically reduced MCF10A *CDH1*$^{-/-}$ cell viability whilst modestly affecting wild-type MCF10A cells up to a concentration of 5 μM. Co-treatment of atorvastatin with our previously identified lead synthetic lethal drugs, entinostat, vorinostat, and saracatinib, maintained synthetic lethality and showed evidence of a synergistic interaction, producing MCF10A *CDH1*$^{-/-}$ ED50 CI values of 0.37, 0.50, and 0.47, respectively. The most potent synergistic and synthetic lethal effect, however, was produced by atorvastatin in combination with the progesterone receptor and glucocorticoid receptor antagonist mifepristone, with MCF10A and MCF10A *CDH1*$^{-/-}$ ED50 CI values of 0.49 and 0.08, respectively.

The atorvastatin and mifepristone combination exclusively arrested MCF10A *CDH1*$^{-/-}$ cells in the G1 phase of the cell cycle. This effect was shown to be independent of

mevalonate and Hippo signalling – key pathways known to be affected by statin treatment. In addition to the non-malignant MCF10A breast cell line, the atorvastatin and mifepristone combination produced a synergistic loss of cell viability in two E-cadherin-deficient breast cancer cell lines, the ILBC-derived line IPH-926 (ED50 CI = 0.69) and the triple-negative breast cancer (TNBC)-derived MDA-MB-231 line (ED50 CI = 0.61). To the best of our knowledge, the combination of a statin and mifepristone has not been previously described in the literature.

In summary, this study has discovered statins as a synthetic lethal drug class in a non-malignant cell line lacking *CDH1* expression. Co-treatment of atorvastatin and mifepristone produced an enhanced synthetic lethal response, a synergistic drug relationship that was maintained across malignant breast cell lines devoid of *CDH1* expression. These findings may serve as a foundation for the development of novel DGC and ILBC treatment options.

RESEARCH OUTPUTS

This research contributed to the following papers, abstracts, and presentations. Publications marked by an asterisk were prepared prior to commencement of the PhD but are relevant to this thesis. Peer-reviewed journal articles can be found in Appendix A-B.

Peer-reviewed Journal Articles

* Telford, B. J., Chen, A., Beetham, H., Frick, J., Brew, T. P., Gould, C. M., **Single, A.**, Godwin, T., Simpson, K. J., and Guilford, P. Synthetic lethal screens identify vulnerabilities in GPCR signaling and cytoskeletal organization in E-cadherin-deficient cells. *Molecular Cancer Therapeutics,* 14, 1213-23 (2015).

Single, A., Beetham, H., Telford, B. J., Guilford, P., and Chen, A. A comparison of real-time and endpoint cell viability assays for improved synthetic lethal drug validation. *Journal of Biomolecular Screening,* 20, 1286-93 (2015).

Published Abstracts

* **Single, A.**, Chen, A., Telford, B., and Guilford, P. Synthetic lethal interactions for the treatment of E-cadherin negative tumours. *The New Zealand Medical Journal,* 126, 1374 (2013).

Single, A., Chen, A., Telford, B., Beetham, H., and Guilford, P. Abstract B41: Statins show synthetic lethality in E-cadherin-deficient cells and are synergistic with SRC and HDAC inhibitors. *Clinical Cancer Research,* 23 (1 Supplement) B41 (2017).

Conference Presentations

Single, A., Chen, A., and Guilford, P. A synergistic synthetic lethal drug combination for the treatment of E-cadherin-deficient tumours. Poster presentation at *Otago Spotlight Series: Cancer Research Symposium*, Wellington, New Zealand, October 2015.

Single, A., Chen, A., Telford, B., Beetham, H., Priya, R., Yap, A., and Guilford, P. Statins show synthetic lethality in E-cadherin-deficient cells and are synergistic with SRC and HDAC inhibitors. Poster presentation at *AACR Precision Medicine Series: Targeting the Vulnerabilities of Cancer*, Miami, USA, May 2016.

Single, A., Chen, A., Telford, B., Beetham, H., Priya, R., Yap, A., and Guilford, P. Statins show synthetic lethality in E-cadherin-deficient cells and are synergistic with SRC and HDAC inhibitors. Poster presentation at *New Zealand Society for Oncology Conference*, Palmerston North, New Zealand, October 2016.

ACKNOWLEDGEMENTS

Firstly, I wish to thank Parry Guilford for your support and supervision over the last few years. I appreciate our numerous discussions relating to this project - your questioning and testing of my knowledge has undoubtedly produced the fruits of this thesis. Under your guidance, I have come to learn that science is a marathon, not a sprint. Or, perhaps more precisely, a half marathon - where, without the right direction, the finish line will always be out of sight.

To my PhD committee members - Anita Dunbier, Augustine Chen, Allan Gamble - thank you for your expert recommendations over our 'regular' meetings throughout this project. Without your signatures on my final progress report, this thesis would have never been submitted.

Thanks to members, both past and present, of the synthetic lethal project. We've made some solid progress over the last few years. I hope we continue on this trajectory and make a real impact for *CDH1* mutation carriers around the globe.

I extend my thanks to members of the Cancer Genetics Lab. The amazing mix of people makes for a great atmosphere that I'm thankful to have been a part of. I've enjoyed our conversations, morning teas, and occasional Bird Dog. I wish you all the best.

A massive thanks must also go to my friends. The futsal, the band gigs, the gym visits, the road trips, the BYOs, the banter – I've loved it all. There aren't many of us left in

Dunedin nowadays, but I'm glad we all keep in touch to share a good laugh now and again. The stories we've picked up over the years would make for a good thesis in itself.

Thanks to my family – Mum, Dad, Daniel, and Courtney. Thanks for your support over the years. My phone calls certainly became less frequent as the workload and writing levels increased, but I'm happy to know I'll always have your support.

Finally, to the families who feel burdened by a *CDH1* mutation, this thesis is dedicated to you. To those I have met, to those I have heard of via email, to those taken too soon, you are the reason I pursue a career in research. One day, we will offer you more than hope.

TABLE OF CONTENTS

LIST OF FIGURES

LIST OF TABLES

ABBREVIATIONS

%	Percent
°C	Degrees celsius
ATP	Adenosine triphosphate
BCA	Bicinchoninic acid
BECN1	Beclin-1
CDH	Cadherin
CDH1	E-cadherin
CDHR	Cadherin-related
CDK	Cyclin-dependent kinase
CI	Combination index
cm	Centimetre
cm^2	Centimetres squared
CO_2	Carbon dioxide
DMSO	Dimethyl sulfoxide
DNA	Deoxyribonucleic acid
DSB	Double stranded break
EC50	Half maximal effective concentration
ECM	Extracellular matrix
ED50	Effective dose providing 50% viability loss
ED75	Effective dose providing 75% viability loss
ED90	Effective dose providing 90% viability loss
EMT	Epithelial-mesenchymal transition
ER-	Oestrogen receptor negative

ER+	Ostrogen receptor positive
Fa	Fraction of cells affected
FAKi	Focal adhesion kinase inhibitor
FBS	Foetal bovine serum
FPP	Farnesyl pyrophosphate
FTase	Farnesyltransferase
GC	Gastric cancer
GEF	Guanine nucleotide exchange factor
GGDP	Geranylgeranyl diphosphate
GGDPS	Geranylgeranyl diphosphate synthase
GGTase-I	Geranylgeranyl transferase type 1
GPCR	G-protein coupled receptor
GR	Glucocorticoid receptor
H_2O	Water
HAT	Histone acetyltransferase
HDACi	Histone deacetylase inhibitor
HDAC	Histone deacetylase
HDGC	Hereditary Diffuse Gastric Cancer
HMG-CoA	3-hydroxy-3-methylglutaryl-coenzyme A
HMGCR	HMG-CoA reductase
h	Hour
IDC	Invasive ductal carcinoma
ILBC	Invasive lobular breast carcinoma
IPP	Isopentenyl-5-pyrophosphate
LATS1	Large tumour suppressor 1

LATS2	Large tumour suppressor 2
mA	Milliamperes
min	Minute
mL	Millilitre
mM	Millimoles per litre
mQH_2O	Ultrapure water with resistivity of the order of 18.2 MΩ·cm at 25 °C
MST1	Mammalian STE20-like protein kinase 1
MST2	Mammalian STE20-like protein kinase 2
MTT	3-[4,5-dimethylthiazolyl-2]-2,5-diphenyltetrazolium bromide
nM	Nanomoles per litre
PARP	Poly(ADP-ribose) polymerase
PARPi	PARP inhibitor
PBS	Phosphate buffered saline
PI3K	Phosphoinositide 3-kinase
PIP_3	Phosphatidylinositol 3,4,5-trisphosphate
PCDH	Protocadherin
PTG	Prophylactic total gastrectomy
Rac1	Ras-related C3 botulinum toxin substrate 1
rpm	Revolutions per minute
RTK	Receptor tyrosine kinase
s	Second
SDS	Sodium dodecyl sulphate
SQS	Squalene synthase
TAZ	Transcriptional co-activator with PDZ binding motif

TEAD1-4	TEA domain family 1-4
TEMED	Tetramethylethylenediamine
TNBC	Triple-negative breast cancer
V	Volts
YAP	Yes-associated protein
Δ	Delta
µg	Microgram
µL	Microlitre
µM	Micromoles per litre
µm	Micrometre

THESIS OUTLINE

This thesis comprises six main chapters with appendices.

Chapter one is a general introduction. This chapter discusses E-cadherin dysregulation in cancer, with an emphasis on diseases caused by germline E-cadherin mutations. Relevant E-cadherin-dependent signalling pathways are also presented, as well as the concept of synthetic lethality and drug synergy. Finally, this chapter concludes with an outline of the project's aims.

Chapter two outlines the materials and methods used in this project.

Chapter three is the first of three results chapters. In addition to presented data, each results chapter contains an introduction and discussion sub-chapter. This results chapter presents data comparing a range of endpoint and real-time cell viability assays. The favoured endpoint assay (nuclei counting) and real-time assay (IncuCyte) are used in the subsequent results chapters.

Chapter four is the second results chapter. This chapter presents data from a screen for synergistic drug combinations that are synthetic lethal in E-cadherin-deficient cells.

Chapter five is the third results chapter. This chapter aims to characterise both the synergistic and synthetic lethal mechanisms of the lead drug combination, atorvastatin and mifepristone, identified in chapter four.

Chapter six outlines potential future directions of this research. This chapter describes a pathway of additional experiments that may lead to clinical use of the atorvastatin and mifepristone drug combination as a chemoprevention option for E-cadherin-deficient cancers.

1. GENERAL INTRODUCTION

1.1 E-CADHERIN DYSREGULATION IN CANCER

The transition from benign tumours to invasive, metastatic cancer cells is known to involve changes in cell motility and intercellular contact mechanisms (Semb and Christofori, 1998). It is therefore not surprising that dysregulation of E-cadherin (*CDH1*), a protein involved in epithelial cell-to-cell adhesion complexes, has been implicated in the development of many cancers types (Hollestelle *et al*., 2013). Downregulation of *CDH1* expression is a common feature of numerous epithelial tumours including gastric, breast, prostate, ovarian, lung, oral, colorectal, and hepatocellular carcinoma (Batlle *et al*., 2000; Guilford *et al*., 1998; van Roy and Berx, 2008). In addition, germline inactivating *CDH1* mutations define hereditary diffuse gastric cancer (HDGC), an inherited cancer syndrome predisposing individuals to increased rates of diffuse gastric cancer (DGC) and invasive lobular breast cancer (ILBC) (Guilford *et al*., 1998; van der Post *et al*., 2015).

1.1.1 Gastric Cancer

Gastric cancer is the fourth most common cause of cancer worldwide; by 2030 deaths from gastric cancer globally are predicted to have risen from the 15th to the 10th leading cause of mortality from all causes (Mathers and Loncar, 2006). In New Zealand, current age-standardised rates of gastric cancer equate to 7.6 per 100,000 for males and 4.0 for females (Torre *et al*., 2016). Although the vast majority of gastric cancers are sporadic, approximately 1-3% of cases arise as a result of inherited gastric cancer predisposition syndromes (La Vecchia *et al*., 1992; Varley *et al*., 1995; Vasen *et al*., 1996).

Gastric cancer is typically characterised using Lauren's classification, where two histotypes are described – intestinal and diffuse (a mixed type is also observed) (Lauren, 1965). Intestinal gastric cancer is more common than the diffuse type, with incidence rates of 8.6 per 100,000 and 4.7 per 100,000, respectively (Ekstrom *et al*., 2000). However, these rates are changing – the rate of intestinal cases is declining, whilst diffuse cases are increasing by approximately 3.7% per year (Guggenheim and Shah, 2013; Henson *et al*., 2004).

1.1.2 Hereditary Diffuse Gastric Cancer (HDGC)

In 1998, linkage analysis demonstrated that germline mutations of the E-cadherin gene (*CDH1*) are the genetic cause of HDGC (Guilford *et al*., 1998). HDGC is an autosomal dominant inherited syndrome that leads to an increased risk for both diffuse gastric and lobular breast cancers. A recent analysis of 75 families with pathogenic *CDH1* mutations has estimated a cumulative penetrance risk of diffuse gastric cancer (DGC) by age 80 years of 70% for males and 56% for females (Hansford *et al*., 2015). *CDH1* mutation carriers develop cancer after somatic inactivation of the *CDH1* second allele. The trigger and molecular mechanism by which the second *CDH1* allele is inactivated appears to be diverse and includes methylation, mutation, and loss of heterozygosity (Barber *et al*., 2008; Oliveira *et al*., 2009). Bisulfite analysis of stomach adenocarcinoma tissue from *CDH1* mutation carriers suggests 50% of early stage cancers have had the second allele inactivated by promoter hypermethylation (Humar *et al*., 2009).

CDH1 mutation carriers develop multiple stage T1a signet ring cell carcinomas (SRCC) from an early age (Figure 1.1) (Charlton *et al*., 2004; Norton *et al*., 2007). These T1a foci present in large numbers as either isolated cells or small clusters in the lining of the stomach, with a median number of 20 and maximum of 500 foci observed in resected tissue (Charlton *et al*.,

2004; Guilford *et al*., 2010). Fortunately, T1a foci display a low proliferative index; showing low Ki67 staining and fewer mitotic cells than adjacent healthy tissue (Barber *et al*., 2008; Humar *et al*., 2009).

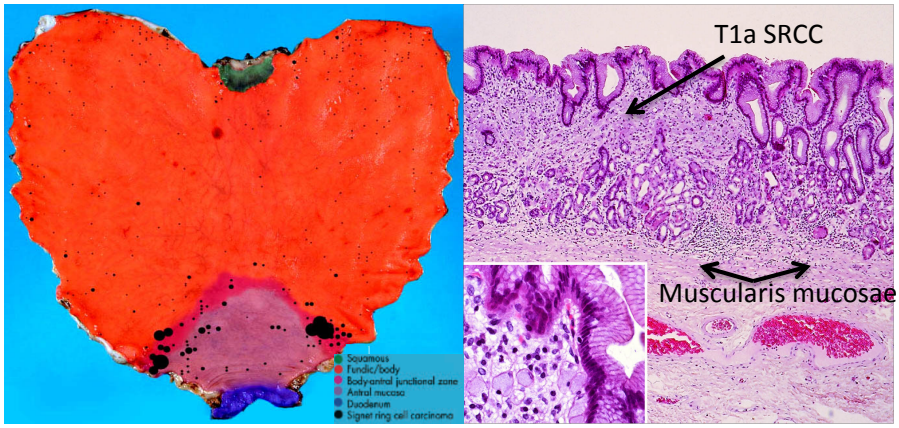

Figure 1.1 Stage T1a signet ring cell carcinoma (SRCC) in a germline *CDH1* mutation carrier

Left: a total gastrectomy specimen from a 15 year *CDH1* mutation carrier showing the anatomical location of 318 stage T1a foci. Black circles are carcinoma foci, to scale, except foci <1 mm are shown arbitrarily as 1 mm for visibility. Right: An example of a 9 mm H&E stained focus showing the location between the mucosal surface and the muscularis mucosae. Signet ring cells can be observed in the bottom left frame. Reproduced from Hereditary diffuse gastric cancer: predominance of multiple foci of signet ring cell carcinoma in distal stomach and transitional zone, Charlton *et al.*, 53, 814-20, 2004 with permission from BMJ Publishing Group Ltd.

Progression from indolent T1a lesions to advanced HDGC presents as *linitis plastica* with diffuse infiltration of the gastric wall. SRCC tend to migrate below an intact mucosa, consequently early stage DGC is difficult to detect by standard gastroscopy and tends to be asymptomatic at early stages (van der Post *et al*., 2015). HDGC is therefore often diagnosed at a late stage with a poor prognosis, with a 5-year survival rate below 30% (Koea *et al*., 2000; Stiekema *et al*., 2013). At present, prophylactic total gastrectomy (PTG) is the single option to remove an inherited risk of gastric cancer and is recommended after age 20 years (van der Post *et al*., 2015).

The low proliferative status of T1a lesions means the progression to advanced DGC is a slow process. In fact, the analysis of 724 foci from resected stomachs of *CDH1* mutation carriers

identified no lesions above T1a stage (Charlton *et al*., 2004). This suggests that advanced HDGC is a rare event, whereby the vast number of T1a foci remain dormant until a chance mutation drives cancer progression. One such gene, *SRC*, has been identified as a key driver of this process (Humar *et al*., 2007). The biology at play presents a potential therapeutic window for *CDH1* mutation carriers, where drug treatment may be used to obliterate the reservoir of T1a foci prior to the acquisition of deleterious mutations and advanced disease. This chemoprevention option would provide a much-needed, novel alternative to PTG surgical intervention.

1.1.3 Invasive Lobular Breast Carcinoma (ILBC)

Breast cancer is the leading cause of cancer-related death in females worldwide, with an estimated 1.7 million cases and 521,900 deaths occurring in 2012 (Torre *et al*., 2016). *CDH1* expression is often decreased in the invasive ductal carcinoma (IDC) subtype, and lost entirely in invasive lobular breast carcinoma (ILBC) – the second most common invasive breast cancer subtype that comprises 10-15% of all breast cancer cases (Arpino *et al*., 2004; Christgen and Derksen, 2015; Singhai *et al*., 2011; Vos *et al*., 1997). Carriers of pathogenic *CDH1* mutations are at an increased risk of developing ILBC (approximately 40% lifetime risk) (Pharoah *et al*., 2001).

ILBCs are typically oestrogen receptor positive (ER+), belonging to the luminal or normal-like molecular subtype, and have a slow proliferation rate (Bertucci *et al*., 2008; Christgen and Derksen, 2015). *ERBB2* amplification and loss of expression of the tumour suppressor *TP53* is rare, however, activating *PIK3CA* mutations are prominent (30-50% of ILBC cases) (Bertucci *et al*., 2008; Christgen and Derksen, 2015; Christgen *et al*., 2013; Christgen *et al*., 2016). An aggressive ILBC variant, termed pleomorphic ILBC, comprises 1-5% of ILBCs and harbours a

contrasting molecular complexion to classical ILBC. Pleomorphic ILBCs are usually oestrogen receptor negative (ER-) and occasionally ERBB2-positive, with inactivating *TP53* mutations observed in most cases (Ercan *et al*., 2012; Simpson *et al*., 2008). As such, *TP53* is considered the 'gatekeeper' between the slow-growing classical and aggressive pleomorphic ILBC variants.

The prognosis for ILBC patients is currently debated in the literature. Some studies have reported a 5-year disease-free survival rate as similar to or slightly greater than that seen for other breast cancer subtypes such as IDC (Biglia *et al*., 2013; Korhonen *et al*., 2013). However, these findings are contested due to anti-oestrogen therapies showing poorer response in ILBC patients than IDC patients – an interesting observation considering ILBCs have a greater proportion of ER+ specimens than IDCs (90% vs. 50%, respectively) (Lehmann, 2015; Rakha *et al*., 2008). It has therefore been suggested that the long-term ILBC prognosis may be worse than IDC (Arpino *et al*., 2004; Lehmann, 2015; Pestalozzi *et al*., 2008).

1.2 E-CADHERIN FUNCTION

E-cadherin is the founding member of the cadherin superfamily, which includes 32 major cadherins (*CDH*), 65 protocadherins (*PCDH*), and 17 cadherin-related (*CDHR*) members (Gul *et al*., 2017). E-cadherin is a transmembrane calcium-dependent cell-to-cell adhesion glycoprotein, located at the adherens junction in the epithelium (Figure 1.2). It consists of five cadherin repeats in the extracellular domain, one transmembrane domain, and an intracellular domain that binds p120-catenin and β-catenin (van Roy and Berx, 2008). As β-catenin is capable of binding to α-catenin (a regulator of actin polymers), E-cadherin thus mediates the connection between the cell and filaments in the cytoskeleton (Onder *et al*., 2008). E-cadherin-actin signalling at the adherens junction recruits and activates myosin II, a protein that generates contractile tension forces at the junction and influences actin organisation (Lecuit and Yap,

2015). Indeed, we have shown a contrasting cytoskeletal framework between E-cadherin-expressing and E-cadherin-deficient cells, with disorganised actin fibre and microtubule patterning apparent following E-cadherin loss (Chen *et al*., 2014a).

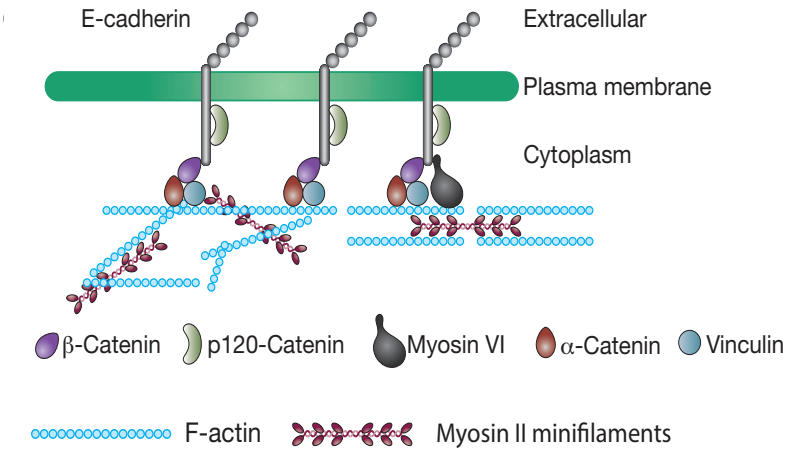

Figure 1.2 E-cadherin association with cytoskeletal filaments at the adherens junction

"Mechanisms for the E-cadherin molecular complex to associate with actin of the actomyosin apparatus. Actin filaments may bind directly to α-catenin, interact with α-catenin-associated proteins, or bind to proteins such as myosin VI, which can associate with E-cadherin independently of α-catenin." Reprinted by permission from RightsLink Permissions Springer Customer Service Centre GmbH: Springer Nature, Nature Cell Biology, E-cadherin junctions as active mechanical integrators in tissue dynamics, Lecuit and Yap, Copyright (2015).

In addition to cytoskeletal binding, E-cadherin forms extracellular contacts with neighbouring cells via homophilic ligation. These cell-to-cell contacts tend to accumulate in groups in the lateral cell membrane, termed 'lateral clusters', and stabilise an apical-basal polarity within the epithelium (Rodriguez-Boulan and Macara, 2014; Yap *et al*., 2015). A polarised phenotype allows epithelial cells to perform a range of functions such as expansion or constriction of apical or lateral membranes, processes central to tubulogenesis and the formation of columnar or squamous epithelia; and orientation of the mitotic spindle, which allows cell division to occur parallel or perpendicular to the epithelial plane (Lechler and Fuchs, 2005; Rodriguez-Boulan and Macara, 2014; Sawyer *et al*., 2010). E-cadherin therefore plays an important role in cell differentiation, stemness, and migration (Onder *et al*., 2008). Downregulation of *CDH1* is central to a process known as the epithelial-mesenchymal transition (EMT) in which epithelial

cells acquire a highly motile, invasive phenotype that is associated with metastasis and drug resistance (Onder *et al*., 2008). The Wnt, phosphoinositide 3-kinase (PI3K)/Akt, Rac, and Hippo signalling pathways are key mediators of these biological processes (Huber *et al*., 2005; Kalluri and Weinberg, 2009; Yang and Weinberg, 2008). Due to their relevance later in this project, the Rac and Hippo pathways are explained in further detail below.

1.2.1 The Rac Pathway

The ubiquitously expressed protein Rac1 belongs to the Rac subfamily of Rho small GTPases. Other members of the Rac subfamily include Rac2, Rac3, and RhoG, although expression of these proteins is generally restricted to specific tissues (Haataja *et al*., 1997; Roberts *et al*., 1999; Vincent *et al*., 1992). As a GTPase, Rac1 cycles between an inactive (GDP-bound) and active (GTP-bound) state to relay signals from membrane-based receptors, including receptor tyrosine kinases (RTKs), G-protein coupled receptors (GPCRs), and cytokine receptors. Functionally, Rac1 has been shown to promote cell growth, inhibit apoptosis, and regulate gene expression, with Rac1 deletion shown to be embryonic lethal due to defective germ layer development (Sugihara *et al*., 1998; Wennerberg and Der, 2004). In addition, Rac1's ability to reorganise the actin cytoskeleton to alter cell polarity and promote motility has led to extensive investigation in the context of cancer (Etienne-Manneville and Hall, 2002).

Further to crosstalk with RTKs, GPCRs, and cytokine receptors, Rac1 has been shown to be activated following E-cadherin homophilic ligation (Kovacs *et al*., 2002). This is achieved by E-cadherin recruiting both Rac1 and the lipid kinase PI3K to adhesive contacts, where the production of phosphatidylinositol 3,4,5-trisphosphate (PIP_3), via PI3K, is sufficient to activate the co-localised Rac1 (Figure 1.3) (Kovacs *et al*., 2002; Rodriguez-Boulan and Macara, 2014). It is possible that the intermediary role played by PI3K in this scenario may explain the high

frequency of activating PI3K mutations in *CDH1*-deficient ILBC, as this would allow Rac1 to drive malignancy in the absence of cell-to-cell contacts. Further to PI3K signalling, cytosolic p120-catenin has been shown to drive Rho/Rock signalling in E-cadherin-deficient ILBC mouse cell lines (Schackmann *et al*., 2011).

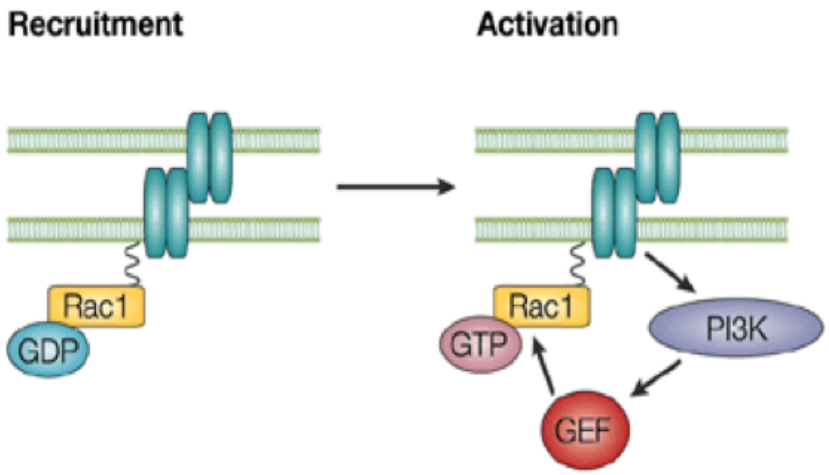

Figure 1.3 Rac1 activation at cell-to-cell contacts

"When cadherin-mediated homophilic interactions occur, GDP-Rac1 is converted to GTP-Rac1 through the action of a guanine nucleotide exchange factor (GEF), downstream of PI3K. Activated Rac1 positively regulates E-cadherin-mediated cell-to-cell adhesion." Reprinted by permission from RightsLink Permissions Springer Customer Service Centre GmbH: Springer Nature, Nature Reviews Molecular Cell Biology, Rho-family GTPases in cadherin-mediated cell – cell adhesion, Fukata and Kaibuchi, Copyright (2001).

1.2.2 The Hippo Pathway

The Hippo pathway, also known as the Salvador-Warts-Hippo pathway, is an evolutionarily conserved pathway involved in the maintenance of cellular proliferation during tissue development and regeneration. Following mutational analysis in *Drosophila melanogaster*, the Hippo pathway has been suspected as a key player in carcinogenesis (Harvey *et al*., 2013; Tapon *et al*., 2002).

Central to the Hippo pathway is a conglomerate of serine/threonine kinases - MST1 and MST2, LATS1 and LATS2, and adaptor proteins MOB1A and MOB1B. This protein complex induces phosphorylation of the oncoproteins YAP and TAZ, which serves to both prevent YAP and TAZ translocation to the nucleus, via 14-3-3 protein binding, and also prime them for ubiquitin-mediated degradation. If unphosphorylated, however, YAP and TAZ translocate to the nucleus and subsequently stimulate cell growth via regulation of the transcription factors TEAD1-4 and SMAD1-3 (Figure 1.4) (Johnson and Halder, 2014).

Mutations in Hippo pathway proteins that induce hyperactivation of YAP or TAZ are known to drive increased cellular proliferation (Harvey *et al*., 2013). Additionally, *in vitro*, the overexpression of YAP in cancer cell lines was shown to promote apoptotic resistance in response to chemotherapeutic agents and anoikis (Overholtzer *et al*., 2006; Zhang *et al*., 2011; Zhao *et al*., 2012). It is therefore noteworthy that few somatic or germline mutations have been identified in Hippo pathway genes in common human cancers (Harvey *et al*., 2013), suggesting that altered Hippo activity may be downstream to other mutational events in carcinoma.

In the context of epithelial cell biology, E-cadherin has been reported to sequester YAP and TAZ to adherens junctions (Schroeder and Halder, 2012). In doing so, E-cadherin regulates the function of YAP and TAZ by preventing their nuclear entry and, additionally, preventing their access to phosphatases which antagonise the activity of YAP and TAZ inhibitory kinases (Schroeder and Halder, 2012). With E-cadherin absent, it is possible that YAP and TAZ would be liberated from the cell periphery, promoting entrance to the nucleus and thus initiating the neoplastic process. Indeed, nuclear localisation of YAP has been reported in ILBC cell lines *in vitro* (Vlug *et al*., 2013).

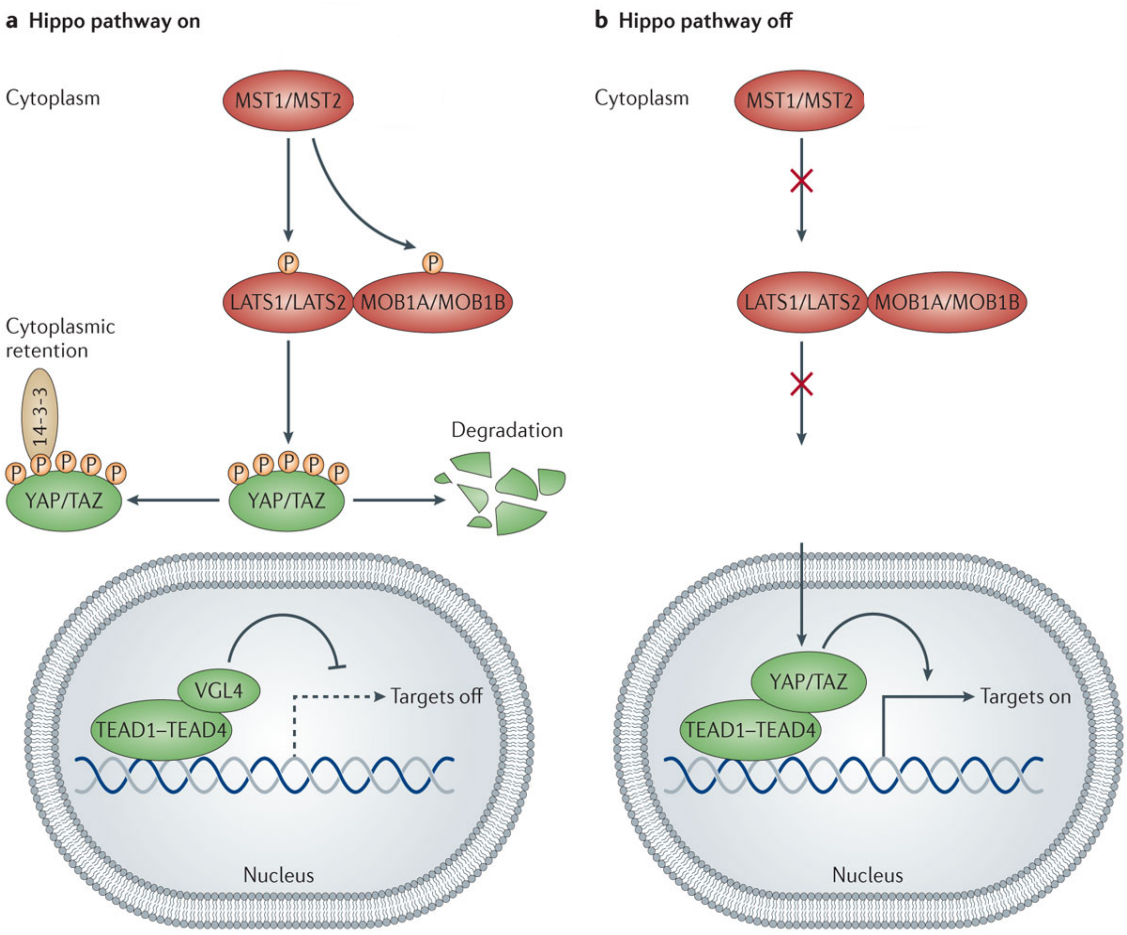

Figure 1.4 The Hippo pathway

"**a)** When the Hippo pathway is on, MST1 or MST2 phosphorylate SAV1, and together they phosphorylate and activate MOB1A, MOB1B, LATS1, and LATS2, which then phosphorylate YAP and TAZ. Phosphorylated YAP and TAZ are sequestered in the cytoplasm by the 14-3-3 protein and shunted for proteasomal degradation. As a result, TEADs associate with the transcriptional cofactor VGL4 and suppress target gene expression. **b)** When the Hippo pathway is off, the kinases MST1, MST2, LATS1, and LATS2 are inactive, so YAP and TAZ are not phosphorylated and instead accumulate in the nucleus where they displace VGL4 and form a complex with TEADs, which promotes the expression of target genes." Reprinted by permission from RightsLink Permissions Springer Customer Service Centre GmbH: Springer Nature, Nature Reviews Drug Discovery, Johnson and Halder, Copyright (2013).

1.3 SYNTHETIC LETHALITY

The inactivation of tumour suppressor genes, such as E-cadherin, is one of the more clear-cut molecular events occurring during tumourigenesis, but one that obviously cannot be exploited by conventional drug development (as no protein is translated from the inactivated gene). One approach, however, that is not precluded by the absence of the tumour suppressor is known as synthetic lethality.

Initially observed in *Drosophila* and explored extensively in yeast, synthetic lethality is classically defined as a genetic interaction in which a combination of mutations in two or more genes leads to cell death (Figure 1.5) (Bender and Pringle, 1991; Canaani, 2013; Dobzhansky, 1946). In a therapeutic setting, the term can refer to the use of a targeted drug to cause cell death exclusively in tumours carrying specific gene alterations. The targeting of cells that carry mutations in common tumour suppressor genes provides a means to achieve a high degree of tumour specificity, enabling better efficacy than standard chemotherapeutic approaches with, theoretically, fewer side effects.

In the context of this thesis, synthetic lethality is used to describe a greater loss of cell number in E-cadherin-deficient cells than E-cadherin-expressing cells, relative to respective control treatment. The use of this definition may therefore not exclusively involve death *per se*.

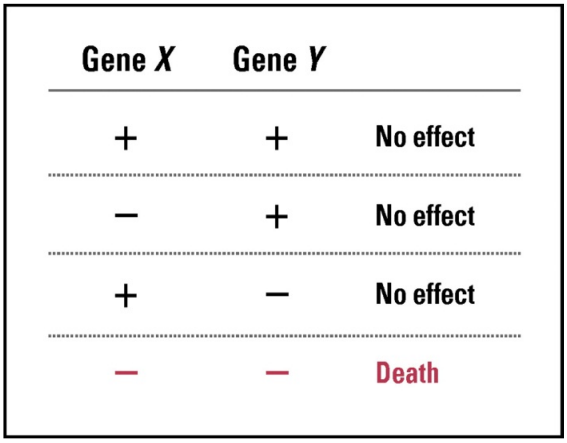

Figure 1.5 The concept of synthetic lethality

Synthetic lethality occurs when a mutation in either two genes individually has no effect but combining the mutations leads to cell death. Drug treatment to inhibit synthetic lethal partners of tumour suppressor genes may lead to novel cancer therapeutic options. Ashworth, A: J Clin Oncol 26 (22), 2008: 3785-90. Reprinted with permission. Copyright (2018) American Society of Clinical Oncology. All rights reserved.

In recent years, researchers have performed compound screens on model knockout cell lines to identify drugs that target cells harbouring tumour suppressor gene mutations (Bryant *et al*., 2005; Farmer *et al*., 2005; Kau *et al*., 2003; Neshat *et al*., 2001; Podsypanina *et al*., 2001). A successful demonstration of synthetic lethality is the development of poly (ADP-ribose) polymerase (PARP) inhibitors that showed an increased sensitivity in cells containing *BRCA1*/*BRCA2* mutations (Ashworth, 2008; Bryant *et al*., 2005). Following this discovery, the PARP inhibitor olaparib has been approved by the FDA and European commission for patients with platinum-sensitive, recurrent, high-grade serous ovarian cancer with *BRCA1* or *BRCA2* mutations (Tangutoori *et al*., 2015). Numerous other PARP inhibitors are currently in clinical trials for *BRCA* mutation carriers, heralding a success for synthetic lethal therapeutics and welcoming a new chapter of personalised medicine.

Our research group has applied a similar strategy and recently performed a screen with over 4,000 known drugs in an attempt to identify synthetic lethal phenotypes in E-cadherin-negative cells (Telford *et al*., 2015). Testing was performed in a non-tumourigenic mammary epithelial

cell line, MCF10A, and an isogenic counterpart harbouring a zinc-finger nuclease-generated four base pair deletion in exon 11 of the *CDH1* gene (MCF10A *CDH1*$^{-/-}$). A non-tumourigenic cell line was selected to best represent 'normal' human cells. From this initial screen, a range of potential drug candidates for E-cadherin-deficient cancers were identified (Table 1.1), with histone deacetylase inhibitors (HDACi) and the SRC inhibitor (SRCi) saracatinib taken on for successful validation (Telford *et al*., 2015).

Table 1.1 Known drugs with greater inhibitory effect on MCF10A *CDH1*$^{-/-}$ cells compared with MCF10A cells. Adapted from Telford *et al.* (2015).

Drug Name	Drug Class
Mocetinostat	HDAC inhibitor
Entinostat	HDAC inhibitor
Quisinostat	HDAC inhibitor
Pracinostat	HDAC inhibitor
LAQ824	HDAC inhibitor
Panobinostat	HDAC inhibitor
Crizotinib	ROS1-like tyrosine kinase inhibitor
PI-103	PI3K inhibitor
GSK2126458	PI3K inhibitor
PIK-75	PI3K inhibitor
CGP 71683	NPY5R inhibitor
Tyrphostin A9	PDGFR and EGFR inhibitor
AZD8055	mTOR inhibitor
Obatoclax mesylate	BCL2 inhibitor
Brefeldin A	Guanidine nucleotide exchange factor inhibitor
LY2784544	JAK family inhibitor
FCCP	Uncoupler of mitochondrial oxidative phosphorylation
JNJ-7706621	CDK and aurora kinase inhibitor
Danusertib	Aurora kinase, BCR-Abl, c-RET, and FGFR inhibitor
PD-166285 hydrate	Broad-spectrum tyrosine kinase inhibitor
10-DEBC hydrochloride	AKT inhibitor
Saracatinib	SRC inhibitor
Mifepristone	Progesterone receptor and glucocorticoid receptor inhibitor

1.3.1 Histone Deacetylase Inhibitors (HDACi)

Histone deacetylation is one of many common epigenetic modifications required for chromatin organisation and gene expression regulation. Whilst acetylated histone residues typically lead to transcriptional activation and gene expression, histone deacetylation has been associated with the formation of a 'condensed' chromatin state linked to transcriptional repression and gene silencing (Glozak and Seto, 2007). Enzymes involved in maintaining these chromatin modifications with opposing activities are the histone acetyltransferases (HATs) and histone deacetylases (HDACs) (Mills, 2010).

There are eighteen characterised mammalian HDAC isozymes (Gupta *et al*., 2012). Eleven of these have been termed 'classical HDACs' because they share a high degree of structural homology and common catalytic mechanism through which they deacetylate both histone and non-histone proteins (Shakespear *et al*., 2011). These classical HDACs are further sub-divided into four classes (classes I, IIa, IIb, and IV) on the basis of domain organisation (Table 1.2) (Gupta *et al*., 2012).

Table 1.2 The four classes and eleven isozymes of the classical HDACs

Class	HDAC Isozyme
I	1 2 3 8
IIa	4 5 7 9
IIb	6 10
IV	11

Aberrant gene expression attributed to epigenetic alterations is crucial for tumour development and is also implicated in response to chemotherapy (Mutze *et al*., 2010). As a consequence of this, HDACs have emerged as promising targets for the treatment of cancers. There are currently five HDACi (vorinostat, romidepsin, belinostat, panobinostat, and pracinostat) that are FDA-approved and used as anti-cancer agents, whilst many others are in various stages of clinical trials for monotherapy or combination chemotherapy treatments (Gupta *et al*., 2012; Manal *et al*., 2016). In addition to cancer therapeutics, HDACi have also shown promise for the treatment of other human diseases, such as inflammatory and metabolic disorders, immunological, cardiovascular, and infectious diseases (Gupta *et al*., 2012). The wide range of diseases that can be treated with HDACi partnered with a reported good tolerability profile in patients is driving the development of novel therapeutic HDACi (Mottamal *et al*., 2015 and references therein).

Most HDACi are comprised of three structural components: an affinity-determining zinc-binding region, a linker region, and a surface recognition domain (cap region) that plugs the entrance to the catalytic site of the HDAC (Figure 1.6) (Gupta *et al*., 2012). Improvements in affinity, potency, and selectivity are achieved via modifications to the recognition group that targets surface residues surrounding the active site (Gupta *et al*., 2012). Successful HDACi modifications have been demonstrated to great effect with the recently FDA-approved pracinostat, a more orally active and therapeutically effective analogue of vorinostat (Novotny-Diermayr *et al*., 2010).

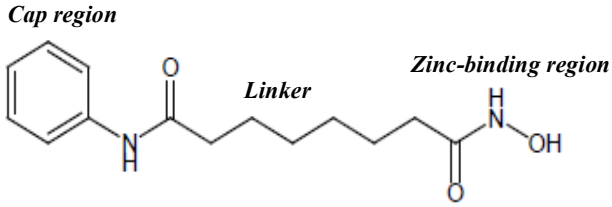

Figure 1.6 Structural components of a histone deacetylase inhibitor (HDACi)

The affinity determining 'zinc-binding region' is attached to the HDAC catalytic site blocking 'cap region' via a 'linker region', as depicted by the pan-HDACi vorinostat. Adapted from Gupta *et al.* (2012). Reprinted with permission. Copyright 2018 Bentham Science.

1.3.2 SRC Inhibitors (SRCi)

SRC is a 536 amino acid non-receptor tyrosine kinase that conveys signals from membrane-based receptors to numerous intracellular survival pathways, including the PI3K and MAPK signalling pathways (Roskoski, 2015; Thomas and Brugge, 1997). The tyrosine kinase receptors, such as EGFR (ERBB1) and HER2 (ERBB2), GPCRs, integrins, and E-cadherin, are among the list of receptors known to regulate SRC activity (Roskoski Jr, 2004; Thomas and Brugge, 1997).

Structurally, from the N- to C-terminus, SRC contains a 14-carbon myristoyl group, a unique domain, an SH3 domain, an SH2 domain, an SH2-kinase linker, a protein-tyrosine kinase domain (SH1), and a C-terminal regulatory segment (Figure 1.7) (Brown and Cooper, 1996; Roskoski, 2015; Thomas and Brugge, 1997). N-terminal myristoylation, occurring at the 14-carbon myristoyl group, is required for SRC to attach to cell membranes and subsequently function (Brown and Cooper, 1996). The SH3 and SH2 domains facilitate binding to left-handed helices and C-terminal phosphotyrosine residues, respectively (Adzhubei *et al*., 2013; Boggon and Eck, 2004; Liu *et al*., 2012). The SH3 domain can therefore bind to the SH2-kinase linker, and SH2 can bind to the C-terminus of SRC, resulting in an auto-inhibitory SRC

conformation (SRC's inactive state) (Boggon and Eck, 2004). Mutations at residues preventing this intramolecular binding result in SRC hyperactivation and have been shown to induce anchorage-independent cell growth (Cooper *et al*., 1986; Kmiecik and Shalloway, 1987).

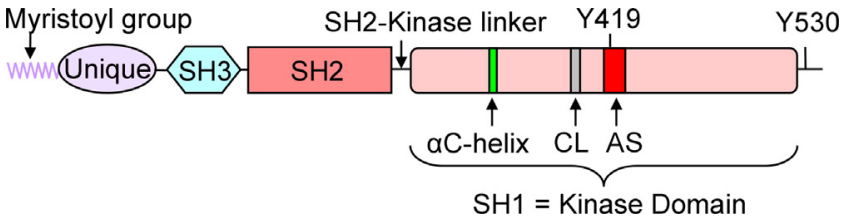

Figure 1.7 Structure of SRC

From the N- to C- terminus, SRC contains a 14-carbon myristoyl group, a unique domain, an SH3 domain, an SH2 domain, an SH2-kinase linker, a protein-tyrosine kinase domain (SH1), and a C-terminal regulatory segment. The catalytic loop (CL) region and activation segment (AS) are highlighted in the SH1 domain. Reprinted from Pharmacological Research, 94, Roskoski, Src protein-tyrosine kinase structure, mechanism, and small molecule inhibitors, 9-25, Copyright (2015), with permission from Elsevier.

Four FDA-approved SRCi (bosutinib, dasatinib, ponatinib, and vandetanib) define the current war chest used to combat SRC hyperactivated tumours in the clinic (Roskoski, 2015). Of this list, only vandetanib is approved for targeting solid tumours (medullary thyroid cancer) and is known to inhibit numerous surface-based receptors in addition to SRC, a likely consequence of its initial development as a VEGFR inhibitor (Hennequin *et al*., 2002). A lead synthetic lethal SRCi identified in our known drug screen, saracatinib, is not FDA-approved but currently in clinical trials for a range of solid tumour malignancies (Roskoski, 2015). Akin to other SRCi, saracatinib shows promise as a safe and well tolerated drug in patients (Nygaard *et al*., 2015).

1.4 DRUG SYNERGY

Our previous discovery of HDACi and SRCi drugs inducing synthetic lethal phenotypes in E-cadherin-deficient cells is of great interest, however, the observed effects are modest and in need of enhancement if such treatments were to be used in the chemoprevention setting. This has led to our interest in investigating synergistic drug combinations which can produce greater synthetic lethal effects.

Derived from the Attic Greek word *synergia*, meaning 'working together', the term 'synergy' is applied to drug studies where a combination of drugs can interact to enhance the effects, or side effects, of the involved individual drugs. Conversely, drug 'antagonism' denotes a response whereby drugs interact in a fashion reducing the effects of the involved drugs. In a therapeutic context, synergistic drug combinations allow for increased efficacy at reduced drug concentrations, ultimately minimising the risk of drug side effects to the patient whilst maximising therapeutic potential.

To investigate the interaction of a drug combination, it must first be predicted what therapeutic response would be observed from an 'additive effect', an interaction where neither drug synergy nor antagonism is observed. The Chou-Talalay combination index equation is currently regarded as the gold standard for determining such drug-based interactions *in vitro*, cited in excess of 5,000 publications (Chou, 2010; Chou and Talalay, 1984). This combination index incorporates facets of Chou's 'median-effect equation', a concept regarded in drug studies as the 'unified theory' due to its amalgamation of enzyme-ligand binding kinetic equations such as Henderson-Hasselbach, Michaelis-Menten, Hill, and Scatchard equations (Chou, 1980). In essence, the Chou-Talalay combination index equation uses the observed cell proliferation inhibition from each individual drug treatment to predict an inhibitory response of combined

treatment in an additive context (an effect denoted by a combination index score of 1; CI = 1). A combination index lower than 1 (CI < 1) denotes a drug combination producing a greater inhibitory effect than the predicted (additive effect) value; conversely, a combination index greater than 1 (CI > 1) denotes a drug combination producing a weaker inhibitory effect than the predicted (additive effect) value (Table 1.3).

Table 1.3 Combination index (CI) scores denoting drug combination interactions

Combination Index (CI)	**Drug Interaction**
> 1	Antagonistic
1	Additive
< 1	Synergistic

1.5 PROJECT AIMS

This project was comprised of three main aims.

(i) To compare the performance of different endpoint and real-time cell viability assays in order to effectively validate candidate synthetic lethal drugs in an isogenic pair of non-malignant MCF10A breast cell lines, one with and one without *CDH1* expression (MCF10A *CDH1*$^{-/-}$).

(ii) To identify a synergistic drug combination that inhibits proliferation preferentially in MCF10A *CDH1*$^{-/-}$ cells (i.e. a synergistic drug combination that inhibits E-cadherin's synthetic lethal partners).

(iii) To characterise the lead drug combination's effect on proliferation in the MCF10A isogenic pair and assess for synergy in E-cadherin-deficient cells with other genetic backgrounds.

2. MATERIALS AND METHODS

2.1 MATERIALS

2.1.1 Reagents

β-mercaptoethanol – Sigma-Aldrich, USA

0.05% trypsin solution - Prepared in lab (Appendix C.2)

0.5% trypsin/EDTA – Thermo Fisher Scientific, USA

30% acrylamide/bis solution 37.5:1 – Bio-Rad, USA

Absolute ethanol - Scharlau, Spain

Actrapid penfil neutral insulin - Novo Nordisk Pharmaceuticals Ltd, New Zealand

Ammonium persulfate (APS) – BDH Laboratory Supplies, UK

Anti-YAP1 (phospho S127) antibody – Abcam, UK

Anti-YAP1 antibody – Abcam, UK

Anti-α-tubulin antibody – Sigma-Aldrich, USA

Atorvastatin - SelleckChem, USA

Bovine insulin – Sigma-Aldrich, USA

Cell Culture Lysis 5X Reagent – Promega, USA

CellTiter-Glo Luminescent Cell Viability Assay - Promega, USA

Cholera toxin - Sigma-Aldrich, USA

cOmplete Mini (EDTA-free) Protease Inhibitor Tablets (Ref: 11836170001) – Sigma-Aldrich, USA

Dimethyl sulfoxide (DMSO) - Sigma-Aldrich, USA

Dulbecco's Modified Eagle Medium/Nutrient Mixture F-12 (DMEM/F-12) – Thermo Fisher Scientific, USA

Entinostat - SelleckChem, USA

Epidermal growth factor (EGF) - PeproTech, USA

Flavopiridol - SelleckChem, USA

Foetal bovine serum (FBS) – Thermo Fisher Scientific, USA

Freezing medium - Prepared in lab (Appendix C.3)

FTI-277 – Tocris Bioscience, UK

GGTI-298 – Tocris Bioscience, UK

Hoechst 33342 – Thermo Fisher Scientific, USA

Horse serum - Thermo Fisher Scientific, USA

HS-173 - SelleckChem, USA

Hydrocortisone - Sigma-Aldrich, USA

IRDye 680LT Goat (ploYclonal) anti-Rabbit IgG (H+L) – LI-COR, USA

IRDye 800CW Goat (polyclonal) anti-Mouse IgG (H+L) – LI-COR, USA

Isopropanol – Scharlau, Spain

K03861 - SelleckChem, USA

Lovastatin - SelleckChem, USA

LY294002 – SelleckChem, USA

Mifepristone - SelleckChem, USA

Olaparib – SelleckChem, USA

Paraformaldehyde - BDH Laboratory Supplies, UK

PD0325901 – SelleckChem, USA

PF-573228 - SelleckChem, USA

PHA-793887 - SelleckChem, USA

Phosphate buffered saline (Dulbecco A) tablets – Oxoid Limited, UK

Phosphate buffered saline solution (PBS) - Prepared in lab (Appendix C.1)

PI-103 – SelleckChem, USA

Pierce BCA Protein Assay Kit – Thermo Fisher Scientific, USA

PIK-75 - SelleckChem, USA

Precision Plus All Blue Prestained Protein Standard – Bio-Rad, USA

Propidium iodide - Thermo Fisher Scientific, USA

Resazurin - Sigma-Aldrich, USA

RNase A - Thermo Fisher Scientific, USA

Roswell Park Memorial Institute 1640 Medium (RPMI 1640) – Thermo Fisher Scientific, USA

RPMI 1640 (ATCC Modification) – Thermo Fisher Scientific, USA

Saponin – Sigma-Aldrich, USA

Saracatinib – SelleckChem, USA

Simvastatin - SelleckChem, USA

Sodium dodecyl sulphate (SDS) – BDH Laboratory Supplies, UK

Sorafenib - SelleckChem, USA

SYTOX - Thermo Fisher Scientific, USA

TAE226 – SelleckChem, USA

Taxol - Sigma-Aldrich, USA

Tetramethylethylenediamine (TEMED) – Riedel-de Haen, Germany

Trim milk powder – Pams, NZ

Tris ultrapure – BioFroxx, Germany

Tunicamycin – Sigma-Aldrich, USA

Tween-20 – Sigma-Aldrich, USA

Ultra-pure DNase/RNase-Free Distilled Water - Thermo Fisher Scientific, USA

Verteporfin – Cayman Chemical, USA

Vorinostat - SelleckChem, USA

Zaragozic acid A – Cayman Chemical, USA

Zoledronic acid - SelleckChem, USA

2.1.2 Equipment

500 mL filter system – Corning, USA

96 well black walled, clear flat bottom plates - Corning, USA

96 well white walled, clear flat bottom plates - Greiner Bio-One, Austria

96 well xCELLigence E-plates - ACEA Biosciences, USA

BD FACSCanto II – BD Biosciences, USA

BD Falcon 5 mL polystyrene round-bottom tube – BD Biosciences, USA

CO_2 cell culture incubator - Binder, Germany

Cytation 5 Imaging Reader – BioTek, USA

Cytell Cell Imaging System – GE Healthcare, UK

Dual chamber cell counting slides - Bio-Rad, USA

Immobilon PVDF transfer membrane – Merck, USA

IncuCyte FLR - Essen BioScience, USA

Milli-Q Ultrapure Water Purification System - Millipore, USA

Mini-PROTEAN II electrophoresis cell – Bio-Rad, USA

Mini Trans-Blot electrophoretic transfer cell – Bio-Rad, USA

Mr. Frosty Cryo 1 °C Freezing Container – Thermo Fisher Scientific, USA

Odyssey Fc Imaging System – LI-COR, USA

POLARstar OPTIMA - BMG Labtech, USA

TC10 Automated Cell Counter - Bio-Rad, USA

Tissue culture hood - EMAIL, Australia

Water bath - Semco, USA

xCELLigence RTCA-MP System – ACEA Biosciences, USA

2.1.3 Software

CellProfiler – Broad Institute, USA

CompuSyn – ComboSyn, Inc., USA

FlowJo – FlowJo, USA

Gen5 Software – BioTek, USA

Image Studio Software – LI-COR, USA

ImageJ - National Institute of Health, USA

IncuCyte Confluence V1.5 - Essen BioScience, USA

xCELLigence RTCA Software 1.2 – ACEA Biosciences, USA

2.2 METHODS

2.2.1 Cell Culture

2.2.1.1 Complete Growth Medium

MCF10A cells were cultured in a 1:1 mixture of Dulbecco's Modified Eagle Medium and F12 medium (DMEM/F-12), supplemented with 5% horse serum, 0.5 μg/mL hydrocortisone, 100 ng/mL cholera toxin, 10 μg/mL human insulin, and 20 ng/mL EGF. Pre-mixed complete media was filter sterilised using a 0.22 μm polyethersulfone filter and aliquoted into 50 mL Falcon tubes.

MDA-MB-231 cells were cultured in RPMI 1640 medium, supplemented with 10% FBS. The ATCC-formulated Leibovitz's L-15 medium was not used as cells were incubated in the presence of 5% CO_2.

IPH-926 cells were cultured in RPMI 1640 (ATCC modification) medium, supplemented with 20% FBS and 10 μg/mL bovine insulin.

2.2.1.2 Cell Culture Maintenance

MCF10A, MCF10A *CDH1*$^{-/-}$, MDA-MB-231, and IPH-926 cells were grown in 75 mL cell culture flasks in a humidified incubator at 37 °C with 5% CO_2 in their respective complete growth medium (Chapter 2.2.1.1).

Prior to passaging, whole growth medium, 0.05% trypsin, and PBS were pre-warmed in a 37 °C water bath. Old growth medium was aspirated from the flask and cells were washed with 3 mL PBS, which was then aspirated and 3 mL 0.05% trypsin added. The cells were then returned to

the incubator (MCF10A and MCF10A *CDH1*$^{-/-}$ cells for approximately 25 min; MDA-MB-231 and IPH-926 cells for approximately 5 min). 4 mL complete growth medium was then added to inactivate the trypsin and cells were transferred to a 15 mL Falcon tube and pelleted via centrifugation. The supernatant was aspirated and the cell pellet was resuspended in 4 mL complete growth medium. MCF10A and MCF10A *CDH1*$^{-/-}$ cells were counted and plated at respective densities of $3.0x10^5$ and $4.5x10^5$ cells in 75 mL culture flasks. MDA-MB-231 and IPH-926 cells were subcultured at ratios of 1:3 and 1:1, respectively. Flasks were then returned to the humidified incubator.

2.2.1.3 Cell Counting

Cells were counted on a dual chamber counter slide using the TC10 Automated Cell Counter. Each slide chamber was filled with approximately 10 µL of resuspended cells. Two measurements of cell density were taken from each chamber and averaged to determine the density of resuspended cells.

2.2.1.4 Thawing Cell Lines

Cells removed from liquid nitrogen storage were quickly thawed in a 37 °C water bath. Recovered cells were then resuspended in 9 mL of warm complete growth medium, pelleted via centrifugation, and the supernatant discarded to remove remaining DMSO. Pelleted cells were resuspended in warm complete growth medium and transferred to a 75 mL cell culture flask, then placed in a humidified incubator at 37 °C and 5% CO_2. Complete growth medium was changed in the cell culture flasks the following day.

2.2.1.5 Cryogenic Preservation

After trypsinisation, pelleted cells were resuspended in freezing medium (Appendix C.3), aliquoted into 1 mL cryovials, and transferred to a Mr. Frosty Cryo 1 °C Freezing Container and placed in a -80 °C freezer for 24 h. This allowed cells to be cooled at a rate of 1 °C per minute before being transferred into liquid nitrogen for long-term storage.

2.2.2 Cell Viability Assays

2.2.2.1 Drug Treatment Protocol

All drugs except zoledronic acid were reconstituted in DMSO to create stock solutions. Zoledronic acid was reconstituted in mQH_2O. Drugs were aliquoted and stored at -80 °C. Individual aliquots were diluted in complete growth medium to create working stocks prior to use in an experiment.

Cells were seeded in 96-well, black-walled, clear-bottomed, tissue culture plates in 100 µL complete growth medium and left to equilibrate at room temperature for 30 min before 37 °C, 5% CO_2 incubation. Cell seeding densities are shown in Table 2.1. After overnight incubation, cells were treated with 10 µL drug or 0.1% DMSO for controls. All endpoint experiments were performed in triplicate.

Table 2.1 Cell seeding densities for 96-well plate experiments

Cell line	Seeding Density (cells per well)
MCF10A	$4x10^3$
MCF10A *CDH1*$^{-/-}$	$4x10^3$
IPH-926	$8x10^3$
MDA-MB-231	$8x10^3$

2.2.2.2 CellTiter-Glo Luminescent Cell Viability Assay

For luminescent assays, CellTiter-Glo was added at 20% final concentration. Earlier optimisation had shown this concentration to consistently reproduce the manufacturer's recommended 1:1 vol/vol ratio (results not shown). Luminescent readings were obtained using a POLARstar Optima after 10 min incubation at room temperature with shaking.

2.2.2.3 Resazurin Reduction Cell Viability Assay

For resazurin reduction assays, resazurin was made to 440 μM stock solutions in PBS and aliquoted for storage at -20 °C. Resazurin solution was added to cells at 20% final concentration, and plates were incubated for 3 h at 37 °C prior to reading fluorescence at 550 nm excitation and 590 nm emission using a POLARstar Optima.

2.2.2.4 Nuclei Counting Cell Viability Assay

For nuclei counting assays, a one-step, no-wash, mild permeabilisation and fixation protocol was adopted from Chan *et al*. (2013), using a final concentration of 0.25% paraformaldehyde, 0.075% saponin, and 1 μg/mL Hoechst 33342. Plates were then incubated for at least 2 h in the

dark at room temperature. Plates were imaged at six fields per well under 4x magnification using the Cytation 5 Imaging Reader and imaged nuclei were enumerated using Gen5 software to obtain a total cell count. Alternatively, plates were imaged at 4 fields per well under 4x magnification using the Cytell Cell Imaging System and imaged nuclei were enumerated using CellProfiler to obtain a total cell count. For direct comparison between total cell count and measured confluency performed in the IncuCyte FLR, 10 nM SYTOX was used in place of Hoechst for nuclei enumeration because this IncuCyte model only has a single, green fluorescence filter.

2.2.2.5 xCELLigence Real-Time Assay

Experiments conducted on the RTCA-MP xCELLigence system were performed in accordance with instructions of the supplier. 100 µL of cell culture medium was added into each well of the E-plate 96, followed by a brief background impedance measurement on the RTCA-MP station. MCF10A and MCF10A *CDH1*$^{-/-}$ cells were seeded at a density of 4x10^3 cells per well in 90 µL complete growth medium. After 30 min equilibration at room temperature, the E-plate was returned to the RTCA-MP station. Cell proliferation as determined by the impedance measurement was recorded in 15 min intervals. At 24 h post-seeding, the assay was paused and cells were treated with 10 µL drug or 0.1% DMSO for controls. The assay was then resumed, taking impedance measurements every 15 min for a further 120 h. The electrical impedance measured by the RTCA software is reflected as the cell index (CI) value and is proportional to the number and attachment strength of the cells. All xCELLigence experiments were performed in duplicate.

2.2.2.6 IncuCyte Real-Time Assay

Cells were seeded in 96-well, black-walled, clear-bottomed, tissue culture plates in 100 µL complete growth medium and left to equilibrate at room temperature for 30 min before 37 °C, 5% CO_2 incubation. Cell seeding densities are shown in Table 2.1. After overnight incubation, cells were treated with 10 µL drug or 0.1% DMSO for controls, and the plate was inserted into the IncuCyte FLR for real-time imaging, with three fields imaged per well under 4x magnification every 2 h for a total of 48 h. Data were analysed using the IncuCyte Confluence version 1.5 software, which quantified cell surface area coverage as confluence values. All IncuCyte experiments were performed in triplicate.

2.2.2.7 Drug Synergy Analysis

Drug synergy/antagonism interactions were analysed using nuclei counting cell viability values and isobologram analysis via CompuSyn software. Isobologram analysis quantifies drug-drug interactions using a combination index (CI) value, whereby CI > 1.1 indicates antagonism, CI = 0.9-1.1 indicates additivity, and CI < 1 indicates synergy.

2.2.3 Cell Cycle Analysis

Cells were seeded at $1.5x10^5$ cells per well into 6-well plates in 2 mL complete growth medium and left to equilibrate to room temperature for 30 min before 37 °C, 5% CO_2 incubation. After 24 h, growth medium was aspirated and replaced with 2 mL drug diluted in complete growth medium, with 0.1% DMSO diluted in 2 mL complete growth medium for vehicle controls and 2 mL complete growth medium for cell-only controls. Plates were then incubated for an additional 24 h. Following incubation, growth medium was transferred from each well into a 15 mL Falcon tube. Wells were washed with 0.5 mL PBS, with wash added to respective 15 mL

Falcon tubes. 250 µL 0.05% trypsin solution was added to each well and plates incubated until cellular detachment. Cells were transferred into their respective Falcon tubes and wells were washed with 0.5 mL PBS, with wash added to the respective tubes. Cells were pelleted by centrifugation, supernatant discarded, and cells resuspended in 1 mL PBS. Cells were pelleted again via centrifugation and supernatant discarded. 800 µL ice-cold 70% ethanol solution was then added dropwise onto pellet whilst vortexing and cells were stored at -20 °C. The fixed, permeabilised cells were pelleted via centrifugation, supernatant discarded, 0.5 mL PBS added, and pelleted again via centrifugation. Supernatant was discarded, 50 µL RNAse A (from a 100 µg/mL working stock) was added to cell pellet, followed by addition of 400 µL propidium iodide solution (from a 50 µg/mL working stock). Cells were vortexed into solution, transferred to 5 mL polystyrene round-bottom FACS tubes, wrapped in foil, and stored at 4 °C for 3 h. Samples were then processed using a FACS Canto II, with 50,000 total cell events recorded for cell cycle analysis via FlowJo software.

2.2.4 Western Blotting

2.2.4.1 Protein Lysate Preparation

Cells were seeded at $1.5x10^5$ cells per well into 6-well plates in 2 mL complete growth medium and left to equilibrate to room temperature for 30 min before 37 °C, 5% CO_2 incubation. After 24 h, growth medium was aspirated and replaced with 2 mL drug diluted in complete growth medium, with 0.1% DMSO diluted in 2 mL complete growth medium for vehicle controls and 2 mL complete growth medium for cell-only controls. Plates were then incubated for an additional 24 h. Following incubation, growth medium was aspirated, cells were washed twice with PBS, and then lysed using 100 µL passive lysis buffer containing 1x cOmplete Protease Inhibitor Cocktail (Appendix C.11). Lysate was transferred to a centrifuge tube and vortexed prior to centrifugation to pellet cell debris. Supernatant was then collected and protein

concentration quantified using a bicinchoninic acid (BCA) assay as per the manufacturer's protocol.

2.2.4.2 Gel Electrophoresis

Protein samples were mixed at a 1:1 ratio with 2x Laemmli buffer (Appendix C.5) and heated at 95 °C for 5 min, then centrifuged for 1 min to remove bubbles after boiling. 20 µg of protein was loaded on a 10% SDS-PAGE gel (Appendix C.6) and submerged in 1x running buffer (Appendix C.7) in the Mini-PROTEAN II electrophoresis cell. 12 µL Precision Plus All Blue Prestained Protein Standard was loaded to determine band sizes. The gel was run at a constant 100 V for 2 h.

2.2.4.3 Protein Transfer to PVDF Membrane

A polyvinylidene fluoride (PVDF) membrane was briefly soaked in 100% methanol before washing with mQH_2O and soaking in 1x cold transfer buffer (Appendix C.8) for 15 min. Proteins were transferred from the gel to the PVDF membrane using the Mini Trans-Blot Electrophoretic Transfer Cell. The gel and membrane were sandwiched between filters, submerged in cold transfer buffer, and transferred using a constant 100 V for 1 h.

2.2.4.4 Primary Antibody Incubation

The PVDF membrane was washed three times for 10 min in Tris-buffered saline with Tween-20 (TBST; Appendix C.10). The membrane was then blocked using 5% w/v trim milk powder in TBST at room temperature for 1 h. Primary antibody was diluted in 5% w/v trim milk powder in TBST and incubated with the PVDF membrane at 4 °C on a rocking platform overnight. Primary antibody dilutions are listed in Table 2.2.

Table 2.2 Primary antibodies used for western blotting

Target	Antibody	Dilution	Product code
YAP	Rabbit mAb	1:1,000	ab52771
YAP pSer127	Rabbit mAb	1:1,000	ab76252
α-tubulin	Mouse mAb	1:2,500	T6199

2.2.4.5 Secondary Antibody Dilution

Following overnight primary antibody incubation, the PVDF membrane was washed four times for 10 min in TBST. Secondary antibody was then added and the membrane was incubated for 1.5 h at room temperature in the dark. Secondary antibody dilutions were performed as per the manufacturer's protocol, with dilution ratios outlined in Table 2.3. Three 10 min TBST washes and one TBS (Appendix C.9) wash was performed, with the membrane in the dark. The membrane was then imaged using an Odyssey Fc Imaging System.

Table 2.3 Secondary antibodies used for western blotting

Target	Antibody	Dilution	Product code
Rabbit	Goat pAb	1:10,000	IRDye 680LT
Mouse	Goat pAb	1:15,000	IRDye 800CW

3. OPTIMISATION OF REAL-TIME AND ENDPOINT CELL VIABILITY ASSAYS

3.1 INTRODUCTION

In vitro viability assays are essential tools for drug development, allowing for the assessment of drug efficacy prior to subsequent *in vivo* analyses. Whether performed as a single plate experiment or as part of a high-throughput screen, the concept remains the same - cells are incubated with a particular compound(s) then assessed for viability to quantify drug-induced cell toxicity.

Numerous commercial cell viability assays that exploit different cellular processes to quantify cytotoxicity are now available, each highlighting the variability that can be obtained from different methodologies (Chan *et al*., 2013; Kepp *et al*., 2011; Quent *et al*., 2010). Consequently, the selection and application of an effective assay(s) should be a major consideration in any drug-based experimental design.

A widely used approach to determine drug-induced cytotoxicity involves measuring cellular metabolic activity at the conclusion of an experiment. Such approaches include the 3-[4,5-dimethylthiazolyl-2]-2,5-diphenyltetrazolium bromide (MTT) assay, resazurin reduction, and the CellTiter-Glo assay, each harnessing a different aspect of cellular metabolism as a means of quantifying live cells. The MTT assay relies upon the mitochondrial activity of live cells to convert a yellow MTT substrate into purple formazan crystals, detectable via spectrophotometry (Mosmann, 1983). The resazurin reduction assay, used in alamarBlue and CellTiter-Blue assays, is a more sensitive alternative to MTT and uses the intracellular reduction potential of

living cells to convert resazurin to the fluorescent product resorufin (O'Brien *et al*., 2000). CellTiter-Glo adopts the use of firefly luciferase, which reacts with available cellular adenosine triphosphate (ATP) to produce a bioluminescent signal proportional to the number of live cells present in the assay (Crouch *et al*., 1993). The nuclei counting method, which is a direct measure of viability, is considered to be the most accurate (Chan *et al*., 2013); however, the ease of mix-and-measure metabolic-based approaches makes them a common feature in high-throughput drug screens.

Unlike endpoint approaches, real-time assay systems allow for the tracking of cellular growth over the entire time course of an experiment. This is particularly effective for assessing the impact of cytostatic compounds, where subtle growth inhibitory effects are easily noticeable but may be missed using endpoint-based methods. Real-time assays are typically performed using equipment capable of capturing images at regular intervals and quantifying cellular surface area coverage as a measure of proliferation, such as the IncuCyte FLR. Such methods also facilitate visualisation of drug-induced cell morphology changes. Alternatives to this approach include the xCELLigence, which uses electrical impedance to measure both cellular adhesion strength and surface area coverage as a combined proxy of cellular proliferation.

In this study, we compared the performance of five different cell-based viability assays. Three endpoint assays (resazurin reduction, CellTiter-Glo, and nuclei enumeration) and two real-time assays (IncuCyte and xCELLigence) were used to investigate the effectiveness of each approach for the validation of candidate synthetic lethal drugs in an isogenic pair of MCF10A breast cell lines.

3.2 RESULTS

3.2.1 Metabolic and Nuclei Counting Endpoint Assays

Firstly, the performance of two metabolic based assays were compared alongside nuclei counting. The resazurin reduction and CellTiter-Glo assays were chosen ahead of the MTT assay as previous studies have reported reduced sensitivity with MTT compared to other endpoint methods (Hamid *et al*., 2004; Haselsberger *et al*., 1996). To compare the efficacy of each assay, MCF10A and MCF10A *CDH1*$^{-/-}$ cells were treated with a previously identified synthetic lethal drug, vorinostat, for 48 hours and assessed for cell viability using each method (Telford *et al*., 2015). A dose-dependent effect was observed in all three methods with increasing vorinostat concentration in both cell lines. In both MCF10A and MCF10A *CDH1*$^{-/-}$ cells, 0.63 μM vorinostat treatment showed negligible viability inhibition, with no marked differences observed between the two metabolic assays. At dosages of 1.25 and 2.5 μM vorinostat, however, the CellTiter-Glo assay gave significantly higher viabilities than the resazurin reduction assay ($P < 0.05$; Figure 3.1A-B). Both metabolic based approaches gave significantly higher viabilities than the nuclei counting approach for all three vorinostat concentrations in both cell lines ($P < 0.05$; Figure 3.1A-B).

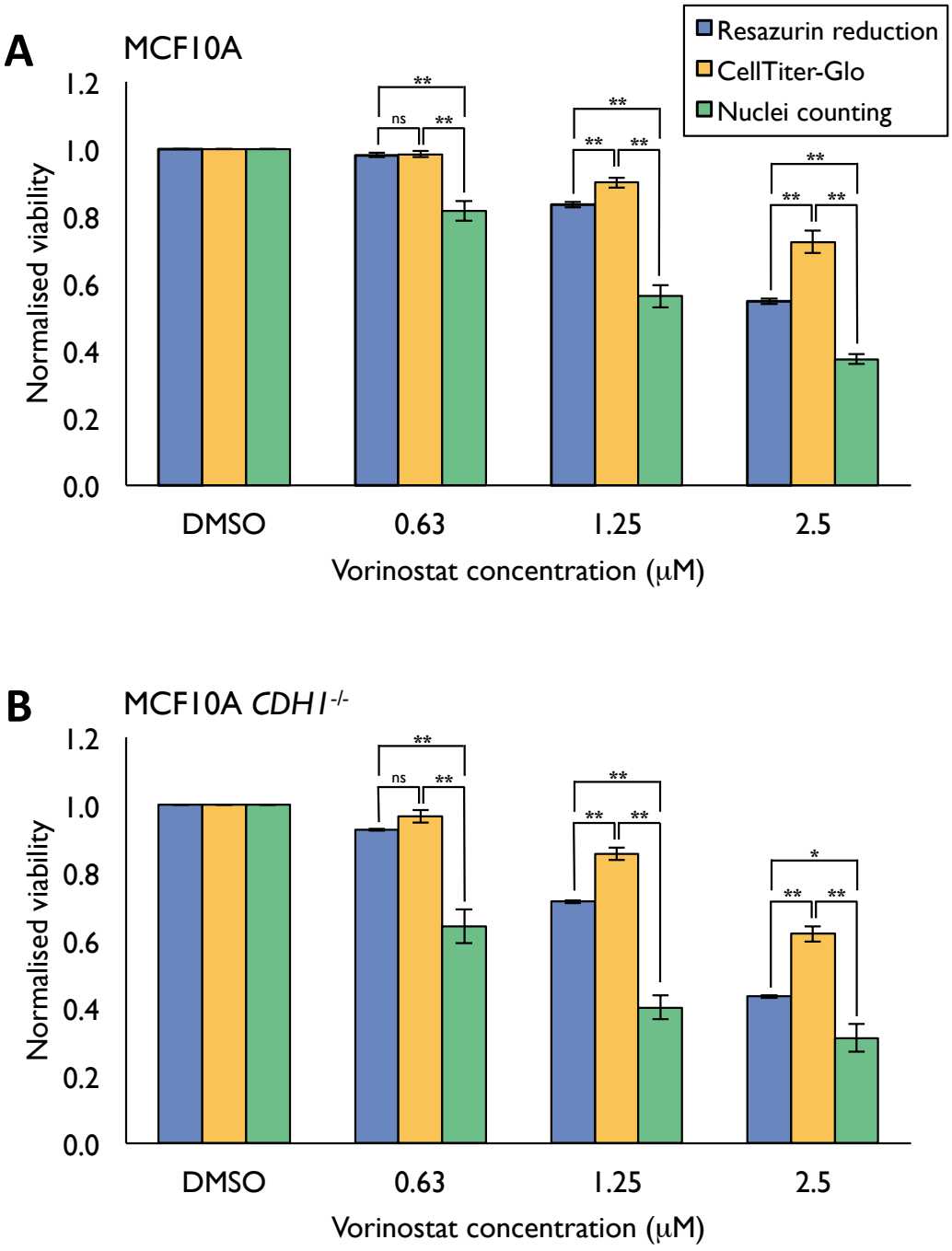

Figure 3.1 Comparison of endpoint viability assays

A comparison of three different endpoint assays (resazurin reduction, CellTiter-Glo, and Hoechst stained nuclei counting) based on their cell viability measurements normalised to their respective DMSO-treated controls in **(A)** MCF10A and **(B)** MCF10A *CDH1*$^{-/-}$ cells. Data represents averaged values of three biological replicates with standard error shown. *P*-values calculated using Student's *t*-test; * $P < 0.05$; ** $P < 0.01$.

3.2.2 Real-Time Assays

To complement the endpoint assays, real-time IncuCyte and xCELLigence assays were performed on MCF10A and MCF10A *CDH1*$^{-/-}$ cell lines treated with vorinostat over 48 hours (Figure 3.2A-B). The IncuCyte uses automated imaging to determine cellular confluence at designated intervals over the time course of an experiment as a measure of viability. The xCELLigence uses gold-plated plates to measure cell surface area coverage and adhesion strength via electrical impedance, combining these factors as a measurement of cell viability.

From the IncuCyte and xCELLigence platforms, both cell lines showed a dose-dependent inhibitory response to vorinostat, although this effect was more pronounced in MCF10A *CDH1*$^{-/-}$ cells (Figure 3.2A-B). In order to compare the two real-time systems, we determined the proliferation rate at logarithmic growth phase (taken from 12 to 36 hours post drugging in Figure 3.2C) between control and drug treatment within the respective MCF10A and MCF10A *CDH1*$^{-/-}$ cells. In both systems, the proliferation rates of vorinostat treated MCF10A cells were quite comparable and differed by no more than 10% across each tested concentration. MCF10A *CDH1*$^{-/-}$ cells showed slower proliferation rates in the xCELLigence than the IncuCyte. From 0.63 and 1.25 μM vorinostat doses, 24% and 53% smaller measurements were observed, respectively.

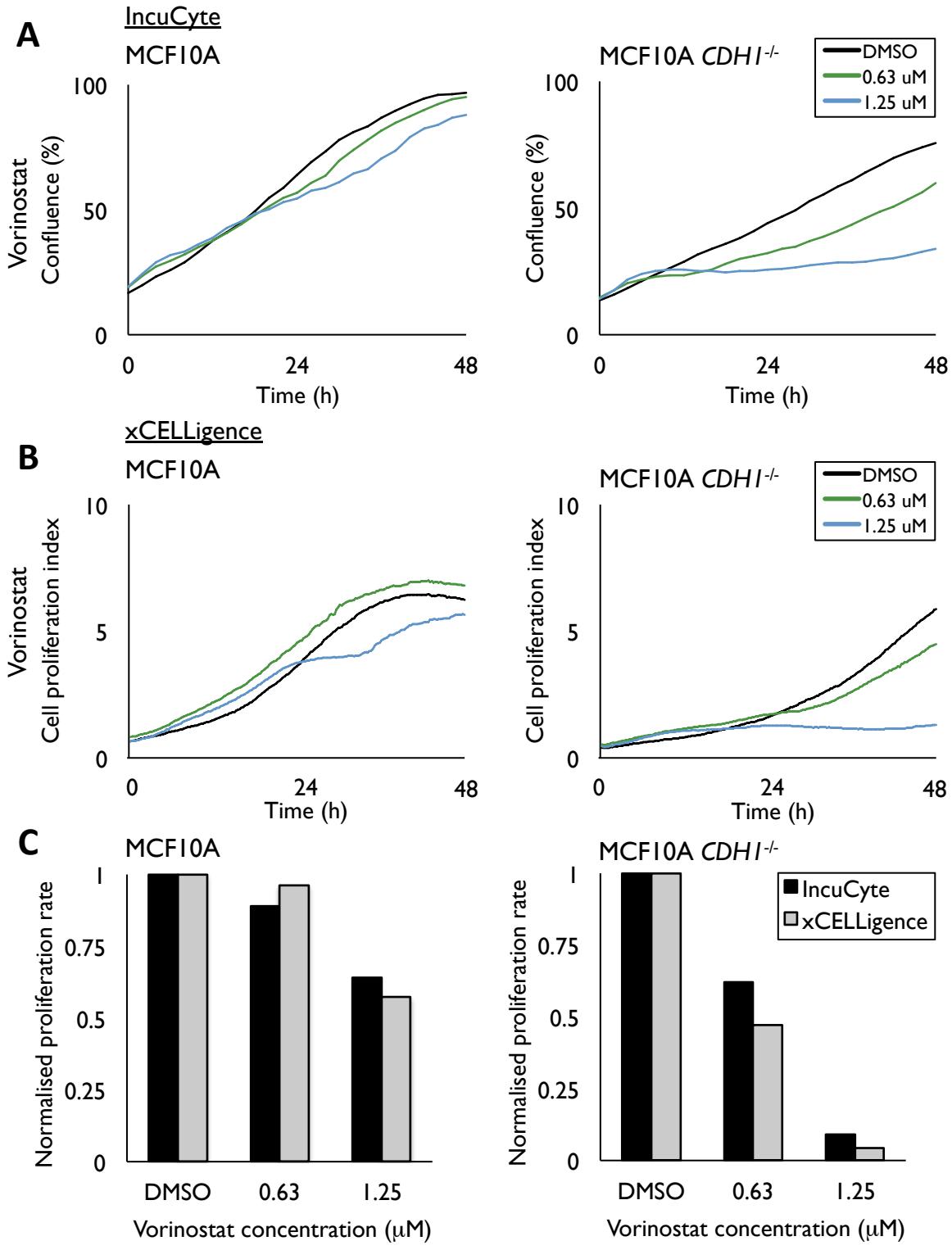

Figure 3.2 Comparison of real-time viability assays

A comparison of real-time viability measurements in MCF10A and MCF10A *CDH1*$^{-/-}$ cells as determined using **(A)** the IncuCyte system, which uses cell surface confluence, and **(B)** the xCELLigence system, which measures cellular surface area coverage and adherence strength. **(C)** A comparison of proliferation rates between the two real-time systems as determined by logarithmic growth phase (between 12 to 36 hours post treatment from **(B)** and **(C)**. The depicted proliferation rates are normalised to DMSO-treated controls. A representative experiment of each real-time assay is shown.

At the conclusion of each assay, both real-time platforms showed that vorinostat treated MCF10A cells had achieved viability values very similar to DMSO-treated controls (Figure 3.2A-B). This was contrary to data from the endpoint methods (Figure 3.1A), which had shown that each vorinostat concentration had produced lower viabilities than control treated cells, particularly in the nuclei counting assay. A closer inspection of representative phase-contrast and fluorescent images from the IncuCyte revealed an observable difference in cell density between control and vorinostat treated MCF10A cells (Figure 3.3A and 3.3C). Even though both control and vorinostat (1.25 μM) treated MCF10A cells showed full growth confluence covering the entire surface area of each respective well (Figure 3.3B), subsequent nuclei counting confirmed significant differences in cell numbers, whereby 39% fewer cells were present following drug treatment than control treatment (Figure 3.3C).

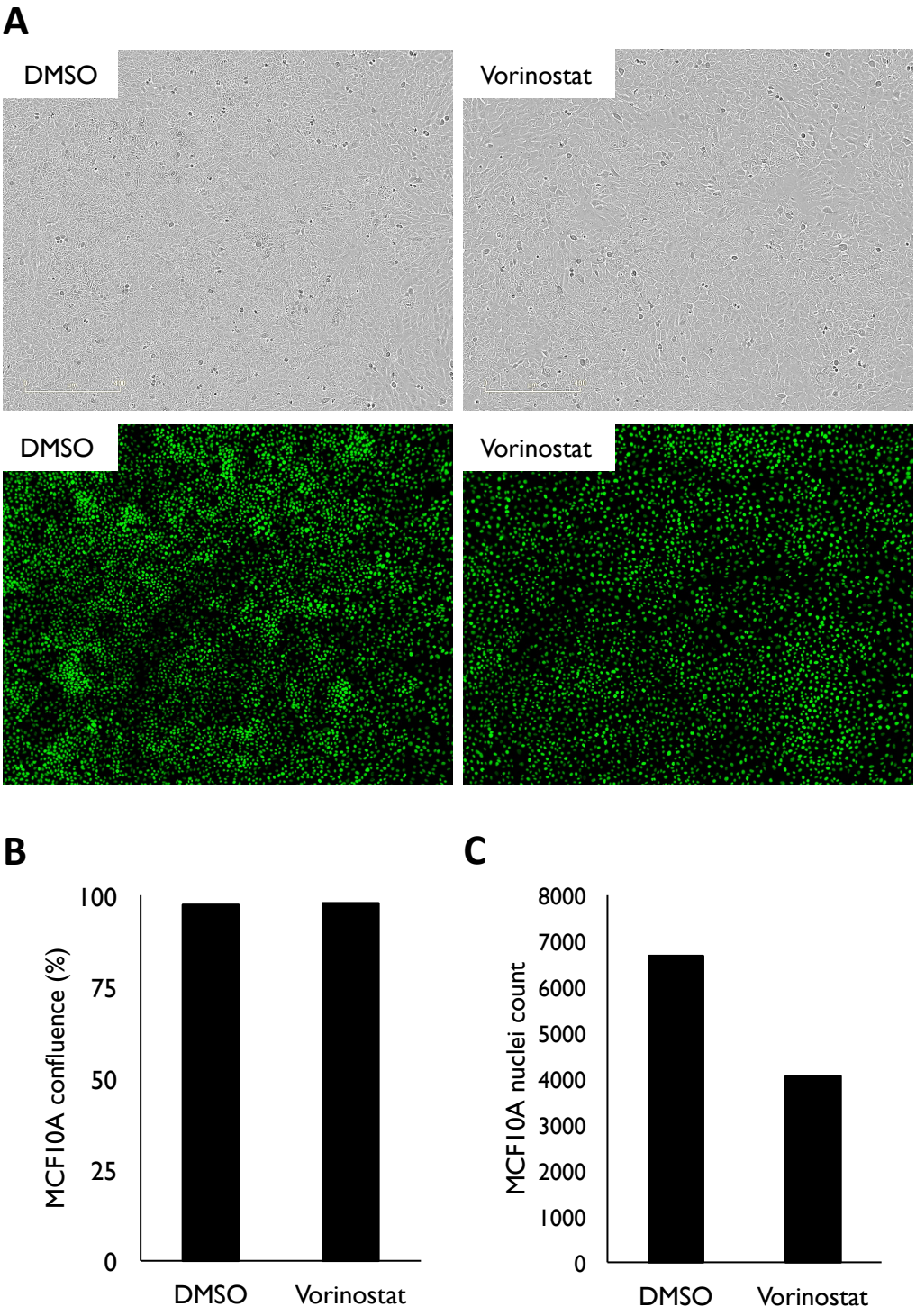

Figure 3.3 Cellular confluence measurements do not reflect cell densities at full surface area coverage

(A) Phase-contrast images of MCF10A cells at 48 h post DMSO and 1.25 μM vorinostat treatment (4X magnification; scale bars = 400 μm in length). A more distinct difference in cell density was observed in SYTOX-stained cell nuclei compared to the phase-contrast from the same field (fluorescent images captured using IncuCyte under 4X magnification). **(B)** Negligible cell viability difference observed between DMSO- and vorinostat-treated MCF10A cells as determined using IncuCyte's cell surface confluence measurements of phase-contrast images in **A**. **(C)** Differential cell densities quantified from nuclei enumeration of control and drug-treated MCF10A cells shown in **A**.

3.2.3 Real-time Assay and Endpoint Assay Multiplexing

To mitigate the shortfalls observed in the endpoint and real-time assays, we combined the IncuCyte real-time assay with both the resazurin reduction and nuclei counting assays. The resazurin reduction and nuclei counting methods were selected as endpoint assays as they have been reported to multiplex together effectively (Wu *et al*., 2009). This multiplexed approach also allowed for more data to be gathered from one drug-treated experiment. We also wanted to investigate if the combined approach was capable of evaluating synthetic lethal properties of two different drugs, where assay sensitivity is essential to distinguish preferential targeting of one cell type over another. In this case, a synthetic lethal effect would involve the selective growth inhibition of MCF10A *CDH1*$^{-/-}$ cells but not MCF10A cells. To test this, MCF10A and MCF10A *CDH1*$^{-/-}$ cells were subjected to either vorinostat or taxol treatment over 48 hours, with cellular growth being tracked in the IncuCyte, followed by resazurin reduction and nuclei counting at the conclusion of the real-time analysis.

At 48 hours following vorinostat treatment (0.63, 1.25, 2.5 μM), the confluence measurements from the IncuCyte showed that MCF10A cells were marginally inhibited and proliferated similarly to control treated cells (Figure 3.4A). However, in MCF10A *CDH1*$^{-/-}$ cells, a significant dose-dependent inhibitory response was observed in which drug treated cells did not reach the confluency of control treated cells (Figure 3.4B). Following the IncuCyte assay, the same plate was then subjected to the resazurin reduction assay. Increasing vorinostat treatment caused a more marked reduction in MCF10A *CDH1*$^{-/-}$ cell viabilities (93%, 71%, and 43%; Figure 3.4C) compared to the corresponding MCF10A treated cells (98%, 83%, 55%; Figure 3.4C). Similarly, the nuclei counting analysis, performed immediately after the resazurin reduction assay, also showed increasing vorinostat treatment causing a more marked effect on

MCF10A *CDH1*$^{-/-}$ cell viabilities (77%, 47%, and 26%; Figure 3.4D) compared to MCF10A cells (79%, 57%, and 37%; Figure 3.4D).

As another measure of synthetic lethality, the viability ratio of MCF10A *CDH1*$^{-/-}$ cells to MCF10A cells was calculated, whereby a ratio of less than 1 indicated an increased susceptibility of MCF10A *CDH1*$^{-/-}$ cells to drug treatment, concordant with a drug-induced synthetic lethal phenotype. Both the resazurin reduction and nuclei counting assays produced comparable viability ratios for 0.63, 1.25, and 2.5 μM vorinostat treatment between the isogenic cell lines (resazurin reduction: 0.95, 0.85, 0.78; nuclei counting: 0.97, 0.82, 0.70). The synthetic lethal effect seen in the endpoint assays was apparent in the IncuCyte confluence analysis, although the extent of this differential was more marked in real-time. Overall, the combined assays demonstrated an increased susceptibility of MCF10A *CDH1*$^{-/-}$ cells compared to MCF10A cells with increasing vorinostat dose.

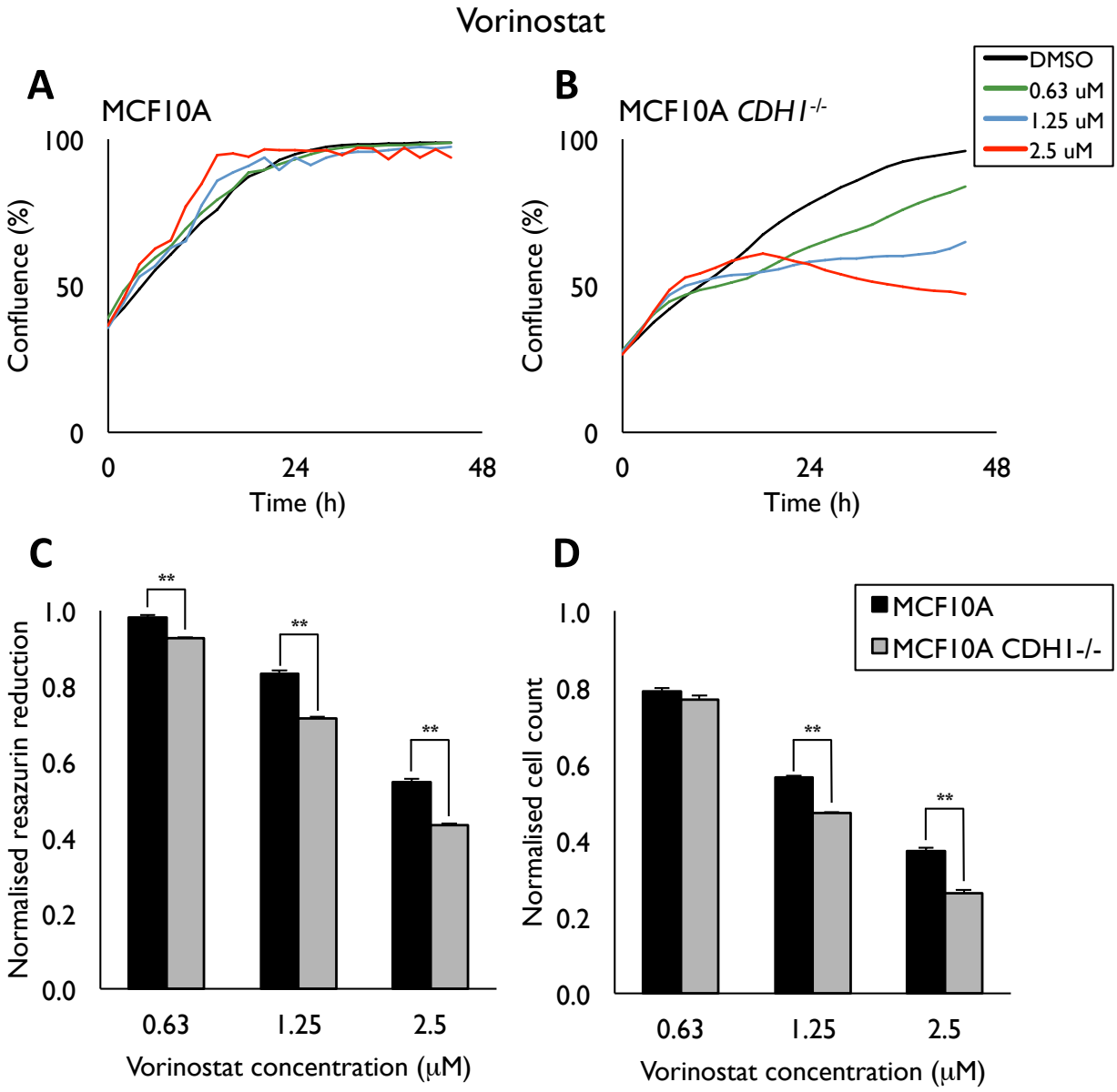

Figure 3.4 Combined real-time and endpoint assays facilitate the evaluation of drugs for synthetic lethal properties in MCF10A isogenic cells

(A-B) IncuCyte real-time confluence measurements demonstrating a selective proliferation inhibition by vorinostat in MCF10A *CDH1*$^{-/-}$ cells compared to MCF10A cells across a range of concentrations over 48 h. Endpoint resazurin reduction **(C)** and Hoechst stained nuclei-counting **(D)** performed immediately after the real-time assay **(A-B)**, showed a greater and selective inhibition of MCF10A *CDH1*$^{-/-}$ cells across three concentrations of vorinostat. Endpoint assays show viabilities normalised to respective controls, representing the averaged values of three biological replicates with standard error shown. *P*-values calculated using Student's *t*-test; ** $P < 0.01$.

We next used the combined endpoint and real-time assay approach to examine a drug that does not induce synthetic lethal effects in the MCF10A isogenic pair. The microtubule-targeting agent taxol was selected from the high-throughput drug screen for this purpose (Telford *et al*., 2015). IncuCyte analysis showed MCF10A cells treated with 1 and 2 nM taxol exhibited negligible inhibition (Figure 3.5A). When treated with 4 nM taxol, MCF10A cell viability was affected within the first 36 hours but eventually attained confluence measurements similar to controls at the conclusion of the real-time assay (Figure 3.5A). A similar effect was seen in taxol treated MCF10A *CDH1*$^{-/-}$ cells, although the highest concentration (4 nM) gave rise to growth inhibition that prevented full confluency observed in control treatment (Figure 3.5B). The resazurin reduction and nuclei counting assays showed that taxol treatment also produced a dose-dependent effect in both MCF10A and MCF10A *CDH1*$^{-/-}$ cells, without showing preferential inhibition in either cell type at the tested concentration range (Figure 3.5C-D). Furthermore, the viability ratios determined from both the resazurin reduction and nuclei counting assays were not less than 1 (resazurin reduction: 1.00, 1.02, and 1.05; nuclei counting: 1.02, 1.03, and 1.03), indicating no synthetic lethality. Taxol treatment at higher concentrations (up to 32 nM) yielded a dose-dependent effect in both isogenic cell lines although no synthetic lethal phenotype was observed at these concentrations (Appendix D.1).

To summarise, the IncuCyte in combination with both resazurin reduction and nuclei counting assays successfully provided a comprehensive analysis of vorinostat- and taxol-induced viability effects in the MCF10A isogenic cell lines.

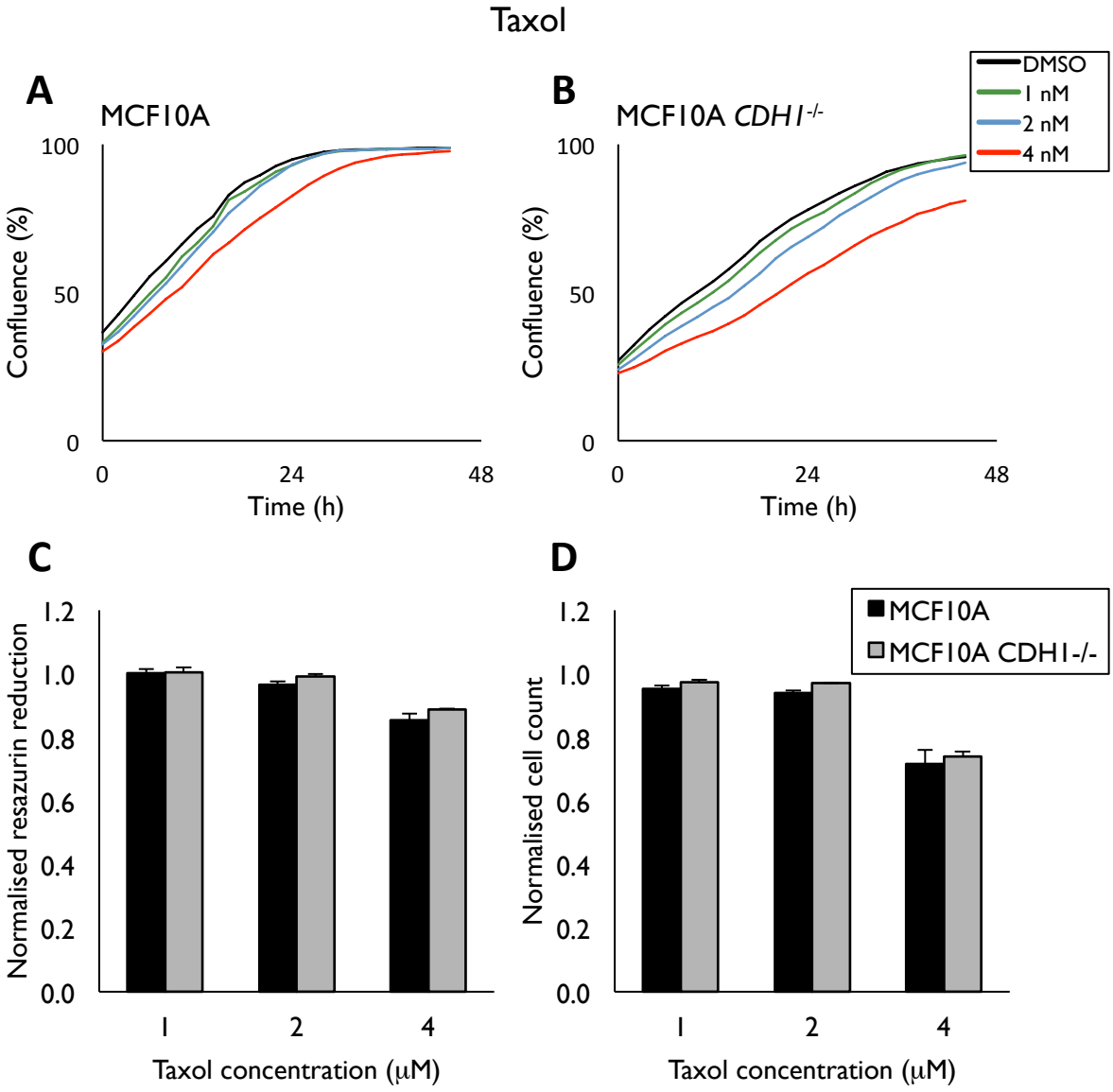

Figure 3.5 Combined real-time and endpoint assays facilitate the evaluation of drugs for synthetic lethal properties in MCF10A isogenic cells

(A-B) IncuCyte real-time confluence measurements demonstrating modest selective proliferation inhibition by taxol in MCF10A *CDH1*$^{-/-}$ cells compared to MCF10A cells across a range of concentrations over 48 h. Endpoint resazurin reduction **(C)** and Hoechst stained nuclei-counting **(D)** performed immediately after the real-time assay **(A-B)**, did not show selective inhibition of MCF10A *CDH1*$^{-/-}$ cells across three concentrations of taxol. Endpoint assays show viabilities normalised to respective controls, representing the averaged values of three biological replicates with standard error shown. *P*-values calculated using Student's *t*-test; ** $P < 0.01$.

3.3 DISCUSSION

In this chapter, we have shown that both metabolic-based endpoint assays examined gave significantly higher viabilities than the nuclei-counting approach, suggesting that resazurin reduction and CellTiter-Glo over-represent cell viability. In addition, viability as measured by nuclei counting was more comparable to that measured using resazurin reduction, suggesting CellTiter-Glo is less sensitive than other endpoint methodologies, at least for cells treated with vorinostat. This is contrary to previous literature reports, which indicate that CellTiter-Glo can provide higher sensitivity than resazurin-based assays (Peternel *et al*., 2009; Riss *et al*., 2004).

In addition to reduced sensitivity, the two metabolic assays also have other potential limitations. For example, the resazurin reduction assay requires a 37 °C incubation step of several hours which has been reported to cause morphological changes in cells (Riss *et al*., 2004). However, we did not observe resazurin-induced morphology changes in our cell lines (data not shown). On the other hand, CellTiter-Glo, which has a shorter incubation phase to permeabilise cells and release their ATP for measurement, has a considerably greater cost, which can be a drawback in high-throughput screening. Furthermore, it is possible that drugs affecting cellular metabolic processes could interfere with the performance of both the resazurin reduction and CellTiter-Glo assays, giving rise to inaccurate viability measurements (Kepp *et al*., 2011).

Overall, the nuclei counting method is still considered to be the most accurate measure of cell viability (Chan *et al*., 2013). A drawback to this approach is the application to high-throughput screening, requiring efficient automated imaging systems with built-in enumeration software, which can be cost prohibitive. Fortunately, more affordable entry-level systems, such as the Cytell (General Electric), Cytation 5 (BioTek), and EVOS (Thermo), are available to provide such technologies at a reduced cost. Alternatively, more standard imaging systems without

accompanying enumeration software can be used with free open sourced applications such as ImageJ (Schneider *et al*., 2012) or CellProfiler (Lamprecht *et al*., 2007).

The IncuCyte and xCELLigence platforms each produced comparable proliferation rates for vorinostat-treated MCF10A cells. When using MCF10A *CDH1*$^{-/-}$ cells, however, discrepancies in recorded proliferation rates from the two systems became apparent, with the xCELLigence producing slower rates than those seen using the IncuCyte. It is possible that this difference could be attributed to the compromised adhesion previously characterised in MCF10A *CDH1*$^{-/-}$ cells (Chen *et al*., 2014a), which may have been further exacerbated by vorinostat treatment. As a result, the xCELLigence, which measures adhesion impedance, would have registered a greater reduction in MCF10A *CDH1*$^{-/-}$ cell viability compared to the IncuCyte, which is incapable of detecting adhesion strength. MCF10A cells showed no marked difference between the two systems, presumably since this cell line does not exhibit compromised cellular adhesion (Chen *et al*., 2014a).

The gold-plated xCELLigence plates used in this study unfortunately lacked clear bottoms which prevented imaging analysis. Newer E-plates with partial clear bottom sections for cell visualisation are now available; however, these were not released prior to our investigation. Conversely, the IncuCyte system was able to provide images which showed no substantial morphological changes over the time course of vorinostat treatment in both cell types (Figure 3.3A). Overall, both real-time platforms showed comparable performance, except for measuring MCF10A *CDH1*$^{-/-}$ cells treated with 0.63 μM vorinostat.

A noteworthy observation was the IncuCyte's inability to discriminate between differing cellular densities when cells had covered the entire surface area of their respective wells. As such, caution should be taken when analysing data at full cellular confluence as further

validation is required from direct cell counting. Nevertheless, the IncuCyte still produced valuable data during sub-confluent growth phases, which was comparable to nuclei counting data (data not shown). These results demonstrate that a combination of distinct methodologies provides a more comprehensive and accurate assessment of drug efficacy than singular assays.

In conclusion, this chapter has shown that the IncuCyte system is well suited for tracking sub-confluent cell growth phases, which can be followed up by nuclei counting to assess drug efficacy when cells are at full confluence. In the absence of a real-time system like the IncuCyte, nuclei counting should be performed as it provided the most accurate measurement of viable cells in this analysis. Overall, we have demonstrated the utility and strengths of five viability assays and have adapted a robust real-time and endpoint multiplexed method for the investigation of synthetic lethal drugs.

4. SYNERGISTIC SYNTHETIC LETHAL DRUG SCREENING

4.1 INTRODUCTION

We have previously identified drugs that are synthetic lethal in a non-malignant breast cell line lacking E-cadherin expression, MCF10A *CDH1*$^{-/-}$, relative to wild-type MCF10A (Single *et al*., 2015; Telford *et al*., 2015). However, these synthetic lethal effects were relatively modest. This led to our goal of discovering synergistic drug combinations capable of accentuating our initial synthetic lethal vulnerabilities. Clinically, this approach would allow for maximal therapeutic outcomes to be achieved for HDGC and ILBC patients with lower risks of drug toxicity.

4.1.1 Drug Combination Testing

The recommended approach for identifying synergistic drug-drug interactions involves the application of Chou-Talalay's median-effect analysis to cell viability data obtained using a constant-ratio experimental design (Chou, 2010; Chou and Martin, 2007; Chou and Talalay, 1984).

The constant-ratio experimental design determines a drug's potency in a particular cell line when given as both a single-agent and combined treatment with another drug. This is important as it allows for the kill-curve, or 'shape', of each drug to be determined prior to assessment of its behaviour in combination. The basis of the constant-ratio experimental design involves treating a particular cell line with a titrated range of two or more single-agent drugs alongside a titrated range of these drugs in combination. This combination treatment must be provided to the cell line with each titration point consisting of a constant-ratio of drug 1 and drug 2.

Following conclusion of the experiment, cell viability data gathered from each single-agent and combination treatment is inputted into Chou-Talalay's equation for determining the combined drug interaction. As previously mentioned, the output of this equation denotes a 'combination index' (CI) whereby: CI < 0.9 indicates a synergistic drug interaction; CI = 0.9-1.1 indicates an additive drug interaction; CI > 1.1 indicates an antagonistic drug interaction (Chou, 2010). It is this Chou-Talalay method and combination index interpretation that has formed the basis of drug combination screening in this chapter.

4.1.2 Synergistic Combinations with HDACi

Multiple reports of drug combinations involving HDACi are evident in the literature. These include descriptions of HDACi in combination with drugs such as microtubule stabilising agents, poly (ADP-ribose) polymerase (PARP) inhibitors, multikinase inhibitors, and inhibitors of the mevalonate pathway. Synergy between HDACi and the microtubule stabilising agent taxol has been observed across numerous cancer cell lines (Cooper *et al*., 2007; Dietrich *et al*., 2010; Dowdy *et al*., 2006; Owonikoko *et al*., 2010; Shi *et al*., 2010; Zuco *et al*., 2011), including the wild-type MCF10A line (Shi *et al*., 2010). We have previously reported that MCF10A *CDH1*$^{-/-}$ cells have grossly disrupted microtubule organisation (Chen *et al*., 2014a; Telford *et al*., 2015). This suggests that taxol has the potential to act synergistically with HDACi, such as vorinostat, in MCF10A *CDH1*$^{-/-}$ cells through the simultaneous targeting of microtubules. One target of vorinostat, a pan-HDACi, is HDAC6. Cytoplasmic HDAC6 mediates the removal of acetylation tags on alpha-tubulin lysine residues, leading to a relaxed microtubule state (Glozak *et al*., 2005; Zhang *et al*., 2003). The inhibition of HDAC6 with vorinostat therefore results in acetylated, stabilised microtubules (Zilberman *et al*., 2009). Simultaneous treatment of HDACi in conjunction with a microtubule stabilising agent such as

taxol, would be predicted to exacerbate this stabilised tubulin state, leading to dysfunction in cell motility, trafficking, and mitotic processes.

In addition to cytoskeleton modifying effects, HDACi have been reported to modulate homologous DNA repair mechanisms (Chao and Goodman, 2014). This is achieved by HDACi-induced downregulation of double stranded break (DSB) repair, a process known to involve the PARP proteins (Chao and Goodman, 2014). It is therefore thought that combined treatment of HDACi with PARP inhibitors (PARPi) may exert a critical decrease in the rate of DNA repair and thus produce a marked cellular apoptotic response. Indeed, current *in vitro* studies across a range of cell lines provide evidence supporting a synergistic interaction between vorinostat and the PARPi, olaparib (Chao and Goodman, 2014; Hegde *et al*., 2016; Konstantinopoulos *et al*., 2014; Rasmussen *et al*., 2016; Zhang *et al*., 2012). It is unlikely that E-cadherin loss will sensitise our normalised MCF10A cell line to DNA repair inhibition, however, HDACi and PARPi combinations will be tested for potential synergistic interactions.

In vitro data have shown combined sorafenib and HDACi treatment induces a synergistic apoptotic response in cell lines derived from tissues including CNS, renal carcinoma, and the liver (Chen *et al*., 2014b; Kim *et al*., 2012; Lachenmayer *et al*., 2012; Tang *et al*., 2012). Sorafenib is a multikinase inhibitor known to inhibit multiple cellular signalling pathways, including Raf kinases, VEGF, and platelet-derived growth factor receptors (Chen *et al*., 2014b). Additionally, sorafenib has been shown to prevent the cellular antiapoptotic response by translationally downregulating Bcl-2 family proteins (Rahmani *et al*., 2005; Yu *et al*., 2005). Sorafenib currently serves as the only FDA-approved drug for patients with advanced hepatocellular carcinoma (HCC), however, recent preclinical studies have shown great promise for the treatment of other malignancies such as melanoma, non-small cell lung cancer, colorectal cancer, and breast cancer (Wilhelm *et al*., 2008 and references therein). Due to the

broad-spectrum nature of multikinase and HDAC inhibition, the synergistic mechanism for this response is yet to be fully understood, however, some reports suggest the ERK signalling pathway may play a key role (Chen *et al*., 2014b). Both epithelial (E-cadherin-expressing) and mesenchymal (E-cadherin-deficient) MCF10A cells require ERK signalling for cell cycle progression (Klein *et al*., 2008), suggesting ERK inhibition alone may not be an exploitable synthetic lethal vulnerability in our isogenic system.

Simultaneous PI3K inhibitor (PI3Ki) and HDACi treatment has been shown to exert synergistic antiproliferative effects both *in vitro* and *in vivo* (Bodo *et al*., 2013; Erlich *et al*., 2012; Pei *et al*., 2016; Piao *et al*., 2016; Wozniak *et al*., 2010; Yamada *et al*., 2013; Yoshioka *et al*., 2013). Interestingly, these studies have spurred development of PI3Ki-HDACi hybrid compounds. CUDC-907 is an example of one such compound containing both HDAC and PI3K inhibition moieties that is currently undergoing phase II clinical trials for non-Hodgkin's lymphoma and multiple myeloma (Rana *et al*., 2015).

The PI3K pathway is regulated, at least in part, by E-cadherin mediated cell-to-cell adhesion dynamics (Fukata and Kaibuchi, 2001; Kovacs *et al*., 2002). Consistent with this, activating PI3K mutations are frequently identified in tumours devoid of E-cadherin expression – particularly in the case of ILBC (Christgen and Derksen, 2015; Christgen *et al*., 2013; Christgen *et al*., 2016). Although the MCF10A cell model used in this study does not harbour an activating PI3K mutation (Isakoff *et al*., 2005; Zhang *et al*., 2008), we hypothesise that inhibition of the PI3K signalling cascade in a drug combination context may be capable of exploiting an underlying vulnerability following E-cadherin loss.

Synergistic combinations between HDACi and mevalonate pathway inhibitors have been described in a range of malignant cell lines (Gan *et al*., 2008; Lin *et al*., 2017; Sonnemann *et al*.,

2007). These studies support investigation of the mevalonate signalling cascade in our E-cadherin-deficient synthetic lethal model. The mevalonate pathway is responsible for the production of cellular steroids, post-translational prenylation modifications, and intracellular cholesterol (Mullen *et al*., 2016). The rate-limiting step of these processes involves conversion of 3-hydroxy-3-methylglutaryl-CoA (HMG-CoA) to mevalonic acid via the enzyme HMG-CoA reductase (HMGCR). The best-known HMGCR inhibitors are statins, which are widely used as lipid-lowering medications (Mullen *et al*., 2016).

Recent studies have highlighted the mevalonate pathway's involvement in cell proliferation, motility, and invasion (Al-Haidari *et al*., 2014; Sanchez *et al*., 2008; Wong *et al*., 2002; Yu *et al*., 2013). Specifically in breast cancer cell lines, the inhibition of multiple mevalonate pathway steps has been shown to induce drastic morphological changes by altering levels of key cytoskeletal regulators such as Rac, Rho, and Cdc42 (Gobel *et al*., 2016). Activation of these cytoskeletal-associated proteins is governed by the mevalonate pathway's addition of post-translational prenylation motifs (Sahai and Marshall, 2002). Prenylation facilitates protein anchoring to the lipid membrane via addition of a 15-carbon or 20-carbon tag to cysteine residues, processes termed farnesylation and geranylgeranylation, respectively (Thurnher *et al*., 2012; Wang and Casey, 2016). Interestingly, statin-mediated mevalonate pathway inhibition reduced proliferation in the E-cadherin devoid MDA-MB-231 cell line whilst minimally affecting an E-cadherin expressing MDA-MB-231 line (Warita *et al*., 2014). Although the underlying mechanism of this susceptibility is not understood, the application of statins to the MCF10A and MCF10A *CDH1*$^{-/-}$ cell lines is an exciting prospect.

In this chapter, candidate HDACi, cytoskeleton-targeting, and statin drug combinations have been tested in an isogenic MCF10A cell line pair to identify synergistic synthetic lethal combinations in E-cadherin-deficient cells, MCF10A *CDH1*$^{-/-}$.

4.2 RESULTS

4.2.1 Histone Deacetylase Inhibitor (HDACi) Combinations

4.2.1.1 HDACi and the SRC Inhibitor Saracatinib

To identify a drug combination that causes a synergistic synthetic lethal effect in E-cadherin-deficient cells, we first tested the combination of our previously identified lead drugs, histone deacetylase inhibitors (HDACi; entinostat and vorinostat; Figure 4.1A-B) and the SRC inhibitor, saracatinib (Figure 4.1C). 24 hours after seeding, MCF10A and MCF10A *CDH1*$^{-/-}$ cells were treated with a range of concentrations of HDACi (entinostat or vorinostat), saracatinib, and a combination of HDACi and saracatinib, and cultured for an additional 48 hours. Cellular viability was then assessed using nuclei counting and potential synergistic drug interactions identified using an isobologram analysis via CompuSyn software. This analysis showed that both entinostat/saracatinib and vorinostat/saracatinib produced marked synthetic lethal effects in MCF10A *CDH1*$^{-/-}$ cells (Figure 4.2A, 4.3A). This was evident by comparing IC_{50} values between the isogenic cell lines, with higher IC_{50} values seen in MCF10A cells than MCF10A *CDH1*$^{-/-}$ cells (Table 4.1). The isobologram analysis, plotted as Combination Index (CI) against cellular viability loss from combination treatment (fraction of cells affected, Fa) showed an antagonistic interaction for both tested HDACi and saracatinib combinations (CI > 1.1; Figure 4.2B-C, 4.3B-C; Table 4.1). In summary, both entinostat and saracatinib or vorinostat and saracatinib produced a significant synthetic lethal effect in E-cadherin-deficient MCF10A cells but did not show evidence of a synergistic drug interaction.

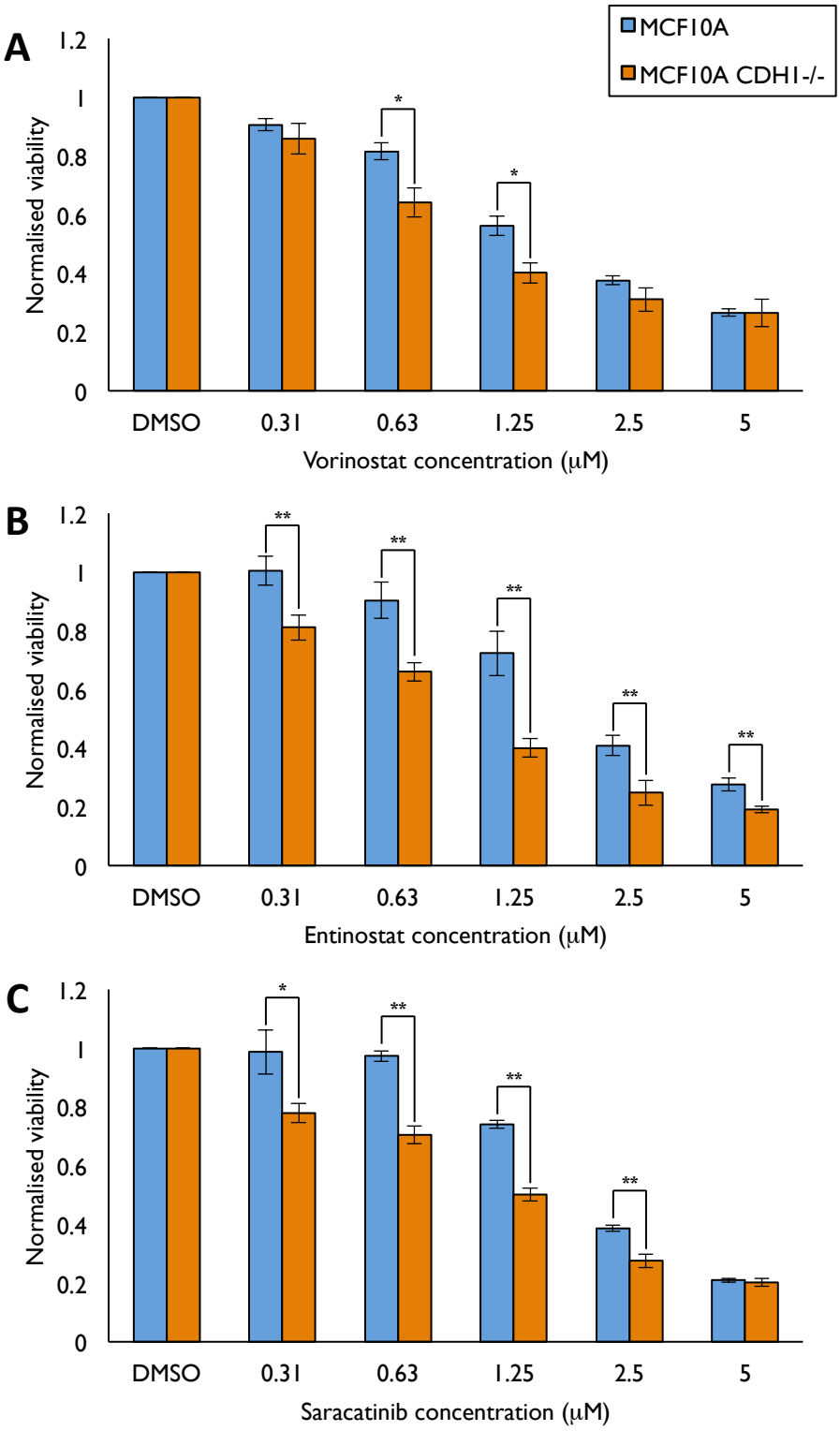

Figure 4.1 Validation of previously identified synthetic lethal drugs in MCF10A *CDH1*$^{-/-}$ cells

MCF10A and MCF10A *CDH1*$^{-/-}$ cells were grown for 24 h and treated with either **(A)** vorinostat, **(B)** entinostat, or **(C)** saracatinib over a range of concentrations. At 48 h post-treatment, cell viability was assessed using a Hoechst-stained nuclei counting assay. MCF10A *CDH1*$^{-/-}$ cells showed greater sensitivity to each drug treatment than MCF10A cells, concordant with a synthetic lethal phenotype. Data represents averaged values of two biological replicates with standard error shown. P-values calculated using Student's t-test; * $P < 0.05$; ** $P < 0.01$.

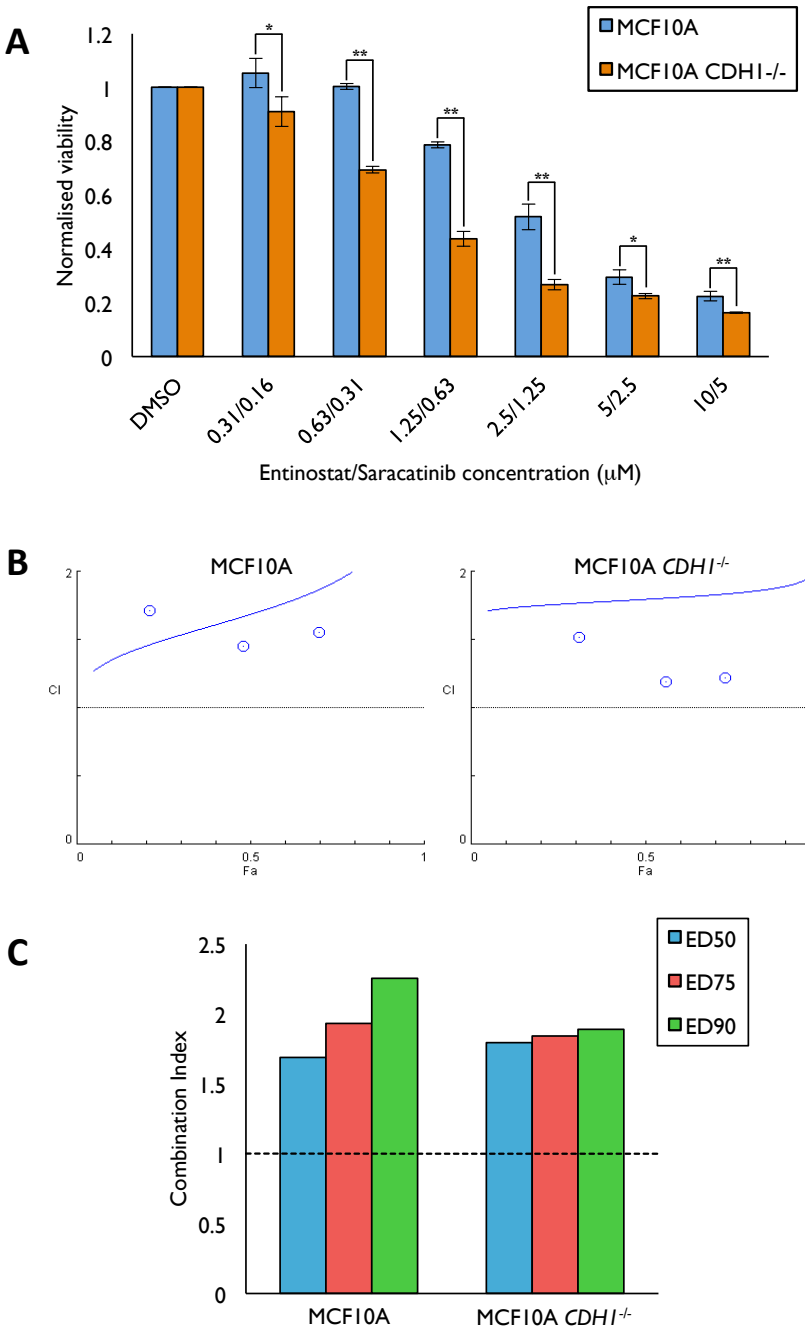

Figure 4.2 Entinostat and saracatinib Treatment is synthetic lethal but not synergistic in MCF10A *CDH1*$^{-/-}$ cells

MCF10A and MCF10A *CDH1*$^{-/-}$ cells were grown for 24 h and treated with single-agent entinostat or saracatinib, or combined entinostat and saracatinib for 48 h. Cell viabilities were determined using a Hoechst-stained nuclei counting assay **(A)** and used to assess drug synergy at ED50, ED75, and ED90 doses via CompuSyn software analysis **(B, C)**. Drug synergy is evaluated using a combination index (CI), whereby CI < 0.9 indicates synergy; CI = 0.9-1.1 indicates additivity; CI > 1.1 indicates antagonism. MCF10A *CDH1*$^{-/-}$ cells showed greater sensitivity to entinostat and saracatinib treatment than MCF10A cells, concordant with a synthetic lethal phenotype. Entinostat and saracatinib treatment was not synergistic in both MCF10A isogenic cell lines (CI > 0.9). **(A)** represents averaged values of two biological replicates with standard error shown; a representative experiment is shown for **(B)** and **(C)**. *P*-values calculated using Student's *t*-test; * $P < 0.05$; ** $P < 0.01$.

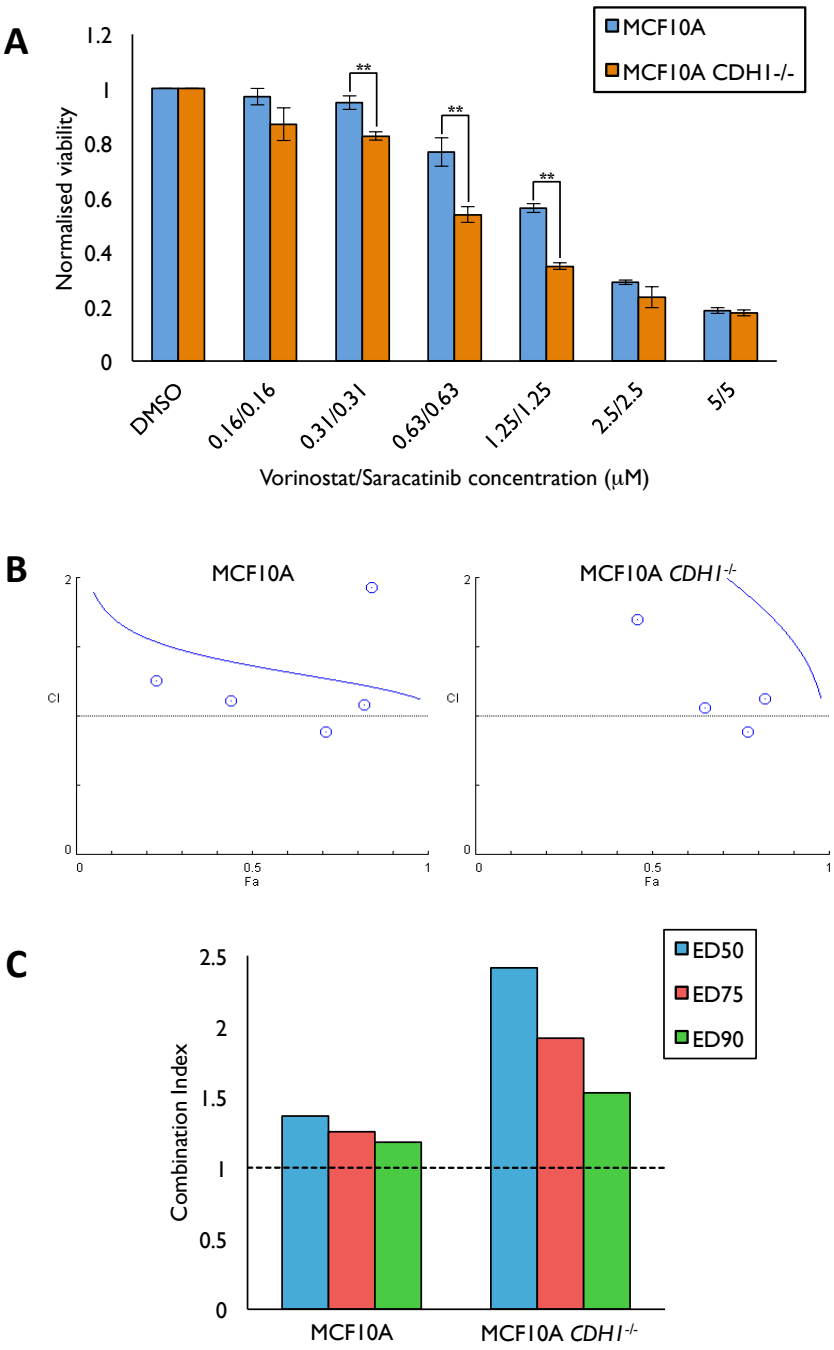

Figure 4.3 Vorinostat and saracatinib treatment is synthetic lethal but not synergistic in MCF10A *CDH1*$^{-/-}$ cells

MCF10A and MCF10A *CDH1*$^{-/-}$ cells were grown for 24 h and treated with single-agent vorinostat or saracatinib, or combined vorinostat and saracatinib for 48 h. Cell viabilities were determined using a Hoechst-stained nuclei counting assay **(A)** and used to assess drug synergy at ED50, ED75, and ED90 doses via CompuSyn software analysis **(B, C)**. Drug synergy is evaluated using a combination index (CI), whereby CI < 0.9 indicates synergy; CI = 0.9-1.1 indicates additivity; CI > 1.1 indicates antagonism. MCF10A *CDH1*$^{-/-}$ cells showed greater sensitivity to vorinostat and saracatinib treatment than MCF10A cells, concordant with a synthetic lethal phenotype. Vorinostat and saracatinib treatment was not synergistic in both MCF10A isogenic cell lines (CI > 0.9). **(A)** represents averaged values of two biological replicates with standard error shown; a representative experiment is shown for **(B)** and **(C)**. *P*-values calculated using Student's *t*-test; ** $P < 0.01$.

Table 4.1 HDACi (entinostat and vorinostat) and saracatinib combination IC_{50} values and ED50 combination indices (CI) in MCF10A and MCF10A *CDH1*$^{-/-}$ cells.

		Combination IC_{50} (HDACi μM/saracatinib μM)	**ED50 CI**
Entinostat + Saracatinib	MCF10A	3.07/1.54	1.69
	MCF10A *CDH1*$^{-/-}$	1.52/0.76	1.80
Vorinostat + Saracatinib	MCF10A	1.87/1.87	1.37
	MCF10A *CDH1*$^{-/-}$	1.14/1.14	2.41

4.2.1.2 HDACi and the Microtubule Stabilising Drug Taxol

We next investigated HDACi in combination with the microtubule stabilising agent taxol in the MCF10A isogenic pair. MCF10A and MCF10A *CDH1*$^{-/-}$ cells were grown for 24 hours, then treated with single-agent vorinostat or taxol, or both drugs in combination for an additional 48 hours. Cell viability was then assessed using nuclei counting and drug synergy quantified using an isobologram analysis via CompuSyn. The nuclei counting analysis showed single-agent taxol treatment did not induce a synthetic lethal phenotype in MCF10A *CDH1*$^{-/-}$ cells (Appendix D.1). Combined vorinostat and taxol treatment also exerted a dose-dependent effect in both MCF10A isogenic cell lines without inducing a synthetic lethal effect in the MCF10A *CDH1*$^{-/-}$ cell line (Figure 4.4A). The lack of synthetic lethality was reflected by similar IC_{50} values in each isogenic cell line following treatment (Table 4.2). In addition, the isobologram analysis showed an antagonistic effect for combined vorinostat and taxol treatment in both MCF10A isogenic cell lines, producing ED50 combination indices of 1.20 and 1.27 for MCF10A and MCF10A *CDH1*$^{-/-}$ cells, respectively (CI > 1.1; Figure 4.4B-C; Table 4.2). To summarise, combined treatment of an HDACi (vorinostat) and microtubule stabilising drug (taxol) failed to increase the synthetic lethal effect of vorinostat-only treatment in MCF10A *CDH1*$^{-/-}$ cells and, additionally, produced a weak antagonistic interaction in both MCF10A isogenic cell lines.

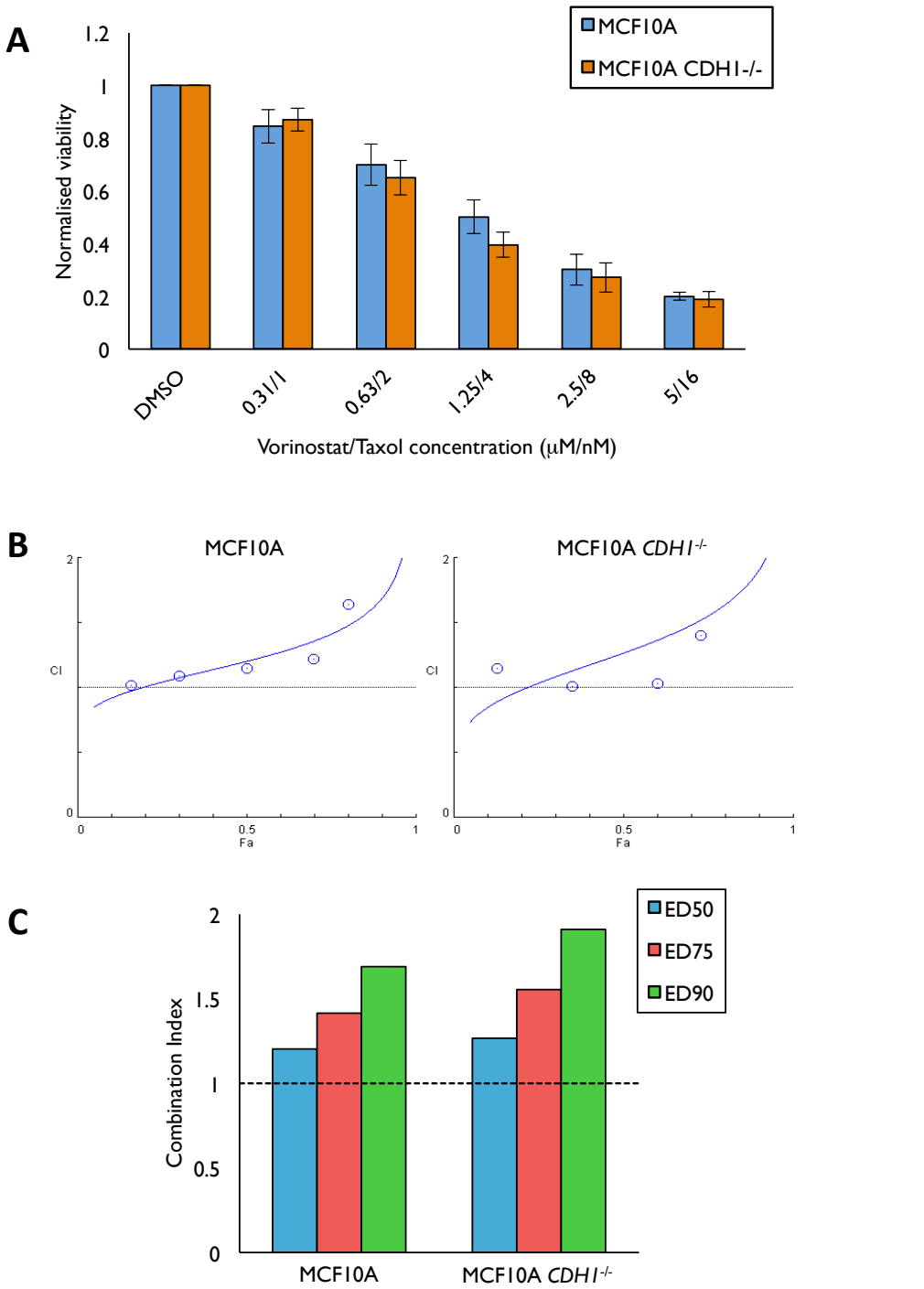

Figure 4.4 Vorinostat and taxol treatment is neither synthetic lethal nor synergistic in MCF10A *CDH1*$^{-/-}$ cells

MCF10A and MCF10A *CDH1*$^{-/-}$ cells were grown for 24 h and treated with single-agent vorinostat or taxol, or combined vorinostat and taxol for 48 h. Cell viabilities were determined using a Hoechst-stained nuclei counting assay **(A)** and used to assess drug synergy at ED50, ED75, and ED90 doses via CompuSyn software analysis **(B, C)**. Drug synergy is evaluated using a combination index (CI), whereby CI < 0.9 indicates synergy; CI = 0.9-1.1 indicates additivity; CI > 1.1 indicates antagonism. MCF10A *CDH1*$^{-/-}$ cells did not show significant increased sensitivity to vorinostat and taxol treatment when compared to MCF10A cells. Vorinostat and taxol treatment was not synergistic in both MCF10A isogenic cell lines (CI > 0.9). **(A)** represents averaged values of two biological replicates with standard error shown; a representative experiment is shown for **(B)** and **(C)**.

Table 4.2 Vorinostat and taxol combination IC_{50} values and ED50 combination indices (CI) in MCF10A and MCF10A *CDH1*$^{-/-}$ cells.

		Combination IC_{50} (vorinostat μM/taxol μM)	**ED50 CI**
Vorinostat + Taxol	MCF10A	1.31/4.20	1.20
	MCF10A *CDH1*$^{-/-}$	1.18/3.79	1.27

4.2.1.3 HDACi and the PARPi Olaparib

To investigate combined HDACi and PARPi treatment in the MCF10A isogenic pair, MCF10A and MCF10A *CDH1*$^{-/-}$ cells were grown for 24 hours then treated for an additional 48 hours with a range of either single-agent vorinostat or olaparib, or combined vorinostat and olaparib. Cell viability was then assessed using nuclei counting and potential drug synergy analysed using an isobologram analysis via CompuSyn. From the nuclei counting assay, single-agent olaparib treatment did not induce a synthetic lethal effect in the MCF10A *CDH1*$^{-/-}$ cell line (Appendix D.2). Additionally, synthetic lethality was not observed in the isogenic pair across each concentration of the vorinostat and olaparib combination (Figure 4.5A). This was supported by similar IC_{50} values for combined HDACi and PARPi treatment in the MCF10A isogenic cell lines (Table 4.3). Furthermore, combined vorinostat and olaparib treatment showed no evidence of synergy in MCF10A *CDH1*$^{-/-}$ cells, producing an ED50 combination index of 1.01 (CI > 0.9; Figure 4.5B-C; Table 4.3). The MCF10A cell line, however, showed a mild synergistic effect for this combination, with an ED50 combination index of 0.80 produced from the isobologram analysis (CI < 0.9; Figure 4.5B-C; Table 4.3). Together, these data show that combined HDACi and PARPi treatment showed no evidence of synthetic lethality or drug synergy in the MCF10A isogenic pair.

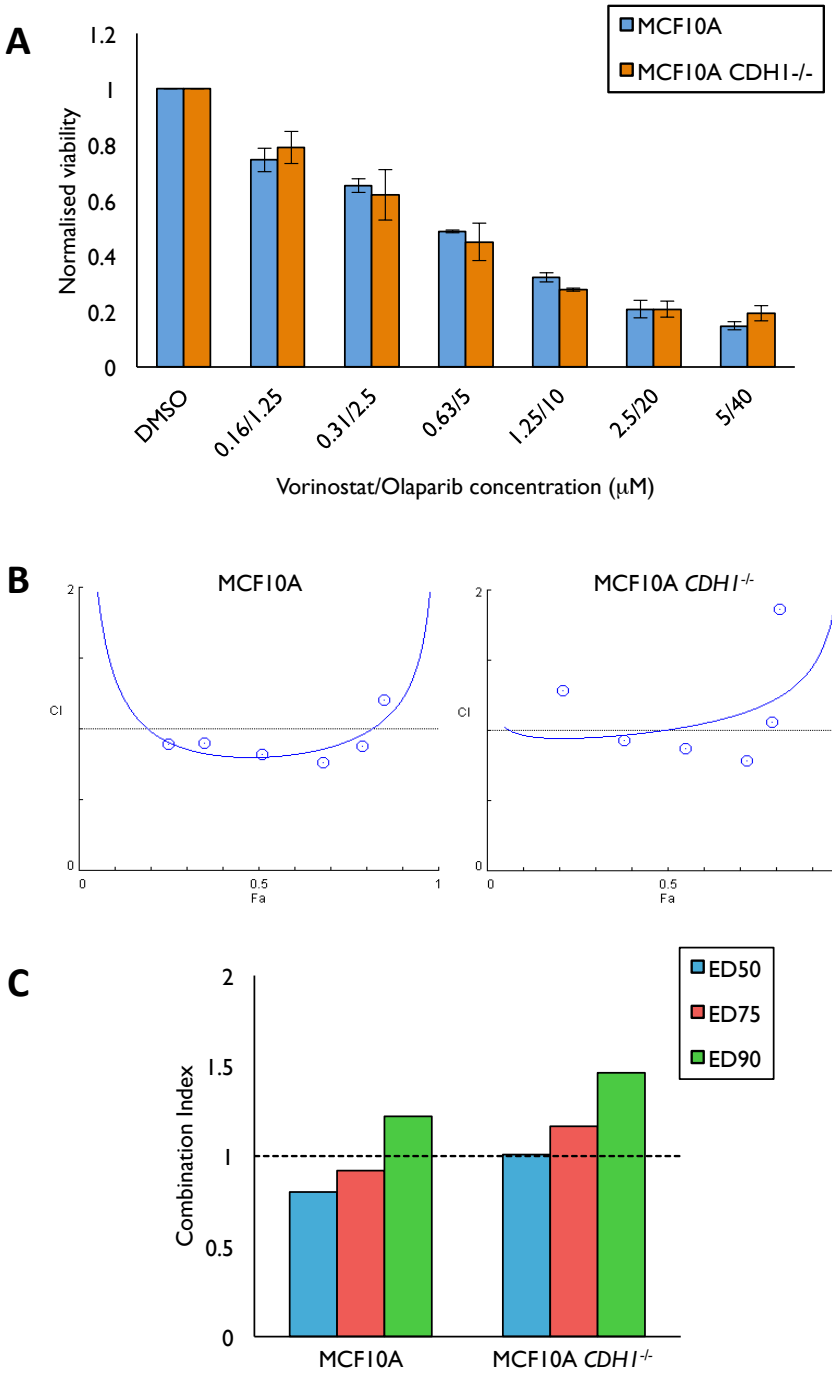

Figure 4.5 Vorinostat and olaparib treatment is neither synthetic lethal nor synergistic in MCF10A *CDH1*$^{-/-}$ cells

MCF10A and MCF10A *CDH1*$^{-/-}$ cells were grown for 24 h and treated with single-agent vorinostat or olaparib, or combined vorinostat and olaparib for 48 h. Cell viabilities were determined using a Hoechst-stained nuclei counting assay **(A)** and used to assess drug synergy at ED50, ED75, and ED90 doses via CompuSyn software analysis **(B, C)**. Drug synergy is evaluated using a combination index (CI), whereby CI < 0.9 indicates synergy; CI = 0.9-1.1 indicates additivity; CI > 1.1 indicates antagonism. MCF10A *CDH1*$^{-/-}$ cells did not show significant increased sensitivity to vorinostat and olaparib treatment when compared to MCF10A cells. Vorinostat and olaparib treatment was not synergistic in both MCF10A isogenic cell lines (CI > 0.9). **(A)** represents averaged values of two biological replicates with standard error shown; a representative experiment is shown for **(B)** and **(C)**.

Table 4.3 Vorinostat and olaparib combination IC_{50} values and ED50 combination indices (CI) in MCF10A and MCF10A *CDH1*$^{-/-}$ cells.

		Combination IC_{50} (vorinostat μM/olaparib μM)	**ED50 CI**
Vorinostat + Olaparib	MCF10A	0.59/4.69	0.80
	MCF10A *CDH1*$^{-/-}$	0.58/4.65	1.01

4.2.1.4 HDACi and the Multikinase Inhibitor Sorafenib

We next tested vorinostat in combination with the multikinase inhibitor sorafenib. Akin to previous HDACi combination testing, MCF10A and MCF10A *CDH1*$^{-/-}$ cells were grown for 24 hours and treated for an additional 48 hours with a range of single-agent vorinostat or sorafenib, or each drug in combination. Cell viability was then assessed using nuclei counting and drug synergy investigated using an isobologram analysis via CompuSyn. The nuclei counting assay showed single-agent sorafenib treatment did not induce a synthetic lethal effect in the MCF10A *CDH1*$^{-/-}$ cell line (Appendix D.3). However, modest synthetic lethality was observed in the isogenic pair following combined vorinostat and sorafenib treatment at two of the five tested drug concentrations (Figure 4.6A). This was reflected by higher IC_{50} values in MCF10A cells than MCF10A *CDH1*$^{-/-}$ cells (Table 4.4). Although slightly synthetic lethal, the vorinostat and sorafenib combination showed evidence for an antagonistic interaction in both isogenic cell lines, with the isobologram analysis producing ED50 combination indices of 2.04 and 1.56 for MCF10A and MCF10A *CDH1*$^{-/-}$ cells, respectively (CI > 1.1; Figure 4.6B-C; Table 4.4). To summarise, combined vorinostat and sorafenib treatment produced a slight synthetic lethal effect in the MCF10A pair; however, an antagonistic combination index for these drugs suggests this combination is no more effective than single-agent vorinostat treatment.

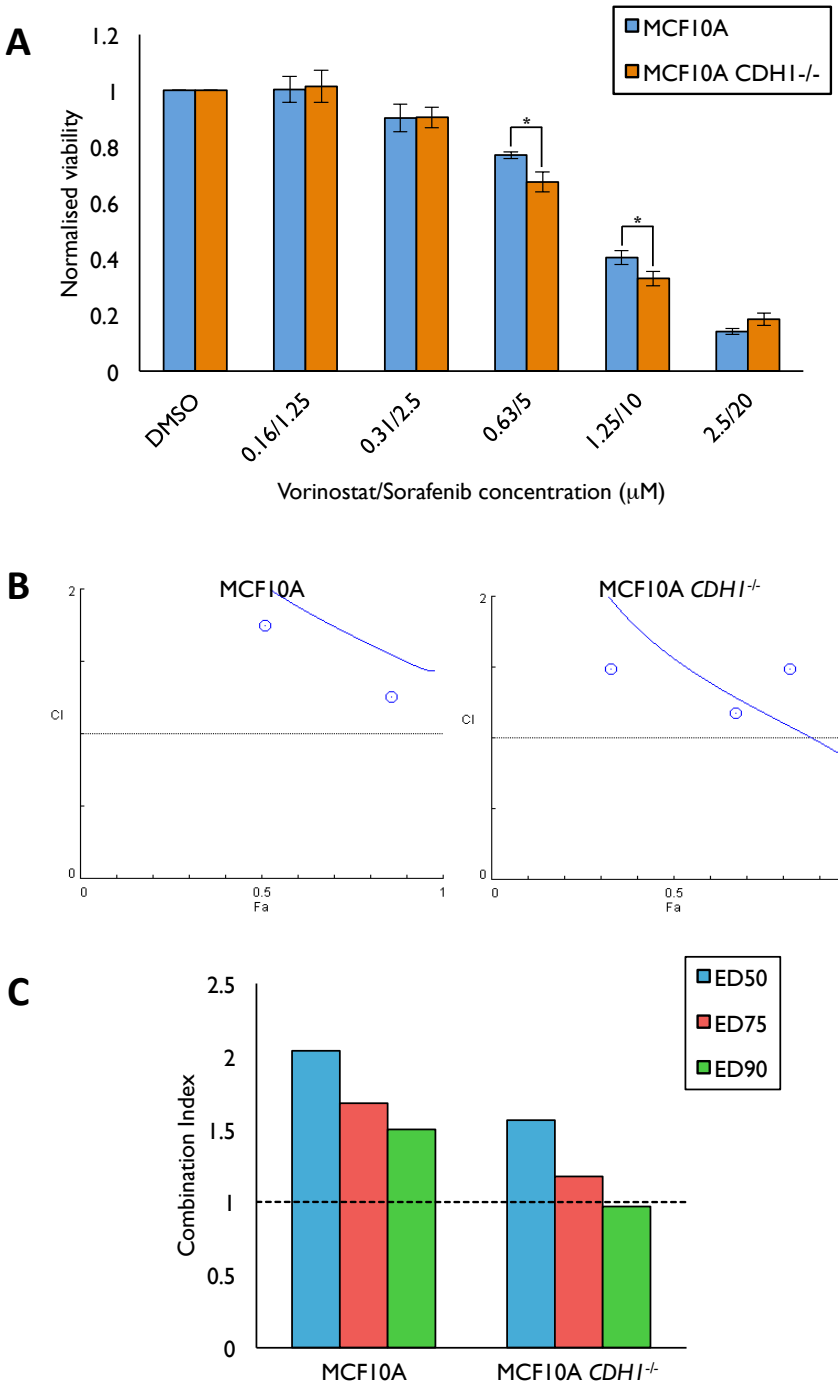

Figure 4.6 Vorinostat and sorafenib treatment is modestly synthetic lethal but not synergistic in MCF10A *CDH1*$^{-/-}$ cells

MCF10A and MCF10A *CDH1*$^{-/-}$ cells were grown for 24 h and treated with single-agent vorinostat or sorafenib, or combined vorinostat and sorafenib for 48 h. Cell viabilities were determined using a Hoechst-stained nuclei counting assay **(A)** and used to assess drug synergy at ED50, ED75, and ED90 doses via CompuSyn software analysis **(B, C)**. Drug synergy is evaluated using a combination index (CI), whereby CI < 0.9 indicates synergy; CI = 0.9-1.1 indicates additivity; CI > 1.1 indicates antagonism. MCF10A *CDH1*$^{-/-}$ cells showed modest sensitivity to vorinostat and sorafenib treatment when compared to MCF10A cells, concordant with a synthetic lethal phenotype. Vorinostat and sorafenib treatment was not synergistic in both MCF10A isogenic cell lines (CI > 0.9). **(A)** represents averaged values of two biological replicates with standard error shown; a representative experiment is shown for **(B)** and **(C)**. *P*-values calculated using Student's *t*-test; * $P < 0.05$.

Table 4.4 Vorinostat and sorafenib combination IC_{50} values and ED50 combination indices (CI) in MCF10A and MCF10A *CDH1*$^{-/-}$ cells.

		Combination IC_{50} (vorinostat μM/sorafenib μM)	**ED50 CI**
Vorinostat + Sorafenib	MCF10A	1.42/11.37	2.04
	MCF10A *CDH1*$^{-/-}$	1.07/8.54	1.56

4.2.1.5 HDACi and Phosphoinositide 3-kinase (PI3K) Inhibition

To investigate potential synergy between HDACi and PI3K signalling, we first tested the PI3K signalling cascade as a potential vulnerability in E-cadherin-deficient cells. MCF10A and MCF10A *CDH1*$^{-/-}$ cells were grown for 24 hours, then incubated for an additional 48 hours with a titration of a PI3K inhibitor; PI-103, PIK-75, HS-173, or LY294002, with cell viability assessed using nuclei counting (Figure 4.7). From the viability analysis, PIK-75, HS-173 and LY294002 treatment each showed a dose-dependent viability reduction in both MCF10A isogenic cell lines without producing a significant synthetic lethal phenotype (Figure 4.7B-D). PI-103 treatment, however, yielded a modest synthetic lethal effect in the MCF10A *CDH1*$^{-/-}$ cell line, producing IC_{50} values of 0.71 and 0.64 μM for MCF10A and MCF10A *CDH1*$^{-/-}$ cells, respectively (Figure 4.7A). PI-103 was therefore selected as the lead PI3K inhibitor for subsequent drug combination studies in the MCF10A isogenic pair.

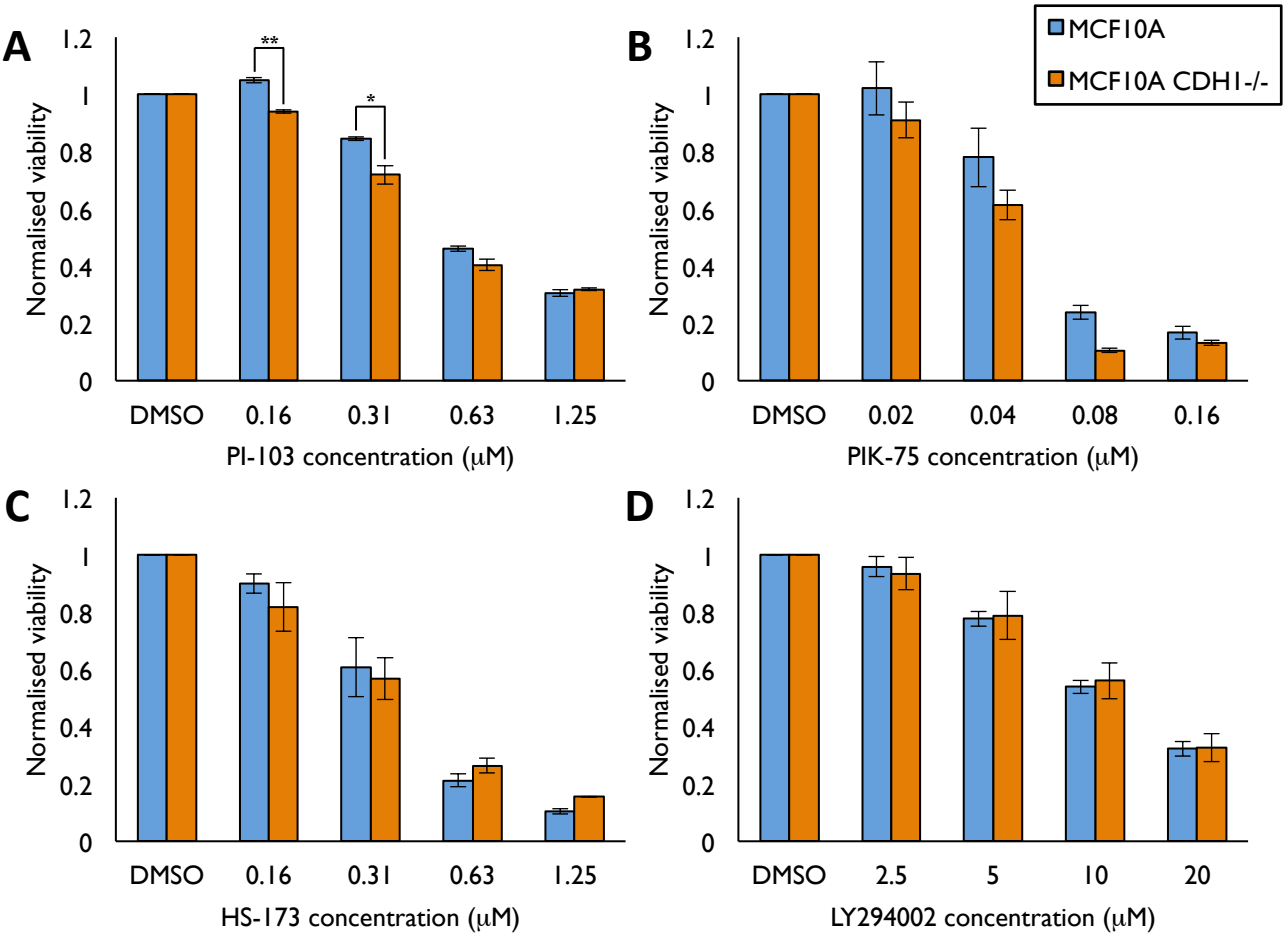

Figure 4.7 MCF10A and MCF10A *CDH1*$^{-/-}$ cell viability following PI3K inhibitor (PI3Ki) treatment

MCF10A and MCF10A *CDH1*$^{-/-}$ cells were grown for 24 h and treated with a PI3Ki over a range of concentrations; either **(A)** PI-103, **(B)** PIK-75, **(C)** HS-173, or **(D)** LY294002. At 48 h post-treatment, cell viability was assessed using a Hoechst-stained nuclei counting assay. A modest synthetic lethal phenotype was seen in MCF10A *CDH1*$^{-/-}$ cells following **(A)** PI-103 treatment. No significant difference between MCF10A and MCF10A *CDH1*$^{-/-}$ cell viability was observed following PIK-75, HS-173, or LY294002 treatment **(B-D)**. Data represents averaged values of two biological replicates with standard error shown. *P*-values calculated using Student's *t*-test; * $P < 0.05$; ** $P < 0.01$.

Next, MCF10A and MCF10A *CDH1*$^{-/-}$ cell lines were grown for 24 hours and treated with a range of concentrations of entinostat, PI-103, and a combination of entinostat and PI-103, for an additional 48 hours. Entinostat was selected as a representative HDACi due to a lack of availability of vorinostat at the time of testing. Cell viability was then assessed using nuclei counting and potential synergistic effects evaluated using an isobologram analysis via CompuSyn. This analysis showed that combined entinostat and PI-103 marginally maintained the synthetic lethal effect of each individual drug at two of the seven tested combination concentrations (Figure 4.8A). A mild synthetic lethal effect was also evident in the IC_{50} values for each isogenic cell line (Table 4.5). The isobologram analysis, however, showed an antagonistic effect for the entinostat and PI-103 combination in both isogenic cell lines, producing ED50 combination indices of 1.33 and 1.35 for MCF10A and MCF10A *CDH1*$^{-/-}$ cells, respectively (CI > 1.1; Figure 4.8B-C; Table 4.5). In summary, combined entinostat and PI-103 treatment produced a mild synthetic lethal effect in MCF10A *CDH1*$^{-/-}$ cells; however, an antagonistic combination index for these drugs suggests the combination is no more effective than single-agent entinostat treatment.

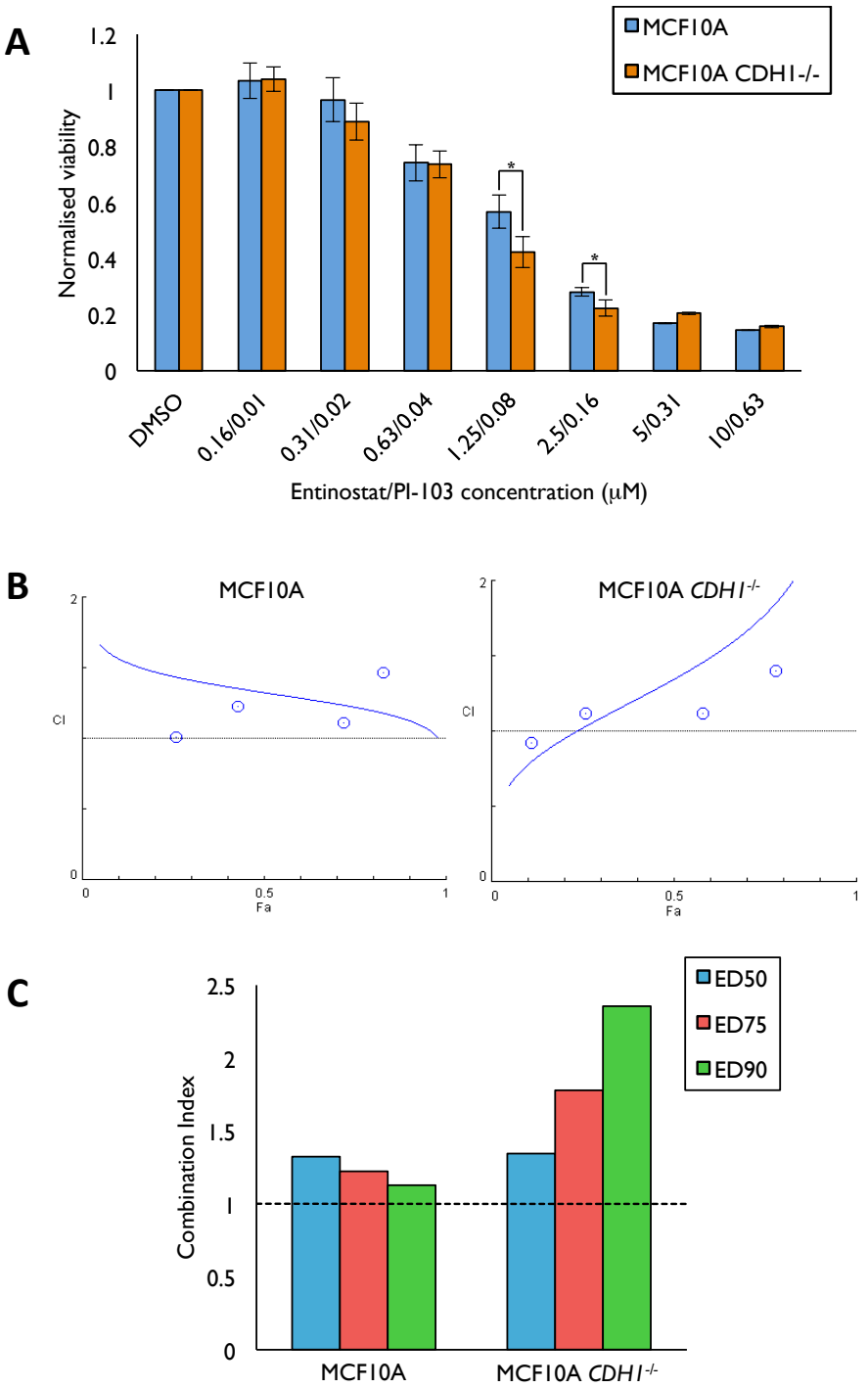

Figure 4.8 Entinostat and PI-103 treatment is modestly synthetic lethal but not synergistic in MCF10A *CDH1*$^{-/-}$ cells

MCF10A and MCF10A *CDH1*$^{-/-}$ cells were grown for 24 h and treated with single-agent PI-103 or entinostat, or combined PI-103 and entinostat for 48 h. Cell viabilities were determined using a Hoechst-stained nuclei counting assay **(A)** and used to assess drug synergy at ED50, ED75, and ED90 doses via CompuSyn software analysis **(B, C)**. Drug synergy is evaluated using a combination index (CI), whereby CI < 0.9 indicates synergy; CI = 0.9-1.1 indicates additivity; CI > 1.1 indicates antagonism. MCF10A *CDH1*$^{-/-}$ cells showed modest sensitivity to PI-103 and entinostat treatment when compared to MCF10A cells, concordant with a synthetic lethal phenotype. PI-103 and entinostat treatment was not synergistic in both MCF10A isogenic cell lines (CI > 0.9). **(A)** represents averaged values of two biological replicates with standard error shown; a representative experiment is shown for **(B)** and **(C)**. *P*-values calculated using Student's *t*-test; * $P < 0.05$.

Table 4.5 Entinostat and PI-103 combination IC_{50} values and ED50 combination indices (CI) in MCF10A and MCF10A *CDH1*$^{-/-}$ cells.

		Combination IC_{50} (entinostat μM/PI-103 μM)	**ED50 CI**
Entinostat + PI-103	MCF10A	1.62/0.10	1.33
	MCF10A *CDH1*$^{-/-}$	1.28/0.08	1.35

4.2.2 Focal Adhesion Signalling Inhibition

4.2.2.1 Saracatinib and PI-103

We next tested focal adhesion signalling inhibition for synergistic synthetic lethal effects in the isogenic MCF10A cell lines. As SRC and PI3K are both involved in the focal adhesion signalling cascade (Zhao and Guan, 2011), the SRC inhibitor saracatinib and PI3K inhibitor PI-103 were tested in combination in the MCF10A isogenic pair. Similarly to combined HDACi and PI3K inhibitor, MCF10A and MCF10A *CDH1*$^{-/-}$ cells were grown for 24 hours and treated for an additional 48 hours with either single-agent saracatinib, PI-103, or both drugs in combination. Cell viability and potential synergy were determined as before. This analysis showed that combined saracatinib and PI-103 treatment produced a marked synthetic lethal effect in the MCF10A pair across a range of concentrations (Figure 4.9A). This was reflected by higher IC_{50} values in MCF10A cells than MCF10A *CDH1*$^{-/-}$ cells (Table 4.6). The isobologram analysis, however, showed a lack of synergy for combined saracatinib and PI-103 treatment, producing ED50 combination indices of 0.98 and 1.12 in MCF10A and MCF10A *CDH1*$^{-/-}$ cell lines, respectively (CI > 0.9; Figure 4.9B-C; Table 4.6). Altogether, SRC inhibition in combination with PI3K inhibition failed to produce a synergistic drug response and did not increase the synthetic lethal phenotype produced by either drug alone in the MCF10A cell line pair.

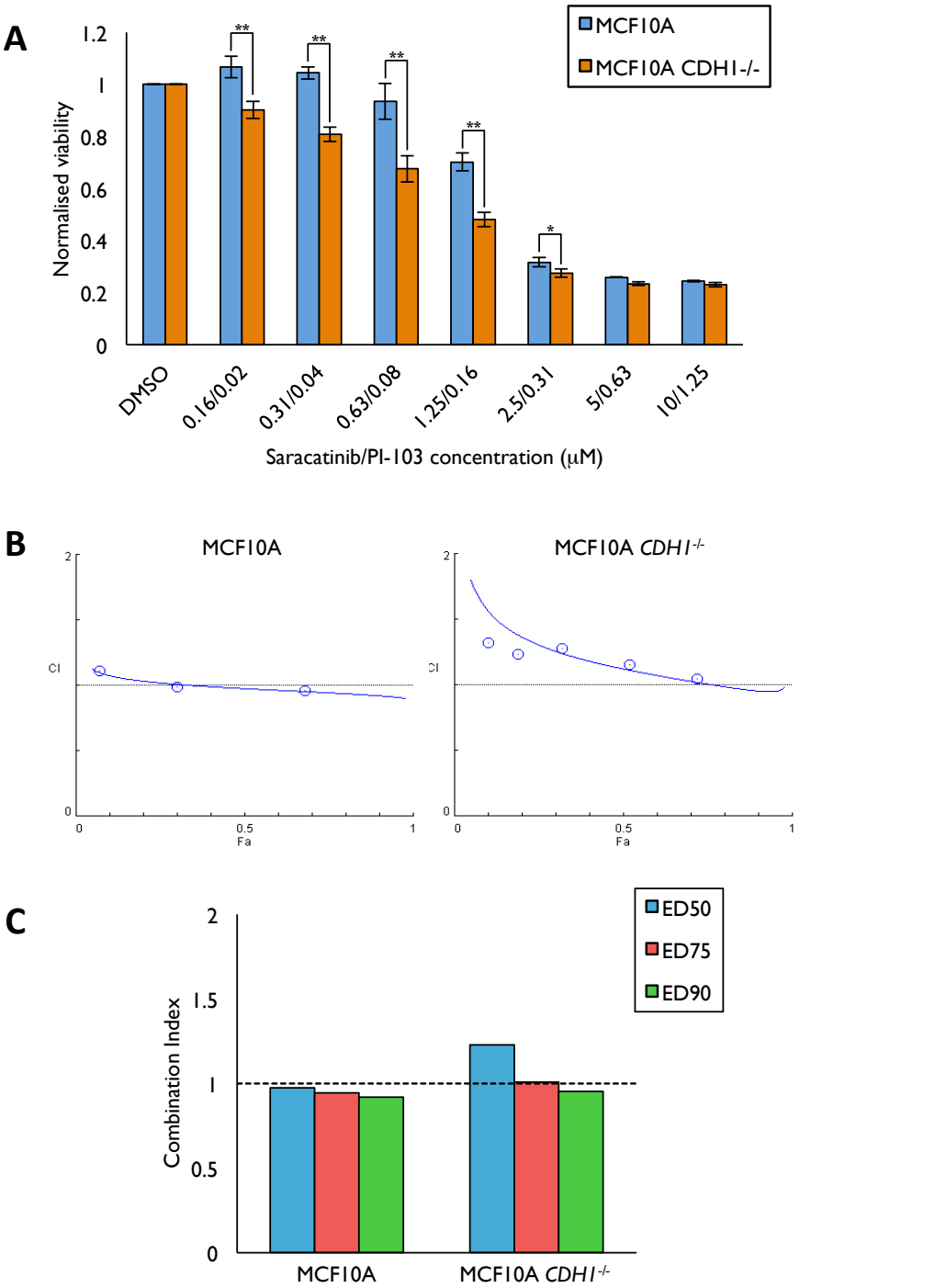

Figure 4.9 Saracatinib and PI-103 treatment is synthetic lethal but not synergistic in MCF10A *CDH1*$^{-/-}$ cells

MCF10A and MCF10A *CDH1*$^{-/-}$ cells were grown for 24 h and treated with single-agent PI-103 or saracatinib, or combined PI-103 and saracatinib for 48 h. Cell viabilities were determined using a Hoechst-stained nuclei counting assay **(A)** and used to assess drug synergy at ED50, ED75, and ED90 doses via CompuSyn software analysis **(B, C)**. Drug synergy is evaluated using a combination index (CI), whereby CI < 0.9 indicates synergy; CI = 0.9-1.1 indicates additivity; CI > 1.1 indicates antagonism. MCF10A *CDH1*$^{-/-}$ cells showed greater sensitivity to PI-103 and saracatinib treatment than MCF10A cells, concordant with a synthetic lethal phenotype. PI-103 and saracatinib treatment was not synergistic in both MCF10A isogenic cell lines (CI > 0.9). **(A)** represents averaged values of two biological replicates with standard error shown; a representative experiment is shown for **(B)** and **(C)**. *P*-values calculated using Student's *t*-test; * $P < 0.05$; ** $P < 0.01$.

Table 4.6 Saracatinib and PI-103 combination IC_{50} values and ED50 combination indices (CI) in MCF10A and MCF10A *CDH1*$^{-/-}$ cells.

		Combination IC_{50} (saracatinib μM/PI-103 μM)	**ED50 CI**
Saracatinib + PI-103	MCF10A	2.24/0.28	0.98
	MCF10A *CDH1*$^{-/-}$	1.27/0.16	1.12

4.2.2.2 Focal Adhesion Kinase Inhibitors (FAKi)

The focal adhesion kinase, FAK, is central to focal adhesion signalling and considered a potential synthetic lethal target that may be synergistic with one or more of our other synthetic lethal drugs. To test this, MCF10A and MCF10A *CDH1*$^{-/-}$ cells were first grown for 24 hours and treated with a range of FAK inhibitors (FAKi), TAE226 or PF-573228, for an additional 48 hours. Cell viability was then assessed using nuclei counting. From this analysis, the MCF10A isogenic cell lines showed a dose-dependent effect in response to FAKi treatment (Figure 4.10). However, neither TAE226 nor PF-573228 treatment induced synthetic lethal effects in the isogenic cells (Figure 4.10A-B). This was reflected by similar IC_{50} values seen in each MCF10A cell line following FAKi treatment (Table 4.7). These data therefore suggest that drug-based FAK inhibition is not a synthetic lethal vulnerability in E-cadherin-deficient MCF10A cells. For this reason, FAKi did not progress to drug combination studies in this synthetic lethal drug synergy project.

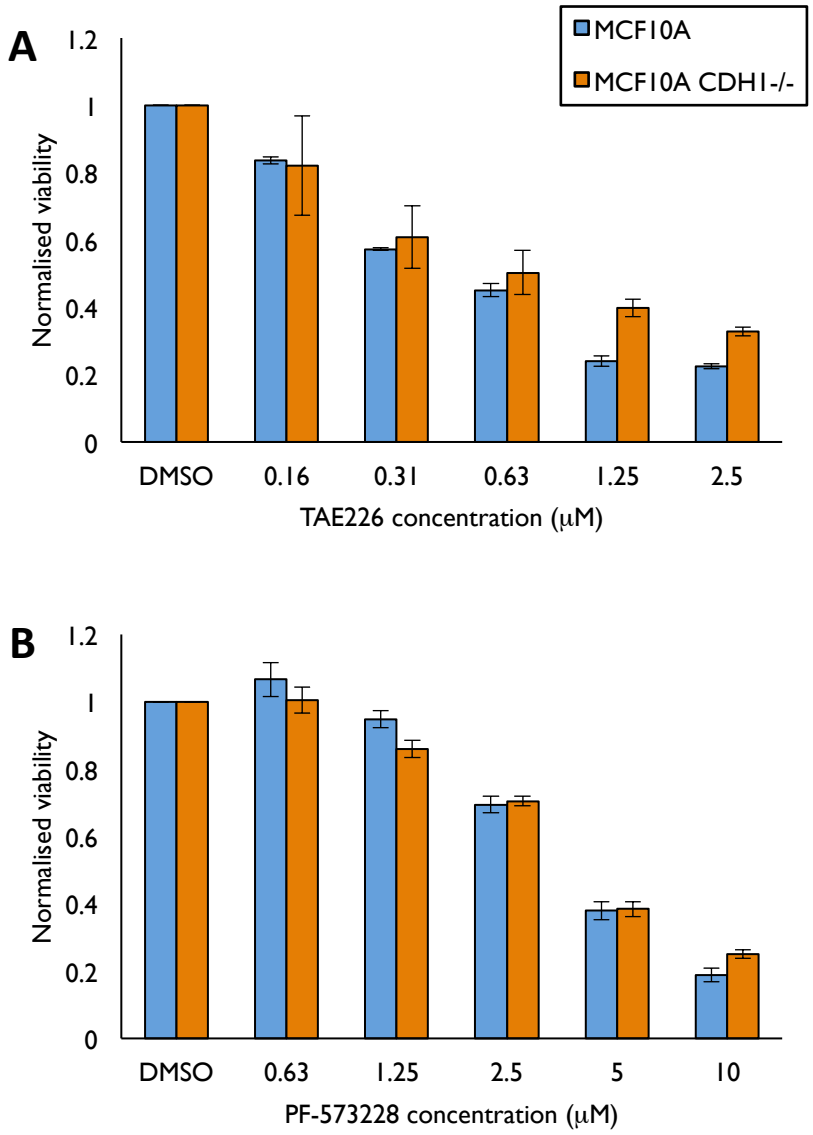

Figure 4.10 MCF10A and MCF10A *CDH1*$^{-/-}$ cell viability following focal adhesion kinase inhibitor (FAKi) treatment

MCF10A and MCF10A *CDH1*$^{-/-}$ cells were grown for 24 h and treated with a FAKi over a range of concentrations; either **(A)** TAE226 or **(B)** PF-573228. At 48 h post-treatment, cell viability was assessed using a Hoechst-stained nuclei counting assay. No marked synthetic lethal phenotype was seen in MCF10A *CDH1*$^{-/-}$ cells following treatment with either FAKi. Data represents averaged values of two biological replicates with standard error shown.

Table 4.7 FAKi (TAE226 and PF-573228) IC_{50} values in MCF10A and MCF10A *CDH1*$^{-/-}$ cells

		IC_{50} (μM)
TAE226	MCF10A	0.56
	MCF10A *CDH1*$^{-/-}$	0.78
PF-573228	MCF10A	4.39
	MCF10A *CDH1*$^{-/-}$	4.25

4.2.3 Statins

A recent report demonstrating that E-cadherin-expressing MDA-MB-231 cells possessed greater resistance to statin treatment than an E-cadherin-deficient counterpart prompted investigation of statins as potential synthetic lethal drugs in the MCF10A isogenic pair (Warita *et al*., 2014). To test this, MCF10A and MCF10A *CDH1*$^{-/-}$ cells were grown for 24 hours, followed by treatment with a concentration range of atorvastatin, lovastatin, or simvastatin over an additional 48 hours, with cell viability assessed using nuclei counting (Figure 4.11). Each tested statin produced a negligible loss of viability in MCF10A cells and a mild viability loss in MCF10A *CDH1*$^{-/-}$ cells, approximately 20% reduced viability relative to controls. This synthetic lethal effect was apparent across a wide concentration range (atorvastatin ≤ 10 μM; lovastatin ≤ 5 μM; simvastatin ≤ 5 μM), with both cell lines exhibiting reduced proliferation and a lack of synthetic lethality when concentrations exceeded this range. Following this observation, atorvastatin was selected as a representative statin for subsequent drug combination testing in the MCF10A isogenic pair.

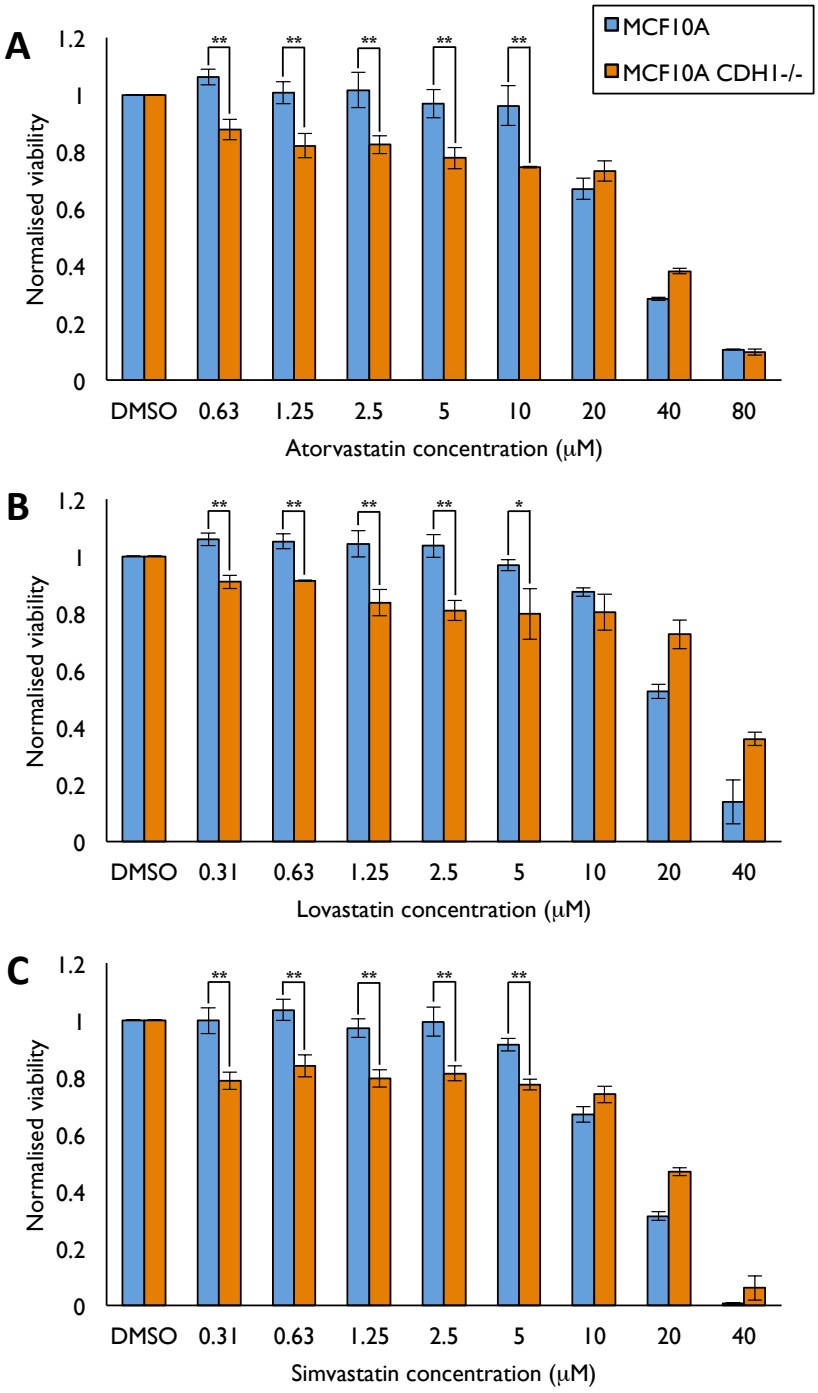

Figure 4.11 Statins induce a synthetic lethal phenotype in MCF10A *CDH1*$^{-/-}$ cells

MCF10A and MCF10A *CDH1*$^{-/-}$ cells were grown for 24 h and treated with either **(A)** atorvastatin, **(B)** lovastatin, or **(C)** simvastatin over a range of concentrations. At 48 h post-treatment, cell viability was assessed using a Hoechst-stained nuclei counting assay. MCF10A *CDH1*$^{-/-}$ cells showed greater sensitivity to statin treatment than MCF10A cells, concordant with a synthetic lethal phenotype. Data represents averaged values of two biological replicates with standard error shown. *P*-values calculated using Student's *t*-test; * $P < 0.05$; ** $P < 0.01$.

4.2.3.1 Atorvastatin and HDACi

To assess atorvastatin in combination with HDACi, MCF10A and MCF10A *CDH1*$^{-/-}$ cells were grown for 24 hours and treated with a range of concentrations of atorvastatin, HDACi (entinostat and vorinostat), and a combination of atorvastatin and HDACi. Cell viability and potential synergistic interactions were identified as before. This analysis showed that atorvastatin/entinostat and atorvastatin/vorinostat produced marked synthetic lethal effects in MCF10A *CDH1*$^{-/-}$ cells (Figure 4.12A, 4.13A). This was supported by lower IC_{50} values in combination-treated MCF10A *CDH1*$^{-/-}$ cells than MCF10A cells (Table 4.8). The isobologram analysis showed evidence for a synergistic interaction for each atorvastatin and HDACi drug combination, with ED50 combination indices below 0.9 in each MCF10A cell line (CI < 0.9; Figure 4.12B-C; Table 4.8). Interestingly, the increased toxicity and synergistic effects of each statin and HDACi combination failed to preserve the wide synthetic lethal concentration range observed following statin-only treatment (Figure 4.11). In summary, combined atorvastatin/entinostat and atorvastatin/vorinostat treatment produced synergistic synthetic lethal effects in MCF10A *CDH1*$^{-/-}$ cells, however, MCF10A cell viability was also compromised by each combination.

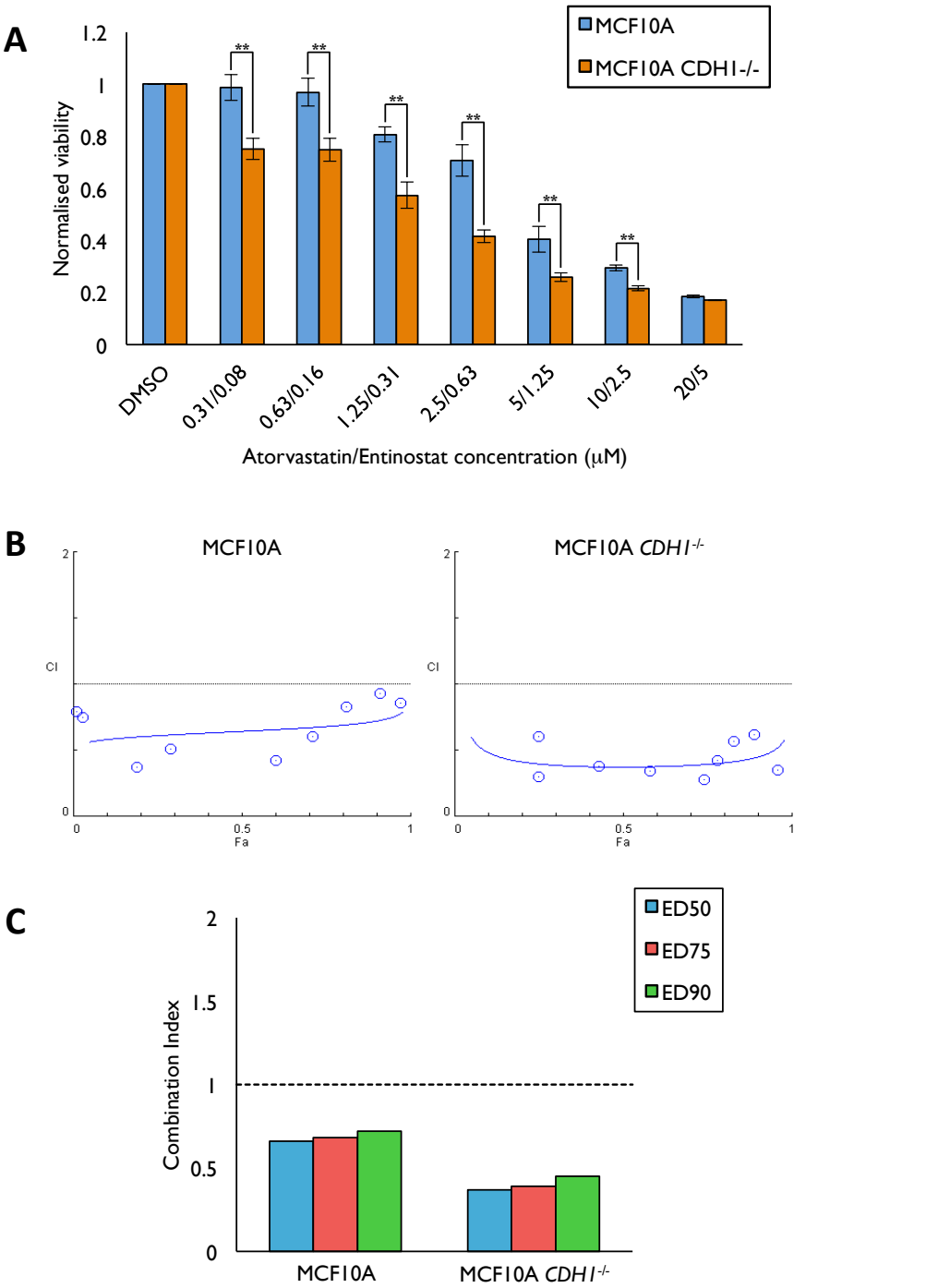

Figure 4.12 Atorvastatin and entinostat treatment is synthetic lethal and synergistic in MCF10A *CDH1*$^{-/-}$ cells

MCF10A and MCF10A *CDH1*$^{-/-}$ cells were grown for 24 h and treated with single-agent atorvastatin or entinostat, or combined atorvastatin and entinostat for 48 h. Cell viabilities were determined using a Hoechst-stained nuclei counting assay **(A)** and used to assess drug synergy at ED50, ED75, and ED90 doses via CompuSyn software analysis **(B, C)**. Drug synergy is evaluated using a combination index (CI), whereby CI < 0.9 indicates synergy; CI = 0.9-1.1 indicates additivity; CI > 1.1 indicates antagonism. MCF10A *CDH1*$^{-/-}$ cells showed greater sensitivity to atorvastatin and entinostat treatment than MCF10A cells, concordant with a synthetic lethal phenotype. Atorvastatin and entinostat treatment was synergistic in both MCF10A isogenic cell lines (CI < 0.9), with a stronger synergistic effect observed in MCF10A *CDH1*$^{-/-}$ cells. **(A)** represents averaged values of two biological replicates with standard error shown; a representative experiment is shown for **(B)** and **(C)**. *P*-values calculated using Student's *t*-test; ** $P < 0.01$.

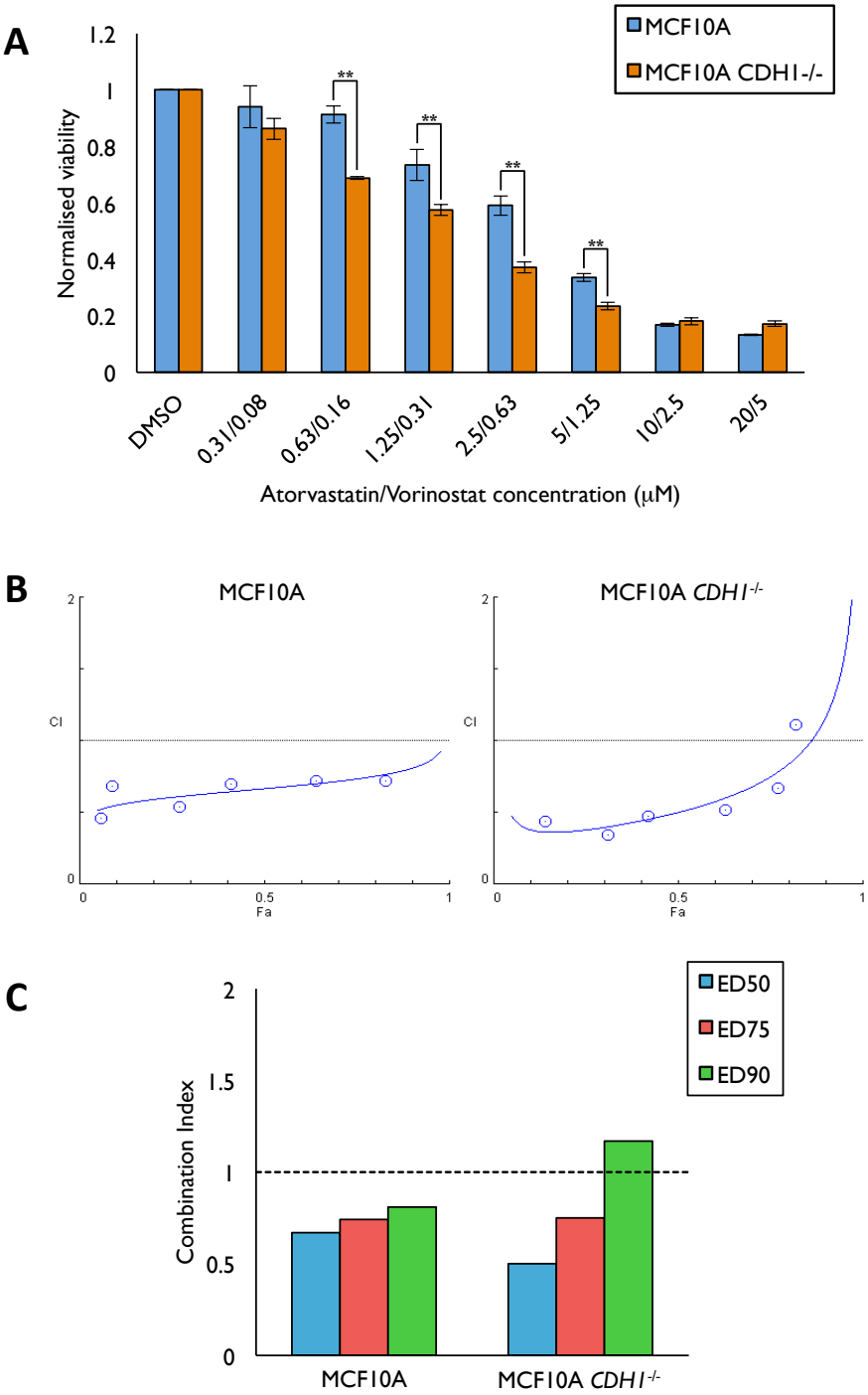

Figure 4.13 Atorvastatin and vorinostat treatment is synthetic lethal and synergistic in MCF10A *CDH1*$^{-/-}$ cells

MCF10A and MCF10A *CDH1*$^{-/-}$ cells were grown for 24 h and treated with single-agent atorvastatin or vorinostat, or combined atorvastatin and vorinostat for 48 h. Cell viabilities were determined using a Hoechst-stained nuclei counting assay **(A)** and used to assess drug synergy at ED50, ED75, and ED90 doses via CompuSyn software analysis **(B, C)**. Drug synergy is evaluated using a combination index (CI), whereby CI < 0.9 indicates synergy; CI = 0.9-1.1 indicates additivity; CI > 1.1 indicates antagonism. MCF10A *CDH1*$^{-/-}$ cells showed greater sensitivity to atorvastatin and vorinostat treatment than MCF10A cells, concordant with a synthetic lethal phenotype. Atorvastatin and vorinostat treatment was synergistic in both MCF10A isogenic cell lines (CI < 0.9), with a stronger synergistic effect observed in MCF10A *CDH1*$^{-/-}$ cells at the ED50 dose. **(A)** represents averaged values of two biological replicates with standard error shown; a representative experiment is shown for **(B)** and **(C)**. *P*-values calculated using Student's *t*-test; ** $P < 0.01$.

Table 4.8 Atorvastatin and HDACi combination IC_{50} values and ED50 combination indices (CI) in MCF10A and MCF10A *CDH1*$^{-/-}$ cells.

		Combination IC_{50} (atorvastatin μM/HDACi μM)	**ED50 CI**
Atorvastatin + Entinostat	MCF10A	5.80/1.50	0.64
	MCF10A *CDH1*$^{-/-}$	1.78/0.44	0.37
Atorvastatin + Vorinostat	MCF10A	3.09/0.77	0.67
	MCF10A *CDH1*$^{-/-}$	1.67/0.42	0.50

4.2.3.2 Atorvastatin and Saracatinib

We next tested atorvastatin in combination with saracatinib in the MCF10A isogenic pair. Similarly to statin and HDACi testing, MCF10A and MCF10A *CDH1*$^{-/-}$ cells were grown for 24 hours and treated for an additional 48 hours with a concentration range of single-agent atorvastatin, saracatinib, or both drugs in combination. Cell viability and potential drug synergy were tested as before. From the viability analysis, combined atorvastatin and saracatinib treatment produced a marked synthetic lethal effect in MCF10A *CDH1*$^{-/-}$ cells across a wide concentration range (Figure 4.14A). This was supported by lower IC_{50} values in MCF10A *CDH1*$^{-/}$ than MCF10A following combined atorvastatin/saracatinib treatment (Table 4.9). The isobologram analysis showed a synergistic interaction for combined atorvastatin and saracatinib treatment in both MCF10A isogenic cell lines, yielding ED50 combination indices of 0.73 and 0.47 in MCF10A and MCF10A *CDH1*$^{-/-}$ cell lines, respectively (CI < 0.9; Figure 4.14B-C; Table 4.9). Although synergistic, combined atorvastatin and saracatinib treatment reduced wild-type MCF10A cell viability across the synthetic lethal concentration range, and thus failed to maintain the synthetic lethal effect produced by atorvastatin treatment alone (Figure 4.11). In summary, the combination of atorvastatin and saracatinib mirrored the effects of combined statin and HDACi treatment, whereby drug toxicity was enhanced in the MCF10A and MCF10A *CDH1*$^{-/-}$ cell lines without enhancing the synthetic lethal effects produced by single-agent statin treatment.

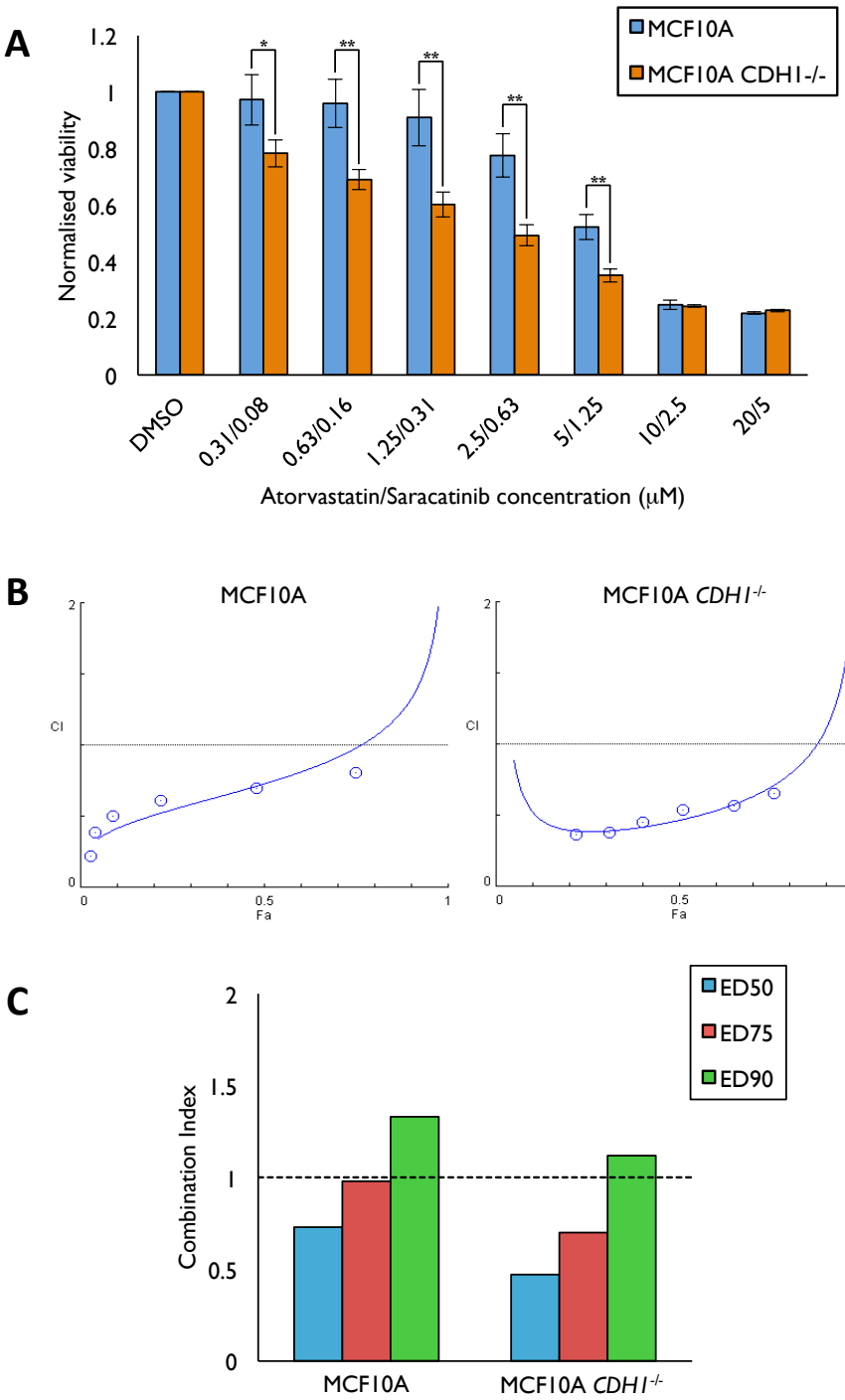

Figure 4.14 Atorvastatin and saracatinib treatment is synthetic lethal and synergistic in MCF10A *CDH1*$^{-/-}$ cells

MCF10A and MCF10A *CDH1*$^{-/-}$ cells were grown for 24 h and treated with single-agent atorvastatin or saracatinib, or combined atorvastatin and saracatinib for 48 h. Cell viabilities were determined using a Hoechst-stained nuclei counting assay **(A)** and used to assess drug synergy at ED50, ED75, and ED90 doses via CompuSyn software analysis **(B, C)**. Drug synergy is evaluated using a combination index (CI), whereby CI < 0.9 indicates synergy; CI = 0.9-1.1 indicates additivity; CI > 1.1 indicates antagonism. MCF10A *CDH1*$^{-/-}$ cells showed greater sensitivity to atorvastatin and saracatinib treatment than MCF10A cells, concordant with a synthetic lethal phenotype. Atorvastatin and saracatinib treatment was synergistic in both MCF10A isogenic cell lines (CI < 0.9), with a stronger synergistic effect observed in MCF10A *CDH1*$^{-/-}$ cells. **(A)** represents averaged values of two biological replicates with standard error shown; a representative experiment is shown for **(B)** and **(C)**. *P*-values calculated using Student's *t*-test; * $P < 0.05$; ** $P < 0.01$.

Table 4.9 Atorvastatin and saracatinib combination IC_{50} values and ED50 combination indices (CI) in MCF10A and MCF10A *CDH1*$^{-/-}$ cells

		Combination IC_{50} (atorvastatin μM/saracatinib μM)	**ED50 CI**
Atorvastatin + Saracatinib	MCF10A	5.43/1.36	0.73
	MCF10A *CDH1*$^{-/-}$	2.07/0.52	0.47

4.2.3.3 Atorvastatin and Mifepristone

In an attempt to identify other potential drugs that would be synergistic and synthetic lethal in MCF10A *CDH1*$^{-/-}$ cells, we searched our previously published drug screen data to find hits displaying a synthetic lethal effect similar to that seen with statins. Specifically, drugs that were synthetic lethal over a wide concentration range without reducing wild-type MCF10A viability. From this search, the progesterone receptor and glucocorticoid receptor antagonist mifepristone was identified and its synthetic lethal effect validated by A. Chen (Figure 4.15). This validation showed that mifepristone treatment yielded a synthetic lethal effect in the MCF10A isogenic pair over a wide concentration range, with both cell lines losing viability and the synthetic lethal effect above 10 μM treatment.

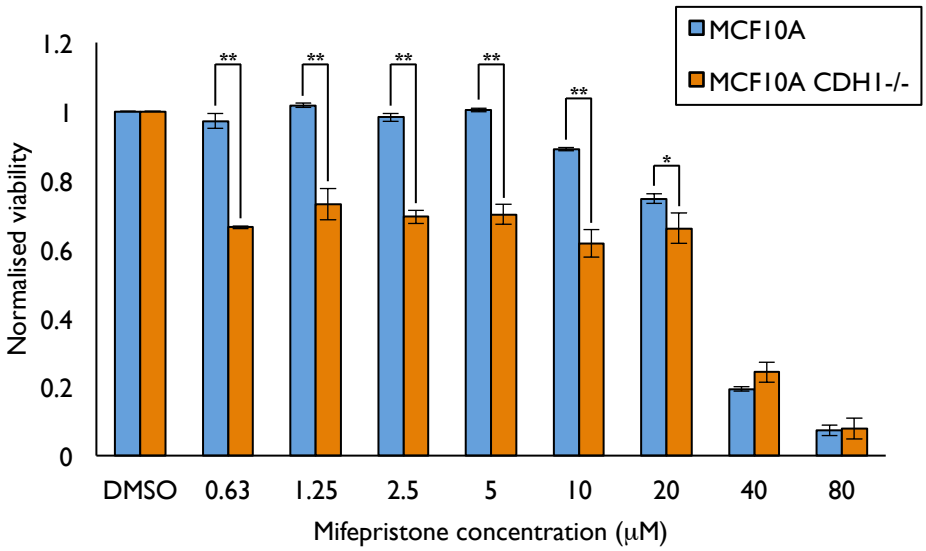

Figure 4.15 Mifepristone induces a synthetic lethal phenotype in MCF10A *CDH1*$^{-/-}$ cells

MCF10A and MCF10A *CDH1*$^{-/-}$ cells were grown for 24 h and treated with mifepristone over a range of concentrations. At 48 h post-treatment, cell viability was assessed using a Hoechst-stained nuclei counting assay. MCF10A *CDH1*$^{-/-}$ cells showed greater sensitivity to mifepristone treatment than MCF10A cells, concordant with a synthetic lethal phenotype. Data represents averaged values of two biological replicates with standard error shown and is a validation of initial work by A.Chen. *P*-values calculated using Student's *t*-test; * $P < 0.05$; ** $P < 0.01$.

To assess potential synergy between atorvastatin and mifepristone, MCF10A and MCF10A *CDH1*$^{-/-}$ cells were grown for 24 hours and treated with a concentration range of single-agent atorvastatin, mifepristone, or both drugs in combination. Following a 48 hour incubation, cellular viability was analysed using nuclei counting and drug synergy assessed using an isobologram analysis via CompuSyn. From this analysis, combined atorvastatin and mifepristone treatment produced a marked synthetic lethal effect in the MCF10A *CDH1*$^{-/-}$ cell line (Figure 4.16A). This was reflected by IC_{50} values for the combination, with MCF10A cells producing an IC_{50} over ten-fold higher than MCF10A *CDH1*$^{-/-}$ cells (Table 4.10). Additionally, combined atorvastatin/mifepristone treatment produced a synthetic lethal effect across a wide concentration range with minimal impact on MCF10A cell viability, akin to single-agent atorvastatin and mifepristone treatment. This effect was apparent up to a maximum concentration of 5/5 μM ([atorvastatin]/[mifepristone]). The isobologram analysis revealed a strong synergistic interaction for the combination in the MCF10A isogenic pair, producing ED50 combination indices of 0.49 and 0.08 in MCF10A and MCF10A *CDH1*$^{-/-}$ cells, respectively (CI < 0.9; Figure 4.16B-C; Table 4.10). Altogether, these data identified combined atorvastatin and mifepristone treatment as the strongest synthetic lethal and synergistic drug combination tested in the MCF10A and MCF10A *CDH1*$^{-/-}$ cell lines.

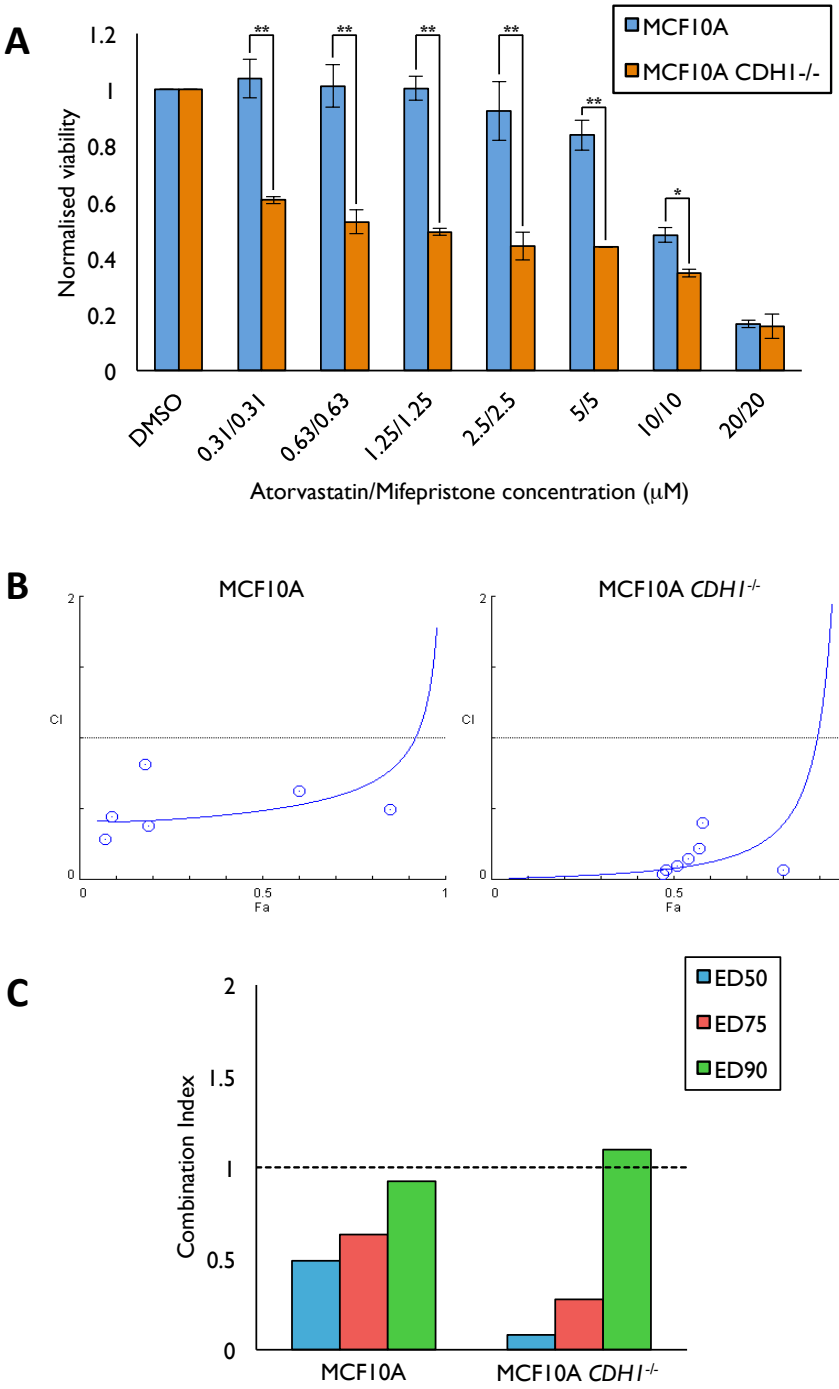

Figure 4.16 Atorvastatin and mifepristone treatment is synthetic lethal and synergistic in MCF10A *CDH1*$^{-/-}$ cells

MCF10A and MCF10A *CDH1*$^{-/-}$ cells were grown for 24 h and treated with single-agent atorvastatin or mifepristone, or combined atorvastatin and mifepristone for 48 h. Cell viabilities were determined using a Hoechst-stained nuclei counting assay **(A)** and used to assess drug synergy at ED50, ED75, and ED90 doses via CompuSyn software analysis **(B, C)**. Drug synergy is evaluated using a combination index (CI), whereby CI < 0.9 indicates synergy; CI = 0.9-1.1 indicates additivity; CI > 1.1 indicates antagonism. MCF10A *CDH1*$^{-/-}$ cells showed greater sensitivity to atorvastatin and mifepristone treatment than MCF10A cells, concordant with a synthetic lethal phenotype. Atorvastatin and mifepristone treatment was synergistic in both MCF10A isogenic cell lines (CI < 0.9), with a stronger synergistic effect observed in MCF10A *CDH1*$^{-/-}$ cells at ED50 and ED75 doses. **(A)** represents averaged values of two biological replicates with standard error shown; a representative experiment is shown for **(B)** and **(C)**. *P*-values calculated using Student's *t*-test; * $P < 0.05$; ** $P < 0.01$.

Table 4.10 Atorvastatin and mifepristone combination IC_{50} values and ED50 combination indices (CI) in MCF10A and MCF10A *CDH1*$^{-/-}$ cells

		Combination IC_{50} (atorvastatin μM/mifepristone μM)	**ED50 CI**
Atorvastatin + Mifepristone	MCF10A	6.06/6.06	0.49
	MCF10A *CDH1*$^{-/-}$	0.58/0.58	0.08

4.3 DISCUSSION

In this chapter, a range of synthetic lethal drug leads and potentially synergistic combinations were applied to MCF10A and MCF10A *CDH1*$^{-/-}$ cell lines. Interestingly, combinations involving our previously identified synthetic lethal drugs, HDACi and saracatinib, did not feature as the strongest synthetic lethal synergistic hits in this study. In addition, drug classes including FAKi and PI3K inhibitors also failed to produce marked antiproliferative effects exclusively in the E-cadherin-deficient cell line. Instead, it was found that statins, alone and in combination, were highly synthetic lethal and synergistic in this pair of isogenic MCF10A cell lines.

We hypothesise that vorinostat, a pan-HDACi, may be exerting its synthetic lethal effect through HDAC6 inhibition and subsequent microtubule stabilisation (Glozak *et al*., 2005; Zhang *et al*., 2003). Combined treatment with taxol would therefore be predicted to exacerbate this effect and enhance the synthetic lethality of vorinostat alone. Interestingly, co-treatment of vorinostat and taxol caused the reverse effect, nullifying the synthetic lethal differential provided by the HDACi (Figure 4.4).

The targeting of DNA repair mechanisms using co-treatment of vorinostat and olaparib (HDACi and PARPi) also failed to induce a synthetic lethal synergistic response in MCF10A *CDH1*$^{-/-}$ cells (Figure 4.5). The apparent lack of synergy between these inhibitors is in contrast to previously published data, although these studies were not performed using the MCF10A line (Chao and Goodman, 2014; Hegde *et al*., 2016; Konstantinopoulos *et al*., 2014; Rasmussen *et al*., 2016; Zhang *et al*., 2012). It seemed unlikely that E-cadherin loss would play a significant role in homologous DNA repair. Therefore, the observed lack of synthetic lethality is perhaps

not surprising, as functional DSB machinery would also be required for maintaining the genetic integrity of wild-type MCF10A cells.

Sorafenib treatment showed that multikinase inhibition is not an exploitable synthetic lethal approach in this study (Appendix D.3). Additionally, a synergistic response was not seen following combined sorafenib and vorinostat treatment in either MCF10A or MCF10A *CDH1*$^{-/-}$ cells (Figure 4.6). It is probable that multiple cell survival pathways are inhibited by sorafenib treatment, blunting any differential dependent on E-cadherin loss. Notably, inhibition of the MEK/ERK signalling cascade was shown to exert a growth advantage to MCF10A *CDH1*$^{-/-}$ cells over MCF10A cells (Appendix D.4), an effect we have termed 'reverse-synthetic lethality'. As the ERK pathway is a known target of sorafenib (Chen *et al*., 2014b), this may explain a lack of synthetic lethality for this combination in the MCF10A isogenic pair.

The majority of the PI3K inhibitors we tested were unsuccessful in exclusively reducing MCF10A *CDH1*$^{-/-}$ cell proliferation (Figure 4.7). Furthermore, combined PI3K inhibitor treatment with our lead synthetic lethal drugs, HDACi and saracatinib, failed to produce a synergistic response and increase the synthetic lethal viability differential provided by single-agent treatment in the MCF10A isogenic pair (Figure 4.8-9). Activating *PIK3CA* mutations are known to drive metastasis in ILBC (Christgen and Derksen, 2015; Christgen *et al*., 2013; Christgen *et al*., 2016). The MCF10A *CDH1*$^{-/-}$ cell line may thus share closer resemblance to very early stage carcinoma, prior to additional mutation events. PI3K inhibitors may therefore hold greater promise in cell lines derived from later stage carcinoma, such as the E-cadherin-deficient, ILBC-derived IPH-926 (Christgen *et al*., 2009; Christgen and Derksen, 2015).

Statin inhibition of HMGCR, the rate-limiting step of the mevalonate pathway, was synthetic lethal in the MCF10A *CDH1*$^{-/-}$ cell line (Figure 4.11) – an effect that was synergistically

enhanced following co-treatment with HDACi, saracatinib, and mifepristone (Figure 4.12-14, 4.16). The exact mechanism underpinning this synthetic lethal effect will provide strong leads in our efforts to develop more powerful synthetic lethal combinations.

E-cadherin is known to modulate lipid-associated signalling molecules such as small GTPases (Rho and Rac) and PI3K (Kovacs *et al*., 2002; Nakagawa *et al*., 2001; Pece and Gutkind, 2000; Ratheesh *et al*., 2012). Subsequently, current literature has hypothesised that alterations to the E-cadherin-localised lipid environment are likely to influence signalling of these pathways (Yap *et al*., 2015). It is therefore possible that cholesterol depletion following statin treatment may underpin the synthetic lethal phenotype in MCF10A *CDH1*$^{-/-}$ cells. Coincidentally, the statins investigated in this study (atorvastatin, simvastatin, and lovastatin) comprise three of the most lipophilic statin variants. As levels of free cholesterol have been shown to differ between lipophilic and hydrophilic statin treatment *in vivo* (Kirsch *et al*., 2003), it would be interesting to test if MCF10A *CDH1*$^{-/-}$ synthetic lethality is preserved following hydrophilic statin treatment.

Recent literature has also identified inhibition of HDACs by statins (Lin *et al*., 2008). As both class-I specific (entinostat) and pan-HDACi (vorinostat) produce a synthetic lethal effect in MCF10A *CDH1*$^{-/-}$ cells, it therefore remains possible that HDAC inhibition may account for the observed statin-mediated synthetic lethality.

Mevalonate pathway-mediated prenylation may also play a role in the observed synthetic lethality. Prenylation, both farnesylation and geranylgeranylation, are known to activate small GTPase proteins, such as Rac and Rho (Etienne-Manneville and Hall, 2002). Rac and Rho are involved in G-protein coupled receptor (GPCR) signal transduction. We have previously noted GPCR signalling as being a synthetic lethal vulnerability in MCF10A *CDH1*$^{-/-}$ cells (Telford *et al*., 2015), suggesting statin-mediated inactivation of GTPases may be active in this pathway.

Mifepristone is a known progesterone receptor (PR) and glucocorticoid receptor (GR) antagonist currently used clinically as an abortifacient agent. It is noteworthy that the MCF10A cell line is devoid of PR expression (Coppock *et al*., 2007; Moran *et al*., 2000), meaning the observed mifepristone-induced synthetic lethal effects in MCF10A *CDH1*$^{-/-}$ cells are a likely result of GR inhibition. As future work, it would be worthwhile investigating the status of PR and GR expression in the isogenic cell lines pre and post mifepristone treatment. Nuclear shuttling of the GR via a chaperone-based interaction with cytoplasmic HDACs suggests another explanation for the observed synthetic lethality in MCF10A *CDH1*$^{-/-}$ cells following both mifepristone and HDACi treatment (Kovacs *et al*., 2005).

Current literature has highlighted mifepristone's ability to inhibit the focal adhesion signalling pathway (Yu *et al*., 2015). The focal adhesion pathway defines one mechanism by which cells interact with their external environment (Miranti and Brugge, 2002). Central to this process are integrins, transmembrane cell surface receptors that bridge the external and internal cellular environments via extracellular matrix (ECM) and cytoskeleton binding, respectively (Hynes, 2002). The nodes where integrins adhere to the ECM are termed focal adhesions. Downstream of integrin receptors are tyrosine protein kinases that play a key role in conveying signals from external stimuli, with an important regulator of this process being the focal adhesion kinase, FAK (Parsons *et al*., 2008). We have previously identified compromised cell adhesion dynamics and abnormal cytoskeletal organisation following E-cadherin loss in MCF10A cells (Chen *et al*., 2014a; Telford *et al*., 2015). Additionally, a recent KEGG pathway analysis using our previously published siRNA screen data in the MCF10A isogenic pair identified focal adhesion signalling genes as highly significant synthetic lethal partners with E-cadherin (P. Guilford, unpublished data). In the current study, we have demonstrated that direct inhibition of FAK, using TAE-226 and PF-573228, failed to induce a synthetic lethal phenotype in the MCF10A *CDH1*$^{-/-}$ cell line (Figure 4.10). We therefore hypothesise that, in addition to GR

antagonism, mifepristone-mediated inhibition of the focal adhesion pathway may be occurring downstream of FAK, targeting a protein less crucial for wild-type MCF10A viability.

To the best of our knowledge, the effects of combined statin and mifepristone treatment has not been reported in the current literature. The exact mechanism explaining the observed synergy between these two drugs is therefore undefined. Studies investigating metabolites of the mevalonate pathway have identified farnesyl pyrophosphate (FPP), produced downstream of HMGCR, serves as a natural ligand for the GR capable of invoking its translocation to the nucleus (Vukelic *et al*., 2010). More recently, the FPP-GR complex has been shown to mimic the effects of GR stimulation via glucocorticoids, meaning mevalonate pathway metabolites can alter the transcriptional regulation of pathways such as interferon, insulin growth factor, and epithelial adherens junction signalling (Pastar *et al*., 2016; Stojadinovic *et al*., 2007). This interplay between the mevalonate pathway, GR, and adherens junction signalling may explain our observed synergistic effect between atorvastatin and mifepristone as well as the synthetic lethal phenotype produced by these drugs in the E-cadherin-deficient MCF10A cell line.

External to the mevalonate pathway, statin and mifepristone treatment have each been shown to alter activity of the Hippo pathway regulator Yes-associated protein, YAP (Sorrentino *et al*., 2014; Sorrentino *et al*., 2017). A screen of 640 FDA-approved drugs in a triple negative breast cancer cell line (MDA-MB-231 cells) identified statins as the lead drug class capable of preventing YAP nuclear translocation, thus activating the Hippo pathway (Sorrentino *et al*., 2014). A follow-up analysis found GR agonists such as dexamethasone and hydrocortisone were the top drug class inducing the reverse effect, deactivating the Hippo pathway by promoting YAP nuclear entry (Sorrentino *et al*., 2017). Treatment with the GR antagonist mifepristone prevented this effect (Sorrentino *et al*., 2017). As nuclear YAP is a hallmark of E-cadherin deficiency in ILBC (Vlug *et al*., 2013), we hypothesise that statin and mifepristone

induced Hippo pathway activation may also explain both the synergistic and synthetic lethal effects of these drugs in the MCF10A isogenic pair.

Regardless of the mechanism at play, we have identified a strongly synergistic and potent drug combination that may hold therapeutic utility in treating E-cadherin-deficient cancers, such as HDGC and ILBC. It would therefore be of interest to investigate if the synergistic and synthetic lethal effects of atorvastatin and mifepristone are also observed in other cell lines devoid of E-cadherin expression. If so, there is the clear opportunity to repurpose these drugs for the prevention and treatment of E-cadherin-deficient cancers.

5. ATORVASTATIN AND MIFEPRISTONE COMBINATION VALIDATION

5.1 INTRODUCTION

In the previous chapter, we discovered a novel synergistic drug combination, comprising atorvastatin and mifepristone, which exclusively reduced the viability of E-cadherin-deficient MCF10A cells (MCF10A *CDH1*$^{-/-}$) at concentrations up to 5/5 μM ([atorvastatin]/[mifepristone]). The exact mechanisms underpinning both the synergistic relationship and synthetic lethal phenotype are currently unknown. Here, we have explored the effects of combined atorvastatin and mifepristone treatment in more detail by investigating the role of key cell signalling pathways, cell cycle arrest, co-treatment with taxol, and employing additional E-cadherin-deficient cell lines.

Atorvastatin is an inhibitor of the rate-limiting enzyme of the mevalonate pathway, HMGCR. The mevalonate pathway is involved in a range of cell signalling pathways, including prenylation events, dolichol synthesis, and cholesterol production. Understanding the potential role of these pathways in our E-cadherin-negative and E-cadherin-expressing cell lines is necessary in order to define the mechanisms of synthetic lethality and synergy with mifepristone.

Downstream of HMGCR in the mevalonate signalling cascade is farnesyl diphosphate synthase (FDPS; Figure 5.1). FDPS is crucial for the conversion of isopentenyl-5-pyrophosphate (IPP) to farnesyl pyrophosphate (FPP). FPP is a metabolite central to downstream functioning of the mevalonate pathway, used to initiate each of the prenylation, dolichol, and cholesterol

production events. In addition to the mevalonate pathway, FPP has been shown to directly stimulate the glucocorticoid receptor (Das *et al*., 2007; Pastar *et al*., 2016; Vukelic *et al*., 2010), a known target inhibited by mifepristone. FDPS is inhibited by bisphosphonates, a drug class predominately used for the treatment of osteoporosis due to their ability to prevent bone mineral density loss. Bisphosphonate treatment in the MCF10A isogenic pair will show potential mevalonate pathway synthetic lethal effects in addition to statin-mediated HMGCR inhibition.

.

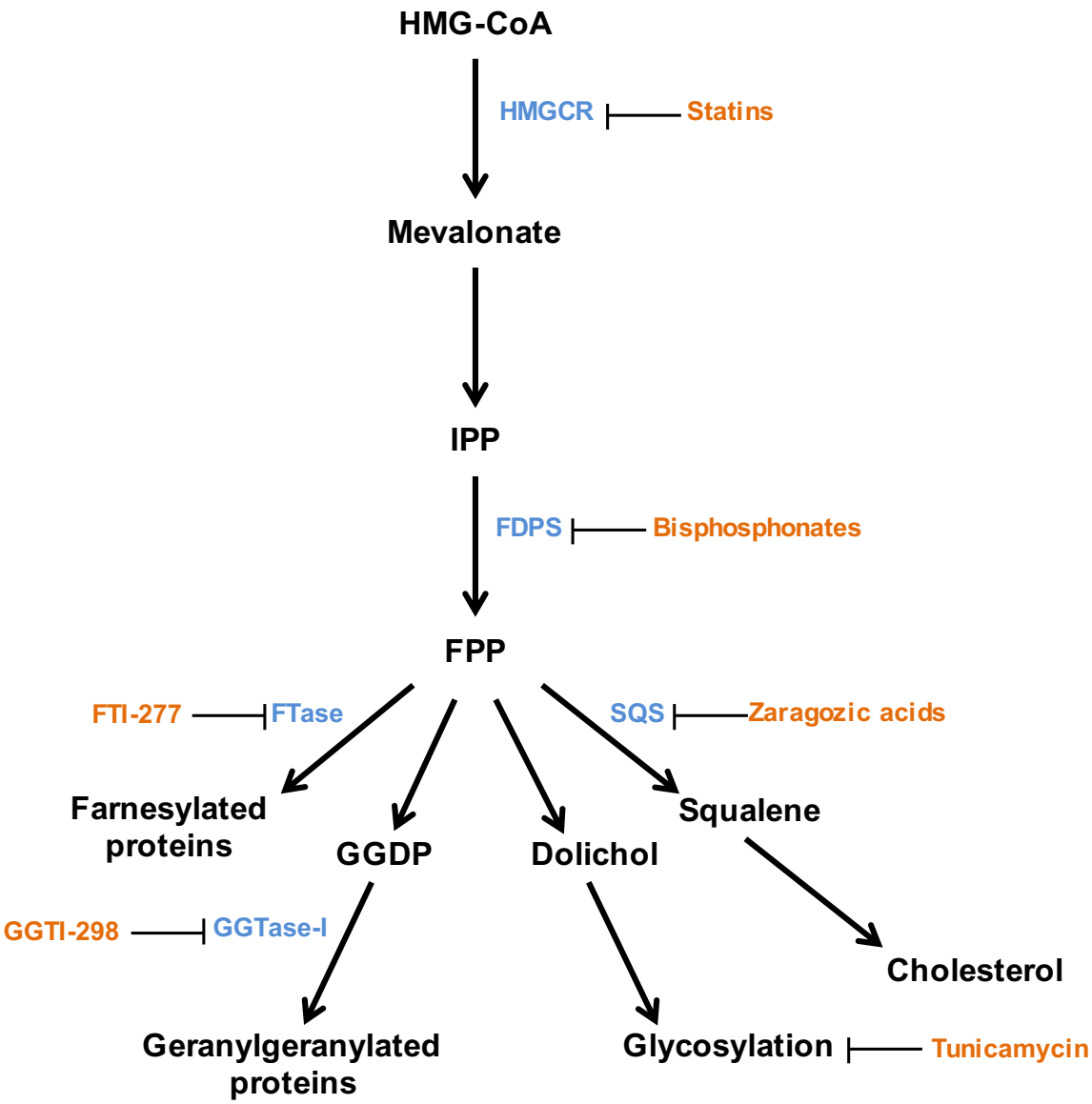

Figure 5.1 The mevalonate pathway

The mevalonate pathway showing key enzymes (blue) and inhibitors (orange). Downstream of HMG-CoA reductase (HMGCR), isopentenyl-5-pyrophosphate (IPP) is converted to farnesyl pyrophosphate (FPP) via the enzyme farnesyl diphosphate synthase (FDPS). FPP is an isoprenoid metabolite central to farnesylation, geranylgeranylation, glycosylation, and cholesterol production within the cell.

FPP is a key metabolite used for the addition of prenylation post-translational modifications, farnesylation and geranylgeranylation (Wang and Casey, 2016). Functionally, prenylation provides membrane-based anchoring for small GTPase proteins. Farnesylation is performed by farnesyltransferase (FTase), which catalyses the transfer of a 15-carbon farnesyl group from FPP to Ras GTPases (Wang and Casey, 2016). Geranylgeranylation first requires conversion of FPP to geranylgeranyl diphosphate (GGDP) via geranylgeranyl diphosphate synthase (GGDPS). GGDPS is an intermediary isoprenoid used by geranylgeranyltransferase type 1 (GGTase-I) to transfer a 20-carbon geranylgeranyl group to Rac and Rho GTPases (Etienne-Manneville and Hall, 2002; Wang and Casey, 2016). Currently, no prenylation inhibitors have successfully attained FDA-approval status, however, the FTase inhibitors lonafarnib and tipifarnib are undergoing clinical trials for treating progeria and a range of cancer subtypes, including acute myeloid leukaemia, breast cancer, chronic myelogenous leukaemia, glioblastoma, non-small cell lung cancer, and advanced metastatic urothelial carcinoma (Head and Johnston, 2004; Wang *et al*., 2017). Inhibitors specific to FTase and GGTase-I will be used to test prenylation pathway function in our MCF10A isogenic cell lines.

FPP is also implicated in the production of the polyprenol dolichol. Interestingly, dexamethasone-induced glucocorticoid receptor stimulation has been shown to increase dolichol levels *in vitro* (Dutta *et al*., 1989). Dolichol is a non-steroid isoprenoid used to form the activated monosaccharides Dol-P-Man and Dol-P-Glc, which are in turn used as substrates for glycosyltransferases. Glycosyltransferases catalyse N-glycosylation, O-mannosylation, C-mannosylation, and glycosylphosphatidylinositol posttranslational modifications (Welti, 2013). E-cadherin is a known target of N-glycosylation, a process shown to alter its adhesive capabilities at the adherens junction (Liwosz *et al*., 2006; Zhao *et al*., 2008). The biological interplay of mevalonate pathway-mediated dolichol production, E-cadherin N-glycosylation,

and glucocorticoid receptor activation highlights this branch of the mevalonate pathway as a potential vulnerability in our E-cadherin-deficient cell model.

FPP is also utilised in the production of cellular cholesterol. This process involves the NADPH-dependent condensation of two FPP molecules to form squalene, a reaction catalysed by squalene synthase (SQS), an enzyme that performs the first committed step of cholesterol synthesis (Charlton-Menys and Durrington, 2007; Do *et al*., 2009; Tansey and Shechter, 2000). Drug-based inhibition of SQS can be achieved using zaragozic acids (Bergstrom *et al*., 1993), however, these compounds are not approved for clinical use.

In addition to the mevalonate pathway, statin and mifepristone treatment have each been shown to induce Hippo pathway activation (Sorrentino *et al*., 2014; Sorrentino *et al*., 2017). When activated, the Hippo pathway effector Yes-associated protein (YAP) is phosphorylated at serine residue 127 by LATS kinases, a process that prevents YAP's nuclear entry and subsequent association with growth-promoting TEAD transcription factors (Johnson and Halder, 2014). The YAP-TEAD nuclear interaction can be inhibited with verteporfin, the only FDA-approved YAP inhibitor, currently used in photodynamic therapy for treating age-related macular degeneration (Henney, 2000; Liu-Chittenden *et al*., 2012). Verteporfin has recently shown promise as a chemotherapeutic agent, however, its use in an E-cadherin-deficient isogenic cell line system is currently unknown.

The E-cadherin-deficient triple-negative breast cancer (TNBC) cell line MDA-MB-231 has been shown to exhibit reduced viability following single-agent statin and mifepristone treatment (Brandhagen *et al*., 2013; Campbell *et al*., 2006; Shen *et al*., 2015; Warita *et al*., 2014). This effect involves both apoptotic and cell cycle arrest mechanisms, the latter occurring in response to low dose treatment (Brandhagen *et al*., 2013; Shen *et al*., 2015). To the best of our

knowledge, combined statin and mifepristone treatment has not yet been described in the literature. Similarly, the use of statins and mifepristone in ILBC cell lines has not been reported, either individually or in combination. Accordingly, in this chapter we have also determined the effect of the atorvastatin and mifepristone combination in two malignant breast cell lines.

5.2 RESULTS

5.2.1 Real-Time Proliferation Analysis

Single-agent and combined atorvastatin and mifepristone treatment showed marked synthetic lethality in MCF10A *CDH1*$^{-/-}$ cells using nuclei counting endpoint assays (Figure 4.11A, 4.15, 4.16A). We next wanted to assess each drug's performance using a real-time assay platform. MCF10A and MCF10A *CDH1*$^{-/-}$ cells were grown for 24 hours and treated with a range of single-agent atorvastatin and mifepristone concentrations, both alone and in combination. Cells were then incubated for an additional 48 hours, with cellular confluence tracked in real-time using an IncuCyte FLR. Firstly, atorvastatin-only treatment showed a modest effect on MCF10A cell proliferation, with drug- and control-treated cells attaining similar confluence readings at 48 hours (Figure 5.2A). Atorvastatin treated MCF10A *CDH1*$^{-/-}$ cells exhibited reduced proliferation over the time course of the assay and failed to achieve comparable confluence to control-treated cells (Figure 5.2B). At 48 hours, atorvastatin-treated MCF10A *CDH1*$^{-/-}$ cellular confluence was at least 18% lower than control-treated cells, consistent with previous endpoint assay testing (Figure 4.11A).

Single-agent mifepristone treatment showed a minor inhibitory effect on MCF10A cell proliferation, however, cellular confluence measurements were comparable between drug-treated and control-treated cells at the conclusion of the assay (Figure 5.2C). Mifepristone-treated MCF10A *CDH1*$^{-/-}$ cells exhibited a marked reduction in cell proliferation over the time-course of the assay, with drug-treated cells yielding confluence measurements at least 25% lower than control treatment at 48 hours (Figure 5.2D). This differential was similar to previous endpoint testing (Figure 4.15).

Similarly to single-agent treatment, combined atorvastatin and mifepristone induced minor growth inhibition in MCF10A cells (Figure 5.2E). At 48 hours, MCF10A cells treated with the highest tested drug concentration (10/10 μM) showed a 4% confluence reduction relative to control treatment. Combined atorvastatin and mifepristone treated MCF10A *CDH1*$^{-/-}$ cells showed a marked proliferation reduction over the assay time course (Figure 5.2F). A confluence differential of at least 31% was evident in drug treated MCF10A *CDH1*$^{-/-}$ cells relative to control treatment at 48 hours. Combined treatment at 10/10 μM induced a 44% confluence reduction in MCF10A *CDH1*$^{-/-}$ cells relative to control treatment at 48 hours, an inhibitory effect 11-fold higher than that seen in MCF10A cells. Overall, the real-time confluence analysis supported the synthetic lethal and synergistic phenotype seen in endpoint assays following combined atorvastatin and mifepristone treatment in the MCF10A isogenic cell lines.

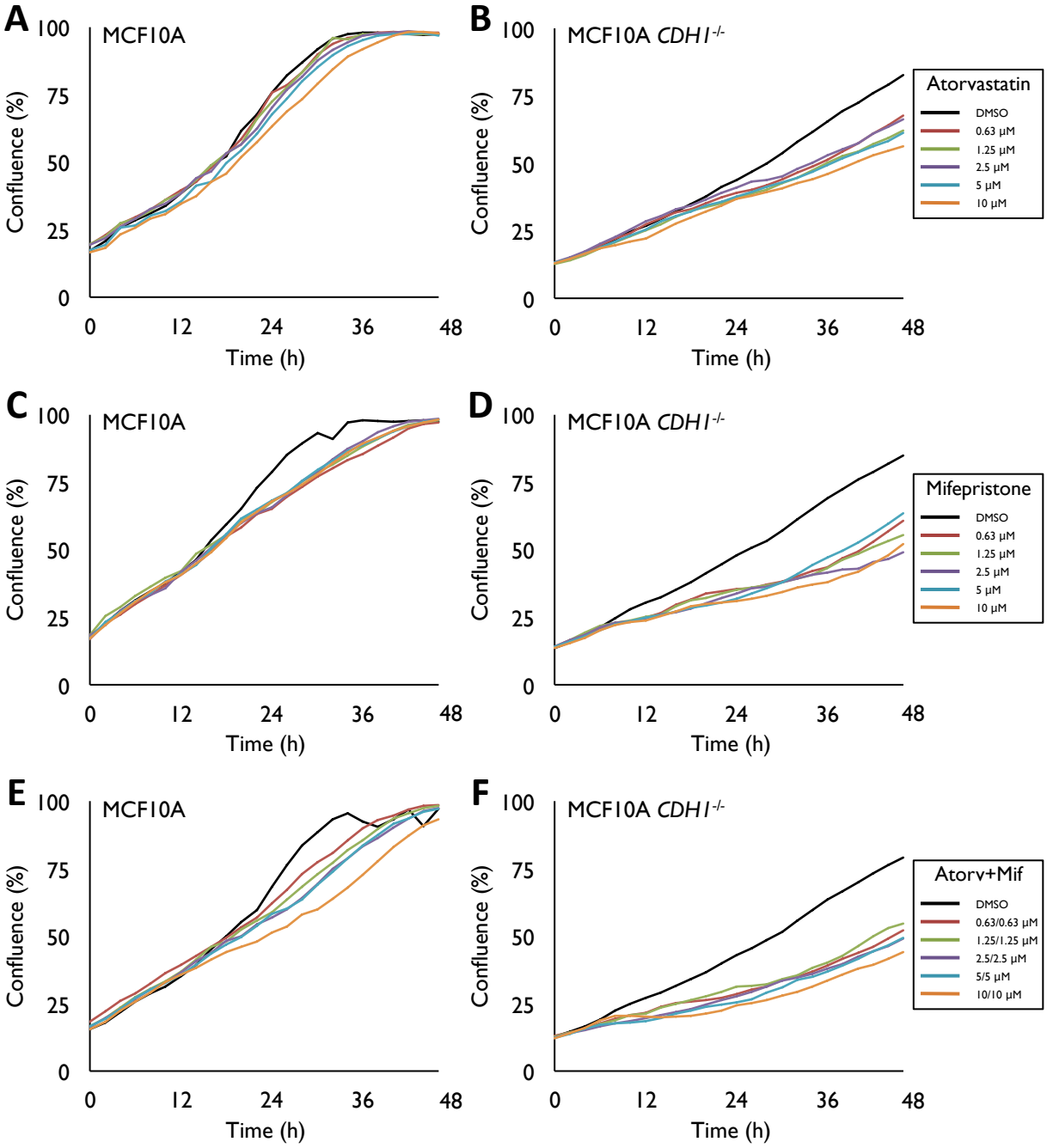

Figure 5.2 Real-time confluence assays show atorvastatin and mifepristone synthetic lethality and synergy in MCF10A *CDH1*$^{-/-}$ cells

MCF10A and MCF10A *CDH1*$^{-/-}$ cells were grown for 24 h and treated with single-agent atorvastatin **(A-B)** or mifepristone **(C-D),** or combined atorvastatin and mifepristone (Atorv+Mif; **E-F**), with cellular confluence measured over 48 h post-treatment. A representative experiment of each real-time assay is shown.

5.2.2 Cell Cycle Analysis

Statins and mifepristone have been shown to prevent cell proliferation via cytostatic mechanisms, specifically via growth arrest in the G1 phase of the cell cycle (Brandhagen *et al*., 2013; Shen *et al*., 2015). A lack of cytotoxicity was evident following single-agent and combined statin and mifepristone treatment in both endpoint and real-time viability assays, where MCF10A *CDH1*$^{-/-}$ cells exhibited reduced proliferation without a complete loss of viability (Figure 4.11A, 4.15, 4.16A, 5.2). Cell cycle analysis was therefore undertaken to characterise cytostatic effects in the drug-treated MCF10A isogenic cell lines.

MCF10A and MCF10A *CDH1*$^{-/-}$ cells were grown for 24 hours and treated with either single-agent atorvastatin and mifepristone, or both drugs in combination. Complete growth medium- and DMSO-treated cells were used as untreated and vehicle-treated controls, respectively. At 24 hours post-treatment, cells were harvested and assessed for cell cycle staging via propidium iodide nuclear staining and flow cytometry. From this analysis, MCF10A cells showed a lack of cell cycle arrest in response to atorvastatin and mifepristone treatment, either as single-agents or in combination (Figure 5.3A). This was concordant with previous endpoint and real-time assay testing. MCF10A *CDH1*$^{-/-}$ cells showed a significant G1 arrest phenotype in response to single-agent atorvastatin and mifepristone treatment across each tested concentration (2.5 and 5 μM), with 40-45% of drug treated cells in G1 compared to 33% following vehicle treatment ($P < 0.01$; Figure 5.3B). Combined atorvastatin and mifepristone treatment induced a marked G1 arrest phenotype in the MCF10A *CDH1*$^{-/-}$ cell line, with G1 arrested cells present at 54, 59, and 60% in order of increasing drug dose (0.63/0.63, 1.25/1.25, 2.5/2.5 μM; $P < 0.01$). G1 arrested MCF10A *CDH1*$^{-/-}$ cells were therefore 29% more prominent following 0.63/0.63 μM combined atorvastatin and mifepristone treatment relative to 2.5 μM single-agent treatment, supporting previous findings of a strong synergistic interaction between these two drugs. Together, these

results demonstrated that atorvastatin and mifepristone both exert a synthetic lethal phenotype in E-cadherin-deficient MCF10A (MCF10A *CDH1*$^{-/-}$) cells via a G1 arrest mechanism and that a greater cytostatic effect is produced when these drugs are treated in combination.

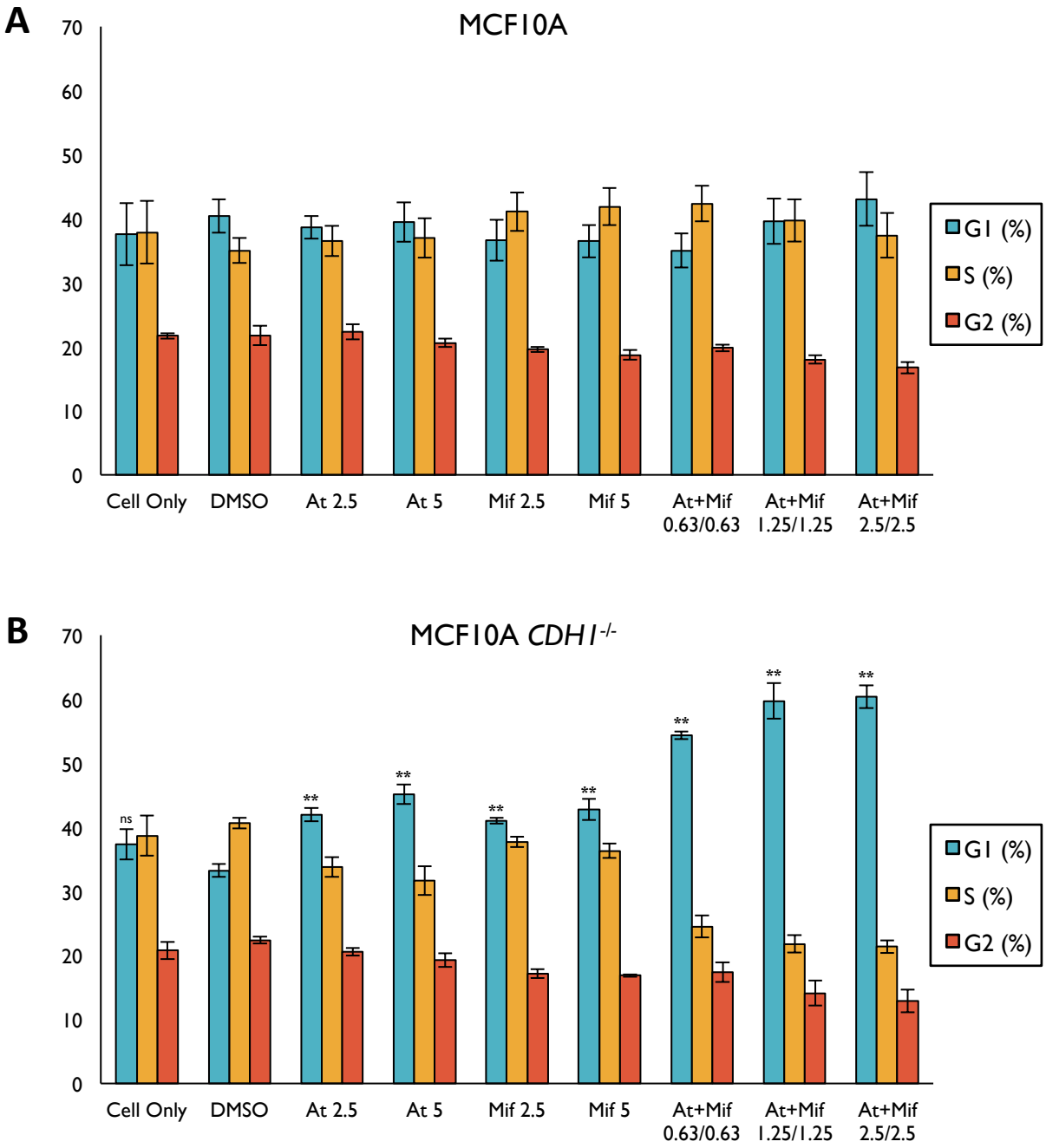

Figure 5.3 Combined atorvastatin and mifepristone treatment induces marked G1 arrest phenotype exclusively in MCF10A *CDH1*$^{-/-}$ cells

MCF10A **(A)** and MCF10A *CDH1*$^{-/-}$ **(B)** cells were grown for 24 h and treated with complete growth medium (Cell Only), vehicle (DMSO), 2.5 and 5 μM single-agent atorvastatin (At) or mifepristone (Mif), or combined atorvastatin and mifepristone (At+Mif; 0.63/0.63, 1.25/1.25, 2.5/2.5 μM) for an additional 24 h. Cells were then harvested and assessed for cell cycle staging via propidium iodide nuclear staining and flow cytometry analysis. Data represents averaged values of three biological replicates with standard error shown. *P*-values calculated using Student's *t*-test compared with vehicle treatment; ns = not significant ($P > 0.05$); ** $P < 0.01$.

5.2.3 Cell Cycle Inhibitor Treatment

Following the observation that MCF10A *CDH1*$^{-/-}$ cells undergo G1 arrest in response to atorvastatin and mifepristone treatment, we hypothesised that inhibition of G1-specific cell cycle regulation might produce a synthetic lethal response in the MCF10A isogenic pair. To test this hypothesis, MCF10A and MCF10A *CDH1*$^{-/-}$ cells were grown for 24 hours and treated with a concentration range of G1-specific cyclin-dependent kinase (CDK) inhibitors; K03861, PHA-793887, and flavopiridol. Cell viability was then assessed at 48 hours post-treatment using a nuclei counting assay. Each tested CDK inhibitor failed to induce a marked synthetic lethal phenotype in the MCF10A *CDH1*$^{-/-}$ cell line, reducing the viability of both MCF10A isogenic cell lines relatively equally (Figure 5.4A-C). A statistically significant viability difference was seen for 160 nM PHA-793887 treatment ($P < 0.01$), however, wild-type MCF10A cells presented with 47% viability and were thus heavily compromised (Figure 5.4B). Overall, these data suggest that CDK inhibition is not a synthetic lethal approach in MCF10A *CDH1*$^{-/-}$ cells.

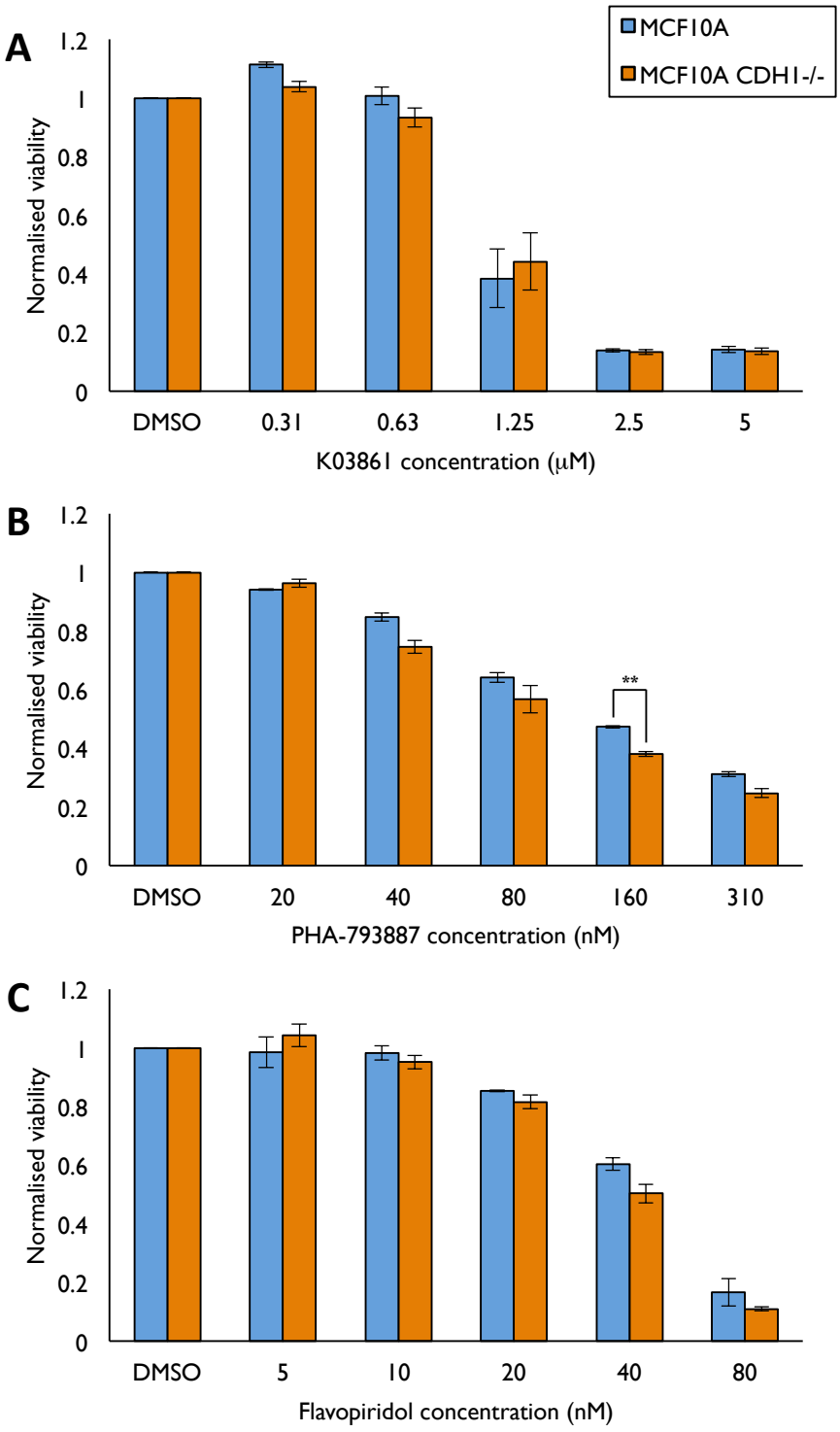

Figure 5.4 MCF10A and MCF10A *CDH1*$^{-/-}$ cell viability following cyclin-dependent kinase (CDK) inhibitor treatment

MCF10A and MCF10A *CDH1*$^{-/-}$ cells were grown for 24 h and treated with either K03861 **(A)**, PHA-793887 **(B)**, or flavopiridol **(C)** over a range of concentrations. At 48 h post-treatment, cell viability was assessed using a Hoechst-stained nuclei counting assay. Data represents averaged values of two biological replicates with standard error shown. *P*-values calculated using Student's *t*-test; ** $P < 0.01$.

5.2.4 Combining Lead Combination with Cytotoxic Agent

As atorvastatin and mifepristone treatment enhanced G1 arrest when co-treated in MCF10A *CDH1*$^{-/-}$ cells, we next hypothesised that the increased proportion of growth-arrested cells may be primed for apoptosis and that use of a cytotoxic agent could push these cells to death. Taxol was selected as the cytotoxic agent as previous testing had shown its ability to induce cell death in the MCF10A isogenic pair (Appendix D.1). The MCF10A isogenic cell lines were grown for 24 hours and incubated for an additional 48 hours with either taxol, combined atorvastatin and mifepristone, or all three drugs (taxol, atorvastatin, and mifepristone) in combination, with cell viability assessed using nuclei counting. An isobologram analysis was then performed using CompuSyn to assess the impact of taxol in the three-part combination. The endpoint viability assay showed that the addition of taxol did not amplify the synthetic lethal differential of combined atorvastatin and mifepristone treatment (Figure 5.5A). This was supported by the isobologram analysis, which showed a lack of synergy for the three-part combination in both MCF10A and MCF10A *CDH1*$^{-/-}$ cell lines (CI > 0.9; Figure 5.5B-C). Interestingly, a strong antagonistic effect was observed for the three-part combination at the calculated ED75 and ED90 doses in MCF10A *CDH1*$^{-/-}$ cells (CI = 2.98 and 4.99, respectively), indicating taxol inclusion impeded the performance of combined atorvastatin and mifepristone treatment (Figure 5.5C). To summarise, atorvastatin and mifepristone treated MCF10A *CDH1*$^{-/-}$ cells did not exhibit increased sensitivity to taxol treatment.

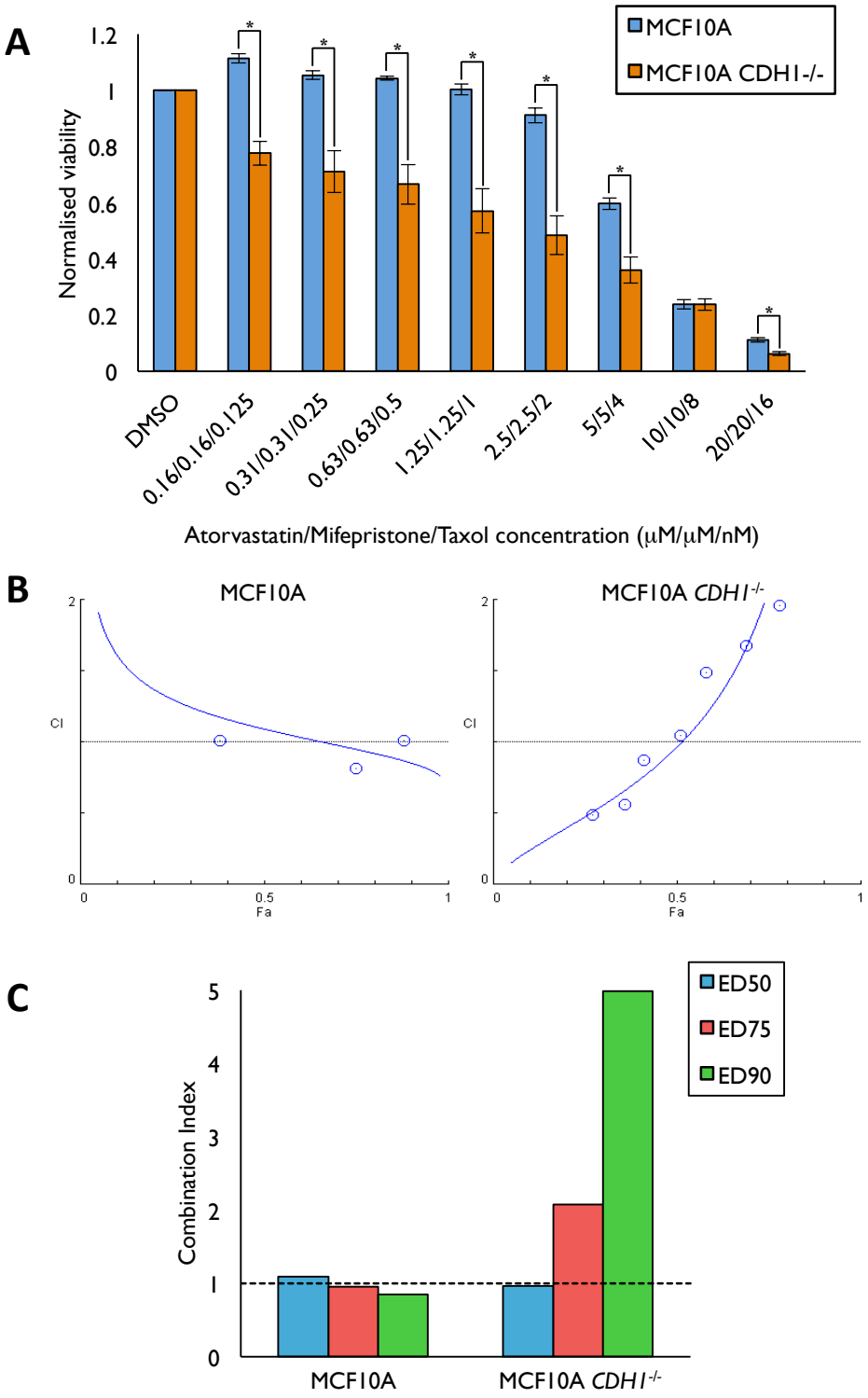

Figure 5.5 Taxol co-treatment does not enhance atorvastatin and mifepristone induced synthetic lethality in MCF10A *CDH1*$^{-/-}$ cells

MCF10A and MCF10A *CDH1*$^{-/-}$ cells were grown for 24 h and treated with single-agent taxol, combined atorvastatin and mifepristone, or all three drugs in combination for 48 h. Cell viabilities were determined using a Hoechst-stained nuclei counting assay **(A)** and used to assess drug synergy at ED50, ED75, and ED90 doses via CompuSyn software analysis **(B, C)**. Drug synergy is evaluated using a combination index (CI), whereby CI < 0.9 indicates synergy; CI = 0.9-1.1 indicates additivity; CI > 1.1 indicates antagonism. Combined atorvastatin and mifepristone and taxol treatment was not synergistic in either MCF10A cell line (CI < 0.9). **(A)** represents averaged values of two biological replicates with standard error shown; a representative experiment is shown for **(B)** and **(C)**. *P*-values calculated using Student's *t*-test; * $P < 0.05$.

5.2.5 Validation in E-cadherin-Deficient Malignant Cell Lines

As the MCF10A and MCF10A *CDH1*$^{-/-}$ cell lines are non-malignant, we wished to determine whether the synergistic effects of atorvastatin and mifepristone would remain in E-cadherin-negative malignant cell lines. The ILBC-derived IPH-926 cell line was kindly provided by Matthias Christgen (Hannover, Germany). IPH-926 cells were derived from a patient with metastatic ILBC and are characteristically similar to the disease (Christgen *et al*., 2009). These features include E-cadherin loss (due to a homozygous *CDH1* frameshift mutation), anti-cancer drug resistance, and a markedly slow proliferation rate *in vitro* and *in vivo* (Christgen *et al*., 2009; Mathieu *et al*., 2004). IPH-926 cells were grown for 24 hours and treated with a range of single-agent atorvastatin and mifepristone concentrations and both drugs in combination. Cell viability was determined at 96 hours post-treatment using a nuclei counting assay. IPH-926 cell viability was analysed over 96 hours post-treatment as drug-induced cytostatic effects were less evident in the slow-growing cell line over 48 hours (Appendix D.5). An isobologram analysis was then performed using CompuSyn to test for potential synergy between atorvastatin and mifepristone in this cell line. Additionally, combined atorvastatin and mifepristone-treated IPH-926 cells were tracked in the IncuCyte to determine if the combination was capable of reducing cell confluence over time. The endpoint assay showed a dose-dependent cell viability reduction in IPH-926 cells following atorvastatin and mifepristone treatment, whether given alone or in combination (Figure 5.6A-C). The highest tested combination concentration, 40/40 μM, induced a 40% viability loss relative to control treatment (Figure 5.6C), whilst 40 μM single-agent atorvastatin and mifepristone treatment provided a 26 and 37% viability reduction, respectively (Figure 5.6A-B). Furthermore, a dose-dependent inhibitory effect for combined atorvastatin and mifepristone treatment was seen in IPH-926 cells in the real-time assay (Figure 5.6D). At 96 hours post-treatment, the real-time assay showed 2.5/2.5, 10/10, and 40/40 μM combined atorvastatin and mifepristone treatment exerted 3, 28, and 45% lower confluence values than

vehicle treatment, respectively (Figure 5.6D). The isobologram analysis provided an ED50 combination index of 0.69, indicating a synergistic interaction for combined atorvastatin and mifepristone treatment in IPH-926 cells (CI < 0.9; Figure 5.6E-F). Together, these results show that atorvastatin and mifepristone treatment induced a dose-dependent viability loss in the E-cadherin-negative IPH-926 ILBC-derived cell line. The effect of the two drugs was synergistic, supporting our previous findings in MCF10A *CDH1*$^{-/-}$ cells.

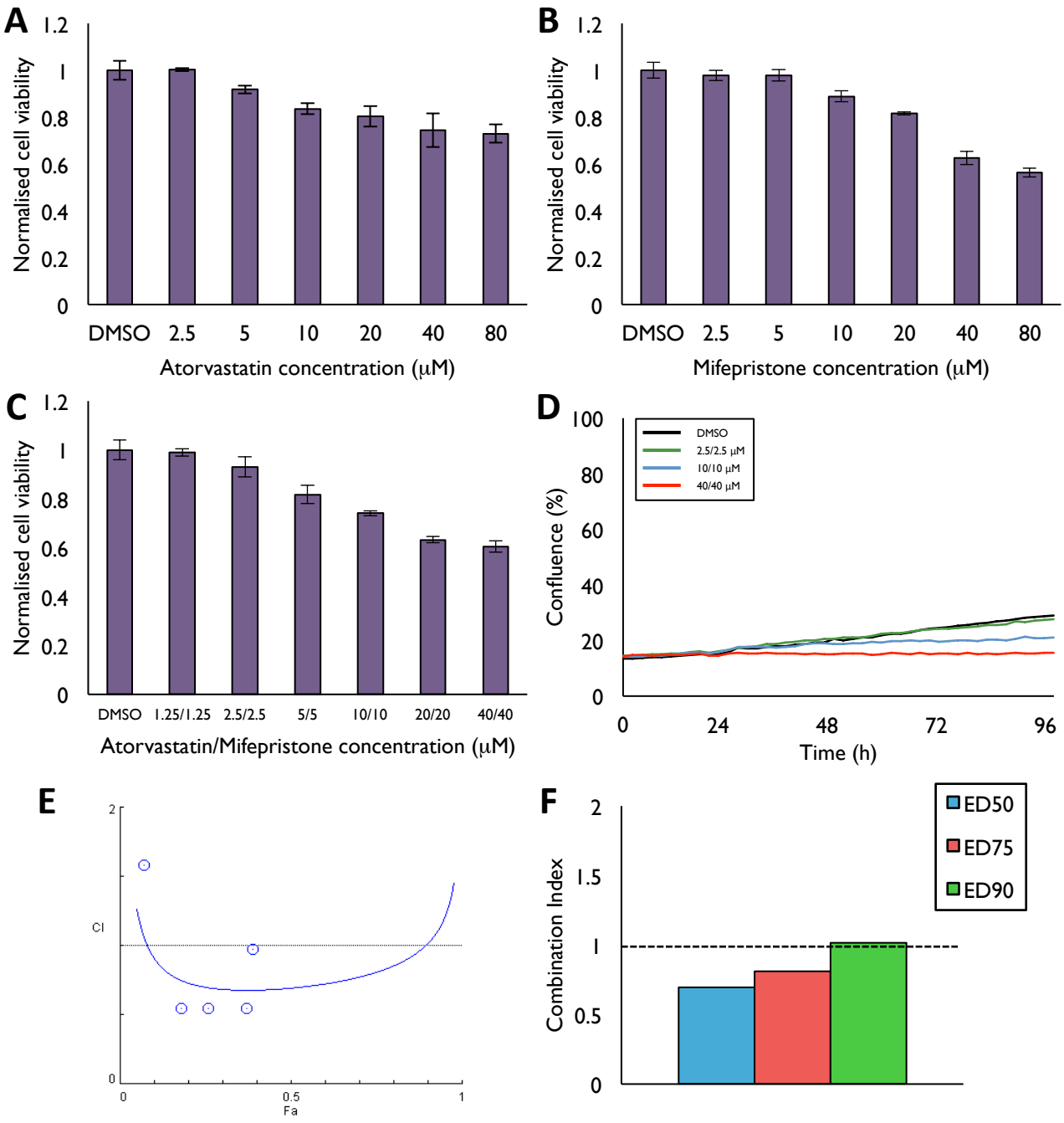

Figure 5.6 IPH-926 cell viability following atorvastatin and mifepristone treatment

IPH-926 cells were grown for 24 h and treated with with single-agent atorvastatin **(A)** or mifepristone **(B)**, or combined atorvastatin and mifepristone (**C**-**D**) for 96 h. Cell viabilities were determined using a Hoechst-stained nuclei counting assay (**A**-**C**) and real-time confluence assay **(D)**. Drug synergy was assessed at ED50, ED75, and ED90 doses via CompuSyn software analysis (**E**-**F**). Drug synergy is evaluated using a combination index (CI), whereby CI < 0.9 indicates synergy; CI = 0.9-1.1 indicates additivity; CI > 1.1 indicates antagonism. Atorvastatin and mifepristone treatment showed a synergistic interaction in IPH-926 cells at ED50 and ED75 doses (CI < 0.9). A representative experiment of each endpoint and real-time assay is shown, with standard deviation shown in (**A**-**C**).

Next we tested the atorvastatin and mifepristone combination in the MDA-MB-231 cell line. The MDA-MB-231 cell line is a triple-negative breast cancer (TNBC) cell line derived from a pleural effusion that lacks E-cadherin expression due to hypermethylation of the *CDH1* promoter (Cailleau *et al*., 1974). MDA-MB-231 cells have a reported faster doubling time than IPH-926 cells (Cailleau *et al*., 1974; Christgen *et al*., 2009; Christgen and Derksen, 2015). Akin to MCF10A testing, MDA-MB-231 cells were grown for 24 hours and treated with a range of single-agent atorvastatin and mifepristone concentrations and both drugs in combination. Cellular confluence was measured in real-time over 48 hours using the IncuCyte FLR, followed by a nuclei counting viability assay. The isobologram analysis was then performed using CompuSyn to assess potential synergy of combined atorvastatin and mifepristone treatment in this cell line. The nuclei counting assay showed a dose-dependent effect on MDA-MB-231 viability following both single-agent and combined atorvastatin and mifepristone treatment (Figure 5.7A-C). Single-agent treatment produced IC_{50} values of 3.86 and 65 μM for atorvastatin and mifepristone, respectively; combined atorvastatin and mifepristone treatment produced an IC_{50} of 2.25/2.25 μM ([atorvastatin]/[mifepristone]). The isobologram analysis reported an ED50 combination index of 0.61, supporting a synergistic interaction for the combination in MDA-MB-231 cells (CI < 0.9; Figure 5.7E-F). Additionally, a dose-dependent inhibitory effect was observed for combined atorvastatin and mifepristone treatment over the time-course of the real-time confluence assay (Figure 5.7D). At 48 hours post-treatment, the real-time assay showed 0.31/0.31, 1.25/1.25, and 5/5 μM treatment produced 6, 42, and 75% lower confluence values than vehicle-treatment (Figure 5.7D). In summary, these findings showed combined atorvastatin and mifepristone treatment maintained a synergistic effect in the E-cadherin-deficient TNBC-derived MDA-MB-231 cell line.

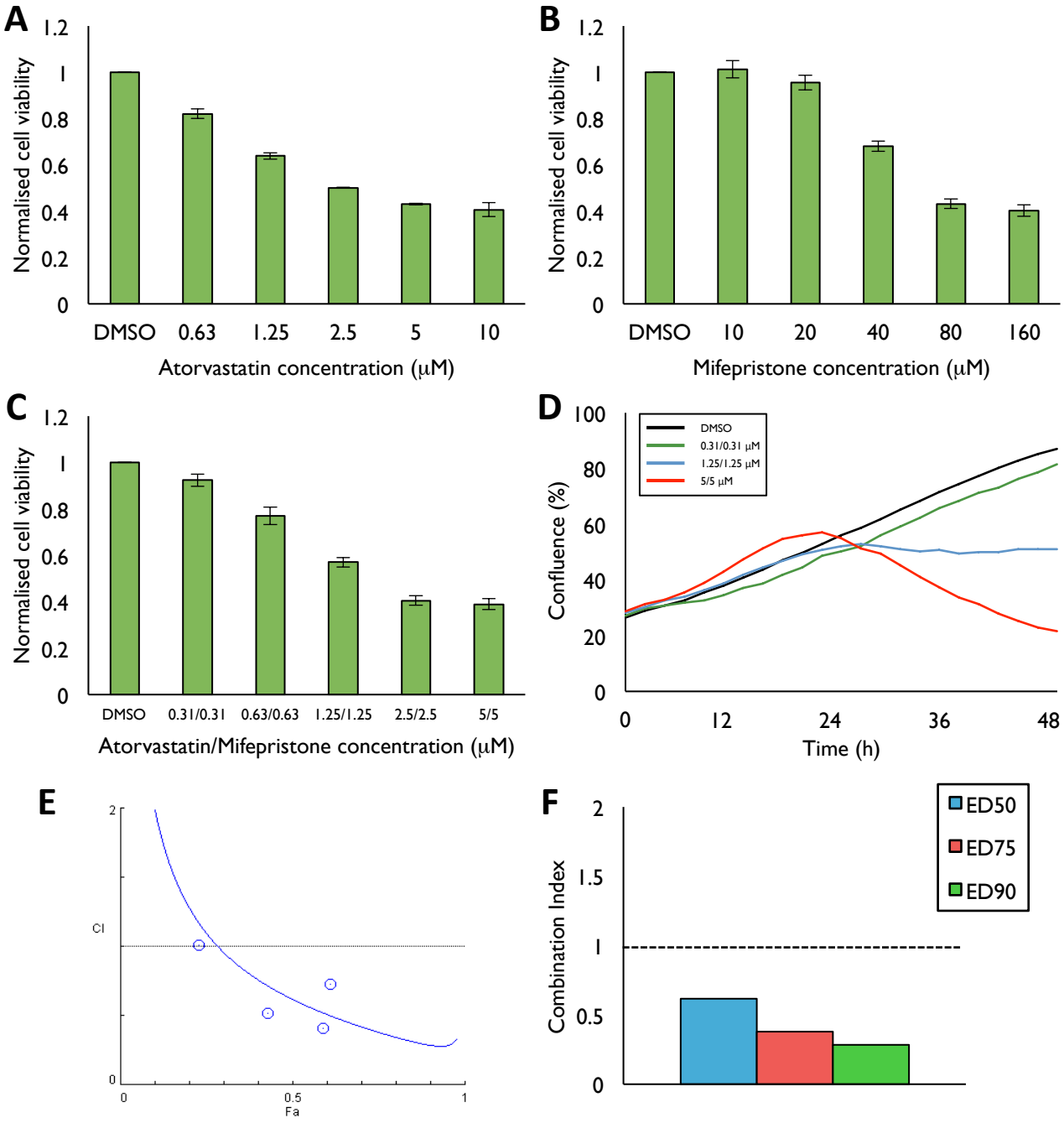

Figure 5.7 MDA-MB-231 cell viability following atorvastatin and mifepristone treatment

MDA-MB-231 cells were grown for 24 h and treated with with single-agent atorvastatin **(A)** or mifepristone **(B)**, or combined atorvastatin and mifepristone **(C-D)** for 48 h. Cell viabilities were determined using a Hoechst-stained nuclei counting assay **(A-C)** and real-time confluence assay **(D)**. Drug synergy was assessed at ED50, ED75, and ED90 doses via CompuSyn software analysis (E-F). Drug synergy is evaluated using a combination index (CI), whereby CI < 0.9 indicates synergy; CI = 0.9-1.1 indicates additivity; CI > 1.1 indicates antagonism. Atorvastatin and mifepristone treatment showed a synergistic interaction in MDA-MB-231 cells (CI < 0.9). Data represents averaged values of two biological replicates with standard error shown.

5.2.6 MDA-MB-231 Cell Cycle Analysis

The MDA-MB-231 cell line was next analysed for the effect of atorvastatin and mifepristone on cell cycle arrest. The MDA-MB-231 cell line was selected over IPH-926 cells due to their inherent faster doubling time that enabled cytostatic analysis at 24 hours post treatment. MDA-MB-231 cells were grown for 24 hours and treated with either single-agent atorvastatin and mifepristone, or both drugs in combination. Complete growth medium- and DMSO-treated cells were used as untreated and vehicle-treated controls, respectively. 24 hours post-treatment, cells were harvested and assessed for cell cycle staging via propidium iodide staining and flow cytometry. From this analysis, MDA-MB-231 cells showed a lack of cell cycle arrest in response to mifepristone treatment (Figure 5.8). A marked cytostatic effect was seen following 2.5 and 5 μM atorvastatin treatment, with G1-arrested cells 72 and 71% more abundant than vehicle-treated cells, respectively ($P < 0.01$; Figure 5.8). Combined atorvastatin and mifepristone treatment also produced a prominent G1-arrested phenotype in the MDA-MB-231 cell line, however, this effect was not greater than atorvastatin-only treatment. Combined atorvastatin and mifepristone treatment induced G1-arrested cell populations 31, 60, and 63% greater than vehicle treatment at concentrations of 0.63/0.63, 1.25/1.25, 2.5/2.5 μM, respectively ($P < 0.05$; Figure 5.8). To summarise, the cell cycle analysis showed combined atorvastatin and mifepristone treatment induced a G1-arrest effect in MDA-MB-231 cells, concordant with previous MCF10A *CDH1*$^{-/-}$ testing. However, combination treatment did not enhance the G1 arrest phenotype produced by atorvastatin-only treatment in MDA-MB-231 cells

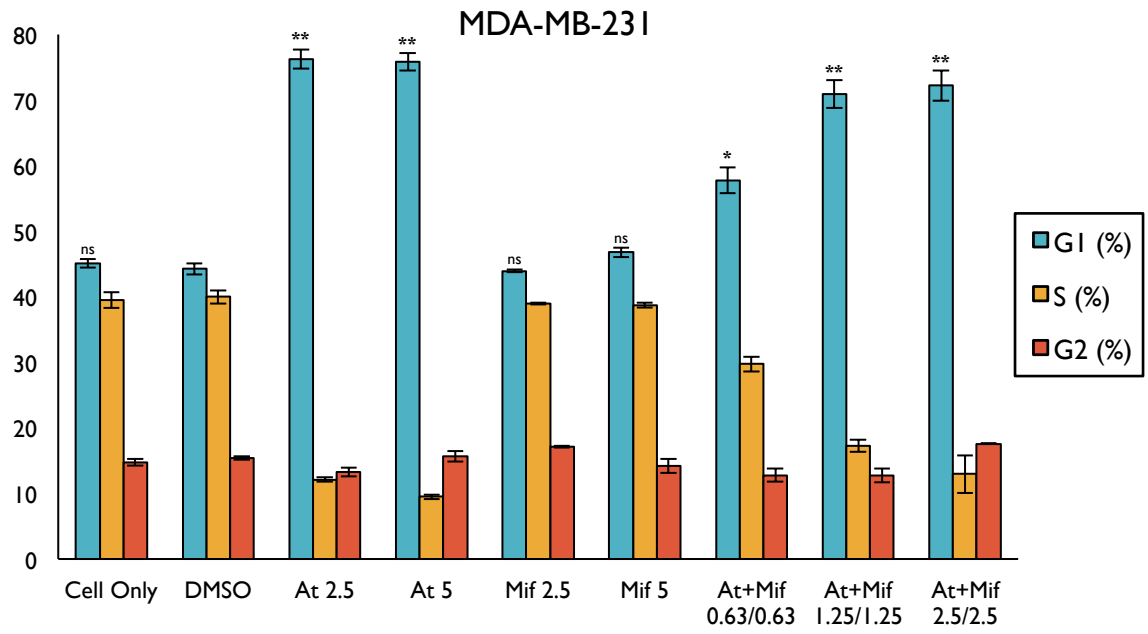

Figure 5.8 MDA-MB-231 cell cycle analysis following atorvastatin and mifepristone treatment

MDA-MB-231 cells were grown for 24 h and treated with complete growth medium (cell only), vehicle (DMSO), 2.5 and 5 μM single-agent atorvastatin (At) or mifepristone (Mif), or combined atorvastatin and mifepristone (At+Mif; 0.63/0.63, 1.25/1.25, 2.5/2.5 μM) for an additional 24 h. Cells were then harvested and assessed for cell cycle staging via propidium iodide nuclear staining and flow cytometry analysis. Data represents averaged values of two biological replicates with standard error shown. *P*-values calculated using Student's *t*-test compared with vehicle treatment; ns = not significant ($P > 0.05$); * $P < 0.05$; ** $P < 0.01$.

5.2.7 Targeting the Mevalonate Pathway

We next aimed to investigate the mevalonate pathway's role in inducing synthetic lethality in E-cadherin-deficient MCF10A cells. Inhibitors for various proteins downstream of HMGCR were therefore tested in the MCF10A isogenic pair. Zoledronic acid, FTI-277, GGTI-298, tunicamycin, and zaragozic acid were used to inhibit FDPS, FTase, GGTase-I, N-glycosylation, and SQS, respectively (Figure 5.1). Following a 24 hour incubation, MCF10A and MCF10A *CDH1*$^{-/-}$ cells were incubated with a range of concentrations of each mevalonate pathway inhibitor for an additional 48 hours, followed by cell viability assessment using nuclei counting. Interestingly, a similar cell viability reduction was seen in both MCF10A cell lines following zoledronic acid, FTI-277, GGTI-298, and tunicamycin treatment (Figure 5.9A-D). A minor synthetic lethal effect was seen in MCF10A *CDH1*$^{-/-}$ cells in response to zaragozic acid treatment, however, this was only achieved at high concentrations when the drug was also highly toxic to the MCF10A cells (Figure 5.9E). The lack of a marked synthetic lethal phenotype from these tested inhibitors suggests the mevalonate pathway may not be a targetable vulnerability in MCF10A *CDH1*$^{-/-}$ cells and that statin-mediated synthetic lethality may be attributed to pleiotropic effects external to HMGCR inhibition. Additionally, the synergistic effects of atorvastatin and mifepristone co-treatment may not be due to interaction of the mevalonate metabolite FPP with the glucocorticoid receptor.

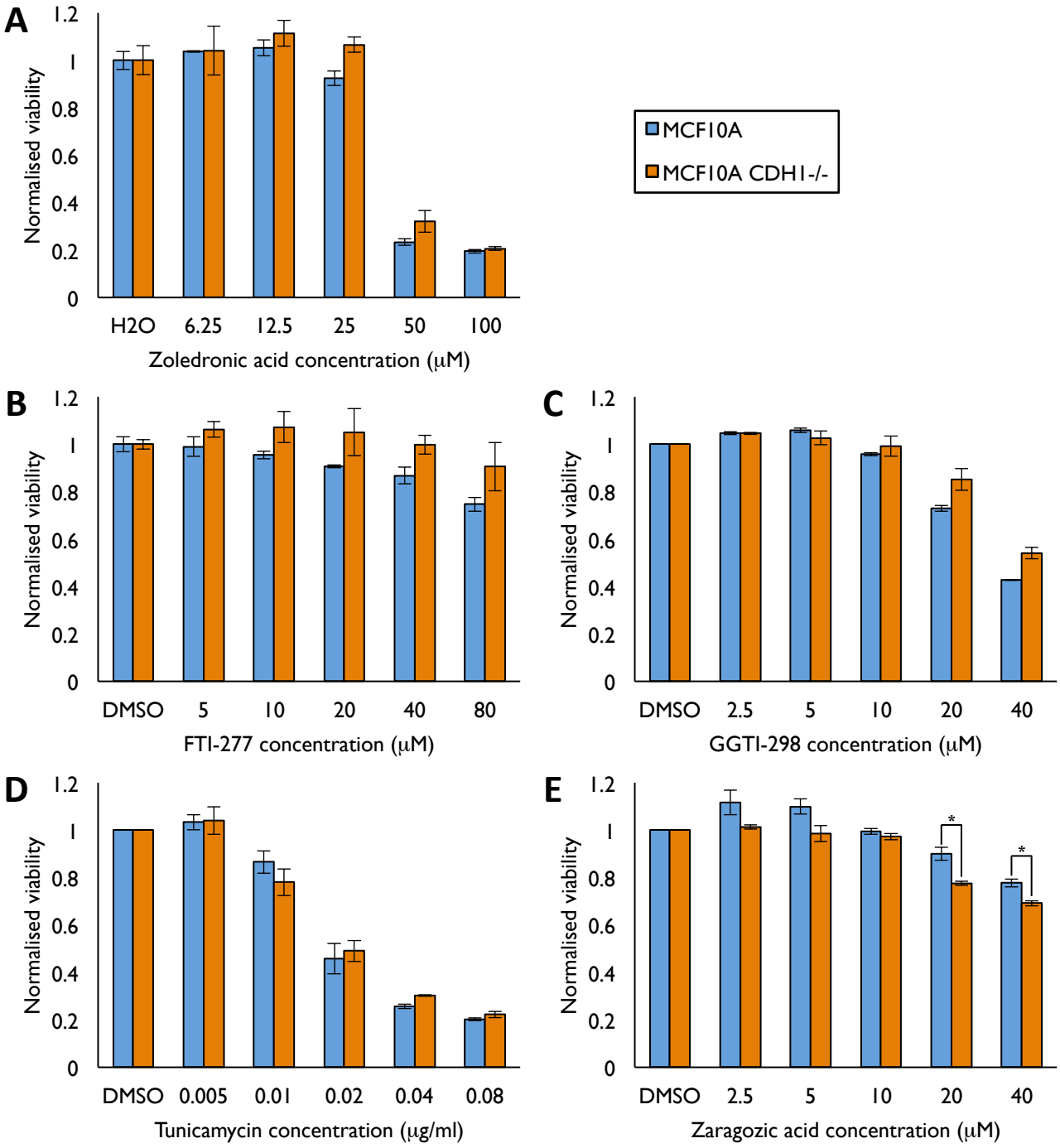

Figure 5.9 MCF10A and MCF10A *CDH1*$^{-/-}$ cell viability following mevalonate pathway inhibition downstream of HMGCR

MCF10A and MCF10A *CDH1*$^{-/-}$ cells were grown for 24 h and treated with either zoledronic acid **(A)**, FTI-277 **(B)**, GGTI-298 **(C)**, tunicamycin **(D)**, or zaragozic acid **(E)** over a range of concentrations. At 48 h post-treatment, cell viability was assessed using a Hoechst-stained nuclei counting assay. Data represents averaged values of two biological replicates with standard error shown. *P*-values calculated using Student's *t*-test; * $P < 0.05$.

5.2.8 Hippo Pathway Activation

Atorvastatin and mifepristone have recently been shown to modulate Hippo pathway activation *in vitro* (Sorrentino *et al*., 2014; Sorrentino *et al*., 2017). This prompted us to analyse YAP regulation as a potential synthetic lethal and synergistic mechanism targeted by atorvastatin and mifepristone in our MCF10A isogenic system. MCF10A and MCF10A *CDH1*$^{-/-}$ cells were grown for 24 hours and treated with either single-agent atorvastatin and mifepristone, or both drugs in combination. Complete growth medium and DMSO were used for untreated and vehicle-treated controls, respectively. 24 hours post-treatment, cell lysates were prepared and immunoblotted for levels of YAP and YAP phosphorylated at serine 127 (pYAP(S127)), the target amino acid of LATS kinases (Johnson and Halder, 2014). pYAP(S127) is retained in the cytoplasm and infers Hippo pathway activation (Johnson and Halder, 2014). The immunoblot analysis showed low YAP expression in MCF10A and MCF10A *CDH1*$^{-/-}$ cells, with no difference observed across both isogenic cell lines (Figure 5.10A). Atorvastatin and mifepristone treatment, either alone or in combination, did not increase pYAP(S127) levels relative to vehicle treatment in either cell line (Figure 5.10B). Additionally, no difference was observed in pYAP(S127) levels between drug-treated MCF10A and MCF10A *CDH1*$^{-/-}$ cell lines (Figure 5.10B). Altogether, the western analysis suggested the Hippo pathway was unlikely to be differentially regulated in the MCF10A isogenic pair and that atorvastatin and mifepristone, whether given alone or in combination, are not exerting synthetic lethality in normalised E-cadherin-deficient cells via YAP manipulation.

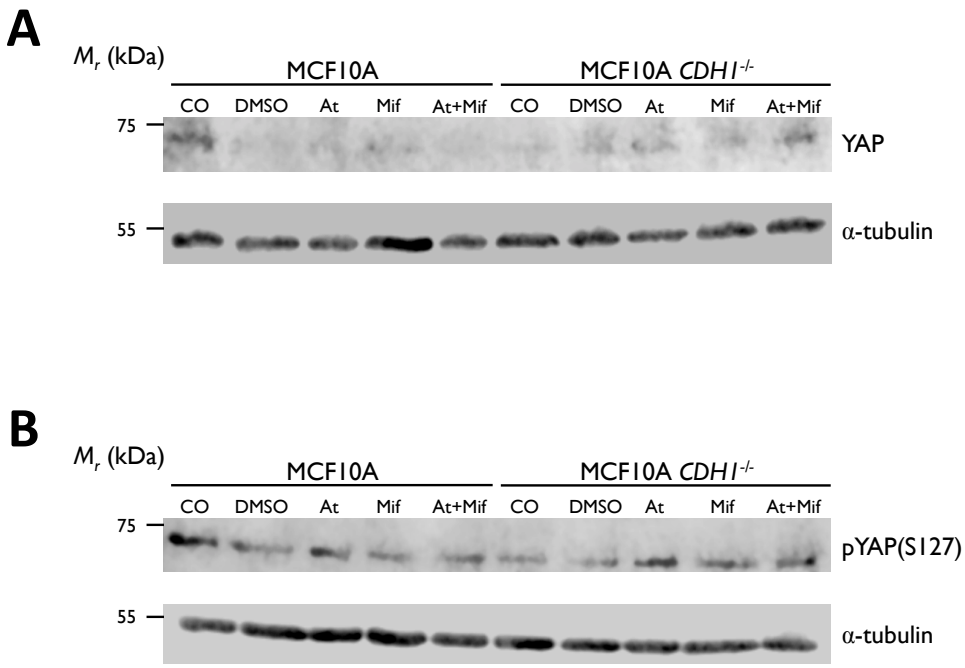

Figure 5.10 Immunoblot for YAP and pYAP(S127) in MCF10A and MCF10A *CDH1*$^{-/-}$ cells following single-agent and combined atorvastatin and mifepristone treatment

MCF10A and MCF10A *CDH1*$^{-/-}$ cells were grown for 24 h and treated with complete growth medium (cell only, CO), vehicle (DMSO), 2.5 μM atorvastatin (At), 2.5 μM mifepristone (Mif), or combined 2.5/2.5 μM atorvastatin and mifepristone (At+Mif) for an additional 24 h. Cell lysates were collected and immunoblotted for YAP **(A)** and YAP phosphorylated at serine residue 127 (pYAP(S127); **(B)**, with α-tubulin used as a loading control. Representative blots (n = 2) are shown.

To confirm the absence of an exploitable Hippo pathway vulnerability in MCF10A *CDH1*$^{-/-}$ cells, we next tested the YAP inhibitor verteporfin in combination with atorvastatin and mifepristone in the MCF10A isogenic cell lines. MCF10A and MCF10A *CDH1*$^{-/-}$ cells were grown for 24 hours and treated with a titrated range of single-agent atorvastatin, mifepristone, or verteporfin; combined atorvastatin and mifepristone, atorvastatin and verteporfin, mifepristone and verteporfin; or all three drugs in combination. Cell viability was determined at 48 hours post-treatment using nuclei counting and an isobologram analysis was used to investigate potential synergistic interactions of the two-part and three-part drug combinations. The viability analysis showed single-agent verteporfin treatment did not induce a marked synthetic lethal phenotype in the MCF10A *CDH1*$^{-/-}$ cell line (Appendix D.6). Further, the addition of verteporfin to atorvastatin and mifepristone failed to increase the synthetic lethal viability differential provided by combined atorvastatin and mifepristone treatment in MCF10A and MCF10A *CDH1*$^{-/-}$ cells (Figure 5.11A). This was supported by a lack of synergy from the isobologram analysis, whereby combined atorvastatin and verteporfin treatment produced combination indices of 1.00 and 0.97, and combined mifepristone and verteporfin treatment produced combination indices of 1.19 and 1.49 for MCF10A and MCF10A *CDH1*$^{-/-}$ cells, respectively (CI > 0.9; Figure 5.11B). To summarise, verteporfin-mediated YAP inhibition showed no evidence for a Hippo pathway vulnerability in the MCF10A *CDH1*$^{-/-}$ cell line.

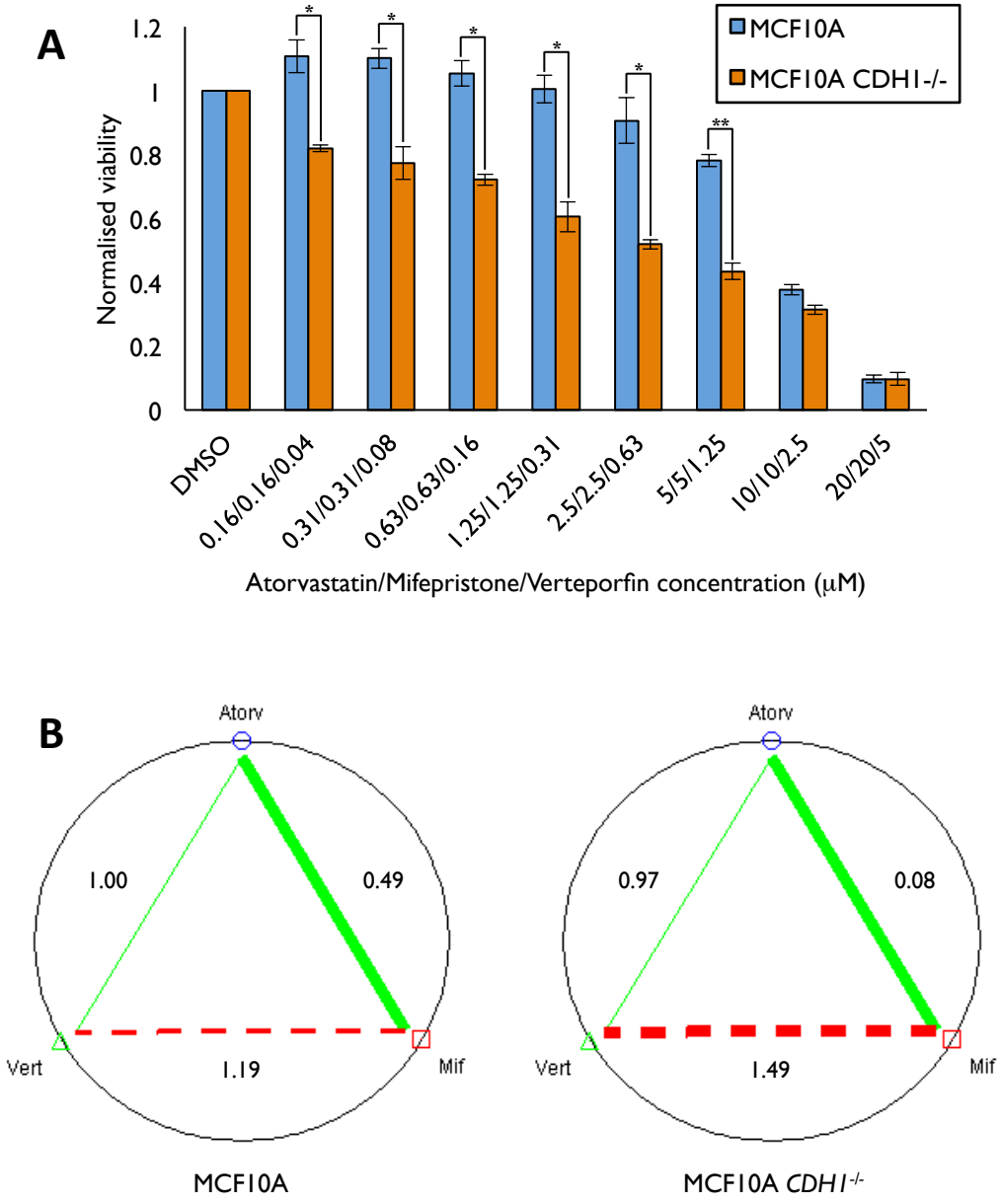

Figure 5.11 Verteporfin co-treatment does not enhance atorvastatin and mifepristone induced synthetic lethality in MCF10A *CDH1*$^{-/-}$ cells

MCF10A and MCF10A *CDH1*$^{-/-}$ cells were grown for 24 h and treated with single-agent verteporfin, atorvastatin, mifepristone; combined verteporfin and atorvastatin, verteporfin and mifepristone, atorvastatin and mifepristone; or all three drugs in combination for 48 h. Cell viabilities were determined using a Hoechst-stained nuclei counting assay **(A)** and used to assess drug synergy at the ED50 dose via CompuSyn software polygonogram analysis **(B)**. Drug synergy is evaluated using a combination index (CI), whereby CI < 0.9 indicates synergy; CI = 0.9-1.1 indicates additivity; CI > 1.1 indicates antagonism. Atorvastatin and verteporfin = additive (CI = 0.9-1.1); verteporfin and mifepristone = antagonistic (CI > 0.9); atorvastatin and mifepristone = synergistic (CI < 0.9). Data represents averaged values of two biological replicates with standard error shown. *P*-values calculated using Student's *t*-test; * $P < 0.05$; ** $P < 0.01$.

5.3 DISCUSSION

In this chapter, the consequences of combined atorvastatin and mifepristone treatment were evaluated in the MCF10A isogenic cell lines. A real-time confluence analysis showed a stronger proliferation reduction in MCF10A cells lacking E-cadherin expression (MCF10A *CDH1*$^{-/-}$) than wild-type MCF10A cells following single-agent atorvastatin and mifepristone treatment, supporting the findings of our previous endpoint testing. This drug-induced confluence loss was enhanced following co-treatment of these drugs, supporting previous findings of a synergistic interaction. A complete loss of cellular confluence, however, was not seen in MCF10A *CDH1*$^{-/-}$ cells in response to atorvastatin and mifepristone treatment at the tested concentration range. This lack of cell death was later attributed to cytostasis, whereby MCF10A *CDH1*$^{-/-}$ cells were exclusively G1-arrested following drug treatment.

In addition to our normalised MCF10A isogenic cell line model, the atorvastatin and mifepristone combination was applied to two malignant cell lines devoid of E-cadherin expression, the ILBC-derived IPH-926 and the TNBC-derived MDA-MB-231. Both IPH-926 and MDA-MB-231 cell lines exhibited a dose-dependent loss in viability in response to atorvastatin and mifepristone treatment. A synergistic response was observed following co-treatment of these drugs in both cell lines, a result similar to our MCF10A isogenic cell line findings. The synergistic response of combined atorvastatin and mifepristone in these malignant breast cancer cell lines suggests that this combination may be robust to a variety of genetic backgrounds. Further studies testing the atorvastatin and mifepristone combination in additional cancer cell lines should be undertaken to further extend these initial observations. This could include testing in malignant cell lines with intact E-cadherin, to see how specific these findings are with respect to E-cadherin loss in a malignant context.

The synergistic effect of co-administered atorvastatin and mifepristone was not as potent in IPH-926 and MDA-MB-231 cells as MCF10A *CDH1*$^{-/-}$, presumably due to background genetic differences. This was also evident in the cell cycle analysis, where MDA-MB-231 cells exhibited a marked G1-arrested effect in response to single-agent statin treatment, an effect unseen using both E-cadherin-expressing and E-cadherin-deficient MCF10A lines, but in line with the previous literature (Shen *et al*., 2015). Interestingly, co-treatment with mifepristone did not amplify the growth-arrested phenotype of atorvastatin treatment in the TNBC-derived cell line. However, this may be attributed to the low mifepristone concentration used in the combination for the MDA-MB-231 cell cycle staging analysis. Mifepristone treatment produced a higher IC_{50} than atorvastatin treatment in MDA-MB-231 endpoint testing, thus a higher mifepristone concentration was likely required in the combination instead of the tested 1:1 (atorvastatin:mifepristone) molar ratio. This effect could be explained by mifepristone targeting hormone receptors (PR and/or GR) in a TNBC context and would therefore be worth examining in additional TNBC cell lines.

Although differences between the isogenic MCF10A cells were detected following atorvastatin and mifepristone treatment, we were unable to confirm a single signalling pathway that correlated with the synthetic lethal phenotype and synergistic drug interaction. Inhibition of multiple mevalonate pathway nodes did not give rise to a marked synthetic lethal phenotype in MCF10A *CDH1*$^{-/-}$ cells, suggesting statin-exploited vulnerabilities in E-cadherin-deficient cells are independent to mevalonate pathway signalling. Additionally, these data suggest that interweaving of mevalonate and glucocorticoid signalling pathways via FPP-GR complex formation may not explain the synergistic link between atorvastatin and mifepristone co-inhibition (Das *et al*., 2007; Pastar *et al*., 2016; Vukelic *et al*., 2010). Follow-up studies involving targeted knockdown of mevalonate pathway enzymes such as HMGCR and FDPS, will likely provide further clarity to this mechanism. Additionally, methodology describing

mevalonate metabolite supplementation to cells following HMGCR inhibition could also be adapted to this analysis (Andres *et al*., 2014; Wang *et al*., 2016).

ILBC exhibits modulated Hippo pathway signalling in addition to E-cadherin loss *in vitro* and *in vivo* (Vlug *et al*., 2013). Furthermore, both atorvastatin and mifepristone have been shown to induce YAP cytoplasmic sequestration, and thus Hippo activation, in breast cancer cell lines (Sorrentino *et al*., 2014; Sorrentino *et al*., 2017). This prompted us to investigate the Hippo pathway in our isogenic MCF10A system. Much to our chagrin, the Hippo pathway regulator YAP was not differentially regulated between MCF10A and MCF10A *CDH1*$^{-/-}$ cells, either pre- or post-treatment with atorvastatin and mifepristone. This infers non-malignant breast cells do not rely on nuclear-localised YAP for proliferation following E-cadherin loss. Atorvastatin and mifepristone treatment is therefore unlikely to be inhibiting MCF10A *CDH1*$^{-/-}$ proliferation via the Hippo pathway, a finding supported by a lack of synthetic lethality following verteporfin (YAP inhibitor) treatment. It is possible that the E-cadherin-deficient cancerous cell lines used in this study, IPH-926 and MDA-MB-231, may utilise YAP signalling to a greater extent than MCF10A cells, however, this was not tested in the investigation.

MCF10A cells have been shown to enter G1 arrest when in agarose suspension cultures (without cell-substratum adhesion) and following knockdown of E-cadherin expression (Fournier *et al*., 2008). This suggests that compromised cell-to-cell adhesion may increase a cell's dependency on basement membrane adhesion (Fournier *et al*., 2008). Both statin and mifepristone treatment are known to alter focal adhesion signalling pathways (Wang *et al*., 2008; Yu *et al*., 2015). It is therefore possible that combined atorvastatin and mifepristone may be acting synergistically through integrin adhesion inhibition. In MCF10A *CDH1*$^{-/-}$ cells, where cell-to-cell adhesion is compromised following E-cadherin loss, atorvastatin and mifepristone

treatment may be inducing a blockade of integrin signalling, which consequently produces our observed G1-arrested synthetic lethal effect.

Additionally, atorvastatin has been shown to reduce the viability of hepatocellular carcinoma and colorectal carcinoma cells via AMPK-mediated autophagy induction, a process that was independent of HMGCR activity (Yang *et al*., 2010). Autophagy involves the self-digestion of cellular proteins and organelles to prolong viability and is usually initiated in response to cellular stress events such as starvation (Meijer and Dubbelhuis, 2004). Atorvastatin-induced cellular starvation involves restriction of insulin-mediated Akt pro-proliferative signalling pathways (Roudier *et al*., 2006). Glucocorticoid removal can also induce cellular starvation, an effect shown to be more potent than combined EGF and insulin deprivation (Moran *et al*., 2000). This may explain mifepristone's greater synthetic lethal effect in MCF10A *CDH1*$^{-/-}$ cells than that seen post-statin treatment. It is noteworthy that EGF, insulin, and the glucocorticoid hydrocortisone are components of MCF10A growth medium. This opens the possibility that atorvastatin-mediated EGF and insulin restriction and mifepristone-mediated hydrocortisone restriction may explain the synergistic interaction following co-treatment of both drugs. This suggests that combining atorvastatin and mifepristone with an autophagy-inducing compound, such as the FDA-approved metformin, may further increase the synthetic lethal differential in the MCF10A isogenic cell lines. Indeed, a recent study has shown combined statin and metformin treatment improves prognosis in gastrointestinal cancer patients (Nimako *et al*., 2017). Additionally, metformin treatment reduces metabolic side effects in patients receiving glucocorticoid therapy (Seelig *et al*., 2017). Taken together, these studies suggest a potential synergistic interaction for combined atorvastatin, mifepristone, and metformin treatment.

If starvation-induced autophagy is responsible for atorvastatin and mifepristone synergy, an impaired autophagic ability must therefore reside in E-cadherin-deficient cells to explain the

synthetic lethality in the isogenic MCF10A cell lines. It has been shown that E-cadherin-mediated cell-to-cell adhesion is required for the formation of an E-cadherin-LKB1-AMPK complex at the cell periphery, which facilitates the activation of AMPK and subsequent induction of autophagy (Bays *et al*., 2017; Sebbagh *et al*., 2009). Interestingly, *LKB1* loss-of-function mutations have been identified in HDGC families who do not harbour *CDH1* mutations (Hansford *et al*., 2015). This suggests that loss of *CDH1* and/or *LKB1* may reduce a cell's ability to perform autophagy via AMPK, a process that may be an exploitable synthetic lethal vulnerability in HDGC. In breast cancer, autophagy-related proteins show differential expression between E-cadherin-negative ILBC and E-cadherin-positive invasive ductal carcinoma (IDC) (Cha *et al*., 2014). Beclin-1 (*BECN1*) is a key regulator of autophagy induction and was identified at lower levels in ILBC than IDC (Cha *et al*., 2014), suggesting ILBC tumours may also have compromised autophagy. Further studies are needed to understand the mechanisms underpinning E-cadherin loss and cellular autophagy, and whether this process can indeed be exploited across DGC and ILBC tumours.

In summary, this chapter has identified a cytostatic effect following combined atorvastatin and mifepristone treatment in both non-malignant and malignant cell lines devoid of E-cadherin expression. We have demonstrated that this response is unrelated to mevalonate and Hippo signalling pathways in non-malignant cells, a finding that will prompt further investigation across a panel of E-cadherin-deficient cancer cell lines. Nonetheless, this study adds further support to the use of statins and mifepristone in cancer therapeutics and provides a novel drug combination alternative for HDGC, ILBC, and potentially TNBC, clinical intervention.

6. FUTURE DIRECTIONS

This thesis characterised a range of real-time and endpoint cell viability assays that were applied to a pair of isogenic non-malignant breast cell lines to screen for synergistic and synthetic lethal drug combinations in E-cadherin-deficient cells. From this screen, statins were identified as a drug class that reduced MCF10A *CDH1*$^{-/-}$ cell viability whilst leaving wild-type MCF10A cells relatively unharmed at concentrations up to 5 μM. Furthermore, statin-induced synthetic lethal interactions were synergistic with HDACi (entinostat and vorinostat), saracatinib, and mifepristone. Combined atorvastatin and mifepristone treatment produced the strongest synthetic lethal and synergistic response via a cytostatic G1-arrest phenotype, and this synergy was maintained in the IPH-926 and MDA-MB-231 breast cancer cell lines. This chapter focuses on potential future directions of this research, highlighting additional steps that may lead to the atorvastatin and mifepristone combination as a chemoprevention and advanced cancer treatment option in the clinic.

To further expand this study's findings, an approach to unravel both the synergistic and synthetic lethal mechanisms of atorvastatin and mifepristone treatment would be useful. As such, this drug combination could be applied to additional isogenic cell lines that differ by *CDH1* expression status. We are currently performing drug testing in a gastric cancer cell line (NCI-N87) and a CRISPR-generated *CDH1* knockout counterpart (unpublished data). Additionally, an RNA sequencing analysis could be undertaken using the MCF10A and MCF10A *CDH1*$^{-/-}$ cells treated with single-agent and combined atorvastatin and mifepristone. On the proteomic scale, a Reverse Phase Protein Array (RPPA) could be used to identify altered phosphoproteome signalling following single-agent and combined drug treatment. Together, these methodologies may uncover a pathway that could be further investigated in the context of cellular vulnerabilities following loss of E-cadherin.

A high-throughput drug screen could also be undertaken to identify additional synthetic lethal drug combinations involving statins and/or mifepristone. This could involve treating MCF10A and MCF10A *CDH1*$^{-/-}$ cells that have been pre-treated with statin and/or mifepristone. An endpoint viability assay would then be used to find drugs that enhance the synthetic lethal effect of statin and mifepristone treatment. Additionally, a caspase assay could be used to discover drugs that drive atorvastatin- and mifepristone-treated cells to apoptosis. Findings from this screen may identify drugs that are more synergistic with atorvastatin than mifepristone. This would provide a better chemoprevention option for female *CDH1* mutation carriers of childbearing age, as mifepristone is used clinically as an abortifacient agent.

An obvious next move for this research is to apply the atorvastatin and mifepristone combination to a more complex system than monolayer cell culture. One such system involves growing cell lines in three-dimensional spheres, termed 'spheroids'. Spheroids can be produced using a number of methods (described in detail by Breslin and O'Driscoll, 2013), with the aim of mimicking aspects of tumour growth *in vivo* (Breslin and O'Driscoll, 2013). Central to this is the formation of a hypoxic core, which is a result of poor oxygen diffusion from the spheroid exterior to the spheroid centre (Tung *et al*., 2011). This resembles conditions of low oxygen permeability observed *in vivo*, where approximately 60% of solid tumours exhibit hypoxic cores (Vaupel and Mayer, 2005). However, it is noteworthy that hypoxic cores are infrequent in lobular carcinomas due to the diffuse and indolent nature of their growth. Hypoxic conditions have been shown to change cellular responses to drug treatment by altering the expression of survival- and apoptosis-related genes (Wilson and Hay, 2011). In addition, hypoxia may cause resistance to drug-induced G1 cell cycle arrest (Wilson and Hay, 2011), an effect that may impact the atorvastatin and mifepristone effects described in this study. Further, the MCF10A and MDA-MB-231 cell lines used in this study are known to become more resistant to doxorubicin-induced cytotoxicity when grown in spheroids versus monolayer cultures (Li *et al*.,

2010). Thus, there is a need to assess the synergistic and synthetic lethal effects of combined atorvastatin and mifepristone treatment in three-dimensional MCF10A, MDA-MB-231, and additional E-cadherin-deficient cell line cultures.

Slightly more complex than spheroids are organoid model systems. Organoids are three-dimensional cell cultures derived from the stem cells of primary tissue that exhibit similar structural and functional properties as the tissue of origin (Clevers, 2016; Fatehullah *et al*., 2016). This allows for a more accurate model of tissue pathology *in vitro*, providing an intermediate between cell culture and animal model systems. Of interest to this study is the development of gastric and mammary tissue organoids, with the aim of inducing E-cadherin loss in these tissues to resemble DGC and ILBC pathologies. Fortunately, the successful culturing of gastric organoids has been described in the literature (Barker *et al*., 2010; Bartfeld *et al*., 2015; McCracken *et al*., 2014), and the technique is now established in our laboratory using neonatal mouse stomachs. Gastric organoids have been developed from both mouse and human primary tissue, containing gastric gland- and pit-like domains, proliferative zones, mucous cells, and endocrine cells, akin to stomach tissue *in vivo* (Clevers, 2016). Recently, Boelens *et al*. (2016) generated an ILBC organoid model from mouse mammary tissue harbouring Cre-conditional inactivation of *Cdh1* and *Pten* (Boelens *et al*., 2016). PTEN loss induces hyperactive signalling of the PI3K pathway and was additionally inactivated as E-cadherin loss alone does not produce mammary tumours in a mouse model (Boussadia *et al*., 2002; Derksen *et al*., 2006).

Similar to Boelens *et al*., we are currently developing a Cre-conditional *Cdh1*$^{-/-}$ mouse as a DGC model. In this model, Cre expression is under a *Cd44* promoter and inducible via tamoxifen treatment. At the time of writing, this *Cd44-Cre*/*Cdh1*$^{-/-}$ mouse is being bred to generate the required numbers for a time course study following tamoxifen-induced *Cdh1* deletion. It is

predicted that lesions akin to T1a signet ring cell carcinoma will develop in the gastric epithelium of these mice in under six months. Lead synthetic lethal drugs, such as atorvastatin and mifepristone, will be used to treat the DGC model mice with the aim of reducing the number of foci in the stomach tissue. Additionally, resected stomach tissue from these mice will be used to form organoids, with tamoxifen treatment used to induce E-cadherin loss *in vitro*. Thus, if the mouse model is successful, we will have two powerful drug testing platforms for advancing synthetic lethal drug testing.

The performance of statin-based combinations in a patient-derived xenograft (PDX) model would also be of interest. PDX models involve the propagation of a patient's tumour tissue inside an immunosuppressed mouse. Following transplantation, PDX models have been found to closely resemble the donor tumour tissue, maintaining features such as gland architecture, mucin production, and cyst development (Hidalgo *et al*., 2014). This provides a useful tool for translational cancer research, as evidenced by the successful use of PDX models in preclinical phase II studies with chemotherapeutic agents (Berger *et al*., 1990). Of immediate relevance to this study would be the testing of atorvastatin and mifepristone in a PDX model consisting of DGC- and/or ILBC-derived tumour tissue. The ability of these synthetic lethal drugs to maintain a synergistic therapeutic effect in a PDX model may expand the combination's application from chemoprevention to advanced cancer therapeutics.

Finally, proof of a therapeutic benefit from statin-based combinations in *CDH1* mutation carriers is needed. This would be a worthwhile investigation as statin concentrations used *in vitro* are markedly higher than what is clinically attainable in human serum (Bjorkhem-Bergman *et al*., 2011). Prior to undergoing prophylactic total gastrectomy (PTG), *CDH1* mutation carriers can face a waiting period of several months. This presents a window where combination treatment could be provided to individuals planning to undergo a PTG. As the

stomach tissue of *CDH1* mutation carriers contain multiple stage T1a lesions (as detailed in Chapter 1.1.2), we would examine the number of foci between the resected stomachs of individuals who received drug combination treatment. No foci in a series of stomachs from patients who received drug treatment would provide evidence of a successful chemoprevention approach.

Overall, co-treatment of atorvastatin and mifepristone is a novel drug combination in cancer chemoprevention. The ability of statin-based combinations to reduce E-cadherin-deficient cell viability whilst modestly affecting wild-type cells demonstrates an exciting overlap between the fields of synergistic drug combination discovery and synthetic lethality. The known safety profile and FDA-approval status of atorvastatin and mifepristone should aid translation of this research to the clinic, where co-treatment of these drugs can potentially serve as a new alternative to current HDGC and ILBC chemoprevention regimes.

APPENDICES

Appendix A.

Synthetic Lethal Screens Identify Vulnerabilities in GPCR Signalling and Cytoskeletal Organization in E-Cadherin-Deficient Cells

Published OnlineFirst March 10, 2015; DOI: 10.1158/1535-7163.MCT-14-1092

Cancer Biology and Signal Transduction

Molecular Cancer Therapeutics

Synthetic Lethal Screens Identify Vulnerabilities in GPCR Signaling and Cytoskeletal Organization in E-Cadherin–Deficient Cells

Bryony J. Telford[1], Augustine Chen[1], Henry Beetham[1], James Frick[1], Tom P. Brew[1], Cathryn M. Gould[2], Andrew Single[1], Tanis Godwin[1], Kaylene J. Simpson[2,3], and Parry Guilford[1]

Abstract

The *CDH1* gene, which encodes the cell-to-cell adhesion protein E-cadherin, is frequently mutated in lobular breast cancer (LBC) and diffuse gastric cancer (DGC). However, because E-cadherin is a tumor suppressor protein and lost from the cancer cell, it is not a conventional drug target. To overcome this, we have taken a synthetic lethal approach to determine whether the loss of E-cadherin creates druggable vulnerabilities. We first conducted a genome-wide siRNA screen of isogenic MCF10A cells with and without *CDH1* expression. Gene ontology analysis demonstrated that G-protein–coupled receptor (GPCR) signaling proteins were highly enriched among the synthetic lethal candidates. Diverse families of cytoskeletal proteins were also frequently represented. These broad classes of E-cadherin synthetic lethal hits were validated using both lentiviral-mediated shRNA knockdown and specific antagonists, including the JAK inhibitor LY2784544, Pertussis toxin, and the aurora kinase inhibitors alisertib and danusertib. Next, we conducted a 4,057 known drug screen and time course studies on the *CDH1* isogenic MCF10A cell lines and identified additional drug classes with linkages to GPCR signaling and cytoskeletal function that showed evidence of E-cadherin synthetic lethality. These included multiple histone deacetylase inhibitors, including vorinostat and entinostat, PI3K inhibitors, and the tyrosine kinase inhibitors crizotinib and saracatinib. Together, these results demonstrate that E-cadherin loss creates druggable vulnerabilities that have the potential to improve the management of both sporadic and familial LBC and DGC. *Mol Cancer Ther; 14(5); 1213–23. ©2015 AACR.*

Introduction

E-cadherin is a cell-to-cell adhesion protein that is localized at the adherens junction of all epithelial cells (1). Other than its roles in cell adhesion, E-cadherin is involved in establishing and maintaining cell polarity and differentiation, the organization of cell migration and architecture and the mediation of signaling through various proliferation and survival pathways, including WNT and EGFR (2, 3).

Abrogation of expression of the E-cadherin gene (*CDH1*) by mutation, deletion, or promoter hypermethylation is a feature common to many epithelial tumors and its downregulation is the hallmark of both diffuse gastric cancer (DGC) and lobular breast cancer (LBC; refs. 1, 4–6). Disrupting E-cadherin's expression or localization has a pronounced impact on a cell's cytoskeletal structure, with changes including misalignment of the microtubule and actin cytoskeletons, defects in cell migration and irregularities in the orientation of the mitotic spindle (7–9).

Germline *CDH1* mutations are responsible for hereditary diffuse gastric cancer (HDGC), a cancer syndrome characterized by the highly penetrant, early onset of multifocal DGC and an elevated rate of LBC. In HDGC, *CDH1* inactivation is an initiating event that may be related to abnormal mitotic spindle orientation resulting in daughter cells being displaced into the lamina propria, outside the epithelial plane (10–12). In other cancer types, its downregulation is considered to be a late event that promotes increased invasive capacity, frequently through association with the epithelial–mesenchymal transition (13).

Although E-cadherin is a tumor suppressor protein that is lost from the cancer cell and therefore not a conventional drug target, the downregulation of such a multifunctional protein during tumorigenesis would be predicted to create vulnerabilities in the cell which are targetable using a synthetic lethal approach. In the context of drug development, synthetic lethality can be defined as a drug that reduces cell viability or fitness only in cells carrying a specific mutation. The utility of synthetic lethal targeting of tumor suppressor genes is well illustrated clinically by olaparib, an inhibitor of the DNA repair enzyme PARP. Olaparib elicits strong clinical responses in breast and ovarian cancer patients who harbor inactivating mutations in the homologous recombination dsDNA repair genes *BRCA1/2* (14, 15).

[1]Cancer Genetics Laboratory, Department of Biochemistry, University of Otago, Dunedin, New Zealand. [2]Victorian Centre for Functional Genomics, Peter MacCallum Cancer Centre, East Melbourne, Victoria, Australia. [3]The Sir Peter MacCallum Department of Oncology, The University of Melbourne, Parkville, Victoria, Australia.

Note: Supplementary data for this article are available at Molecular Cancer Therapeutics Online (http://mct.aacrjournals.org/).

Current address for C.M. Gould: Garvan Institute of Medical Research, Darlinghurst, New South Wales 2010, Australia.

Corresponding Author: Parry Guilford, Cancer Genetics Laboratory, Centre for Translational Cancer Research, Department of Biochemistry, University of Otago, P.O. Box 56, Dunedin 9054, New Zealand. Phone: 643-479-7673; Fax: 643-479-5077; E-mail: parry.guilford@otago.ac.nz

doi: 10.1158/1535-7163.MCT-14-1092

Published OnlineFirst March 10, 2015; DOI: 10.1158/1535-7163.MCT-14-1052

In addition to providing new therapeutic avenues for the treatment of sporadic epithelial cancers, synthetic lethal targeting of E-cadherin–deficient cells also has the potential to improve the clinical management of HDGC. To identify druggable synthetic lethal vulnerabilities in E-cadherin–deficient cells, we have conducted both a genome-wide siRNA synthetic lethal screen and a four thousand compound known drug screen on isogenic breast MCF10A cells with and without *CDH1* expression. Together, these screens have identified multiple druggable targets that suggest new therapeutic strategies for the treatment of E-cadherin–deficient cancers and the chemoprevention of HDGC.

Materials and Methods

Cell lines and media

The MCF10A breast cell line and its paired isogenic MCF10A *CDH1*$^{-/-}$ line (here designated *CDH1*$^{-/-}$) were obtained from Sigma Aldrich in 2011 (parental line ATCC CRL-10317) and had been authenticated using short terminal repeat analysis. *CDH1*$^{-/-}$ had been created by homozygous deletion of 4 bp from exon 11 of the *CDH1* gene. The lines were resuscitated within one week of receipt and early passage cells (passage 3–7) were aliquoted and frozen. All experiments were conducted with cells between passages 6–15 in DMEM F12 media with glutamate, 5% horse serum, 20 ng/mL EGF, 0.5 μg/mL hydrocortisone, 100 ng/mL cholera toxin, and 10 μg/mL insulin. Characterization of the cell line pair is described elsewhere (7).

siRNA high-throughput screen

Cells were transfected with siRNAs from the Dharmacon SMARTpool whole genome protein-coding siRNA library (RefSeq 27) housed in the Victorian Center for Functional Genomics. Each SMARTpool contained four siRNAs that targeted different regions of each gene in one well. Each reaction, in a white walled, clear-bottom 384-well plate format, contained 0.125% DharmaFECT 3 (0.05 μL), 27.4% OptiMEM (Invitrogen), and 40 nmol/L of the siRNA SMARTpool (total volume 37.5 μL). Cells were reverse transfected and seeded onto the siRNA cocktail at a density of 700 MCF10A cells per well and 900 *CDH1*$^{-/-}$ cells/well to enable the two cell lines to reach confluence at the same time point (72 hours after seeding). The following controls were included in each plate: the death controls si*EGFR* and si*PLK1* (4 wells each), a synthetic lethal control si*CTNNB1* (6 wells) and two negative controls, siRISC free and mock (lipid only, 9 wells each). After 24 hours, the media was replaced and at 72 hours 10 μL CellTiter-Glo was added to each well (final concentration 1/5), shaken on an orbital shaker for 2 minutes and incubated for a further 30 minutes at room temperature before measuring luminescence using a Synergy H4 microplate reader (Biotek). siRNA was dispensed using a Caliper Sciclone ALH3000 (PerkinElmer). All other liquid handling steps were performed using a Biotek406 liquid handling workstation. Primary screen analysis was performed by normalizing genes in each cell line individually to the average mock value (across all screen plates) for the respective cell line. The level of increased kill was determined by the ratio of *CDH1*$^{-/-}$ viability to MCF10A viability. Candidates with MCF10A viability $\geq$50% and a fold change ratio of $\leq$0.85 were considered synthetic lethal candidates. Selection of the final 500 genes chosen for secondary screening was based on further analysis of druggability and biologic relevance. Secondary siRNA screening was performed using four individual siRNAs targeting each gene arrayed in individual wells, separately using the same transfection conditions described above with a final siRNA concentration of 25 nmol/L. The secondary screen was analyzed using the same normalization strategy and cutoffs as the primary screen.

Viral knockdown

Dharmacon pGIPZ lentiviral shRNA mir30 plasmids were prepared from cultures using the Machery Nagel EasyPure Miniprep Kit. 293FT cells were cotransfected 24 hours after seeding with 18.6 μg pGIPZ, 9.6 μg PAX2, and 4.8 μg VSVG plasmids using 55.7 μL Lipofectamine 2000 (Invitrogen). Media was changed at 24 hours, and after a further 24 hours, viral particles were harvested by aspirating media, centrifugation at 3,000 rpm for 15 minutes to remove cellular debris and filtration through a 0.45 μmol/L polyvinylidene difluoride filter. Virus was aliquoted and snap frozen for subsequent use.

Viral titer was determined by seeding MCF10A cells at 4,000 cells per well and transducing with a 1/32 dilution of virus 24 hours later. Media was changed after 24 hours, and after a further 24 hours, GFP-expressing cells were quantitated over 5 fields at 10× magnification. The average number of transduced cells per well was used to determine the number of transducing units per mL.

For knockdown experiments, 1,000 MCF10A and 2,000 *CDH1*$^{-/-}$ cells per well were seeded in black walled, clear bottomed 96-well plates and allowed to adhere overnight. The following day, virus was added at a multiplicity of infection (MOI) of 10. Media were changed at 24 hours and 1 μg/mL puromycin added. Seventy-four hours after transduction, media was aspirated and 1 μg/mL Hoechst 33342 and 0.5 μg/mL propidium iodide in PBS added. After 30 minutes, incubation plates were imaged with 4 fields per well on the Cytell (GE) at 4× magnification and 10 fields per well at 10× magnification using the "Cell Viability BioApp". CellProfiler (16) was used to quantitate the total nuclei, as well as the proportion stained with propidium iodide.

RNA was extracted at 72 hours to determine gene knockdown using the RNAgem-PLUS Kit (ZyGem). cDNA was synthesized using the Primescript cDNA Synthesis Kit (Takara), and qPCR performed using Sybr Fast kit (KAPA) on an ABI7900HT with an enzyme activation step of 95°C for 3 minutes followed by 40 cycles of 95°C for 15 seconds, 57°C for 15 seconds, and 72°C for 15 seconds. *GAPDH* and *PPIA* were used as reference genes and results were analyzed using the efficiency method as described by Pfaffl (17).

Known drug screen

Assay ready plates containing 20 nL of 4,057 compounds diluted in DMSO at four concentrations (2, 1, 0.5, and 0.25 μmol/L) were prepared by the Walter and Eliza Hall Institute (WEHI, Parkville, Victoria, Australia) High-Throughput Chemical Screening Facility. Cells were seeded directly onto these plates in a volume of 50 μL at a density of 1,000 cells per well for MCF10A and 1,200 cells per well for *CDH1*$^{-/-}$ in 384-well clear bottom plates. After 48 hours, 20 μL of CellTiter-Glo (Promega) was added to each well, shaken for 2 minutes on an orbital shaker, and incubated for 30 minutes before reading. Values were normalised to the average DMSO control value of the whole screen for each cell line at each concentration.

The secondary drug screen was performed on 316 compounds selected from the primary screen. These were provided at 5 mmol/L

and 11 1:1 dilutions were made with DMSO to create a 10 μmol/L to 10 nmol/L concentration range. Cells were seeded at a density of 700 cells per well for MCF10A and 900 cells per well for *CDH1*$^{-/-}$ for 24 hours before 100 nL of each compound was added to the plates robotically. Thirty-two DMSO control wells were included in each plate. Plates were incubated for a further 48 hours before assaying with CellTiter-Glo.

Drug titrations and time course assays

To determine drug EC_{50}, cells were seeded in white walled, clear-bottom 384 well plates at a density of 800 cells per well in a volume of 45 μL. After 24 hours incubation, 5 μL of drug (rehydrated in DMSO to an 80 mmol/L stock and diluted in complete media) was added to each well. A DMSO control and a cell only control were used on each plate. The 11 drug concentrations used were dependent on the individual drug. After 48 hours of treatment, cell viability was assayed using either the CellTiter-Glo (Promega) or Alamar blue assay. All results were normalized to the average DMSO control for individual cell types. EC_{50} values were calculated by plotting viability against the log drug concentration and fitting a nonlinear regression curve using Prism version 6.0 for Mac (GraphPad Software).

Drug time course assays were carried out by seeding equal numbers of MCF10A or *CDH1*$^{-/-}$ at 4,000 cells per well in xCELLigence plates (Roche), except for crizotinib which was seeded at 2,000 cells per well. The xCELLigence system measures relative changes in electrical impedance in a well ("cell proliferation index") which can be used as a measure of cell number. After 24 hours, three concentrations of each drug were added and growth followed in real time for a further 72 hours. Assays were carried out in duplicate and the data averaged. Time course assays were also performed on the IncuCyte Imaging System (Essen Bioscience). Cells were seeded at 4,000 cells per well in black walled clear-bottom 96-well plates. After 24 hours, five concentrations of each drug were added and 3 fields were imaged per well at 4× magnification every 2 hours for 48 hours. Plates were then removed and cell numbers determined using metabolic assays and nuclei imaging as described above.

For drug synergy studies, the combination index was determined using CompuSyn software (ComboSyn Inc) and the Chou–Talalay method (18). EC_{50} was estimated for both drugs and cells treated with each drug alone and in combination at this concentration and concentrations 2- and 4-fold higher and lower. Viability was calculated by nuclei counting and normalized values imported into CompuSyn.

Results

Genome-wide siRNA screen of *CDH1* isogenic MCF10A cells

To identify genes potentially involved in a synthetic lethal interaction with E-cadherin, we conducted a genome-wide functional screen using the Dharmacon siGENOME SMARTpool library targeting 18,120 genes in a pooled format, with 4 individual siRNAs targeting each gene. Isogenic MCF10A cells with and without *CDH1* expression were screened in parallel, and viability was assayed 72 hours after transduction using CellTiter-Glo. si*PLK1* and si*EGFR* were used as positive death controls (Fig. 1A) and si*CTNNB1* used as a positive synthetic lethal control, after showing a mild synthetic lethal effect in a pilot screen (Supplementary Fig. S1). Mock (lipid only) and RISC-free control (Dharmacon) were included as nontargeting controls. Little variability was observed between these controls; consequently, we normalized the values of each gene to the average screen-wide mock value within each cell line. Hits were selected on the basis of

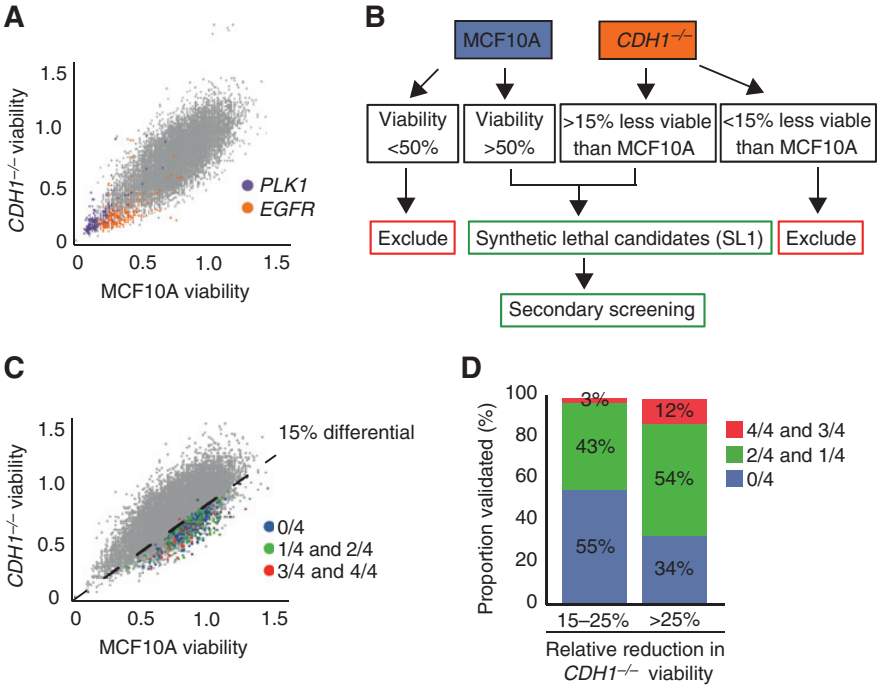

Figure 1.
siRNA screening overview of outcomes and analysis strategy. A, the resulting effect on cell viability after knockdown of each protein-coding target in MCF10A and *CDH1*$^{-/-}$ cells. The positive death controls si*PLK1* and si*EGFR* both consistently cause death in both cell lines. B, the analysis workflow used to select synthetic lethal candidates based on MCF10A and *CDH1*$^{-/-}$ viability. C, correlation between primary and secondary screens. The dotted line marks where *CDH1*$^{-/-}$ has 15% less viability than MCF10A. The primary screen identified 500 candidates that were selected for validation in a secondary screen. Five percent of these validates as with 3 of 4 or 4 of 4 individual siRNA. D, candidates tested in the secondary screen were split into two categories, based on the decrease in viability of *CDH1*$^{-/-}$ compared with MCF10A. Candidates with a greater differential were more likely to be validated in the secondary screen.

Published OnlineFirst March 18, 2015; DOI: 10.1158/1535-7163.MCT-14-1092

the ratio of cell viability between the MCF10A and *CDH1*$^{-/-}$ cells 72 hours after transduction (Fig. 1B). We rejected siRNAs that were highly toxic to the MCF10A cells (a decrease in viability of ≥50%) and selected those for which the viability of *CDH1*$^{-/-}$ cells decreased by ≥15% more than the corresponding knockdown in MCF10A cells. These targets were classed as *CDH1* synthetic lethal candidate genes (List SL1, 2,437 genes; Supplementary Table S1). From this set, 501 genes were manually selected for secondary screening using criteria, including predicted druggability of the encoded proteins and biologic significance. The secondary screen was performed by deconvoluting the four individual siRNAs that consititute the SMARTpool. Using the same stringent threshold as the primary screen (i.e., MCF10A viability ≥50% and ≥15% more death in *CDH1*$^{-/-}$), 21 genes (5%) had 3 of 4 or 4 of 4 of the individual siRNAs show a synthetic lethal effect. One hundred eighty-three genes (44%) had 1 of 4 or 2 of 4 siRNAs validated. Fifty-one percent of genes were not validated (0/4) by this approach. Division of the selected genes into groups based on the strength of the synthetic lethal phenotype in the primary screen demonstrated that candidates which showed a greater viability differential between MCF10A and *CDH1*$^{-/-}$ cells were more likely to be validated in the secondary screen (Fig. 1C and D). Of the candidates that reduced *CDH1*$^{-/-}$ cell number by ≥25% more than MCF10A cells, 12% validated with 3 of 4 or 4 of 4 individual siRNAs, a validation rate comparable with other genome-wide RNAi studies (19, 20).

Functional diversity: gene ontology analysis

To search for functional enrichment in the 2,437 synthetic lethal candidates identified in the primary screen (List SL1), we conducted a gene ontology analysis using DAVID (21). Using the Functional Annotation Clustering tool, the most enriched functional cluster was a group of ten terms associated with G-protein–coupled receptor (GPCR) signaling (enrichment score = 10.01; Supplementary Table S2A). Accordingly, the two most significant biologic process terms (Supplementary Table S2B) were "G-protein–coupled receptor protein signaling pathway" (Benjamini-adjusted *P* value = 4.1×10^{-8}) and "cell surface receptor linked signal transduction" (adj. *P* value = 1.7×10^{-5}). These cell signaling processes were strongly reflected in the DAVID gene ontology molecular function terms (Supplementary Table S2C) which included peptide, neuropeptide, and purinergic nucleotide receptor activity and protein kinase activity (adj. *P* value 3.5×10^{-7} to 3.2×10^{-2}).

Because our ultimate goal is to identify targeted drugs for E-cadherin–deficient tumors that have minimal toxicity against nonmalignant tissues, we also performed gene ontology analysis on a subset of genes from List SL1 whose corresponding siRNA SMARTpools had little or no impact on MCF10A cells (MCF10A viability ≥0.85 mock). 1,136 genes met this revised threshold (List SL2; Supplementary Table S3). Notably, this more stringent cutoff led to further enrichment of both the GPCR-associated functional cluster (enrichment score, 12.14) and the biologic process terms "GPCR protein signaling pathway" (adj. *P* value = $9.0 \times 10^{-}16$) and "cell surface receptor linked signal transduction" (adj. *P* value = 4.8×10^{-10}; Supplementary Table S2D).

Our earlier observation of abnormal cytoskeletal organization in E-cadherin–deficient MCF10A cells (7) prompted us to look for specific cytoskeletal functions associated with synthetic lethality. Although the adjusted *P* values for cytoskeletal-like terms in List SL1 and SL2 did not reach significance, DAVID functional clusters associated with each of cell motility, cell polarity, and cell adhesion were among the top five clusters observed in the group of synthetic lethal candidate genes which reduced MCF10A viability to <0.85 of the mock controls (enrichment scores, 2.18, 1.97, and 1.84, respectively; Supplementary Table S2E). This greater representation of cytoskeletal genes among synthetic lethal candidates that seriously affect MCF10A cell viability presumably reflects the essential role of many cytoskeletal proteins. Cyto- or nucleoskeletal functions that were represented in List SL1, often by multiple family members, included microtubule nucleation, organization, and function (e.g., *TUBA1C*, *TUBG1*, *TUBB2A*, *MZT2A*, *ARPC3*, *NME4*, *NME7*, *MAST1*, *MAST2*, *MAST3*, *NEK1*, *NEK3*, *NEK4*, *NEK10*, *CLIP1*, *CLIP2*, *TEKT3*, *TEKT4*, *TEKT5*), Rho-mediated motility (e.g., *RHOB*, *RHOC*, *RHOH*, *RAC1*, *PAK2*, *TIAM1*), linkages between the cytoskeleton and nucleoskeleton (e.g., *SUN1*, *SUN2*, *SUN5*, *NSUN3*, *NSUN6*, *SYNE1*), polarity (e.g., *DLG1*, *DLG2*, *DLG4*, *DLG5*, *CELSR1*, *CELSR3*), and actin filament organization and remodeling (e.g., *AVIL*, *ARF6*, *CYTH2*, *CTYH3*, *CYTH4*).

E-cadherin–deficient MCF10A cells are sensitive to downregulation of microtubule-associated genes and the aurora kinase A inhibitor alisertib

To validate the apparent synthetic lethal interaction between E-cadherin and the microtubule cytoskeleton, we selected three microtubule-associated genes, *MAST2*, *MAP1B*, and *MAPRE3* for confirmation using lentiviral shRNA knockdown. MAST2 is a microtubule-associated serine–threonine kinase (22); MAP1B is a microtubule-binding and -stabilizing protein that can also interact with actin microfilaments (23) and MAPRE3 is a microtubule plus end-binding protein involved in regulating the dynamics of microtubules and their interactions with intracellular structures such as the cell cortex or mitotic kinetochore (24). These three genes had previously been validated in the secondary screen, with 3 of 4, 2 of 4, and 1 of 4 siRNAs, respectively, decreasing the viability of *CDH1*$^{-/-}$ cells by at least 15% more than the MCF10A (Fig. 2A). shRNAs targeting these three genes resulted in 51%–86% mRNA knockdown in both cell lines (Fig. 2B). Seventy-two hours after transduction, cell viability was measured using nuclei counting (Fig. 2C). Knockdown of each of *MAP1B*, *MAST2*, and *MAPRE3* resulted in 15%–29% more cell death in the *CDH1*$^{-/-}$ cells compared with the MCF10A cells, confirming the siRNA data.

To determine whether the synthetic lethal phenotype observed with downregulation of microtubule-associated genes could be recapitulated using known inhibitors of microtubule function, we treated the isogenic MCF10A cell line pair with the microtubule stabilizing drug taxol and inhibitors of the microtubule-associated proteins aurora kinase A and aurora kinase B. Increasing concentrations of taxol (1–16 nmol/L) led to a small increase in cell death in *CDH1*$^{-/-}$ cells compared with MCF10A cells (Supplementary Fig. S2). The aurora kinase A inhibitor alisertib and the aurora kinase B inhibitor danusertib both showed a minor synthetic lethal effect (Fig. 2D and E), with 18% (at 25 nmol/L) and 12% (50 nmol/L) more death in the *CDH1*$^{-/-}$ line, respectively. Together, the RNAi and aurora kinase inhibitor data demonstrate that E-cadherin–deficient MCF10A cells are more vulnerable to disruption of specific microtubule-related functions than E-cadherin–expressing MCF10A cells.

Published OnlineFirst March 18, 2015; DOI: 10.1158/1535-7163.MCT-14-1092

Table 1. Known drugs with greater inhibitory effect on *CDH1*$^{-/-}$ cells compared with MCF10A cells

Drug name	Drug class	MCF10A EC_{50} (μmol/L)	*CDH1*$^{-/-}$ EC_{50} (μmol/L)	*CDH1*$^{-/-}$ to MCF10A ratio
Mocetinostat	HDAC inhibitor	1.76	1.02	0.58
Entinostat	HDAC inhibitor	4.31	2.50	0.58
Quisinostat	HDAC inhibitor	0.05	0.04	0.72
Pracinostat	HDAC inhibitor	0.73	0.54	0.74
LAQ824	HDAC inhibitor	0.09	0.06	0.76
Panobinostat	HDAC inhibitor	0.08	0.07	0.84
Crizotinib	ROS1-like tyrosine kinase inhibitor	5.53	3.98	0.72
PI103	PI3K inhibitor	0.75	0.59	0.79
GSK2126458	PI3K inhibitor	0.05	0.04	0.79
PIK-75 hydrochloride	PI3K inhibitor	0.08	0.07	0.89
CGP 71683 hydrochloride	NPY5R inhibitor	3.92	3.47	0.89
Tyrphostin A9	PDGFR and EGFR inhibitor	1.30	0.65	0.50
AZD8055	mTOR inhibitor	0.22	0.12	0.53
Obatoclax Mesylate	BCL2 inhibitor	0.63	0.47	0.74
Brefeldin A	Guanine nucleotide exchange factor inhibitor	0.20	0.15	0.76
LY2784544	JAK family inhibitor	5.64	4.70	0.83
FCCP	uncoupler of mitochondrial oxidative phosphorylation	3.74	2.90	0.78
JNJ-7706621	CDK and aurora kinase inhibitor	3.37	2.77	0.82
Danusertib	Inhibitor of aurora kinases, Bcr-Abl, c-RET, and FGFR	1.25	1.07	0.86
PD-166285 hydrate	Broad-spectrum tyrosine kinase inhibitor	0.66	0.58	0.88
10-DEBC hydrochloride	AKT/protein kinase B inhibitor	8.10	7.26	0.90

NOTE: EC_{50} values were obtained from 11-point dilution curves carried out in duplicate. Cell viability was determined using the CellTiter-Glo assay 48 hours after drug addition. The *CDH1*$^{-/-}$ to MCF10A ratio is a measure of the reduced viability of the *CDH1*$^{-/-}$ cells in the presence of drug.

lethal drugs were selected for further characterization if they met two criteria: (i) modest toxicity to MCF10A cells (a decrease in viability of no more than 30%) and (ii) a minimum of 15% greater reduction in *CDH1*$^{-/-}$ viability compared with the MCF10A cells at one or more concentrations. Three-hundred sixteen compounds were selected for secondary analysis using an 11 point serial dilution from 10 μmol/L to 10 nmol/L. Twenty-one of 316 compounds in this secondary screen had EC_{50} values that were 10%–50% lower in the *CDH1*$^{-/-}$ cells compared with the MCF10A cells (Table 1). These included multiple histone deacetylase (HDAC) and PI3K inhibitors, crizotinib (an inhibitor of receptor tyrosine kinases c-MET, ALK, and ROS1), CGP 71683 hydrochloride (an inhibitor of the neuropeptide receptor NPY5R) and the guanine nucleotide exchange factor inhibitor Brefeldin A. The synthetic lethality of the majority of drug classes shown in Table 1 was supported by the siRNA primary screen data with one or more targets (or associated proteins) for each being included in List SL1 (Supplementary Table S4).

The E-cadherin synthetic lethal effects of crizotinib and several HDAC inhibitors were further characterized in time course and direct cell counting studies. Saracatinib, a c-SRC kinase inhibitor not included in the 11-point screen was also further examined because of a borderline effect in the original four-point screen. Crizotinib had little effect on the growth of MCF10A cells at 0.63, 1.25, and 2.50 μmol/L up to 48 hours after drug addition, as observed using the xCELLigence system. The same concentrations, however, reduced the growth of *CDH1*$^{-/-}$ cells to 86%, 76%, and 46% of mock (Fig. 4A). Nuclei counting at 48 hours confirmed the synthetic lethal effect, although an inhibitory effect was observed on the MCF10A cells at all three concentrations (Fig. 4B). The difference between the nuclei counting method and the IncuCyte and xCELLigence methods is primarily due to cell density differences at full confluency that can only be determined by direct nuclei counting.

Treatment with saracatinib caused greater growth inhibition in the *CDH1*$^{-/-}$ cells compared with the MCF10A cells at three different concentrations in two different assay systems, cell confluence (IncuCyte) and direct nuclei counting. In the IncuCyte system, a dose-dependent inhibition was observed in both isogenic cells with the *CDH1*$^{-/-}$ cells demonstrating greater susceptibility (Fig. 4C). At 0.63 μmol/L, saracatinib had negligible effect on the confluence of MCF10A cells but caused a 26% inhibition of *CDH1*$^{-/-}$ cells (relative to DMSO) after 48 hours. Similarly, differentials of 0.17 ($P = 0.06$), 0.30 ($P = 0.02$), and 0.15 ($P = 0.10$) were observed in normalized cell counts of the *CDH1*$^{-/-}$ cells compared with the MCF10A cells at saracatinib concentrations of 0.63, 1.25, and 2.5 μmol/L, respectively (Fig. 4D).

Entinostat selectively targets class I HDACs, in particular HDAC1–3 (26). The 0.63, 1.25, and 2.5 μmol/L entinostat had a negligible effect on cell proliferation of MCF10A as determined using the xCELLigence system. In contrast, *CDH1*$^{-/-}$ cells showed 18%, 67%, and 78% growth inhibition at these concentrations 48 hours after drug addition (Fig. 4E). Comparable results were obtained using the IncuCyte (Supplementary Fig. S3). Nuclei counting also showed a significant synthetic lethal effect across the three entinostat concentrations, although, as observed previously for crizotinib, reduced nuclei count was observed in both cell lines with increasing drug concentration using this more direct method. At concentrations of 0.63, 1.25, and 2.5 μmol/L, a cell viability differential of 0.13 ($P = 0.04$), 0.23 ($P = 0.004$), and 0.14 ($P = 0.02$) was observed between the *CDH1*$^{-/-}$ cells and the MCF10A cells (Fig. 4F).

Vorinostat (SAHA) is a pan-HDAC inhibitor, acting on both class I and class II HDACs (26). Assays using the IncuCyte system showed preferential inhibition of *CDH1*$^{-/-}$ cells over 48 hours of drug treatment at 0.63, 1.25, and 2.5 μmol/L, with little effect on the MCF10A cells (Fig. 4G). This effect was confirmed on the xCELLigence system (Supplementary Fig. S3). Similar to entinostat, direct nuclei counting showed a greater effect of vorinostat on the MCF10A cells than was observed using the real-time proliferation assay platforms. A significant cell viability differential was still observed between the *CDH1*$^{-/-}$ and MCF10A cells with cell

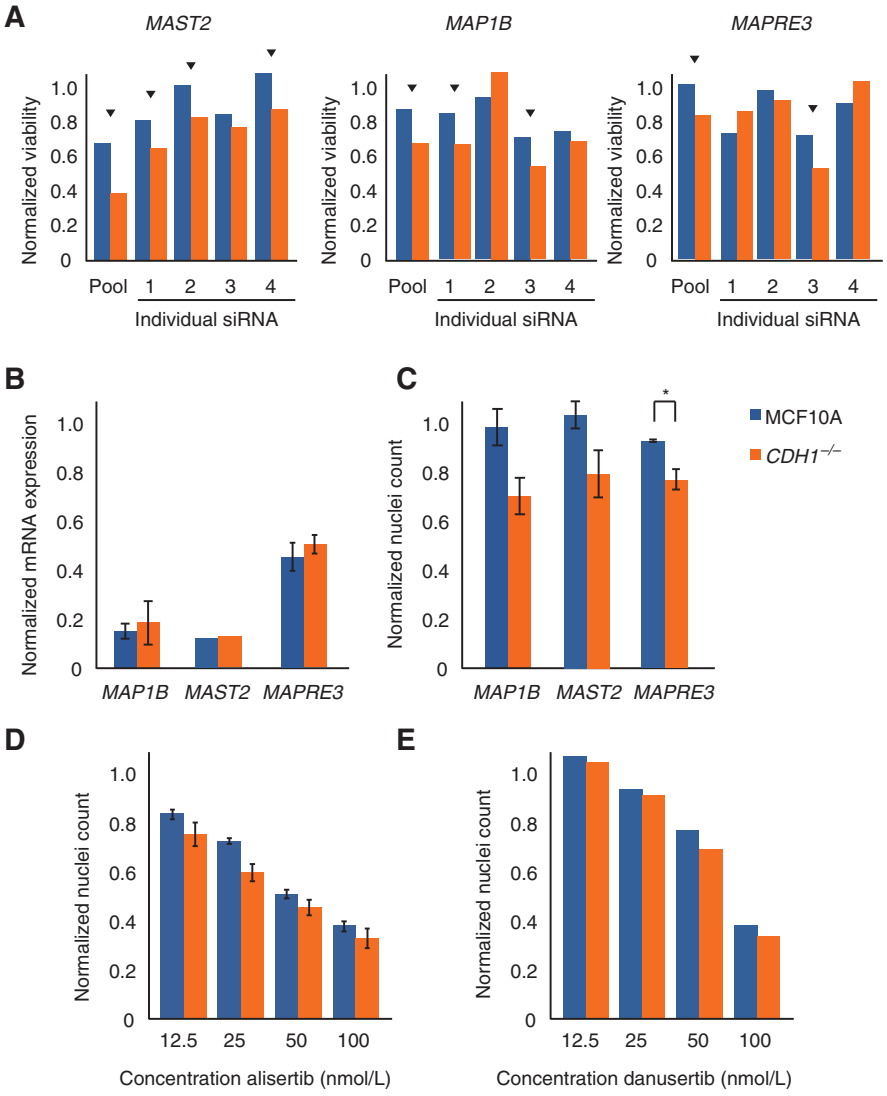

Figure 2.
Disruption of microtubule-associated proteins induces synthetic lethal effect. A, bar graphs with primary and secondary screen viability normalized to mock for *MAST2*, *MAP1B*, and *MAPRE3*. Each value is the average of two technical replicates. The arrowheads mark siRNAs that reached the synthetic lethal criteria (15% less viability in *CDH1*$^{-/-}$ cells). B, level of mRNA knockdown 72 hours after transduction with shRNA lentivirus constructs. Error bars show SE of two independent experiments, except for *MAST2* which was only assayed once. C, nuclei count normalized to nonsilencing control after knockdown with *MAP1B*, *MAST2*, and *MAPRE3* shRNA. Error bars show SE of two independent experiments. *, $P < 0.05$ by one-tailed, equal variance Student *t* test. D, nuclei count normalized to DMSO control 48 hours after alisertib treatment. Error bars show SEM of two independent experiments. E, nuclei count normalized to DMSO control 48 hours after danusertib treatment. A single experiment is shown.

E-cadherin–deficient MCF10A cells show vulnerabilities in GPCR signaling

Gene ontology analysis (21) identified >200 genes from our list of synthetic lethal candidates (List SL1) that were associated with GPCR protein signaling pathways. These candidates included several proteins involved in signal transduction from activated GPCRs such as the G protein subunits GNAS, GNAT1, GNG2, and GNG5, the membrane bound adenyl cyclase ADCY7 and the downstream signaling protein JAK2. *ADCY7* validated in the secondary screen with 4 of 4 siRNAs recapitulating the SMARTpool phenotype (Fig. 3A). The synthetic lethal effect of the *JAK2* siRNA SMARTpool was confirmed using lentiviral-mediated shRNA transduction. Both the siRNA SMARTpool and lentiviral shRNA knocked down *JAK2* mRNA by >44% (Fig. 3B). Normalized cell numbers after transduction were significantly lower in the *CDH1*$^{-/-}$ cells compared with the MCF10A cells for both the siRNA pool and the shRNA (Fig. 3C). To determine whether the synthetic lethality of *JAK2* downregulation could be mimicked using a JAK2 antagonist, we treated the isogenic *CDH1* MCF10A cell line pair with the JAK inhibitor LY2784544. Using the xCELLigence system to monitor cell growth in real time, LY2784544 had only a modest effect on MCF10A cells at 0.32, 0.63, and 1.25 μmol/L concentrations; however, the cell proliferation index was reduced in the *CDH1*$^{-/-}$ cells in a concentration-dependent manner. Forty-eight hours after drug addition, the three concentrations of LY2784544 resulted in a 15%, 29%, and 51% reduction in *CDH1*$^{-/-}$ cell number, respectively (Fig. 3D). In contrast, the three drug concentrations reduced MCF10A cell number by 0%, 11%, and 10%, respectively. A second JAK2 inhibitor, AG490, showed a similar synthetic lethal response in xCELLigence assays (data not shown). Further real-time assays using the IncuCyte replicated this effect (Supplementary Fig. S3). Nuclei counting confirmed a significant synthetic lethal effect at LY2784544 concentrations of 1.25 μmol/L

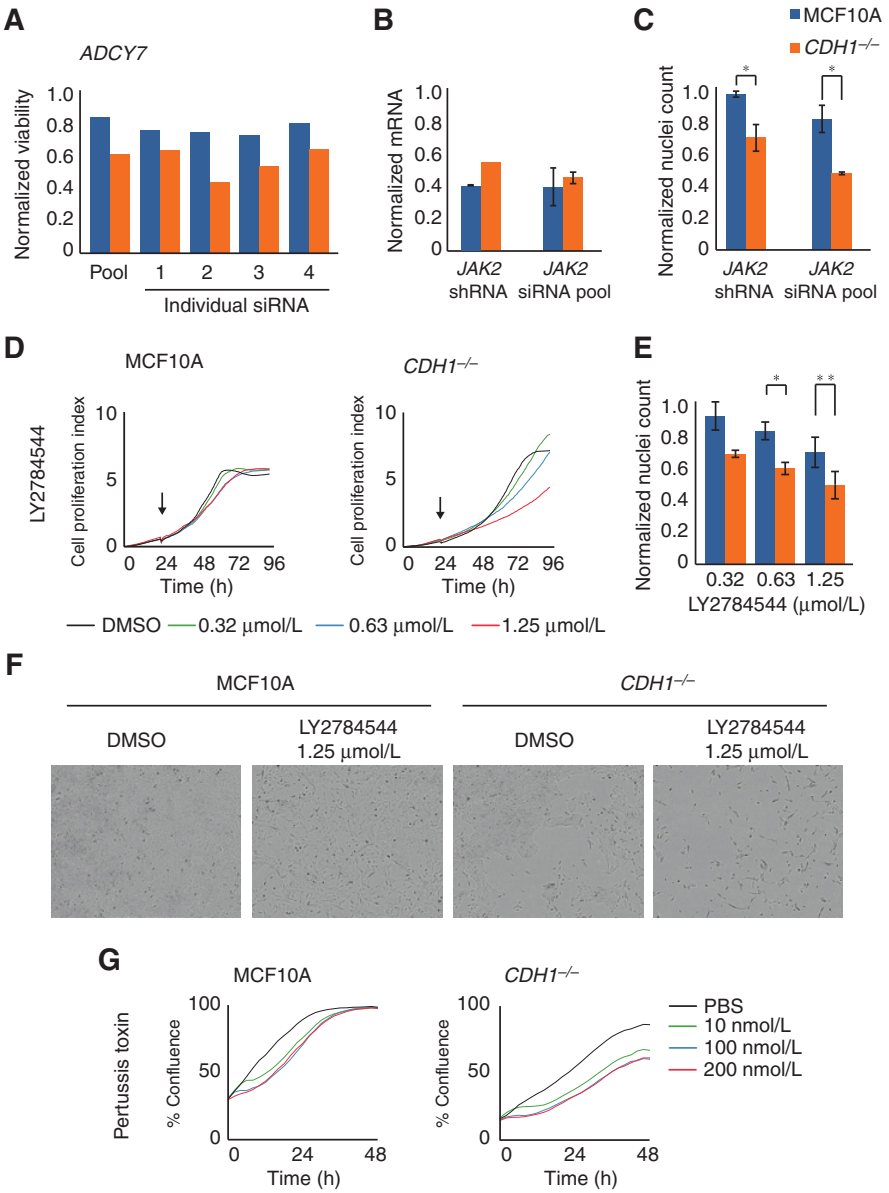

Figure 3.
Disruption of GPCR-associated proteins causes synthetic lethality. A, bar graphs with primary and secondary screen viability normalized to mock for *ADCY7*. Each value is the average of two technical replicates. All siRNA reached the synthetic lethal criteria. B, normalized mRNA levels after knockdown by *JAK2* shRNA and siRNA pool. C, nuclei counts normalized to nonsilencing (shRNA) or mock (siRNA) controls after knockdown by *JAK2* RNAi. D, representative xCELLigence experiment for cells treated with LY2784544. Arrow marks time when compound was added. E, nuclei count normalized to DMSO 48 hours after LY2784544 treatment. F, images taken 48 hours after LY2784544 treatment showing reduced confluence and morphologic changes. G, representative IncuCyte assay showing confluence over 48 hours after Pertussis toxin treatment. Error bars show SE of at least two independent experiments. *, $P < 0.05$; **, $P < 0.01$ by the one-tailed, equal variance Student *t* test.

($P = 0.005$) and 0.63 µmol/L ($P = 0.03$) (Fig. 3E). LY2784544 resulted in cells becoming more spindle shaped, with an increased number of extended filopodia; this effect was particularly marked in the $CDH1^{-/-}$ cells (Fig. 3F).

The presence of G protein subunits in list SL1 prompted us to examine *CDH1* synthetic lethality using the Gαi and Gαo subunit inhibitor Pertussis toxin (25). Treatment of MCF10A and $CDH1^{-/-}$ cells with 10, 100, and 200 ng/mL of Pertussis toxin over a period of 48 hours resulted in growth inhibition of both MCF10A and $CDH1^{-/-}$ cell lines in a concentration-dependent manner (Fig. 3G). However, the MCF10A cells recovered and reached the same confluence as the PBS control after 48 hours, whereas the $CDH1^{-/-}$ cells showed 20%–30% less confluence at that time point for the three drug concentrations.

E-cadherin loss sensitizes MCF10A cells to HDAC inhibitors and other drug classes

To explore how E-cadherin loss alters sensitivity of MCF10A cells to other known drugs, we screened 4,057 compounds against the *CDH1* MCF10A isogenic cell line pair. The compounds comprised the WEHI known drug library (3,600 compounds from the Tocriscreen Total library, the Prestwick Chemical Library and the "Lopac 1280" library), the Selleck Chemistry inhibitor library (326 compounds consisting of approximately half known drugs and half kinase inhibitors) and a kinase inhibitor library (131 compounds supplied by SYNthesis Medicinal Chemistry). The initial screen covered four drug concentrations ranging from 0.25 to 2 µmol/L, with cell viability measured at 48 hours after drug addition using the CellTiter-Glo assay. Potential synthetic

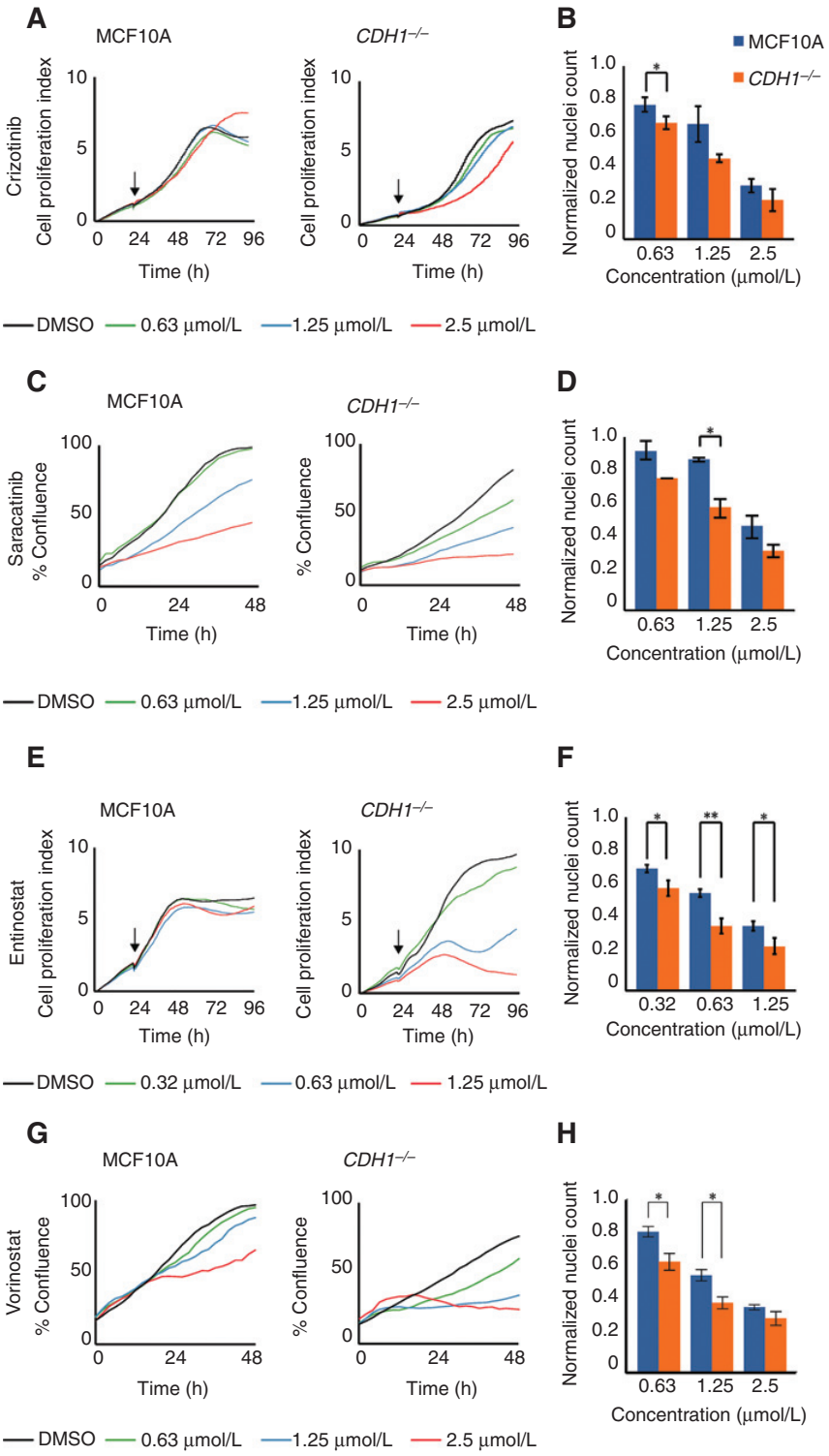

Figure 4.
Treatment with various known drugs causes *CDH1* synthetic lethality. A and E, representative xCELLigence assay of cells treated with crizotinib (A) and entinostat (E). Cells were seeded at 4,000 or 2,000 (crizotinib) cells per well and drug was added at 24 hours. Cells were grown for an additional 72 hours. C and G, representative IncuCyte assays of cells treated with saracatinib (C) and vorinostat (G). Cells were seeded at 4,000 cells per well and drug was added at 24 hours. Cells were then grown for an additional 48 hours. B, D, F and H, nuclei counts normalized to DMSO after treatment with crizotinib (B), saracatinib (D), entinostat (F), and vorinostat (H). Error bars show SE of at least two independent experiments. *, $P < 0.05$; **, $P < 0.01$ determined by the one-tailed, equal variance Student t test.

viability differentials of 0.21 ($P = 0.02$), 0.29 ($P = 0.01$), and 0.17 ($P = 0.10$) between *CDH1*$^{-/-}$ and MCF10A at concentrations of 0.63, 1.25, and 2.5 μmol/L (Fig. 4H). The HDAC inhibitors mocetinostat and pracinostat showed comparable synthetic lethal effects when assayed at 0.63, 1.25, and 2.5 μmol/L on the xCELLigence system (Supplementary Fig. S4A and S4B). The class

Published OnlineFirst March 16, 2015; DOI: 10.1158/1535-7163.MCT-14-1062

I/II HDAC inhibitor valproic acid also showed a minor synthetic lethal effect when assayed by direct nuclei counting (Supplementary Fig. S4C).

Previous reports of synergy between HDAC inhibitors and taxol (27–30) prompted us to test combinations of taxol and each of vorinostat and entinostat in our isogenic cell line pair. CompuSyn (ComboSyn Inc) was used to calculate EC_{50} concentrations, and to determine the Combination Index. In contrast to other studies, we found no evidence for synergy between taxol and these HDAC inhibitors (Supplementary Fig. S2).

Discussion

Synthetic lethality provides a potential method to target cancers carrying inactivating mutations in tumor suppressor genes such as the E-cadherin gene, *CDH1*. To provide an initial survey of E-cadherin's synthetic lethal interactions, we conducted a genome-wide functional screen of nonmalignant, isogenic MCF10A cells with and without E-cadherin expression. Thirteen percent of the 18,120 genes in the siRNA screen met our threshold for synthetic lethality of at least 15% more death in the $CDH1^{-/-}$ cells than the wild-type MCF10A cells. Although this threshold is low stringency and subsequently not highly specific, it is clear that E-cadherin deficiency creates large numbers of vulnerabilities in nonmalignant cells which are exposed by genetic knockdown of additional genes.

Gene ontology analysis identified a striking enrichment for GPCR signaling proteins among the synthetic lethal candidates. Notably, this enrichment was greater for hits that showed minimal impact on the viability of the E-cadherin–expressing MCF10A cells, suggesting that drug targeting of GPCR signaling in *CDH1*-mutant tumors may be a means to obtain clinical gain while minimizing collateral damage to normal tissues. The nature of the synthetic lethal relationship between E-cadherin and GPCR signaling is not yet known, although the functional diversity of the candidate synthetic lethal GPCR signaling proteins would suggest that the interaction involves a common downstream mechanism such as interplay with the actin and microtubule cytoskeletons (31–33). The importance of cytoskeletal functions to the E-cadherin synthetic lethal phenotype is supported by the abundance of cytoskeletal genes associated with synthetic lethality in our primary siRNA screen. These genes were involved in all aspects of cytoskeletal function, including the nucleation, organization, and function of microtubules mitotic spindle organization and control, linkages between the cytoskeleton and nucleoskeleton, polarity, actin filament organization, vesicle transport, focal adhesion kinase signaling, and Rho-mediated motility (8, 34–36). The increased vulnerability of E-cadherin–deficient MCF10A cells to knockdown of so many diverse but inter-related functions is consistent with the widespread disorganization of cytoskeletal networks observed in the $CDH1^{-/-}$ cells (7). Notably, after *CDH1* and *TP53*, *RHOA* is the most commonly mutated gene in DGC (37–39), emphasizing the importance of dysregulated cytoskeletal function to development of the diffuse phenotype.

The increased vulnerability of E-cadherin–deficient MCF10A cells to RNAi knockdown of cytoskeletal and GPCR signaling genes was supported by the increased sensitivity of these cells to antagonists of multiple protein families associated with GPCR signaling and cytoskeletal function, including HDACs (40, 41), JAK (42), aurora kinases (43), c-SRC tyrosine kinase (44), G-protein subunits and PI3K (45). The enrichment for GPCR signaling genes among our synthetic lethal candidates does not, however, exclude the possibility that other signaling functions, such as the cytokine responses of JAK2, may also be associated with synthetic lethality. EC_{50} differences between MCF10A and $CDH1^{-/-}$ cells for these known drugs were on average only approximately 25% less in the $CDH1^{-/-}$ cells. This small differential is to be expected as neither MCF10A or $CDH1^{-/-}$ cells are tumorigenic and therefore these lines cannot be distinguished by the presence/absence of addiction to the targeted pathways. Synthetic lethal drugs which are significantly more potent in E-cadherin–deficient cells will be more readily identified using fit-for-purpose, high-throughput compound screens across the MCF10A and other *CDH1* isogenic cell line pairs. Differences between the E-cadherin–expressing and E-cadherin–deficient cells may also be more pronounced in phenotypes other than cell viability, such as invasive capability.

This research demonstrates for the first time that loss of the tumor suppressor protein E-cadherin creates druggable vulnerabilities in cells. It remains to be determined whether any of the observed drug sensitivities in $CDH1^{-/-}$ cells will be robust to the genetic dysregulation of advanced tumors, and therefore able to provide additional clinical benefit in the treatment of sporadic *CDH1*-mutant tumors. Instead, the observed sensitivities may have more near term application to HDGC chemoprevention. The natural history of cancer development in *CDH1* germline mutation carriers involves the development of multifocal lobular carcinoma *in situ* (46, 47) and tens to hundreds of gastric stage T1a signet ring cell carcinomas before the onset of advanced disease (11, 48, 49). The high multiplicity of these early stage foci argues against additional genetic hits being required for their initiation. These early breast and gastric cancers are therefore relatively genetically homogenous and distinguished from normal tissue predominantly by the cellular changes associated with deficiency of E-cadherin. As a consequence, the E-cadherin synthetic lethal interactions identified in the nonmalignant breast MCF10A cells provide strong leads for drugs that may eliminate early-stage disease in germline *CDH1* mutation carriers, potentially providing a new clinical management option for HDGC families.

Disclosure of Potential Conflicts of Interest

No potential conflicts of interest were disclosed.

Authors' Contributions

Conception and design: A. Chen, K.J. Simpson, P. Guilford

Development of methodology: B.J. Telford, A. Chen, H. Beetham, J. Frick, T.P. Brew, A. Single, T. Godwin, K.J. Simpson, P. Guilford

Acquisition of data (provided animals, acquired and managed patients, provided facilities, etc.): B.J. Telford, A. Chen, J. Frick, T.P. Brew, A. Single, T. Godwin, K.J. Simpson, P. Guilford

Analysis and interpretation of data (e.g., statistical analysis, biostatistics, computational analysis): B.J. Telford, A. Chen, J. Frick, T.P. Brew, C.M. Gould, A. Single, K.J. Simpson, P. Guilford

Writing, review, and/or revision of the manuscript: B.J. Telford, A. Chen, H. Beetham, T.P. Brew, A. Single, K.J. Simpson, P. Guilford

Administrative, technical, or material support (i.e., reporting or organizing data, constructing databases): B.J. Telford, A. Chen, H. Beetham, C.M. Gould, P. Guilford

Study supervision: A. Chen, K.J. Simpson, P. Guilford

Acknowledgments

VCFG technical expertise was provided by Daniel Thomas and Yanny Handoko. Lentiviral expertise and training was provided by Dr. Stephanie Hughes and Hollie Wicky. Compound screening was performed at the Walter Eliza Hall Institute under the supervision of Dr. Kurt Lackovic.

Published OnlineFirst March 16, 2015; DOI: 10.1158/1535-7163.MCT-14-1052

Grant Support

This work was supported by the New Zealand Health Research Council (grant number 11/513 to P. Guilford) and the University of Otago (PhD Fellowships to B. Telford, H. Beetham, and A. Single). Additional funding support was received from No Stomach for Cancer Inc, the Degregario Family Foundation and the New Zealand Breast Cancer Research Partnership. The Victorian Centre for Functional Genomics (to K. Simpson) is funded by the Australian Cancer Research Foundation (ACRF), the Victorian Department of Industry, Innovation and Regional Development (DIIRD), the Australian Phenomics Network (APN) supported by funding from the Australian Government's Education Investment Fund through the Super Science Initiative, the Australasian Genomics Technologies Association (AMATA), the Brockhoff Foundation, and the Peter MacCallum Cancer Centre Foundation.

The costs of publication of this article were defrayed in part by the payment of page charges. This article must therefore be hereby marked *advertisement* in accordance with 18 U.S.C. Section 1734 solely to indicate this fact.

Received December 26, 2014; revised February 16, 2015; accepted March 6, 2015; published OnlineFirst March 16, 2015.

References

1. Berx G, van Roy F. Involvement of members of the cadherin superfamily in cancer. Cold Spring Harb Perspect Biol 2009;1:a003129.
2. Mohamet L, Hawkins K, Ward CM. Loss of function of e-cadherin in embryonic stem cells and the relevance to models of tumorigenesis. J Oncol 2011;2011:352616.
3. Jeanes A, Gottardi CJ, Yap AS. Cadherins and cancer: how does cadherin dysfunction promote tumor progression? Oncogene 2008;27:6920–9.
4. Guilford P, Hopkins J, Harraway J, McLeod M, McLeod N, Harawira P, et al. E-cadherin germline mutations in familial gastric cancer. Nature 1998; 392:402–5.
5. Corso G, Carvalho J, Marrelli D, Vindigni C, Carvalho B, Seruca R, et al. Somatic mutations and deletions of the E-cadherin gene predict poor survival of patients with gastric cancer. J Clin Oncol 2013;31:868–75.
6. Vlug E, Ercan C, van der Wall E, van Diest PJ, Derksen PW. Lobular breast cancer: pathology, biology, and options for clinical intervention. Arch Immunol Ther Exp 2013;62:7–21.
7. Chen A, Beetham H, Black MA, Priya R, Telford BJ, Guest J, et al. E-cadherin loss alters cytoskeletal organization and adhesion in non-malignant breast cells but is insufficient to induce an epithelial-mesenchymal transition. BMC Cancer 2014;14:552.
8. Brieher WM, Yap AS. Cadherin junctions and their cytoskeleton(s). Curr Opin Cell Biol 2013;25:39–46.
9. den Elzen N, Buttery CV, Maddugoda MP, Ren G, Yap AS. Cadherin adhesion receptors orient the mitotic spindle during symmetric cell division in mammalian epithelia. Mol Biol Cell 2009;20:3740–50.
10. Zou D, Yoon HS, Perez D, Weeks RJ, Guilford P, Humar B. Epigenetic silencing in non-neoplastic epithelia identifies E-cadherin (CDH1) as a target for chemoprevention of lobular neoplasia. J Pathol 2009;218: 265–72.
11. Humar B, Blair V, Charlton A, More H, Martin I, Guilford P. E-cadherin deficiency initiates gastric signet-ring cell carcinoma in mice and man. Cancer Res 2009;69:2050–6.
12. Humar B, Guilford P. Hereditary diffuse gastric cancer and lost cell polarity: a short path to cancer. Future Oncol (London, England) 2008;4:229–39.
13. Thiery JP, Acloque H, Huang RY, Nieto MA. Epithelial-mesenchymal transitions in development and disease. Cell 2009;139:871–90.
14. Fong PC, Yap TA, Boss DS, Carden CP, Mergui-Roelvink M, Gourley C, et al. Poly(ADP)-ribose polymerase inhibition: frequent durable responses in BRCA carrier ovarian cancer correlating with platinum-free interval. J Clin Oncol 2010;28:2512–9.
15. Gelmon KA, Tischkowitz M, Mackay H, Swenerton K, Robidoux A, Tonkin K, et al. Olaparib in patients with recurrent high-grade serous or poorly differentiated ovarian carcinoma or triple-negative breast cancer: a phase 2, multicentre, open-label, non-randomised study. Lancet Oncol 2011; 12:852–61.
16. Kamentsky L, Jones TR, Fraser A, Bray MA, Logan DJ, Madden KL, et al. Improved structure, function and compatibility for CellProfiler: modular high-throughput image analysis software. Bioinformatics 2011;27:1179–80.
17. Pfaffl MW. A new mathematical model for relative quantification in real-time RT-PCR. Nucleic Acids Res 2001;29:2002–7.
18. Chou TC, Talalay P. Quantitative analysis of dose-effect relationships: the combined effects of multiple drugs or enzyme inhibitors. Adv Enzyme Regul 1984;22:27–55.
19. Petrocca F, Altschuler G, Tan SM, Mendillo ML, Yan H, Jerry DJ, et al. A genome-wide siRNA screen identifies proteasome addiction as a vulnerability of basal-like triple-negative breast cancer cells. Cancer Cell 2013;24:182–96.
20. Lee AS, Burdeinick-Kerr R, Whelan SP. A genome-wide small interfering RNA screen identifies host factors required for vesicular stomatitis virus infection. J Virol 2014;88:8355–60.
21. Huang da W, Sherman BT, Lempicki RA. Systematic and integrative analysis of large gene lists using DAVID bioinformatics resources. Nat Protoc 2009;4:44–57.
22. Garland P, Quraishe S, French P, O'Connor V. Expression of the MAST family of serine/threonine kinases. Brain Res 2008;1195:12–9.
23. Villarroel-Campos D, Gonzalez-Billault C. The MAP1B case: an old MAP that is new again. Dev Neurobiol 2014;74:953–71.
24. Akhmanova A, Steinmetz MO. Tracking the ends: a dynamic protein network controls the fate of microtubule tips. Nat Rev Mol Cell Biol 2008;9:309–22.
25. Clark MJ, Traynor JR. Assays for G-protein-coupled receptor signaling using RGS-insensitive Galpha subunits. Methods Enzymol 2004;389:155–69.
26. Dickinson M, Johnstone RW, Prince HM. Histone deacetylase inhibitors: potential targets responsible for their anti-cancer effect. Invest New Drugs 2010;28 Suppl 1:S3–20.
27. Shi YK, Li ZH, Han XQ, Yi JH, Wang ZH, Hou JL, et al. The histone deacetylase inhibitor suberoylanilide hydroxamic acid induces growth inhibition and enhances taxol-induced cell death in breast cancer. Cancer Chemother Pharmacol 2010;66:1131–40.
28. Dietrich CS III, Greenberg VL, DeSimone CP, Modesitt SC, van Nagell JR, Craven R, et al. Suberoylanilide hydroxamic acid (SAHA) potentiates paclitaxel-induced apoptosis in ovarian cancer cell lines. Gynecol Oncol 2010;116:126–30.
29. Owonikoko TK, Ramalingam SS, Kanterewicz B, Balius TE, Belani CP, Hershberger PA. Vorinostat increases carboplatin and paclitaxel activity in non-small-cell lung cancer cells. Int J Cancer 2010;126:743–55.
30. Dowdy SC, Jiang S, Zhou XC, Hou X, Jin F, Podratz KC, et al. Histone deacetylase inhibitors and paclitaxel cause synergistic effects on apoptosis and microtubule stabilization in papillary serous endometrial cancer cells. Mol Cancer Ther 2006;5:2767–76.
31. Ganguly S, Saxena R, Chattopadhyay A. Reorganization of the actin cytoskeleton upon G-protein coupled receptor signaling. Biochim Biophys Acta 2011;1808:1921–9.
32. Schappi JM, Krbanjevic A, Rasenick MM. Tubulin, actin and heterotrimeric G proteins: coordination of signaling and structure. Biochim Biophys Acta 2014;1838:674–81.
33. Saengsawang W, Rasenick MM. Heterotrimeric G proteins and microtubules. Methods Cell Biol 2013;115:173–89.
34. Kollman JM, Merdes A, Mourey L, Agard DA. Microtubule nucleation by gamma-tubulin complexes. Nat Rev Mol Cell Biol 2011;12:709–21.
35. Sulzmaier FJ, Jean C, Schlaepfer DD. FAK in cancer: mechanistic findings and clinical applications. Nat Rev 2014;14:598–610.
36. Hall A. The cytoskeleton and cancer. Cancer Metastasis Rev 2009;28:5–14.
37. Kakiuchi M, Nishizawa T, Ueda H, Gotoh K, Tanaka A, Hayashi A, et al. Recurrent gain-of-function mutations of RHOA in diffuse-type gastric carcinoma. Nat Genet 2014;46:583–7.
38. Cancer Genome Atlas Research N. Comprehensive molecular characterization of gastric adenocarcinoma. Nature 2014;513:202–9.
39. Wang K, Yuen ST, Xu J, Lee SP, Yan HH, Shi ST, et al. Whole-genome sequencing and comprehensive molecular profiling identify new driver mutations in gastric cancer. Nat Genet 2014;46:573–82.

Published OnlineFirst March 16, 2015; DOI: 10.1158/1535-7163.MCT-14-1092

40. Spiegelberg BD. G protein coupled-receptor signaling and reversible lysine acetylation. J Recept Signal Transduct Res 2013;33:261–6.
41. Schemies J, Sippl W, Jung M. Histone deacetylase inhibitors that target tubulin. Cancer Lett 2009;280:222–32.
42. Pelletier S, Duhamel F, Coulombe P, Popoff MR, Meloche S. Rho family GTPases are required for activation of Jak/STAT signaling by G protein-coupled receptors. Mol Cell Biol 2003;23:1316–33.
43. Hochegger H, Hegarat N, Pereira-Leal JB. Aurora at the pole and equator: overlapping functions of Aurora kinases in the mitotic spindle. Open Biol 2013;3:120185.
44. Luttrell LM, Hawes BE, van Biesen T, Luttrell DK, Lansing TJ, Lefkowitz RJ. Role of c-Src tyrosine kinase in G protein-coupled receptor- and Gbeta-gamma subunit-mediated activation of mitogen-activated protein kinases. J Biol Chem 1996;271:19443–50.
45. Fritsch R, de Krijger I, Fritsch K, George R, Reason B, Kumar MS, et al. RAS and RHO families of GTPases directly regulate distinct phosphoinositide 3-kinase isoforms. Cell 2013;153:1050–63.
46. Blair VR. Hereditary diffuse gastric cancer: Of mice and man. Auckland, New Zealand: PhD thesis, University of Auckland; 2008.
47. Petridis C, Shinomiya I, Kohut K, Gorman P, Caneppele M, Shah V, et al. Germline CDH1 mutations in bilateral lobular carcinoma in situ. Br J Cancer 2014;110:1053–7.
48. Charlton A, Blair V, Shaw D, Parry S, Guilford P, Martin IG. Hereditary diffuse gastric cancer: predominance of multiple foci of signet ring cell carcinoma in distal stomach and transitional zone. Gut 2004;53:814–20.
49. Fitzgerald RC, Hardwick R, Huntsman D, Carneiro F, Guilford P, Blair V, et al. Hereditary diffuse gastric cancer: updated consensus guidelines for clinical management and directions for future research. J Med Genet 2010;47:436–44.

Appendix B.

A Comparison of Real-Time and Endpoint Cell Viability Assays for Improved Synthetic Lethal Drug Validation

Technical Note

A Comparison of Real-Time and Endpoint Cell Viability Assays for Improved Synthetic Lethal Drug Validation

Journal of Biomolecular Screening
2015, Vol. 20(10) 1286–1293

DOI: 10.1177/1087057115605765
jbx.sagepub.com
SAGE

Andrew Single[1], Henry Beetham[1], Bryony J. Telford[1], Parry Guilford[1], and Augustine Chen[1]

Abstract

Cell viability assays fulfill a central role in drug discovery studies. It is therefore important to understand the advantages and disadvantages of the wide variety of available assay methodologies. In this study, we compared the performance of three endpoint assays (resazurin reduction, CellTiter-Glo, and nuclei enumeration) and two real-time systems (IncuCyte and xCELLigence). Of the endpoint approaches, both the resazurin reduction and CellTiter-Glo assays showed higher cell viabilities when compared directly to stained nuclei counts. The IncuCyte and xCELLigence real-time systems were comparable, and both were particularly effective at tracking the effects of drug treatment on cell proliferation at sub-confluent growth. However, the real-time systems failed to evaluate contrasting cell densities between drug-treated and control-treated cells at full growth confluency. Here, we showed that using real-time systems in combination with endpoint assays alleviates the disadvantages posed by each approach alone, providing a more effective means to evaluate drug toxicity in monolayer cell cultures. Such approaches were shown to be effective in elucidating the toxicity of synthetic lethal drugs in an isogenic pair of MCF10A breast cell lines.

Keywords

cell-based assays, imaging technologies, label-free technologies, multiplex assays and technology

Introduction

In vitro viability assays are essential tools for drug development, allowing for the assessment of drug efficacy prior to subsequent in vivo analyses. Whether performed as a single-plate experiment or as part of a high-throughput screen, the concept remains the same—cells are incubated with a particular compound(s), then assessed for viability to quantify drug-induced cell toxicity.

Numerous commercial cell viability assays that exploit different cellular processes to quantify cytotoxicity are now available, each highlighting the variability that can be obtained from different methodologies.[1–3] Consequently, the selection and application of an effective assay(s) should be a major consideration in any drug-based experimental design.

A widely used approach to determine drug-induced cytotoxicity involves measuring cellular metabolic activity at the conclusion of an experiment. Such approaches include the 3-[4,5-dimethylthiazolyl-2]-2,5-diphenyltetrazolium bromide (MTT) assay, resazurin reduction, and the CellTiter-Glo assay, each using a different aspect of cellular metabolism as a means of quantifying live cells. The MTT assay relies on the mitochondrial activity of live cells to convert a yellow MTT substrate into purple formazan crystals, detectable via spectrophotometry.[4] The resazurin reduction assay, used in alamarBlue and CellTiter-Blue assays, is a more sensitive alternative to MTT and uses the intracellular reduction potential of living cells to convert resazurin to the fluorescent product resorufin.[5] CellTiter-Glo adopts the use of firefly luciferase, which reacts with available cellular adenosine triphosphate (ATP) to produce a bioluminescent signal proportional to the number of live cells present in the assay.[6] The nuclei counting method, which is a direct measure of viability, is considered to be the most accurate;[1] however, the ease of mix-and-measure metabolic-based approaches makes them a common feature in high-throughput drug screens.

Unlike endpoint approaches, real-time assay systems allow for the tracking of cellular growth over the entire time course of an experiment. This is particularly effective for

[1]Cancer Genetics Laboratory, Department of Biochemistry, University of Otago, Dunedin, New Zealand

Received Jun 21, 2015, and in revised form Jul 31, 2015. Accepted for publication Aug 23, 2015.

Corresponding Author:
Augustine Chen, Cancer Genetics Laboratory, Department of Biochemistry, University of Otago, P.O. Box 56, 710 Cumberland Street, Dunedin, 9054, New Zealand.
Email: augustine.chen@otago.ac.nz

assessing the impact of cytostatic compounds, where subtle growth inhibitory effects are easily noticeable but may be missed using endpoint-based methods. Real-time assays are typically performed using equipment capable of capturing images at regular intervals and quantifying cellular surface area coverage as a measure of proliferation (e.g., IncuCyte FLR; Essen BioScience, Ann Arbor, MI). Such methods also facilitate visualization of drug-induced cell morphology changes. Alternatives to this approach include the xCELLigence (ACEA Biosciences, San Diego, CA), which uses electrical impedance to measure both cellular adhesion strength and surface area coverage as a combined proxy of cellular proliferation.

In this study, we compared the performance of five different cell-based viability assays. Three endpoint assays (resazurin reduction, CellTiter-Glo, and nuclei enumeration) and two real-time assays (IncuCyte and xCELLigence) were used to investigate the effectiveness of each approach for the validation of candidate synthetic lethal drugs in an isogenic pair of MCF10A breast cell lines.

Materials and Methods

Cell Culture

MCF10A and the derived *CDH1*-negative isogenic line (MCF10A *CDH1*$^{-/-}$) were purchased from Sigma-Aldrich (St. Louis, MO). Cells were cultured in Dulbecco's modified Eagle's medium (DMEM)/F12 (1:1; Life Technologies, Carlsbad, CA) with 5% horse serum (Life Technologies), 10 μg/ml insulin (Novo Nordisk Pharmaceuticals Ltd, Bagsvaerd, Denmark), 20 ng/ml human epidermal growth factor (Peprotech, Rocky Hill, NJ), 100 ng/ml cholera toxin (Sigma-Aldrich), and 500 ng/ml hydrocortisone (Sigma-Aldrich).[7] The cells were cultured in exponential growth phase at 37 °C and 5% CO_2.[7,8] An isogenic MCF10A cell line pair was selected to demonstrate drug-induced synthetic lethal phenotypes against *CDH1* in a nonmalignant cell background.

Vorinostat was purchased from SelleckChem (Houston, TX), and paclitaxel (Taxol) was purchased from Sigma-Aldrich. Both drugs were reconstituted in 100% DMSO, stored at −80 °C, and individual aliquots were diluted to working stocks in complete growth medium prior to use in an experiment. Vorinostat, a histone deacetylase inhibitor, was selected because it has previously demonstrated selective lethality toward *CDH1*-deficient MCF10A cells.[9] Taxol was chosen as a chemotherapeutic agent that demonstrated nondiscriminate lethality in the MCF10A isogenic cell line pair.

Endpoint Assays

MCF10A and MCF10A *CDH1*$^{-/-}$ cells were seeded at 4×10^3 cells per well in 96-well, black-walled, clear-bottomed tissue culture plates (Corning, Corning, NY) in 100 μL complete growth medium and left to equilibrate at room temperature for 30 min before incubation at 37 °C. After overnight incubation, cells were treated in triplicate with drug or DMSO for controls. Endpoint assays were performed at 48 h post drug treatment. For resazurin reduction assays, resazurin (Sigma-Aldrich) was made to 440 μM stock solutions in phosphate buffered saline (PBS) and aliquoted for storage at −20 °C. Resazurin solution was added to cells at 20% final concentration, and plates were incubated for 3 h at 37 °C prior to reading fluorescence at 550 nm excitation and 590 nm emission using a POLARstar Optima (BMG Labtech, Ortenberg, Germany). For luminescent assays, CellTiter-Glo (Promega, Madison, WI) was added at 20% final concentration. Earlier optimization had shown this concentration to consistently reproduce the manufacturer's recommended 1:1 vol/vol ratio (results not shown). Luminescent readings were obtained using a POLARstar Optima after 10 min incubation at room temperature with shaking. For nuclei counting assays, Hoechst 33342 (Life Technologies) was added at 1 μg/mL final concentration and incubated for 30 min in the dark at 37 °C with shaking. Plates were then imaged at four fields per well under 4× magnification using the Cytell Cell Imaging System (GE Healthcare, Buckinghamshire, United Kingdom), and imaged nuclei were enumerated using CellProfiler[10] to obtain a total cell count. For direct comparison between total cell count and measured confluency performed in the IncuCyte FLR, SYTOX (Life Technologies) was used in place of Hoechst for nuclei enumeration because this IncuCyte model only has a single, green fluorescence filter. A one-step, no-wash, mild permeabilization and fixation protocol was adopted from Chan et al. (2013),[1] using a final concentration of 0.25% paraformaldehyde, 0.075% saponin, and 10 nM SYTOX. Because the SYTOX dye stains only membrane-compromised cells, permeabilization was required to obtain a total cell count.

xCELLigence Assays

Experiments conducted on the RTCA-MP xCELLigence system (ACEA Biosciences, San Diego, CA) were performed in accordance with the instructions of the supplier. Complete growth medium (100 μL) was added into each well of the E-plate 96 (ACEA Biosciences), followed by a brief background impedance measurement on the RTCA-MP station. MCF10A and MCF10A *CDH1*$^{-/-}$ cells were seeded at 4×10^3 cells per well in 100 μL complete growth medium, and, after 30 min equilibration at room temperature, the E-plate was placed in the RTCA-MP station. The RTCA-MP station was housed in a humidified cell culture incubator at 37 °C and 5% CO_2. Cell proliferation, as determined by electrical impedance, was recorded at 15-min intervals. After overnight incubation, the assay was paused, 10 μL medium was removed from each well, and cells were treated

with 10 µL drug or 0.1% DMSO for controls. The assay was then resumed, taking impedance measurements every 15 min for a further 48 h. All xCELLigence experiments were performed in duplicate.

IncuCyte Assays

MCF10A and MCF10A *CDH1*$^{-/-}$ cells were seeded at 4×10^3 cells per well in 96-well, black-walled, clear-bottomed, tissue culture plates in 100 µL complete growth medium and left to equilibrate at room temperature for 30 min before 37 °C, 5% CO_2 incubation. After overnight incubation, cells were treated with 10 µL drug or 0.1% DMSO for controls, and the plate was inserted into the IncuCyte FLR for real-time imaging, with three fields imaged per well under 4× magnification every 2 h for a total of 48 h. Data were analyzed using the IncuCyte Confluence version 1.5 software, which quantified cell surface area coverage as confluence values. All IncuCyte experiments were performed in triplicate.

Results and Discussion

Metabolic and Nuclei-Counting Endpoint Assays

First, we compared the performance of two metabolic-based assays alongside a nuclei-counting one. The resazurin reduction and CellTiter-Glo assays were chosen ahead of the MTT assay because previous studies have reported reduced sensitivity with MTT compared to other endpoint methods.[11,12] To compare the efficacy of each assay, MCF10A and MCF10A *CDH1*$^{-/-}$ cells were treated with vorinostat for 48 h and assessed for cell viability using each method. A dose-dependent effect was observed in all three methods with increasing vorinostat concentration in both cell lines. In both MCF10A and MCF10A *CDH1*$^{-/-}$ cells, 0.63 µM vorinostat treatment showed negligible viability inhibition with no marked differences observed between the two metabolic assays. At dosages of 1.25 and 2.5 µM vorinostat, however, the CellTiter-Glo assay gave significantly higher viabilities than the resazurin reduction assay ($P < 0.05$; **Fig. 1A**). Both metabolic-based approaches gave significantly higher viabilities than the nuclei-counting approach for all three vorinostat concentrations in both cell lines ($P < 0.05$; **Fig. 1A**), suggesting that resazurin reduction and CellTiter-Glo were overrepresenting cell viability. In addition, viability as measured by nuclei counting was more comparable to that measured using resazurin reduction, suggesting CellTiter-Glo gave less sensitivity to the other endpoint methodologies for cells treated with vorinostat. This is contrary to previous literature reports, which indicate that CellTiter-Glo can provide higher sensitivity than resazurin-based assays.[13,14]

In addition to reduced sensitivity, the two metabolic assays also have other potential limitations. For example, the resazurin reduction assay requires a 37 °C incubation step of several hours, which has been reported to cause morphological changes in cells.[13] However, we did not observe resazurin-induced morphology changes in both cell lines (data not shown). In comparison, CellTiter-Glo, which has a shorter incubation phase to permeabilize cells and release their ATP for measurement, has a considerably greater cost, which can be a drawback in high-throughput screening. Furthermore, it is possible that drugs affecting cellular metabolic processes could interfere with the performance of both the resazurin reduction and CellTiter-Glo assays, giving rise to inaccurate viability measurements.[2]

Overall, the nuclei-counting method is still considered to be the most accurate measure of cell viability.[1] However, its application to high-throughput screening requires efficient automated imaging systems with built-in enumeration software, which can be cost prohibitive. Fortunately, more affordable entry-level systems, such as the Cytell (GE Healthcare, Buckinghamshire, UK), Cytation 5 (BioTek, Winooski, VT), and EVOS (Thermo, Waltham, MA), are available to provide such technologies at a reduced cost. Alternatively, more standard imaging systems without accompanying enumeration software can be used with free open-sourced applications such as ImageJ[15] or CellProfiler.[10]

Real-Time Assays

To complement the endpoint assays, real-time IncuCyte and xCELLigence assays were performed on MCF10A and MCF10A *CDH1*$^{-/-}$ cell lines treated with vorinostat over 48 h (**Fig. 1B** and **1C**). The IncuCyte uses automated imaging to determine cellular confluence at designated intervals over the time course of an experiment as a measure of viability. The xCELLigence uses gold-plated plates to measure cell surface area coverage and adhesion strength via electrical impedance, combining these factors as a measurement of cell viability.

From the IncuCyte and xCELLigence platforms, both cell lines showed a dose-dependent inhibitory response to vorinostat, although this effect was more pronounced in MCF10A *CDH1*$^{-/-}$ cells (**Fig. 1B** and **1C**). To compare the two real-time systems, we determined the proliferation rate at logarithmic growth phase (taken from 12 to 36 hours post drugging in **Fig. 1B** and **1C**) between control and drug treatment within the respective MCF10A and MCF10A *CDH1*$^{-/-}$ cells. In both systems, the proliferation rates of vorinostat-treated MCF10A cells were quite comparable and differed by no more than 10% across each tested concentration (**Fig. 1D**). MCF10A *CDH1*$^{-/-}$ cells showed slower proliferation rates in the xCELLigence than in the IncuCyte. From 0.63 and 1.25 µM vorinostat doses, 24% and 53% smaller measurements were observed, respectively (**Fig. 1D**). This difference could possibly be attributed to the compromised adhesion previously characterized

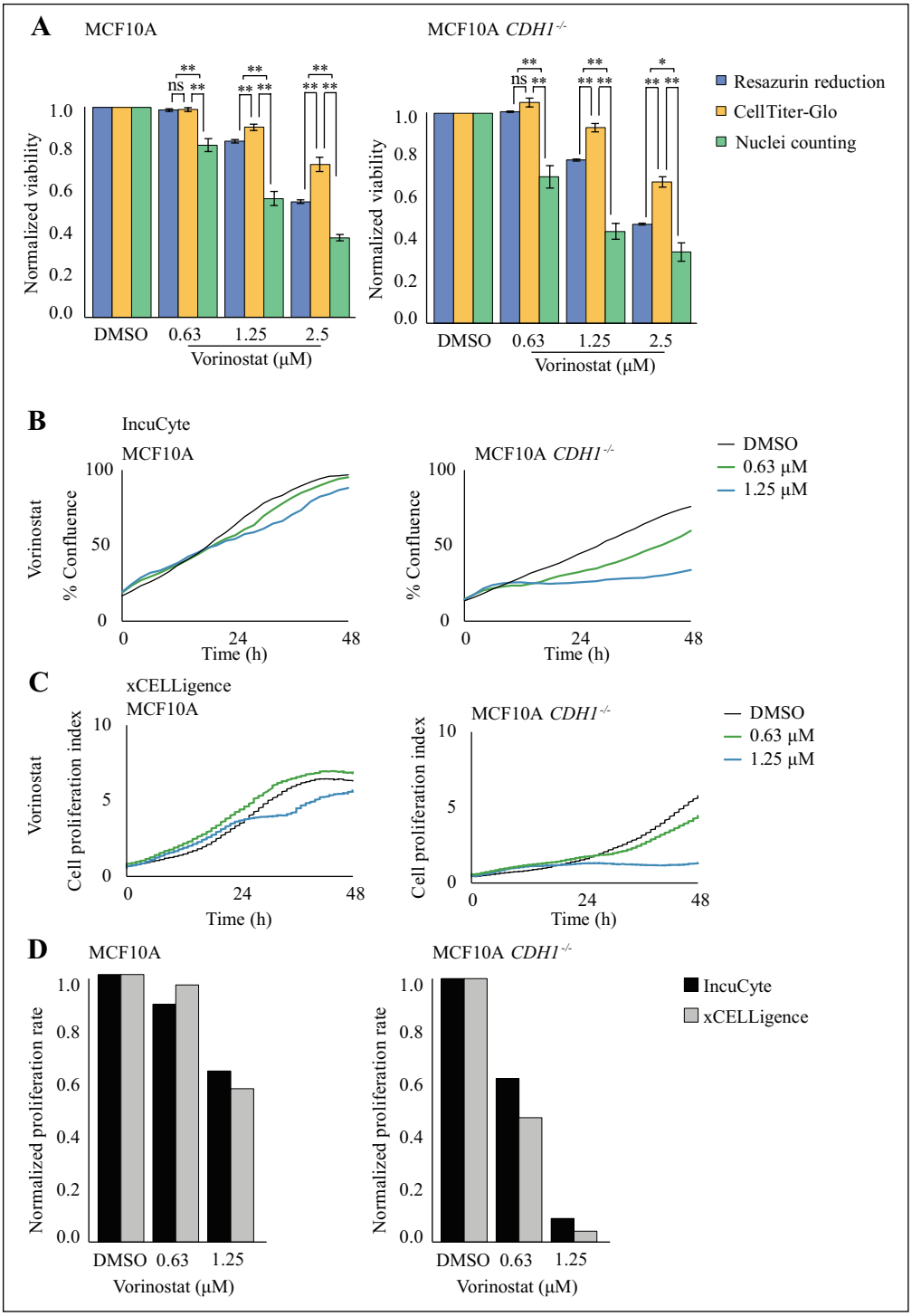

Figure 1. Comparison of endpoint and real-time cell viability assays. (**A**) A comparison of three different endpoint assays (resazurin reduction, CellTiter-Glo, and Hoechst stained nuclei counting) based on their cell viability measurements normalized to their respective DMSO-treated controls in MCF10A and MCF10A *CDH1*$^{-/-}$ cells. A comparison of real-time viability measurements in MCF10A and MCF10A *CDH1*$^{-/-}$ cells as determined using (**B**) the IncuCyte system, which uses cell surface confluence, and (**C**) the xCELLigence system, which measures cellular surface area coverage and adherence strength. (**D**) A comparison of proliferation rates between the two real-time systems as determined at logarithmic growth phase (between 12 to 36 hours post treatment from **B** and **C**). The depicted proliferation rates are normalized to DMSO-treated controls. Endpoint assays represent averaged values of three biological replicates with standard error shown; a representative experiment of each real-time assay is shown. *P*-values calculated using Student's *t*-test; * $P < 0.05$; ** $P < 0.01$.

in MCF10A *CDH1*$^{-/-}$ cells,[8] which may have been further exacerbated by vorinostat treatment. As a result, the xCELLigence, which measures adhesion impedance, would have registered a greater reduction in MCF10A *CDH1*$^{-/-}$ cell viability compared to the IncuCyte, which is incapable of detecting adhesion strength. MCF10A cells showed no marked difference between the two systems, presumably because this cell line does not exhibit compromised cellular adhesion.[8] Unfortunately, the gold-plated xCELLigence plates used in this study lacked clear bottoms, which prevented imaging analysis. Newer E-plates with partially clear-bottomed sections for cell visualization are now

available; however, these were not released prior to our investigation. Conversely, the IncuCyte system was able to provide images that showed no substantial morphological changes over the time course of vorinostat treatment in both cell types (**Fig. 2A**). Overall, both real-time platforms showed comparable performance, except for measuring MCF10A *CDH1*$^{-/-}$ cells treated with 0.63 μM vorinostat.

At the conclusion of each assay, both real-time platforms showed that vorinostat-treated MCF10A cells had achieved viability values very similar to those of DMSO-treated controls (**Fig. 1B** and **1C**). This was contrary to data from our endpoint methods (**Fig. 1A**), which had shown that each vorinostat concentration had produced lower viabilities than control-treated cells, particularly in the nuclei-counting assay. A closer inspection of representative phase-contrast and fluorescent images from the IncuCyte revealed an observable difference in cell density between control and vorinostat-treated MCF10A cells (**Fig. 2A** and **2C**). Even though both control and vorinostat (1.25 μM) treated MCF10A cells showed full growth confluence covering the entire surface area of each respective well (**Fig. 2B**), subsequent nuclei counting confirmed significant differences in cell numbers, whereby 39% fewer cells were present following drug treatment compared to control treatment (**Fig. 2C**). This key observation demonstrated the IncuCyte's inability to discriminate between differing cellular densities when cells had covered the entire surface area of their respective wells. As such, caution should be taken when analyzing data at full cellular confluence because further validation is required from direct cell counting. Nevertheless, the IncuCyte still produced valuable data during sub-confluent growth phases, which was comparable to nuclei-counting data (data not shown). These results demonstrate that a combination of distinct methodologies provides a more comprehensive and accurate assessment of drug efficacy than singular assays.

Real-Time Assay and Endpoint Assay Multiplexing

To mitigate the shortfalls observed in the endpoint and real-time assays, we combined the IncuCyte real-time assay with both the resazurin reduction and nuclei-counting assays. The resazurin reduction and nuclei-counting methods were selected as endpoint assays because they have been reported to multiplex together effectively.[16] This multiplexed approach also allowed for more data to be gathered from one drug-treated experiment. We also wanted to investigate if the combined approach was capable of evaluating synthetic lethal properties of two different drugs, in which assay sensitivity is essential to distinguish preferential targeting of one cell type over another. In this case, a synthetic lethal effect would involve the selective growth inhibition of MCF10A *CDH1*$^{-/-}$ cells but not MCF10A cells. To test this, we subjected MCF10A and MCF10A *CDH1*$^{-/-}$ cells to either vorinostat or Taxol treatment over 48 hours, with cellular growth being tracked in the IncuCyte, followed by resazurin reduction and nuclei counting at the conclusion of the real-time analysis.

At 48 h following vorinostat treatment (0.63, 1.25, 2.5 μM), the confluence measurements from the IncuCyte showed that MCF10A cells were marginally inhibited and proliferated similarly to control treated cells (**Fig. 3A**). However, in MCF10A *CDH1*$^{-/-}$ cells, a significant dose-dependent inhibitory response was observed in which drug-treated cells did not reach the confluency of control-treated cells (**Fig. 3B**). Following the IncuCyte assay, the same plate was then subjected to the resazurin reduction assay. Increasing vorinostat treatment caused a more marked reduction in MCF10A *CDH1*$^{-/-}$ cell viabilities (93%, 71%, and 43%; **Fig. 3E**) compared to the corresponding MCF10A treated cells (98%, 83%, 55%; **Fig. 3E**). Similarly, the nuclei-counting analysis, performed immediately after the resazurin reduction assay, also showed increasing vorinostat treatment causing a more marked effect on MCF10A *CDH1*$^{-/-}$ cell viabilities (77%, 47%, and 26%; **Fig. 3F**) compared to MCF10A cells (79%, 57%, and 37%; **Fig. 3F**). These results infer synthetic lethality, which in the context of cancer therapeutics allows for greater target specificity toward tumor cells with reduced side effects.

As another measure of synthetic lethality, we calculated the viability ratio of MCF10A *CDH1*$^{-/-}$ cells to MCF10A cells, whereby a ratio of less than 1 indicated an increased susceptibility of MCF10A *CDH1*$^{-/-}$ cells to drug treatment, concordant with a drug-induced synthetic lethal phenotype. Both the resazurin reduction and nuclei-counting assays produced comparable viability ratios for 0.63, 1.25, and 2.5 μM vorinostat treatment between the isogenic cell lines (resazurin reduction: 0.95, 0.85, 0.78; nuclei counting: 0.97, 0.82, 0.70). This result is consistent with the IncuCyte confluence analysis, although the extent of this differential was more marked in real time. Overall, the combined assays demonstrated an increased susceptibility of MCF10A *CDH1*$^{-/-}$ cells compared to MCF10A cells with increasing vorinostat dose.

IncuCyte analysis showed that MCF10A cells treated with 1 and 2 nM Taxol exhibited negligible inhibition. When treated with 4 nM Taxol, MCF10A cell viability was affected within the first 36 hours but eventually attained confluence measurements similar to those of controls at the conclusion of the real-time assay (**Fig. 3C**). A similar effect was seen in Taxol-treated MCF10A *CDH1*$^{-/-}$ cells, although the highest concentration (4 nM) gave rise to growth inhibition that prevented full confluency observed in control treatment (**Fig. 3D**). The resazurin reduction and nuclei-counting assays showed that Taxol treatment also produced a dose-dependent effect in both MCF10A and MCF10A *CDH1*$^{-/-}$ cells, without showing preferential inhibition in

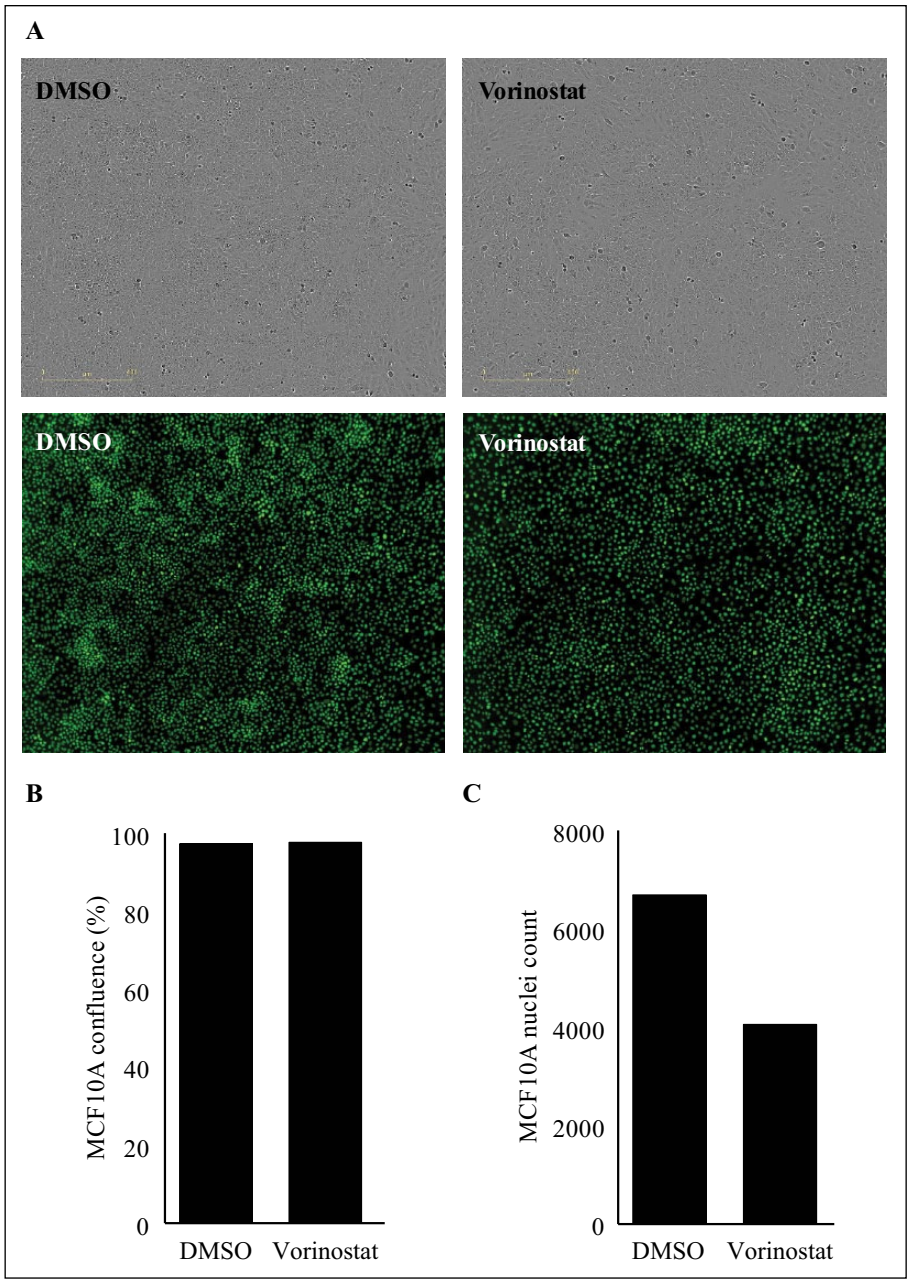

Figure 2. Cellular confluence measurements do not reflect cell densities at full surface area coverage. (**A**) Phase-contrast images of MCF10A cells at 48 h post DMSO and 1.25 μM vorinostat treatment (4× magnification; scale bars = 400 μm in length). A more distinct difference in cell density was observed in SYTOX-stained cell nuclei compared to the phase-contrast images from the same field (fluorescent images captured using IncuCyte under 4× magnification). (**B**) Negligible cell viability difference observed between DMSO- and vorinostat-treated MCF10A cells as determined using IncuCyte's cell surface confluence measurement of phase-contrast images in **A**. (**C**) A significant difference in cell density as quantified from nuclei enumeration of control and drug-treated MCF10A cells shown in **A**.

either cell type at the tested concentration range (**Fig. 3G** and **3H**). Furthermore, the viability ratios determined from both the resazurin reduction and nuclei-counting assays were not less than 1 (resazurin reduction: 1.00, 1.02, and 1.05; nuclei counting: 1.02, 1.03, and 1.03), indicating no synthetic lethality. Taxol treatment at higher concentrations (up to 16 nM) yielded a dose-dependent effect in both isogenic cells lines, although no synthetic lethal phenotype was observed at these concentrations (data not shown). Here, we have shown that our combined real-time and endpoint assay approach reliably identified drug-induced synthetic lethal effects in the tested MCF10A isogenic cell lines. We have also previously used the combined IncuCyte and endpoint method to uncover other drugs that induce synthetic lethality in MCF10A *CDH1*$^{-/-}$ cells.[9] The IncuCyte and nuclei counting were used to show that drugs such as crizotinib, LY2784544, and saracatinib each caused significantly reduced viabilities in MCF10A *CDH1*$^{-/-}$ cells compared to MCF10A cells.[9]

Our current study has shown that the IncuCyte system is well suited for tracking sub-confluent cell growth phases, which can be followed up by nuclei counting to assess drug

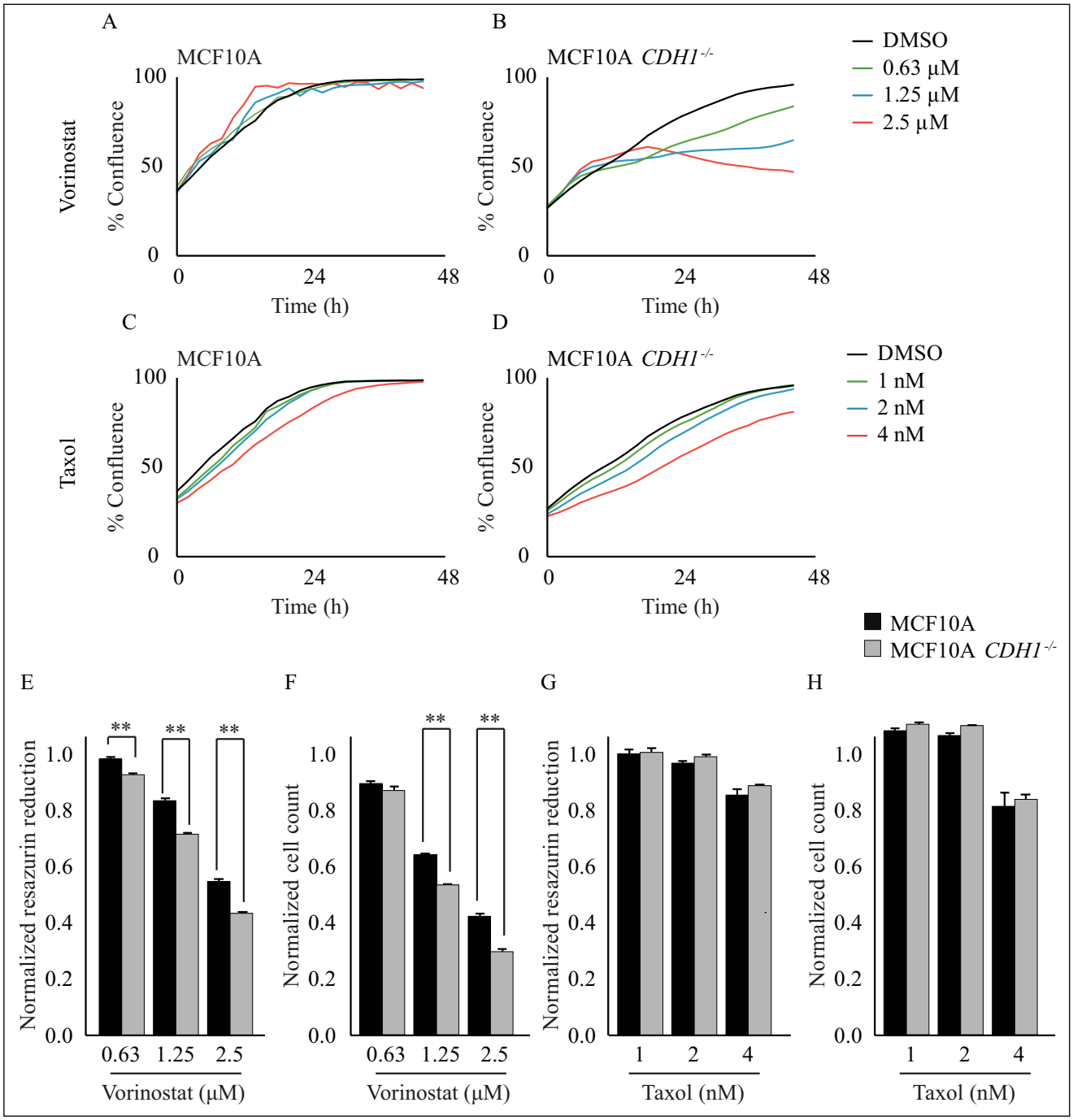

Figure 3. Combined real-time and endpoint assays facilitate the evaluation of drugs for synthetic lethal properties in MCF10A isogenic cells. (**A**–**D**) IncuCyte real-time confluence measurements demonstrating a selective proliferation inhibition by vorinostat and, to a lesser extent, by Taxol in MCF10A *CDH1*$^{-/-}$ cells compared to MCF10A cells across a range of concentrations over 48 h. Endpoint resazurin reduction (**E**, **G**) and Hoechst stained nuclei-counting (**F**, **H**) assays, performed immediately after the real-time assay (**A**–**D**), showed a greater and selective inhibition in MCF10A *CDH1*$^{-/-}$ cells across three concentrations of vorinostat but not Taxol. Endpoint assays show cell viabilities normalized to respective controls, representing the averaged values of three biological replicates with standard error shown. *P*-values calculated using Student's *t*-test; ** $P < 0.01$.

efficacy when cells are at full confluence. In the absence of a real-time system like the IncuCyte, nuclei counting should be performed because it provided the most accurate measurement of viable cells in our analysis. Overall, we have demonstrated the utility and strengths of five viability assays and have adapted a robust real-time and endpoint

multiplexed method for the investigation of synthetic lethal drugs.

Acknowledgments

We thank Dr. Michelle McConnell and Ms. Clare Fitzpatrick (Department of Microbiology and Immunology, University of Otago) for assistance with the xCELLigence real-time system; Dr. Adele Woolley and Mr. Michael Algie (Department of Pathology, University of Otago) for the use of the IncuCyte FLR; and Dr. Kenny Chitcholtan (Department of Obstetrics and Gynaecology, University of Otago) for providing the resazurin dye recipe and associated assay recommendations.

Declaration of Conflicting Interests

The authors declared no potential conflicts of interest with respect to the research, authorship, and/or publication of this article.

Funding

The authors disclosed receipt of the following financial support for the research, authorship, and/or publication of this article: This work was supported by the Health Research Council of New Zealand and the University of Otago (PhD scholarships to A. Single, H. Beetham, and B. Telford).

References

1. Chan, G. K.; Kleinheinz, T. L.; Peterson, D.; et al. A Simple High-Content Cell Cycle Assay Reveals Frequent Discrepancies between Cell Number and ATP and MTS Proliferation Assays. *PLoS One*. **2013**, *8*, e63583.
2. Kepp, O.; Galluzzi, L.; Lipinski, M.; et al. Cell Death Assays for Drug Discovery. *Nat. Rev. Drug Discov*. **2011**, *10*, 221–237.
3. Quent, V. M.; Loessner, D.; Friis, T.; et al. Discrepancies between Metabolic Activity and DNA Content as Tool to Assess Cell Proliferation in Cancer Research. *J. Cell Mol. Med*. **2010**, *14*, 1003–1013.
4. Mosmann, T. Rapid Colorimetric Assay for Cellular Growth and Survival: Application to Proliferation and Cytotoxicity Assays. *J. Immunol. Methods*. **1983**, *65*, 55–63.
5. O'Brien, J.; Wilson, I.; Orton, T.; et al. Investigation of the Alamar Blue (Resazurin) Fluorescent Dye for the Assessment of Mammalian Cell Cytotoxicity. *Eur. J. Biochem*. **2000**, *267*, 5421–5426.
6. Crouch, S. P.; Kozlowski, R.; Slater, K. J.; et al. The Use of ATP Bioluminescence as a Measure of Cell Proliferation and Cytotoxicity. *J. Immunol. Methods*. **1993**, *160*, 81–88.
7. Debnath, J.; Muthuswamy, S. K.; Brugge, J. S. Morphogenesis and Oncogenesis of MCF-10A Mammary Epithelial Acini Grown in Three-Dimensional Basement Membrane Cultures. *Methods*. **2003**, *30*, 256–268.
8. Chen, A.; Beetham, H.; Black, M. A.; et al. E-Cadherin Loss Alters Cytoskeletal Organization and Adhesion in Non-Malignant Breast Cells but Is Insufficient to Induce an Epithelial-Mesenchymal Transition. *BMC Cancer*. **2014**, *14*, 552.
9. Telford, B. J.; Chen, A.; Beetham, H.; et al. Synthetic Lethal Screens Identify Vulnerabilities in GPCR Signaling and Cytoskeletal Organization in E-Cadherin-Deficient Cells. *Mol. Cancer Ther*. **2015**, *14*, 1213–1223.
10. Lamprecht, M. R.; Sabatini, D. M.; Carpenter, A. E. CellProfiler: Free, Versatile Software for Automated Biological Image Analysis. *Biotechniques*. **2007**, *42*, 71–75.
11. Haselsberger, K.; Peterson, D. C.; Thomas, D. G.; et al. Assay of Anticancer Drugs in Tissue Culture: Comparison of a Tetrazolium-Based Assay and a Protein Binding Dye Assay in Short-Term Cultures Derived from Human Malignant Glioma. *Anticancer Drugs*. **1996**, *7*, 331–338.
12. Hamid, R.; Rotshteyn, Y.; Rabadi, L.; et al. Comparison of Alamar Blue and MTT Assays for High Through-put Screening. *Toxicol. in Vitro*. **2004**, *18*, 703–710.
13. Riss, T. L.; Moravec, R. A.; Niles, A. L.; et al. Cell Viability Assays. In *Assay Guidance Manual*; Sittampalam, G. S.; et al., Eds.; Eli Lilly & Company and the National Center for Advancing Translational Sciences: Bethesda, MD, **2004**.
14. Peternel, L.; Kotnik, M.; Prezelj, A.; et al. Comparison of 3 Cytotoxicity Screening Assays and Their Application to the Selection of Novel Antibacterial Hits. *J. Biomol. Screen*. **2009**, *14*, 142–150.
15. Schneider, C. A.; Rasband, W. S.; Eliceiri, K. W. NIH Image to ImageJ: 25 Years of Image Analysis. *Nat. Meth*. **2012**, *9*, 671–675.
16. Wu, Y.; Connors, D.; Barber, L.; et al. Multiplexed Assay Panel of Cytotoxicity in HK-2 Cells for Detection of Renal Proximal Tubule Injury Potential of Compounds. *Toxicol. in Vitro*. **2009**, *23*, 1170–1178.

Appendix C.

Reagent Preparations

C.1 Phosphate buffered saline (PBS)

Phosphate buffered saline (PBS) was made by dissolving 1 PBS tablet per 100 mL mQH_2O, then autoclaving to sterilise.

C.2 0.05% trypsin solution

0.05% trypsin solution was made by diluting 0.5% trypsin at a 1:10 ratio with PBS.

C.3 Cell culture freezing medium

Cell culture freezing medium was made with a final concentration of 70% complete growth medium, 20% horse serum or FBS (respective to serum in complete growth medium), and 10% DMSO.

C.4 Resazurin solution

Resazurin solution was prepared by dissolving resazurin in PBS to create a 440 μM stock solution. Stock solutions were aliquoted and stored at -20 °C.

C.5 Laemmli buffer

A 5x laemmli buffer stock consisted of 164.5 mM Tris-HCl (pH 6.8), 65.75% (w/v) glycerol, 6.25% SDS, and 0.025% bromophenol blue mixed in mQH_2O.

C.6 SDS-PAGE

Gels were cast in pairs using the Mini-PROTEAN II casting stand and a 15 tooth comb.

Two resolving gels consisted of: 6.6 mL 30% acrylamide/bis solution, 5 mL 1.5 M Tris-HCl containing 0.4% SDS (pH 8.8), 26 μL TEMED, 120 μL 10% APS, and 8.26 mL mQH_2O. This was poured to below the comb level and covered with 1 mL isopropanol while setting.

Two stacking gels consisted of: 1.4 mL 30% acrylamide/bis solution, 2.5 mL 0.5 M Tris-HCl contacting 0.4% SDS (pH 6.8), 40 µL TEMED, 50 µL 10% APS, and 6 mL mQH_2O added. Following isopropanol removal, stacking gel solution was added on top of each set resolving gel.

C.7 Running buffer

A 10x running buffer stock consisted of 250 mM Tris, 1.9 M glycine, and 1 % SDS mixed thoroughly in mQH_2O.

A 1 L 1x working stock consisted of: 100 mL 10x running buffer stock was mixed with 900 mL mQH_2O.

C.8 Transfer buffer

A 10x transfer buffer stock consisted of 250 mM Tris, 1.9 M glycine, and 0.5% SDS mixed thoroughly in mQH_2O.

A 1 L 1x transfer buffer solution with 20% methanol consisted of: 100 mL 10x transfer buffer stock, 200 mL methanol, and 700 mL mQH_2O.

C.9 Tris buffered saline (TBS)

A 10x Tris buffered saline (TBS) stock consisted of 200mM Tris and 1.5 M NaCl mixed thoroughly in 900 mL mQH_2O. This was adjusted to pH 7.6 and made to 1 L with mQH_2O.

A 1L 1x TBS working stock consisted of: 100 mL 10x TBS stock was mixed with 900 mL mQH_2O.

C.10 Tris buffered saline and 0.1% Tween-20 (TBST)

A 1 L 1x working stock of Tris-buffered saline and 0.1% Tween-20 (TBST) solution consisted of 100 mL 10x TBS, 900 mL mQ H_2O, and 1 mL Tween-20.

C.11 Protease inhibitor cocktail

A 25x protease inhibitor stock consisted of 1 cOmplete mini (EDTA-free) tablet dissolved in 2 mL mQH_2O.

C.12 Cell culture lysis buffer containing protease inhibitors

A 1.5 mL 1x cell culture lysis buffer containing protease inhibitors consisted of: 60 µL 25x protease inhibitor stock, 300 µL Cell Culture Lysis 5X Reagent, and 1.14 mL mQH_2O.

Appendix D.

Supplementary Drug Viability Assays

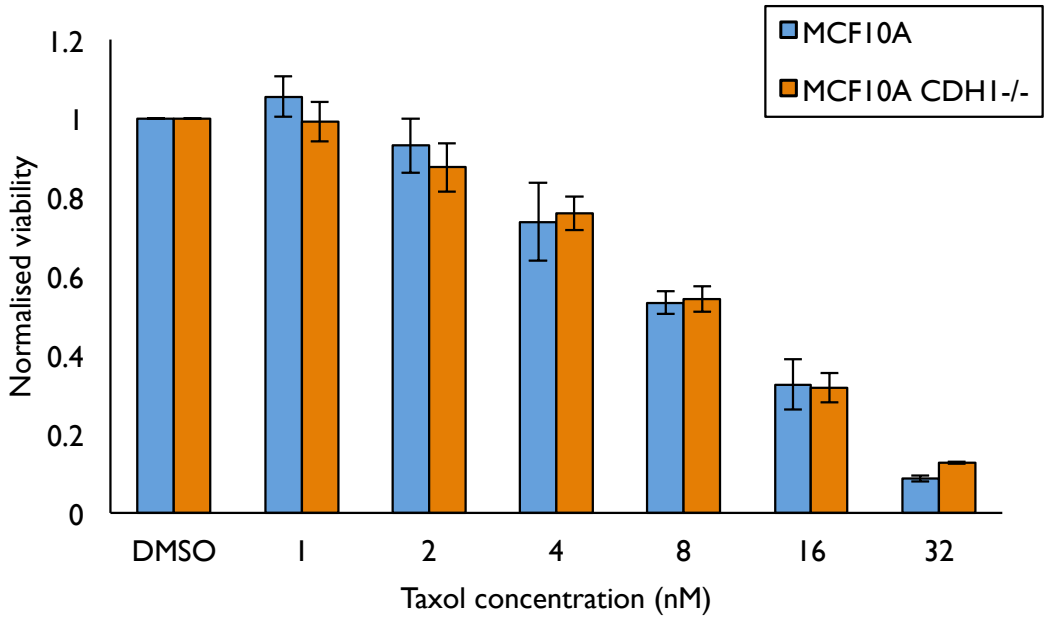

Figure D.1 MCF10A and MCF10A *CDH1*$^{-/-}$ cells following taxol treatment

MCF10A and MCF10A *CDH1*$^{-/-}$ cells were grown for 24 h and treated with taxol over a range of concentrations. At 48 h post-treatment, cell viability was assessed using a Hoechst-stained nuclei counting assay. Data represents averaged values of two biological replicates with standard error shown.

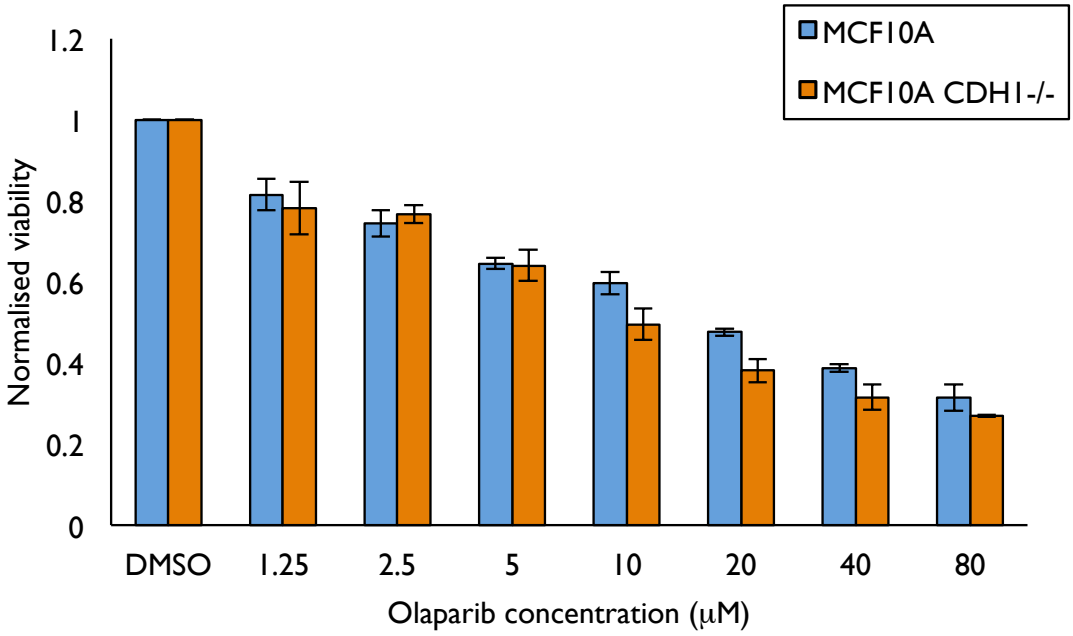

Figure D.2 MCF10A and MCF10A *CDH1*$^{-/-}$ cells following olaparib treatment

MCF10A and MCF10A *CDH1*$^{-/-}$ cells were grown for 24 h and treated with olaparib over a range of concentrations. At 48 h post-treatment, cell viability was assessed using a Hoechst-stained nuclei counting assay. Data represents averaged values of two biological replicates with standard error shown.

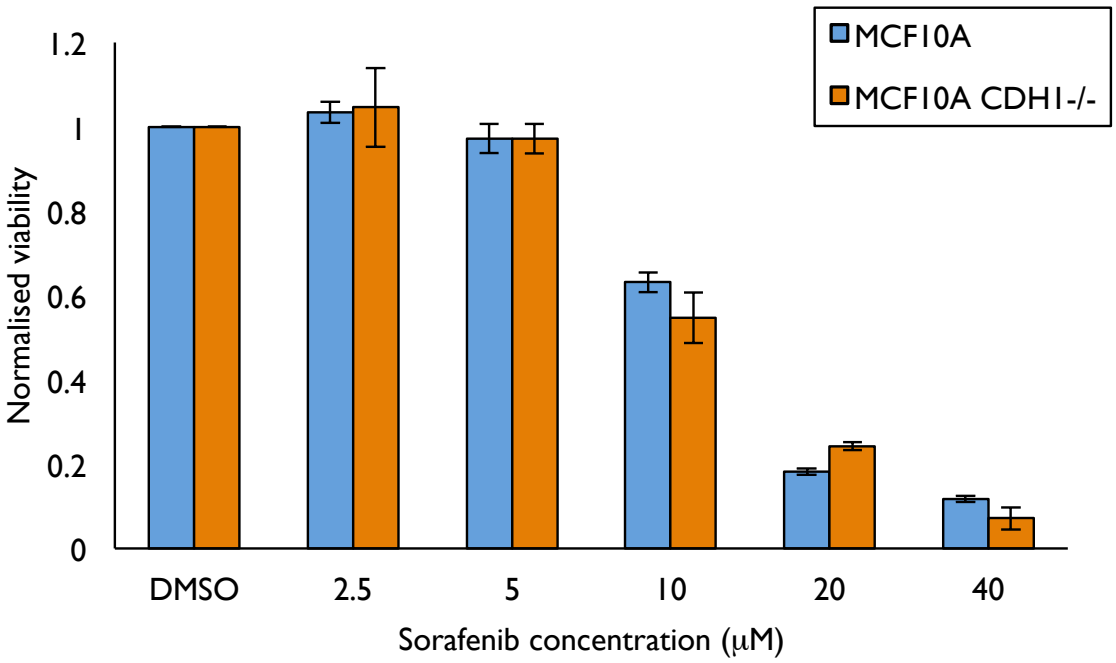

Figure D.3 MCF10A and MCF10A *CDH1*$^{-/-}$ cells following sorafenib treatment

MCF10A and MCF10A *CDH1*$^{-/-}$ cells were grown for 24 h and treated with sorafenib over a range of concentrations. At 48 h post-treatment, cell viability was assessed using a Hoechst-stained nuclei counting assay. Data represents averaged values of two biological replicates with standard error shown.

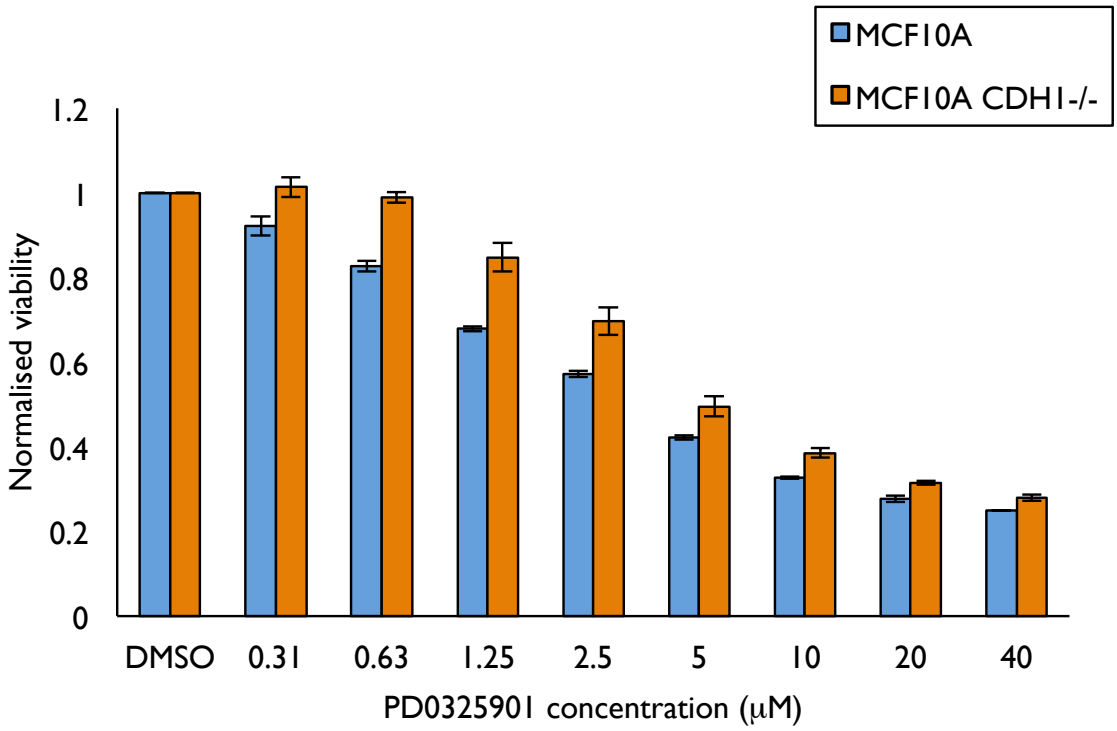

Figure D.4 MCF10A and MCF10A *CDH1*$^{-/-}$ cells following PD0325901 treatment

MCF10A and MCF10A *CDH1*$^{-/-}$ cells were grown for 24 h and treated with PD0325901 over a range of concentrations. At 48 h post-treatment, cell viability was assessed using a Hoechst-stained nuclei counting assay. Data represents averaged values of two biological replicates with standard error shown.

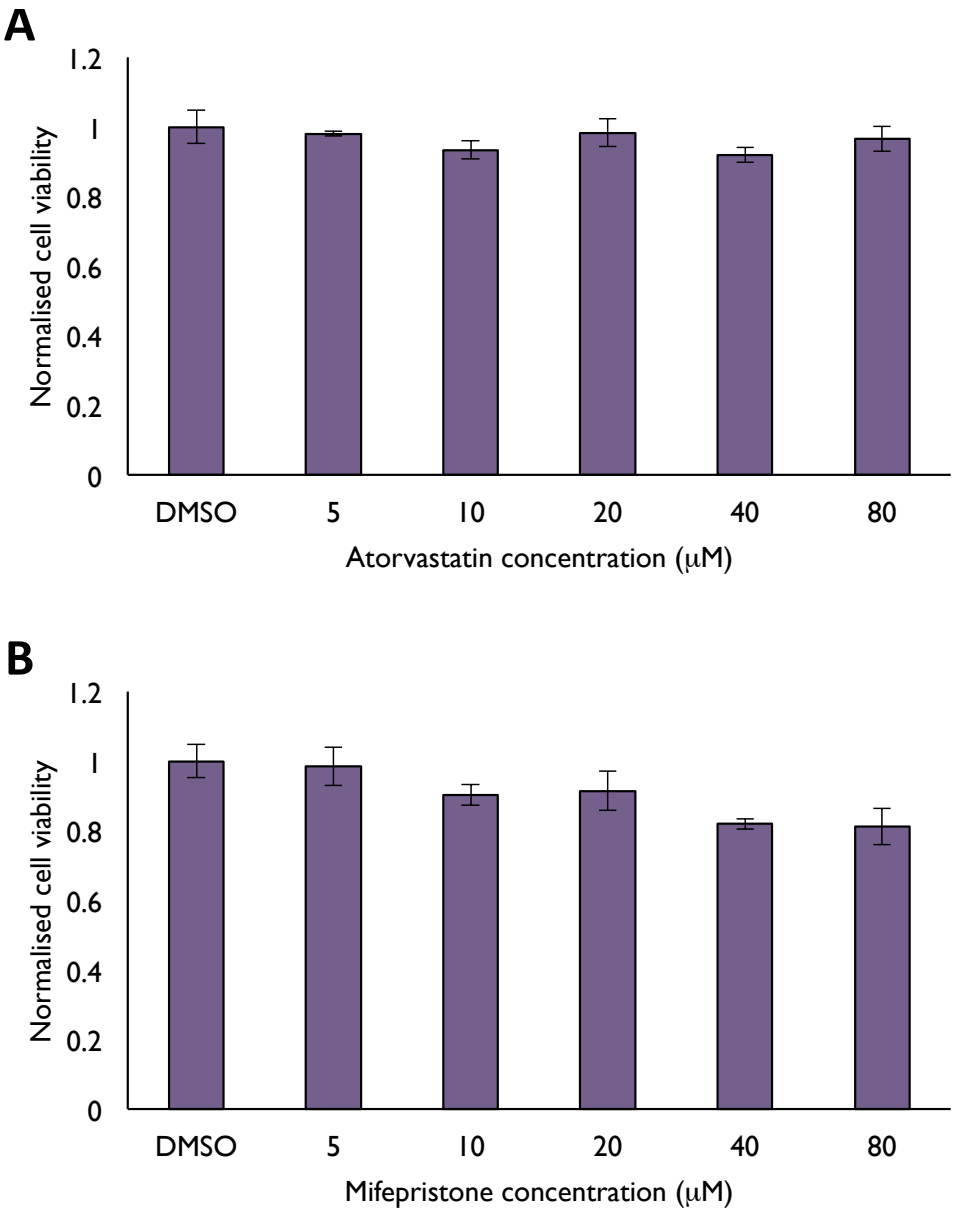

Figure D.5 IPH-926 cell viability following atorvastatin and mifepristone treatment over 48 hours

IPH-926 cells were grown for 24 h and treated with either atorvastatin **(A)** or mifepristone **(B)** over a range of concentrations. At 48 h post-treatment, cell viability was assessed using a Hoechst-stained nuclei counting assay. A representative experiment of each endpoint assay with standard deviation is shown.

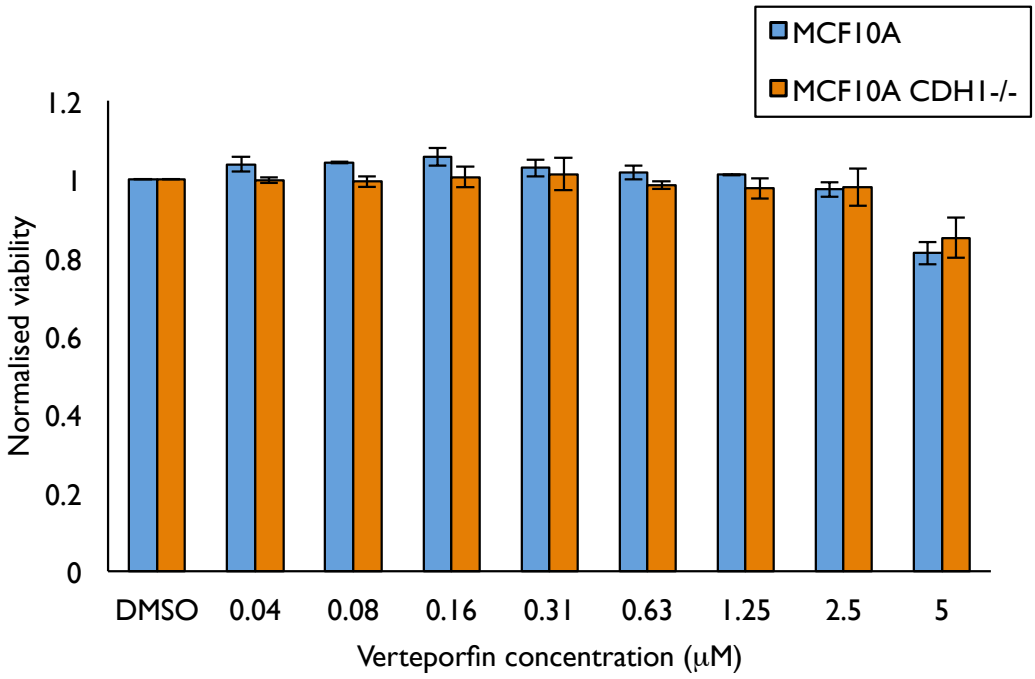

Figure D.6 MCF10A and MCF10A *CDH1*$^{-/-}$ cells following verteporfin treatment

MCF10A and MCF10A *CDH1*$^{-/-}$ cells were grown for 24 h and treated with verteporfin over a range of concentrations. At 48 h post-treatment, cell viability was assessed using a Hoechst-stainednuclei counting assay. Data represents averaged values of two biological replicates with standarderror shown.

REFERENCES

Adzhubei, A. A., Sternberg, M. J., and Makarov, A. A. Polyproline-II helix in proteins: structure and function. *J Mol Biol,* 425, 2100-32 (2013).

Al-Haidari, A. A., Syk, I., and Thorlacius, H. HMG-CoA reductase regulates CCL17-induced colon cancer cell migration via geranylgeranylation and RhoA activation. *Biochem Biophys Res Commun,* 446, 68-72 (2014).

Andres, A. M., Hernandez, G., Lee, P., Huang, C., Ratliff, E. P., Sin, J., Thornton, C. A., Damasco, M. V., and Gottlieb, R. A. Mitophagy is required for acute cardioprotection by simvastatin. *Antioxid Redox Signal,* 21, 1960-73 (2014).

Arpino, G., Bardou, V. J., Clark, G. M., and Elledge, R. M. Infiltrating lobular carcinoma of the breast: tumor characteristics and clinical outcome. *Breast Cancer Res,* 6, R149-56 (2004).

Ashworth, A. A synthetic lethal therapeutic approach: poly(ADP) ribose polymerase inhibitors for the treatment of cancers deficient in DNA double-strand break repair. *J Clin Oncol,* 26, 3785-90 (2008).

Barber, M., Murrell, A., Ito, Y., Maia, A. T., Hyland, S., Oliveira, C., Save, V., Carneiro, F., Paterson, A. L., Grehan, N.*, et al.* Mechanisms and sequelae of E-cadherin silencing in hereditary diffuse gastric cancer. *J Pathol,* 216, 295-306 (2008).

Barker, N., Huch, M., Kujala, P., van de Wetering, M., Snippert, H. J., van Es, J. H., Sato, T., Stange, D. E., Begthel, H., van den Born, M.*, et al.* Lgr5(+ve) stem cells drive self-renewal in the stomach and build long-lived gastric units in vitro. *Cell Stem Cell,* 6, 25-36 (2010).

Bartfeld, S., Bayram, T., van de Wetering, M., Huch, M., Begthel, H., Kujala, P., Vries, R., Peters, P. J., and Clevers, H. In vitro expansion of human gastric epithelial stem cells and their responses to bacterial infection. *Gastroenterology,* 148, 126-136 e6 (2015).

Batlle, E., Sancho, E., Franci, C., Dominguez, D., Monfar, M., Baulida, J., and Garcia De Herreros, A. The transcription factor snail is a repressor of E-cadherin gene expression in epithelial tumour cells. *Nat Cell Biol,* 2, 84-9 (2000).

Bays, J. L., Campbell, H. K., Heidema, C., Sebbagh, M., and DeMali, K. A. Linking E-cadherin mechanotransduction to cell metabolism through force-mediated activation of AMPK. *Nat Cell Biol,* 19, 724-731 (2017).

Bender, A., and Pringle, J. R. Use of a screen for synthetic lethal and multicopy suppressee mutants to identify two new genes involved in morphogenesis in Saccharomyces cerevisiae. *Mol Cell Biol,* 11, 1295-305 (1991).

Berger, D. P., Fiebig, H. H., Winterhalter, B. R., Wallbrecher, E., and Henss, H. Preclinical phase II study of ifosfamide in human tumour xenografts in vivo. *Cancer Chemother Pharmacol,* 26 Suppl, S7-11 (1990).

Bergstrom, J. D., Kurtz, M. M., Rew, D. J., Amend, A. M., Karkas, J. D., Bostedor, R. G., Bansal, V. S., Dufresne, C., VanMiddlesworth, F. L., Hensens, O. D., and et al. Zaragozic acids: a family of fungal metabolites that are picomolar competitive inhibitors of squalene synthase. *Proc Natl Acad Sci U S A,* 90, 80-4 (1993).

Bertucci, F., Orsetti, B., Negre, V., Finetti, P., Rouge, C., Ahomadegbe, J. C., Bibeau, F., Mathieu, M. C., Treilleux, I., Jacquemier, J.*, et al.* Lobular and ductal carcinomas of the breast have distinct genomic and expression profiles. *Oncogene,* 27, 5359-72 (2008).

Biglia, N., Maggiorotto, F., Liberale, V., Bounous, V. E., Sgro, L. G., Pecchio, S., D'Alonzo, M., and Ponzone, R. Clinical-pathologic features, long term-outcome and surgical treatment in a large series of patients with invasive lobular carcinoma (ILC) and invasive ductal carcinoma (IDC). *Eur J Surg Oncol,* 39, 455-60 (2013).

Bjorkhem-Bergman, L., Lindh, J. D., and Bergman, P. What is a relevant statin concentration in cell experiments claiming pleiotropic effects? *Br J Clin Pharmacol,* 72, 164-5 (2011).

Bodo, J., Zhao, X., Sharma, A., Hill, B. T., Portell, C. A., Lannutti, B. J., Almasan, A., and Hsi, E. D. The phosphatidylinositol 3-kinases (PI3K) inhibitor GS-1101 synergistically potentiates histone deacetylase inhibitor-induced proliferation inhibition and apoptosis through the inactivation of PI3K and extracellular signal-regulated kinase pathways. *Br J Haematol,* 163, 72-80 (2013).

Boelens, M. C., Nethe, M., Klarenbeek, S., de Ruiter, J. R., Schut, E., Bonzanni, N., Zeeman, A. L., Wientjens, E., van der Burg, E., Wessels, L.*, et al.* PTEN loss in E-cadherin-deficient mouse mammary epithelial cells rescues apoptosis and results in development of classical invasive lobular carcinoma. *Cell Rep,* 16, 2087-101 (2016).

Boggon, T. J., and Eck, M. J. Structure and regulation of Src family kinases. *Oncogene,* 23, 7918-27 (2004).

Boussadia, O., Kutsch, S., Hierholzer, A., Delmas, V., and Kemler, R. E-cadherin is a survival factor for the lactating mouse mammary gland. *Mech Dev,* 115, 53-62 (2002).

Brandhagen, B. N., Tieszen, C. R., Ulmer, T. M., Tracy, M. S., Goyeneche, A. A., and Telleria, C. M. Cytostasis and morphological changes induced by mifepristone in human metastatic cancer cells involve cytoskeletal filamentous actin reorganization and impairment of cell adhesion dynamics. *BMC Cancer,* 13, 35 (2013).

Breslin, S., and O'Driscoll, L. Three-dimensional cell culture: the missing link in drug discovery. *Drug Discov Today,* 18, 240-9 (2013).

Brown, M. T., and Cooper, J. A. Regulation, substrates and functions of src. *Biochim Biophys Acta,* 1287, 121-49 (1996).

Bryant, H. E., Schultz, N., Thomas, H. D., Parker, K. M., Flower, D., Lopez, E., Kyle, S., Meuth, M., Curtin, N. J., and Helleday, T. Specific killing of BRCA2-deficient tumours with inhibitors of poly(ADP-ribose) polymerase. *Nature,* 434, 913-7 (2005).

Cailleau, R., Young, R., Olive, M., and Reeves, W. J., Jr. Breast tumor cell lines from pleural effusions. *J Natl Cancer Inst,* 53, 661-74 (1974).

Campbell, M. J., Esserman, L. J., Zhou, Y., Shoemaker, M., Lobo, M., Borman, E., Baehner, F., Kumar, A. S., Adduci, K., Marx, C.*, et al.* Breast cancer growth prevention by statins. *Cancer Res,* 66, 8707-14 (2006).

Canaani, D. Application of the concept synthetic lethality toward anticancer therapy: A promise fulfilled? *Cancer Lett,* (2013).

Cha, Y. J., Kim, Y. H., Cho, N. H., and Koo, J. S. Expression of autophagy related proteins in invasive lobular carcinoma: comparison to invasive ductal carcinoma. *Int J Clin Exp Pathol,* 7, 3389-98 (2014).

Chan, G. K., Kleinheinz, T. L., Peterson, D., and Moffat, J. G. A simple high-content cell cycle assay reveals frequent discrepancies between cell number and ATP and MTS proliferation assays. *PLoS One,* 8, e63583 (2013).

Chao, O. S., and Goodman, O. B. Synergistic loss of prostate cancer cell viability by coinhibition of HDAC and PARP. *Mol Cancer Res,* 12, 1755-1766 (2014).

Charlton, A., Blair, V., Shaw, D., Parry, S., Guilford, P., and Martin, I. G. Hereditary diffuse gastric cancer: predominance of multiple foci of signet ring cell carcinoma in distal stomach and transitional zone. *Gut,* 53, 814-20 (2004).

Charlton-Menys, V., and Durrington, P. N. Squalene synthase inhibitors: clinical pharmacology and cholesterol-lowering potential. *Drugs,* 67, 11-6 (2007).

Chen, A., Beetham, H., Black, M. A., Priya, R., Telford, B. J., Guest, J., Wiggins, G. A., Godwin, T. D., and Guilford, P. J. E-cadherin loss alters cytoskeletal organization and adhesion in non-malignant breast cells but is insufficient to induce an epithelial-mesenchymal transition. *BMC Cancer,* 14, 552 (2014a).

Chen, C. H., Chen, M. C., Wang, J. C., Tsai, A. C., Chen, C. S., Liou, J. P., Pan, S. L., and Teng, C. M. Synergistic interaction between the HDAC inhibitor, MPT0E028, and sorafenib in liver cancer cells in vitro and in vivo. *Clin Cancer Res,* 20, 1274-87 (2014b).

Chou, T. C. Comparison of dose-effect relationships of carcinogens following low-dose chronic exposure and high-dose single injection: an analysis by the median-effect principle. *Carcinogenesis,* 1, 203-13 (1980).

Chou, T. C. Drug combination studies and their synergy quantification using the Chou-Talalay method. *Cancer Res,* 70, 440-446 (2010).

CompuSyn software for drug combinations and for general dose-effect analysis, and user's guide., ComboSyn, Inc., Paramus, NJ.

Chou, T. C., and Talalay, P. Quantitative analysis of dose-effect relationships: the combined effects of multiple drugs or enzyme inhibitors. *Adv Enzyme Regul,* 22, 27-55 (1984).

Christgen, M., Bruchhardt, H., Hadamitzky, C., Rudolph, C., Steinemann, D., Gadzicki, D., Hasemeier, B., Römermann, D., Focken, T., Krech, T.*, et al.* Comprehensive genetic and functional characterization of IPH-926: a novel CDH1-null tumour cell line from human lobular breast cancer. *J Pathol,* 217, 620-632 (2009).

Christgen, M., and Derksen, P. Lobular breast cancer: molecular basis, mouse and cellular models. *Breast Cancer Res,* 17, 16 (2015).

Christgen, M., Noskowicz, M., Schipper, E., Christgen, H., Heil, C., Krech, T., Langer, F., Kreipe, H., and Lehmann, U. Oncogenic PIK3CA mutations in lobular breast cancer progression. *Genes Chromosomes Cancer,* 52, 69-80 (2013).

Christgen, M., Steinemann, D., Kuhnle, E., Langer, F., Gluz, O., Harbeck, N., and Kreipe, H. Lobular breast cancer: Clinical, molecular and morphological characteristics. *Pathol Res Pract,* 212, 583-97 (2016).

Clevers, H. Modeling development and disease with organoids. *Cell,* 165, 1586-97 (2016).

Cooper, A. L., Greenberg, V. L., Lancaster, P. S., van Nagell, J. R., Jr., Zimmer, S. G., and Modesitt, S. C. In vitro and in vivo histone deacetylase inhibitor therapy with suberoylanilide hydroxamic acid (SAHA) and paclitaxel in ovarian cancer. *Gynecol Oncol,* 104, 596-601 (2007).

Cooper, J. A., Gould, K. L., Cartwright, C. A., and Hunter, T. Tyr527 is phosphorylated in pp60c-src: implications for regulation. *Science,* 231, 1431-4 (1986).

Coppock, H. A., Gilham, D. E., Howell, A., and Clarke, R. B. Cyclin-dependent kinase inhibitors and basement membrane interact to regulate breast epithelial cell differentiation and acinar morphogenesis. *Cell Prolif,* 40, 721-40 (2007).

Crouch, S. P., Kozlowski, R., Slater, K. J., and Fletcher, J. The use of ATP bioluminescence as a measure of cell proliferation and cytotoxicity. *J Immunol Methods,* 160, 81-8 (1993).

Das, S., Schapira, M., Tomic-Canic, M., Goyanka, R., Cardozo, T., and Samuels, H. H. Farnesyl pyrophosphate is a novel transcriptional activator for a subset of nuclear hormone receptors. *Mol Endocrinol,* 21, 2672-86 (2007).

Derksen, P. W., Liu, X., Saridin, F., van der Gulden, H., Zevenhoven, J., Evers, B., van Beijnum, J. R., Griffioen, A. W., Vink, J., Krimpenfort, P*., et al.* Somatic inactivation of E-cadherin and p53 in mice leads to metastatic lobular mammary carcinoma through induction of anoikis resistance and angiogenesis. *Cancer Cell,* 10, 437-49 (2006).

Dietrich, C. S., 3rd, Greenberg, V. L., DeSimone, C. P., Modesitt, S. C., van Nagell, J. R., Craven, R., and Zimmer, S. G. Suberoylanilide hydroxamic acid (SAHA) potentiates paclitaxel-induced apoptosis in ovarian cancer cell lines. *Gynecol Oncol,* 116, 126-30 (2010).

Do, R., Kiss, R. S., Gaudet, D., and Engert, J. C. Squalene synthase: a critical enzyme in the cholesterol biosynthesis pathway. *Clin Genet,* 75, 19-29 (2009).

Dobzhansky, T. Genetics of Natural Populations. Xiii. Recombination and Variability in Populations of Drosophila Pseudoobscura. *Genetics,* 31, 269-90 (1946).

Dowdy, S. C., Jiang, S., Zhou, X. C., Hou, X., Jin, F., Podratz, K. C., and Jiang, S. W. Histone deacetylase inhibitors and paclitaxel cause synergistic effects on apoptosis and microtubule stabilization in papillary serous endometrial cancer cells. *Mol Cancer Ther,* 5, 2767-76 (2006).

Dutta, A., Parikh, B., Maben, R., and Melnykovych, G. Increased dolichol content in glucocorticoid-sensitive human T-cell leukemia line grown in the presence of dexamethasone. *Biochem Biophys Res Commun,* 158, 163-9 (1989).

Ekstrom, A. M., Hansson, L. E., Signorello, L. B., Lindgren, A., Bergstrom, R., and Nyren, O. Decreasing incidence of both major histologic subtypes of gastric adenocarcinoma--a population-based study in Sweden. *Br J Cancer,* 83, 391-6 (2000).

Ercan, C., van Diest, P. J., van der Ende, B., Hinrichs, J., Bult, P., Buerger, H., van der Wall, E., and Derksen, P. W. B. p53 mutations in classic and pleomorphic invasive lobular carcinoma of the breast. *Cell Oncol (Dordr),* 35, 111-118 (2012).

Erlich, R. B., Kherrouche, Z., Rickwood, D., Endo-Munoz, L., Cameron, S., Dahler, A., Hazar-Rethinam, M., de Long, L. M., Wooley, K., Guminski, A., and Saunders, N. A. Preclinical evaluation of dual PI3K-mTOR inhibitors and histone deacetylase inhibitors in head and neck squamous cell carcinoma. *Br J Cancer,* 106, 107-15 (2012).

Etienne-Manneville, S., and Hall, A. Rho GTPases in cell biology. *Nature,* 420, 629-35 (2002).

Farmer, H., McCabe, N., Lord, C. J., Tutt, A. N., Johnson, D. A., Richardson, T. B., Santarosa, M., Dillon, K. J., Hickson, I., Knights, C.*, et al.* Targeting the DNA repair defect in BRCA mutant cells as a therapeutic strategy. *Nature,* 434, 917-21 (2005).

Fatehullah, A., Tan, S. H., and Barker, N. Organoids as an in vitro model of human development and disease. *Nat Cell Biol,* 18, 246-54 (2016).

Fournier, A. K., Campbell, L. E., Castagnino, P., Liu, W. F., Chung, B. M., Weaver, V. M., Chen, C. S., and Assoian, R. K. Rac-dependent cyclin D1 gene expression regulated by cadherin- and integrin-mediated adhesion. *J Cell Sci,* 121, 226-33 (2008).

Fukata, M., and Kaibuchi, K. Rho-family GTPases in cadherin-mediated cell-cell adhesion. *Nat Rev Mol Cell Biol,* 2, 887-897 (2001).

Gan, Y., Wang, J., Coselli, J., and Wang, X. L. Synergistic induction of apoptosis by HMG-CoA reductase inhibitor and histone deacetylases inhibitor in HeLa cells. *Biochem Biophys Res Commun,* 365, 386-92 (2008).

Glozak, M. A., Sengupta, N., Zhang, X., and Seto, E. Acetylation and deacetylation of non-histone proteins. *Gene,* 363, 15-23 (2005).

Glozak, M. A., and Seto, E. Histone deacetylases and cancer. *Oncogene,* 26, 5420-32 (2007).

Gobel, A., Thiele, S., Browne, A. J., Rauner, M., Zinna, V. M., Hofbauer, L. C., and Rachner, T. D. Combined inhibition of the mevalonate pathway with statins and zoledronic acid potentiates their anti-tumor effects in human breast cancer cells. *Cancer Lett,* 375, 162-71 (2016).

Guggenheim, D. E., and Shah, M. A. Gastric cancer epidemiology and risk factors. *J Surg Oncol,* 107, 230-6 (2013).

Guilford, P., Hopkins, J., Harraway, J., McLeod, M., McLeod, N., Harawira, P., Taite, H., Scoular, R., Miller, A., and Reeve, A. E. E-cadherin germline mutations in familial gastric cancer. *Nature,* 392, 402-5 (1998).

Guilford, P., Humar, B., and Blair, V. Hereditary diffuse gastric cancer: translation of CDH1 germline mutations into clinical practice. *Gastric Cancer,* 13, 1-10 (2010).

Gul, I. S., Hulpiau, P., Saeys, Y., and van Roy, F. Evolution and diversity of cadherins and catenins. *Exp Cell Res,* 358, 3-9 (2017).

Gupta, P., Reid, R. C., Iyer, A., Sweet, M. J., and Fairlie, D. P. Towards isozyme-selective HDAC inhibitors for interrogating disease. *Curr Top Med Chem,* 12, 1479-99 (2012).

Haataja, L., Groffen, J., and Heisterkamp, N. Characterization of RAC3, a novel member of the Rho family. *J Biol Chem,* 272, 20384-8 (1997).

Hamid, R., Rotshteyn, Y., Rabadi, L., Parikh, R., and Bullock, P. Comparison of alamar blue and MTT assays for high through-put screening. *Toxicol In Vitro,* 18, 703-10 (2004).

Hansford, S., Kaurah, P., Li-Chang, H., Woo, M., Senz, J., Pinheiro, H., Schrader, K. A., Schaeffer, D. F., Shumansky, K., Zogopoulos, G.*, et al.* Hereditary diffuse gastric cancer syndrome: CDH1 mutations and beyond. *JAMA Oncol,* 1, 23-32 (2015).

Harvey, K. F., Zhang, X., and Thomas, D. M. The Hippo pathway and human cancer. *Nat Rev Cancer,* 13, 246-57 (2013).

Haselsberger, K., Peterson, D. C., Thomas, D. G., and Darling, J. L. Assay of anticancer drugs in tissue culture: comparison of a tetrazolium-based assay and a protein binding dye assay in short-term cultures derived from human malignant glioma. *Anticancer Drugs,* 7, 331-8 (1996).

Head, J., and Johnston, S. R. New targets for therapy in breast cancer: farnesyltransferase inhibitors. *Breast Cancer Res,* 6, 262-8 (2004).

Hegde, M., Mantelingu, K., Pandey, M., Pavankumar, C. S., Rangappa, K. S., and Raghavan, S. C. Combinatorial study of a novel poly (ADP-ribose) polymerase inhibitor and an HDAC inhibitor, SAHA, in leukemic cell lines. *Target Oncol,* 11, 655-665 (2016).

Hennequin, L. F., Stokes, E. S., Thomas, A. P., Johnstone, C., Ple, P. A., Ogilvie, D. J., Dukes, M., Wedge, S. R., Kendrew, J., and Curwen, J. O. Novel 4-anilinoquinazolines with C-7 basic side chains: design and structure activity relationship of a series of potent, orally active, VEGF receptor tyrosine kinase inhibitors. *J Med Chem,* 45, 1300-12 (2002).

Henney, J. E. From the Food and Drug Administration. *JAMA,* 283, 2779 (2000).

Henson, D. E., Dittus, C., Younes, M., Nguyen, H., and Albores-Saavedra, J. Differential trends in the intestinal and diffuse types of gastric carcinoma in the United States, 1973-2000: increase in the signet ring cell type. *Arch Pathol Lab Med,* 128, 765-70 (2004).

Hidalgo, M., Amant, F., Biankin, A. V., Budinska, E., Byrne, A. T., Caldas, C., Clarke, R. B., de Jong, S., Jonkers, J., Maelandsmo, G. M.*, et al.* Patient-derived xenograft models: an

emerging platform for translational cancer research. *Cancer Discov,* 4, 998-1013 (2014).

Hollestelle, A., Peeters, J. K., Smid, M., Timmermans, M., Verhoog, L. C., Westenend, P. J., Heine, A. A., Chan, A., Sieuwerts, A. M., Wiemer, E. A.*, et al.* Loss of E-cadherin is not a necessity for epithelial to mesenchymal transition in human breast cancer. *Breast Cancer Res Treat,* 138, 47-57 (2013).

Huber, M. A., Kraut, N., and Beug, H. Molecular requirements for epithelial-mesenchymal transition during tumor progression. *Curr Opin Cell Biol,* 17, 548-58 (2005).

Humar, B., Blair, V., Charlton, A., More, H., Martin, I., and Guilford, P. E-cadherin deficiency initiates gastric signet-ring cell carcinoma in mice and man. *Cancer Res,* 69, 2050-6 (2009).

Humar, B., Fukuzawa, R., Blair, V., Dunbier, A., More, H., Charlton, A., Yang, H. K., Kim, W. H., Reeve, A. E., Martin, I., and Guilford, P. Destabilized adhesion in the gastric proliferative zone and c-Src kinase activation mark the development of early diffuse gastric cancer. *Cancer Res,* 67, 2480-9 (2007).

Hynes, R. O. Integrins: bidirectional, allosteric signaling machines. *Cell,* 110, 673-87 (2002).

Isakoff, S. J., Engelman, J. A., Irie, H. Y., Luo, J., Brachmann, S. M., Pearline, R. V., Cantley, L. C., and Brugge, J. S. Breast cancer-associated PIK3CA mutations are oncogenic in mammary epithelial cells. *Cancer Res,* 65, 10992-1000 (2005).

Johnson, R., and Halder, G. The two faces of Hippo: targeting the Hippo pathway for regenerative medicine and cancer treatment. *Nat Rev Drug Discov,* 13, 63-79 (2014).

Kalluri, R., and Weinberg, R. A. The basics of epithelial-mesenchymal transition. *J Clin Invest,* 119, 1420-8 (2009).

Kau, T. R., Schroeder, F., Ramaswamy, S., Wojciechowski, C. L., Zhao, J. J., Roberts, T. M., Clardy, J., Sellers, W. R., and Silver, P. A. A chemical genetic screen identifies inhibitors of regulated nuclear export of a Forkhead transcription factor in PTEN-deficient tumor cells. *Cancer Cell,* 4, 463-76 (2003).

Kepp, O., Galluzzi, L., Lipinski, M., Yuan, J., and Kroemer, G. Cell death assays for drug discovery. *Nat Rev Drug Discov,* 10, 221-37 (2011).

Kim, M. J., Kim, D. E., Jeong, I. G., Choi, J., Jang, S., Lee, J. H., Ro, S., Hwang, J. J., and Kim, C. S. HDAC inhibitors synergize antiproliferative effect of sorafenib in renal cell carcinoma cells. *Anticancer Res,* 32, 3161-8 (2012).

Kirsch, C., Eckert, G. P., and Mueller, W. E. Statin effects on cholesterol micro-domains in brain plasma membranes. *Biochem Pharmacol,* 65, 843-56 (2003).

Klein, E. A., Campbell, L. E., Kothapalli, D., Fournier, A. K., and Assoian, R. K. Joint requirement for Rac and ERK activities underlies the mid-G1 phase induction of cyclin D1 and S phase entry in both epithelial and mesenchymal cells. *J Biol Chem,* 283, 30911-8 (2008).

Kmiecik, T. E., and Shalloway, D. Activation and suppression of pp60c-src transforming ability by mutation of its primary sites of tyrosine phosphorylation. *Cell,* 49, 65-73 (1987).

Koea, J. B., Karpeh, M. S., and Brennan, M. F. Gastric cancer in young patients: demographic, clinicopathological, and prognostic factors in 92 patients. *Ann Surg Oncol,* 7, 346-51 (2000).

Konstantinopoulos, P. A., Wilson, A. J., Saskowski, J., Wass, E., and Khabele, D. Suberoylanilide hydroxamic acid (SAHA) enhances olaparib activity by targeting homologous recombination DNA repair in ovarian cancer. *Gynecol Oncol,* 133, 599-606 (2014).

Korhonen, T., Kuukasjarvi, T., Huhtala, H., Alarmo, E. L., Holli, K., Kallioniemi, A., and Pylkkanen, L. The impact of lobular and ductal breast cancer histology on the metastatic behavior and long term survival of breast cancer patients. *Breast,* 22, 1119-24 (2013).

Kovacs, E. M., Ali, R. G., McCormack, A. J., and Yap, A. S. E-cadherin homophilic ligation directly signals through Rac and phosphatidylinositol 3-kinase to regulate adhesive contacts. *J Biol Chem,* 277, 6708-18 (2002).

Kovacs, J. J., Murphy, P. J., Gaillard, S., Zhao, X., Wu, J. T., Nicchitta, C. V., Yoshida, M., Toft, D. O., Pratt, W. B., and Yao, T. P. HDAC6 regulates Hsp90 acetylation and chaperone-dependent activation of glucocorticoid receptor. *Mol Cell,* 18, 601-7 (2005).

La Vecchia, C., Negri, E., Franceschi, S., and Gentile, A. Family history and the risk of stomach and colorectal cancer. *Cancer,* 70, 50-5 (1992).

Lachenmayer, A., Toffanin, S., Cabellos, L., Alsinet, C., Hoshida, Y., Villanueva, A., Minguez, B., Tsai, H. W., Ward, S. C., Thung, S.*, et al.* Combination therapy for hepatocellular carcinoma: additive preclinical efficacy of the HDAC inhibitor panobinostat with sorafenib. *J Hepatol,* 56, 1343-50 (2012).

Lamprecht, M. R., Sabatini, D. M., and Carpenter, A. E. CellProfiler: free, versatile software for automated biological image analysis. *Biotechniques,* 42, 71-5 (2007).

Lauren, P. The two histological main types of gastric carcinoma: diffuse and so-called intestinal-type carcinoma. An attempt at a histo-clinical classification. *Acta Pathol Microbiol Scand,* 64, 31-49 (1965).

Lechler, T., and Fuchs, E. Asymmetric cell divisions promote stratification and differentiation of mammalian skin. *Nature,* 437, 275-80 (2005).

Lecuit, T., and Yap, A. S. E-cadherin junctions as active mechanical integrators in tissue dynamics. *Nat Cell Biol,* 17, 533-9 (2015).

Lehmann, U. Lobular breast cancer--the most common special subtype or a most special common subtype? *Breast Cancer Res,* 17, 99 (2015).

Li, Q., Chow, A. B., and Mattingly, R. R. Three-dimensional overlay culture models of human breast cancer reveal a critical sensitivity to mitogen-activated protein kinase kinase inhibitors. *J Pharmacol Exp Ther,* 332, 821-8 (2010).

Lin, Y. C., Lin, J. H., Chou, C. W., Chang, Y. F., Yeh, S. H., and Chen, C. C. Statins increase p21 through inhibition of histone deacetylase activity and release of promoter-associated HDAC1/2. *Cancer Res,* 68, 2375-83 (2008).

Lin, Z., Zhang, Z., Jiang, X., Kou, X., Bao, Y., Liu, H., Sun, F., Ling, S., Qin, N., Jiang, L., and Yang, Y. Mevastatin blockade of autolysosome maturation stimulates LBH589-induced cell death in triple-negative breast cancer cells. *Oncotarget,* 8, 17833-17848 (2017).

Liu, B. A., Engelmann, B. W., and Nash, P. D. The language of SH2 domain interactions defines phosphotyrosine-mediated signal transduction. *FEBS Lett,* 586, 2597-605 (2012).

Liu-Chittenden, Y., Huang, B., Shim, J. S., Chen, Q., Lee, S. J., Anders, R. A., Liu, J. O., and Pan, D. Genetic and pharmacological disruption of the TEAD-YAP complex suppresses the oncogenic activity of YAP. *Genes Dev,* 26, 1300-5 (2012).

Liwosz, A., Lei, T., and Kukuruzinska, M. A. N-glycosylation affects the molecular organization and stability of E-cadherin junctions. *J Biol Chem,* 281, 23138-49 (2006).

Manal, M., Chandrasekar, M. J., Gomathi Priya, J., and Nanjan, M. J. Inhibitors of histone deacetylase as antitumor agents: A critical review. *Bioorg Chem,* 67, 18-42 (2016).

Mathers, C. D., and Loncar, D. Projections of Global Mortality and Burden of Disease from 2002 to 2030. *PLoS Med,* 3, e442 (2006).

Mathieu, M. C., Rouzier, R., Llombart-Cussac, A., Sideris, L., Koscielny, S., Travagli, J. P., Contesso, G., Delaloge, S., and Spielmann, M. The poor responsiveness of infiltrating lobular breast carcinomas to neoadjuvant chemotherapy can be explained by their biological profile. *Eur J Cancer,* 40, 342-51 (2004).

McCracken, K. W., Cata, E. M., Crawford, C. M., Sinagoga, K. L., Schumacher, M., Rockich, B. E., Tsai, Y. H., Mayhew, C. N., Spence, J. R., Zavros, Y., and Wells, J. M. Modelling human development and disease in pluripotent stem-cell-derived gastric organoids. *Nature,* 516, 400-4 (2014).

Meijer, A. J., and Dubbelhuis, P. F. Amino acid signalling and the integration of metabolism. *Biochem Biophys Res Commun,* 313, 397-403 (2004).

Mills, A. A. Throwing the cancer switch: reciprocal roles of polycomb and trithorax proteins. *Nat Rev Cancer,* 10, 669-82 (2010).

Miranti, C. K., and Brugge, J. S. Sensing the environment: a historical perspective on integrin signal transduction. *Nat Cell Biol,* 4, E83-90 (2002).

Moran, T. J., Gray, S., Mikosz, C. A., and Conzen, S. D. The glucocorticoid receptor mediates a survival signal in human mammary epithelial cells. *Cancer Res,* 60, 867-72 (2000).

Mosmann, T. Rapid colorimetric assay for cellular growth and survival: Application to proliferation and cytotoxicity assays. *J Immunol Methods,* 65, 55-63 (1983).

Mottamal, M., Zheng, S., Huang, T. L., and Wang, G. Histone deacetylase inhibitors in clinical studies as templates for new anticancer agents. *Molecules,* 20, 3898-941 (2015).

Mullen, P. J., Yu, R., Longo, J., Archer, M. C., and Penn, L. Z. The interplay between cell signalling and the mevalonate pathway in cancer. *Nat Rev Cancer,* 16, 718-731 (2016).

Mutze, K., Langer, R., Becker, K., Ott, K., Novotny, A., Luber, B., Hapfelmeier, A., Gottlicher, M., Hofler, H., and Keller, G. Histone deacetylase (HDAC) 1 and 2 expression and chemotherapy in gastric cancer. *Ann Surg Oncol,* 17, 3336-43 (2010).

Nakagawa, M., Fukata, M., Yamaga, M., Itoh, N., and Kaibuchi, K. Recruitment and activation of Rac1 by the formation of E-cadherin-mediated cell-cell adhesion sites. *J Cell Sci,* 114, 1829-38 (2001).

Neshat, M. S., Mellinghoff, I. K., Tran, C., Stiles, B., Thomas, G., Petersen, R., Frost, P., Gibbons, J. J., Wu, H., and Sawyers, C. L. Enhanced sensitivity of PTEN-deficient tumors to inhibition of FRAP/mTOR. *Proc Natl Acad Sci U S A,* 98, 10314-9 (2001).

Nimako, G. K., Wintrob, Z. A., Sulik, D. A., Donato, J. L., and Ceacareanu, A. C. Synergistic benefit of statin and metformin in gastrointestinal malignancies. *J Pharm Pract,* 30, 185-194 (2017).

Norton, J. A., Ham, C. M., Van Dam, J., Jeffrey, R. B., Longacre, T. A., Huntsman, D. G., Chun, N., Kurian, A. W., and Ford, J. M. CDH1 truncating mutations in the E-cadherin gene: an indication for total gastrectomy to treat hereditary diffuse gastric cancer. *Ann Surg,* 245, 873-9 (2007).

Novotny-Diermayr, V., Sangthongpitag, K., Hu, C. Y., Wu, X., Sausgruber, N., Yeo, P., Greicius, G., Pettersson, S., Liang, A. L., Loh, Y. K.*, et al.* SB939, a novel potent and orally active histone deacetylase inhibitor with high tumor exposure and efficacy in mouse models of colorectal cancer. *Mol Cancer Ther,* 9, 642-52 (2010).

Nygaard, H. B., Wagner, A. F., Bowen, G. S., Good, S. P., MacAvoy, M. G., Strittmatter, K. A., Kaufman, A. C., Rosenberg, B. J., Sekine-Konno, T., Varma, P.*, et al.* A phase Ib multiple ascending dose study of the safety, tolerability, and central nervous system availability of AZD0530 (saracatinib) in Alzheimer's disease. *Alzheimers Res Ther,* 7, 35 (2015).

O'Brien, J., Wilson, I., Orton, T., and Pognan, F. Investigation of the Alamar Blue (resazurin) fluorescent dye for the assessment of mammalian cell cytotoxicity. *Eur J Biochem,* 267, 5421-6 (2000).

Oliveira, C., Sousa, S., Pinheiro, H., Karam, R., Bordeira-Carrico, R., Senz, J., Kaurah, P., Carvalho, J., Pereira, R., Gusmao, L.*, et al.* Quantification of epigenetic and genetic 2nd hits in CDH1 during hereditary diffuse gastric cancer syndrome progression. *Gastroenterology,* 136, 2137-48 (2009).

Onder, T. T., Gupta, P. B., Mani, S. A., Yang, J., Lander, E. S., and Weinberg, R. A. Loss of E-Cadherin Promotes Metastasis via Multiple Downstream Transcriptional Pathways. *Cancer Res,* 68, 3645-3654 (2008).

Overholtzer, M., Zhang, J., Smolen, G. A., Muir, B., Li, W., Sgroi, D. C., Deng, C. X., Brugge, J. S., and Haber, D. A. Transforming properties of YAP, a candidate oncogene on the chromosome 11q22 amplicon. *Proc Natl Acad Sci U S A,* 103, 12405-10 (2006).

Owonikoko, T. K., Ramalingam, S. S., Kanterewicz, B., Balius, T. E., Belani, C. P., and Hershberger, P. A. Vorinostat increases carboplatin and paclitaxel activity in non-small-cell lung cancer cells. *Int J Cancer,* 126, 743-55 (2010).

Parsons, J. T., Slack-Davis, J., Tilghman, R., and Roberts, W. G. Focal adhesion kinase: targeting adhesion signaling pathways for therapeutic intervention. *Clin Cancer Res,* 14, 627-32 (2008).

Pastar, I., Stojadinovic, O., Sawaya, A. P., Stone, R. C., Lindley, L. E., Ojeh, N., Vukelic, S., Samuels, H. H., and Tomic-Canic, M. Skin metabolite, farnesyl pyrophosphate, regulates epidermal response to inflammation, oxidative stress, and migration. *J Cell Physiol,* 231, 2452-63 (2016).

Pece, S., and Gutkind, J. S. Signaling from E-cadherins to the MAPK pathway by the recruitment and activation of epidermal growth factor receptors upon cell-cell contact formation. *J Biol Chem,* 275, 41227-33 (2000).

Pei, Y., Liu, K. W., Wang, J., Garancher, A., Tao, R., Esparza, L. A., Maier, D. L., Udaka, Y. T., Murad, N., Morrissy, S.*, et al.* HDAC and PI3K antagonists cooperate to inhibit growth of MYC-driven medulloblastoma. *Cancer Cell,* 29, 311-23 (2016).

Pestalozzi, B. C., Zahrieh, D., Mallon, E., Gusterson, B. A., Price, K. N., Gelber, R. D., Holmberg, S. B., Lindtner, J., Snyder, R., Thurlimann, B.*, et al.* Distinct clinical and prognostic features of infiltrating lobular carcinoma of the breast: combined results of 15 International Breast Cancer Study Group clinical trials. *J Clin Oncol,* 26, 3006-14 (2008).

Peternel, L., Kotnik, M., Prezelj, A., and Urleb, U. Comparison of 3 cytotoxicity screening assays and their application to the selection of novel antibacterial hits. *J Biomol Screen,* 14, 142-50 (2009).

Pharoah, P. D., Guilford, P., and Caldas, C. Incidence of gastric cancer and breast cancer in CDH1 (E-cadherin) mutation carriers from hereditary diffuse gastric cancer families. *Gastroenterology,* 121, 1348-53 (2001).

Piao, J., Chen, L., Quan, T., Li, L., Quan, C., Piao, Y., Jin, T., and Lin, Z. Superior efficacy of co-treatment with the dual PI3K/mTOR inhibitor BEZ235 and histone deacetylase inhibitor Trichostatin A against NSCLC. *Oncotarget,* 7, 60169-60180 (2016).

Podsypanina, K., Lee, R. T., Politis, C., Hennessy, I., Crane, A., Puc, J., Neshat, M., Wang, H., Yang, L., Gibbons, J.*, et al.* An inhibitor of mTOR reduces neoplasia and normalizes p70/S6 kinase activity in Pten+/- mice. *Proc Natl Acad Sci U S A,* 98, 10320-5 (2001).

Quent, V. M., Loessner, D., Friis, T., Reichert, J. C., and Hutmacher, D. W. Discrepancies between metabolic activity and DNA content as tool to assess cell proliferation in cancer research. *J Cell Mol Med,* 14, 1003-13 (2010).

Rahmani, M., Davis, E. M., Bauer, C., Dent, P., and Grant, S. Apoptosis induced by the kinase inhibitor BAY 43-9006 in human leukemia cells involves down-regulation of Mcl-1 through inhibition of translation. *J Biol Chem,* 280, 35217-27 (2005).

Rakha, E. A., El-Sayed, M. E., Powe, D. G., Green, A. R., Habashy, H., Grainge, M. J., Robertson, J. F., Blamey, R., Gee, J., Nicholson, R. I.*, et al.* Invasive lobular carcinoma of the breast: response to hormonal therapy and outcomes. *Eur J Cancer,* 44, 73-83 (2008).

Rana, A., Alex, J. M., Chauhan, M., Joshi, G., and Kumar, R. A review on pharmacophoric designs of antiproliferative agents. *Med Chem Res,* 24, 903-920 (2015).

Rasmussen, R. D., Gajjar, M. K., Jensen, K. E., and Hamerlik, P. Enhanced efficacy of combined HDAC and PARP targeting in glioblastoma. *Mol Oncol,* 10, 751-63 (2016).

Ratheesh, A., Gomez, G. A., Priya, R., Verma, S., Kovacs, E. M., Jiang, K., Brown, N. H., Akhmanova, A., Stehbens, S. J., and Yap, A. S. Centralspindlin and alpha-catenin regulate Rho signalling at the epithelial zonula adherens. *Nat Cell Biol,* 14, 818-28 (2012).

Riss, T. L., Moravec, R. A., Niles, A. L., Benink, H. A., Worzella, T. J., and Minor, L. 2004. Cell viability assays. In *Assay Guidance Manual,* eds. Sittampalam, G. S., Gal-Edd, N., Arkin, M., Auld, D., Austin, C., Bejcek, B., Glicksman, M., Inglese, J., Lemmon, V., Li, Z., McGee, J., McManus, O., Minor, L., Napper, A., Riss, T., Trask, O. J. & Weidner, J. Bethesda MD.

Roberts, A. W., Kim, C., Zhen, L., Lowe, J. B., Kapur, R., Petryniak, B., Spaetti, A., Pollock, J. D., Borneo, J. B., Bradford, G. B.*, et al.* Deficiency of the hematopoietic cell-specific Rho family GTPase Rac2 is characterized by abnormalities in neutrophil function and host defense. *Immunity,* 10, 183-96 (1999).

Rodriguez-Boulan, E., and Macara, I. G. Organization and execution of the epithelial polarity programme. *Nat Rev Mol Cell Biol,* 15, 225-42 (2014).

Roskoski Jr, R. Src protein–tyrosine kinase structure and regulation. *Biochem Biophys Res Commun,* 324, 1155-1164 (2004).

Roskoski, R., Jr. Src protein-tyrosine kinase structure, mechanism, and small molecule inhibitors. *Pharmacol Res,* 94, 9-25 (2015).

Roudier, E., Mistafa, O., and Stenius, U. Statins induce mammalian target of rapamycin (mTOR)-mediated inhibition of Akt signaling and sensitize p53-deficient cells to cytostatic drugs. *Mol Cancer Ther,* 5, 2706-15 (2006).

Sahai, E., and Marshall, C. J. RHO-GTPases and cancer. *Nat Rev Cancer,* 2, 133-42 (2002).

Sanchez, C. A., Rodriguez, E., Varela, E., Zapata, E., Paez, A., Masso, F. A., Montano, L. F., and Loopez-Marure, R. Statin-induced inhibition of MCF-7 breast cancer cell proliferation is related to cell cycle arrest and apoptotic and necrotic cell death mediated by an enhanced oxidative stress. *Cancer Invest,* 26, 698-707 (2008).

Sawyer, J. M., Harrell, J. R., Shemer, G., Sullivan-Brown, J., Roh-Johnson, M., and Goldstein, B. Apical constriction: a cell shape change that can drive morphogenesis. *Dev Biol,* 341, 5-19 (2010).

Schackmann, R. C., van Amersfoort, M., Haarhuis, J. H., Vlug, E. J., Halim, V. A., Roodhart, J. M., Vermaat, J. S., Voest, E. E., van der Groep, P., van Diest, P. J., *et al.* Cytosolic p120-catenin regulates growth of metastatic lobular carcinoma through Rock1-mediated anoikis resistance. *J Clin Invest,* 121, 3176-88 (2011).

Schneider, C. A., Rasband, W. S., and Eliceiri, K. W. NIH Image to ImageJ: 25 years of image analysis. *Nat Meth,* 9, 671-675 (2012).

Schroeder, M. C., and Halder, G. Regulation of the Hippo pathway by cell architecture and mechanical signals. *Semin Cell Dev Biol,* 23, 803-11 (2012).

Sebbagh, M., Santoni, M. J., Hall, B., Borg, J. P., and Schwartz, M. A. Regulation of LKB1/STRAD localization and function by E-cadherin. *Curr Biol,* 19, 37-42 (2009).

Seelig, E., Meyer, S., Timper, K., Nigro, N., Bally, M., Pernicova, I., Schuetz, P., Muller, B., Korbonits, M., and Christ-Crain, M. Metformin prevents metabolic side effects during systemic glucocorticoid treatment. *Eur J Endocrinol,* 176, 349-358 (2017).

Semb, H., and Christofori, G. The Tumor-Suppressor Function of E-Cadherin. *The American Journal of Human Genetics,* 63, 1588-1593 (1998).

Shakespear, M. R., Halili, M. A., Irvine, K. M., Fairlie, D. P., and Sweet, M. J. Histone deacetylases as regulators of inflammation and immunity. *Trends Immunol,* 32, 335-43 (2011).

Shen, Y. Y., Yuan, Y., Du, Y. Y., and Pan, Y. Y. Molecular mechanism underlying the anticancer effect of simvastatin on MDA-MB-231 human breast cancer cells. *Mol Med Rep,* 12, 623-30 (2015).

Shi, Y.-k., Li, Z.-h., Han, X.-q., Yi, J.-h., Wang, Z.-h., Hou, J.-l., Feng, C.-r., Fang, Q.-h., Wang, H.-h., Zhang, P.-f., *et al.* The histone deacetylase inhibitor suberoylanilide hydroxamic acid induces growth inhibition and enhances taxol-induced cell death in breast cancer. *Cancer Chemoth Pharm,* 66, 1131-1140 (2010).

Simpson, P. T., Reis-Filho, J. S., Lambros, M. B., Jones, C., Steele, D., Mackay, A., Iravani, M., Fenwick, K., Dexter, T., Jones, A., *et al.* Molecular profiling pleomorphic lobular carcinomas of the breast: evidence for a common molecular genetic pathway with classic lobular carcinomas. *J Pathol,* 215, 231-44 (2008).

Singhai, R., Patil, V. W., Jaiswal, S. R., Patil, S. D., Tayade, M. B., and Patil, A. V. E-Cadherin as a diagnostic biomarker in breast cancer. *N Am J Med Sci,* 3, 227-33 (2011).

Single, A., Beetham, H., Telford, B. J., Guilford, P., and Chen, A. A comparison of real-time and endpoint cell viability assays for improved synthetic lethal drug validation. *J Biomol Screen,* 20, 1286-93 (2015).

Sonnemann, J., Bumbul, B., and Beck, J. F. Synergistic activity of the histone deacetylase inhibitor suberoylanilide hydroxamic acid and the bisphosphonate zoledronic acid against prostate cancer cells in vitro. *Mol Cancer Ther,* 6, 2976-84 (2007).

Sorrentino, G., Ruggeri, N., Specchia, V., Cordenonsi, M., Mano, M., Dupont, S., Manfrin, A., Ingallina, E., Sommaggio, R., Piazza, S.*, et al.* Metabolic control of YAP and TAZ by the mevalonate pathway. *Nat Cell Biol,* 16, 357-66 (2014).

Sorrentino, G., Ruggeri, N., Zannini, A., Ingallina, E., Bertolio, R., Marotta, C., Neri, C., Cappuzzello, E., Forcato, M., Rosato, A.*, et al.* Glucocorticoid receptor signalling activates YAP in breast cancer. *Nat Commun,* 8, 14073 (2017).

Stiekema, J., Cats, A., Kuijpers, A., van Coevorden, F., Boot, H., Jansen, E. P., Verheij, M., Balague Ponz, O., Hauptmann, M., and van Sandick, J. W. Surgical treatment results of intestinal and diffuse type gastric cancer. Implications for a differentiated therapeutic approach? *Eur J Surg Oncol,* 39, 686-93 (2013).

Stojadinovic, O., Lee, B., Vouthounis, C., Vukelic, S., Pastar, I., Blumenberg, M., Brem, H., and Tomic-Canic, M. Novel genomic effects of glucocorticoids in epidermal keratinocytes: inhibition of apoptosis, interferon-gamma pathway, and wound healing along with promotion of terminal differentiation. *J Biol Chem,* 282, 4021-34 (2007).

Sugihara, K., Nakatsuji, N., Nakamura, K., Nakao, K., Hashimoto, R., Otani, H., Sakagami, H., Kondo, H., Nozawa, S., Aiba, A., and Katsuki, M. Rac1 is required for the formation of three germ layers during gastrulation. *Oncogene,* 17, 3427-33 (1998).

Tang, Y., Yacoub, A., Hamed, H. A., Poklepovic, A., Tye, G., Grant, S., and Dent, P. Sorafenib and HDAC inhibitors synergize to kill CNS tumor cells. *Cancer Biol Ther,* 13, 567-74 (2012).

Tangutoori, S., Baldwin, P., and Sridhar, S. PARP inhibitors: A new era of targeted therapy. *Maturitas,* 81, 5-9 (2015).

Tansey, T. R., and Shechter, I. Structure and regulation of mammalian squalene synthase. *Biochim Biophys Acta,* 1529, 49-62 (2000).

Tapon, N., Harvey, K. F., Bell, D. W., Wahrer, D. C., Schiripo, T. A., Haber, D., and Hariharan, I. K. Salvador promotes both cell cycle exit and apoptosis in Drosophila and is mutated in human cancer cell lines. *Cell,* 110, 467-78 (2002).

Telford, B. J., Chen, A., Beetham, H., Frick, J., Brew, T. P., Gould, C. M., Single, A., Godwin, T., Simpson, K. J., and Guilford, P. Synthetic lethal screens identify vulnerabilities in GPCR signaling and cytoskeletal organization in E-cadherin-deficient cells. *Mol Cancer Ther,* 14, 1213-23 (2015).

Thomas, S. M., and Brugge, J. S. Cellular functions regulated by Src family kinases. *Annu Rev Cell Dev Biol,* 13, 513-609 (1997).

Thurnher, M., Nussbaumer, O., and Gruenbacher, G. Novel aspects of mevalonate pathway inhibitors as antitumor agents. *Clin Cancer Res,* 18, 3524-31 (2012).

Torre, L. A., Siegel, R. L., Ward, E. M., and Jemal, A. Global cancer incidence and mortality rates and trends—an update. *Cancer Epidemiol Biomarkers Prev,* 25, 16-27 (2016).

Tung, Y. C., Hsiao, A. Y., Allen, S. G., Torisawa, Y. S., Ho, M., and Takayama, S. High-throughput 3D spheroid culture and drug testing using a 384 hanging drop array. *Analyst,* 136, 473-8 (2011).

van der Post, R. S., Vogelaar, I. P., Carneiro, F., Guilford, P., Huntsman, D., Hoogerbrugge, N., Caldas, C., Schreiber, K. E., Hardwick, R. H., Ausems, M. G.*, et al.* Hereditary diffuse gastric cancer: updated clinical guidelines with an emphasis on germline CDH1 mutation carriers. *J Med Genet,* 52, 361-74 (2015).

van Roy, F., and Berx, G. The cell-cell adhesion molecule E-cadherin. *Cell Mol Life Sci,* 65, 3756-88 (2008).

Varley, J. M., McGown, G., Thorncroft, M., Tricker, K. J., Teare, M. D., Santibanez-Koref, M. F., Martin, J., Birch, J. M., and Evans, D. G. An extended Li-Fraumeni kindred with gastric carcinoma and a codon 175 mutation in TP53. *J Med Genet,* 32, 942-5 (1995).

Vasen, H. F., Wijnen, J. T., Menko, F. H., Kleibeuker, J. H., Taal, B. G., Griffioen, G., Nagengast, F. M., Meijers-Heijboer, E. H., Bertario, L., Varesco, L.*, et al.* Cancer risk in families with hereditary nonpolyposis colorectal cancer diagnosed by mutation analysis. *Gastroenterology,* 110, 1020-7 (1996).

Vaupel, P., and Mayer, A. Hypoxia and anemia: effects on tumor biology and treatment resistance. *Transfus Clin Biol,* 12, 5-10 (2005).

Vincent, S., Jeanteur, P., and Fort, P. Growth-regulated expression of rhoG, a new member of the ras homolog gene family. *Mol Cell Biol,* 12, 3138-48 (1992).

Vlug, E. J., van de Ven, R. A., Vermeulen, J. F., Bult, P., van Diest, P. J., and Derksen, P. W. Nuclear localization of the transcriptional coactivator YAP is associated with invasive lobular breast cancer. *Cell Oncol (Dordr),* 36, 375-84 (2013).

Vos, C. B., Cleton-Jansen, A. M., Berx, G., de Leeuw, W. J., ter Haar, N. T., van Roy, F., Cornelisse, C. J., Peterse, J. L., and van de Vijver, M. J. E-cadherin inactivation in lobular carcinoma in situ of the breast: an early event in tumorigenesis. *Br J Cancer,* 76, 1131-3 (1997).

Vukelic, S., Stojadinovic, O., Pastar, I., Vouthounis, C., Krzyzanowska, A., Das, S., Samuels, H. H., and Tomic-Canic, M. Farnesyl pyrophosphate inhibits epithelialization and wound healing through the glucocorticoid receptor. *J Biol Chem,* 285, 1980-8 (2010).

Wang, C. Y., Liu, P. Y., and Liao, J. K. Pleiotropic effects of statin therapy: molecular mechanisms and clinical results. *Trends Mol Med,* 14, 37-44 (2008).

Wang, J., Yao, X., and Huang, J. New tricks for human farnesyltransferase inhibitor: cancer and beyond. *Med Chem Commun,* 8, 841-854 (2017).

Wang, M., and Casey, P. J. Protein prenylation: unique fats make their mark on biology. *Nat Rev Mol Cell Biol,* 17, 110-22 (2016).

Wang, T., Seah, S., Loh, X., Chan, C. W., Hartman, M., Goh, B. C., and Lee, S. C. Simvastatin-induced breast cancer cell death and deactivation of PI3K/Akt and MAPK/ERK

signalling are reversed by metabolic products of the mevalonate pathway. *Oncotarget,* 7, 2532-44 (2016).

Warita, K., Warita, T., Beckwitt, C. H., Schurdak, M. E., Vazquez, A., Wells, A., and Oltvai, Z. N. Statin-induced mevalonate pathway inhibition attenuates the growth of mesenchymal-like cancer cells that lack functional E-cadherin mediated cell cohesion. *Sci Rep,* 4, 7593 (2014).

Welti, M. Regulation of dolichol-linked glycosylation. *Glycoconj J,* 30, 51-6 (2013).

Wennerberg, K., and Der, C. J. Rho-family GTPases: it's not only Rac and Rho (and I like it). *J Cell Sci,* 117, 1301-12 (2004).

Wilhelm, S. M., Adnane, L., Newell, P., Villanueva, A., Llovet, J. M., and Lynch, M. Preclinical overview of sorafenib, a multikinase inhibitor that targets both Raf and VEGF and PDGF receptor tyrosine kinase signaling. *Mol Cancer Ther,* 7, 3129-40 (2008).

Wilson, W. R., and Hay, M. P. Targeting hypoxia in cancer therapy. *Nat Rev Cancer,* 11, 393-410 (2011).

Wong, W. W., Dimitroulakos, J., Minden, M. D., and Penn, L. Z. HMG-CoA reductase inhibitors and the malignant cell: the statin family of drugs as triggers of tumor-specific apoptosis. *Leukemia,* 16, 508-19 (2002).

Wozniak, M. B., Villuendas, R., Bischoff, J. R., Aparicio, C. B., Martinez Leal, J. F., de La Cueva, P., Rodriguez, M. E., Herreros, B., Martin-Perez, D., Longo, M. I., *et al.* Vorinostat interferes with the signaling transduction pathway of T-cell receptor and synergizes with phosphoinositide-3 kinase inhibitors in cutaneous T-cell lymphoma. *Haematologica,* 95, 613-21 (2010).

Wu, Y., Connors, D., Barber, L., Jayachandra, S., Hanumegowda, U. M., and Adams, S. P. Multiplexed assay panel of cytotoxicity in HK-2 cells for detection of renal proximal tubule injury potential of compounds. *Toxicol In Vitro,* 23, 1170-8 (2009).

Yamada, T., Horinaka, M., Shinnoh, M., Yoshioka, T., Miki, T., and Sakai, T. A novel HDAC inhibitor OBP-801 and a PI3K inhibitor LY294002 synergistically induce apoptosis via the suppression of survivin and XIAP in renal cell carcinoma. *Int J Oncol,* 43, 1080-6 (2013).

Yang, J., and Weinberg, R. A. Epithelial-mesenchymal transition: at the crossroads of development and tumor metastasis. *Dev Cell,* 14, 818-29 (2008).

Yang, P. M., Liu, Y. L., Lin, Y. C., Shun, C. T., Wu, M. S., and Chen, C. C. Inhibition of autophagy enhances anticancer effects of atorvastatin in digestive malignancies. *Cancer Res,* 70, 7699-709 (2010).

Yap, A. S., Gomez, G. A., and Parton, R. G. Adherens junctions revisualized: Organizing cadherins as nanoassemblies. *Dev Cell,* 35, 12-20 (2015).

Yoshioka, T., Yogosawa, S., Yamada, T., Kitawaki, J., and Sakai, T. Combination of a novel HDAC inhibitor OBP-801/YM753 and a PI3K inhibitor LY294002 synergistically

induces apoptosis in human endometrial carcinoma cells due to increase of Bim with accumulation of ROS. *Gynecol Oncol,* 129, 425-32 (2013).

Yu, C., Bruzek, L. M., Meng, X. W., Gores, G. J., Carter, C. A., Kaufmann, S. H., and Adjei, A. A. The role of Mcl-1 downregulation in the proapoptotic activity of the multikinase inhibitor BAY 43-9006. *Oncogene,* 24, 6861-9 (2005).

Yu, S., Yang, X., Zhu, Y., Xie, F., Lu, Y., Yu, T., Yan, C., Shao, J., Gao, Y., Mo, F*., et al.* Systems pharmacology of mifepristone (RU486) reveals its 47 hub targets and network: comprehensive analysis and pharmacological focus on FAK-Src-Paxillin complex. *Sci Rep,* 5, 7830 (2015).

Yu, X., Pan, Y., Ma, H., and Li, W. Simvastatin inhibits proliferation and induces apoptosis in human lung cancer cells. *Oncol Res,* 20, 351-7 (2013).

Zhang, H., Liu, G., Dziubinski, M., Yang, Z., Ethier, S. P., and Wu, G. Comprehensive analysis of oncogenic effects of PIK3CA mutations in human mammary epithelial cells. *Breast Cancer Res Treat,* 112, 217-27 (2008).

Zhang, J. X., Li, D. Q., He, A. R., Motwani, M., Vasiliou, V., Eswaran, J., Mishra, L., and Kumar, R. Synergistic inhibition of hepatocellular carcinoma growth by cotargeting chromatin modifying enzymes and poly (ADP-ribose) polymerases. *Hepatology,* 55, 1840-51 (2012).

Zhang, X., George, J., Deb, S., Degoutin, J. L., Takano, E. A., Fox, S. B., Bowtell, D. D., and Harvey, K. F. The Hippo pathway transcriptional co-activator, YAP, is an ovarian cancer oncogene. *Oncogene,* 30, 2810-22 (2011).

Zhang, Y., Li, N., Caron, C., Matthias, G., Hess, D., Khochbin, S., and Matthias, P. HDAC-6 interacts with and deacetylates tubulin and microtubules in vivo. *EMBO J,* 22, 1168-79 (2003).

Zhao, B., Li, L., Wang, L., Wang, C. Y., Yu, J., and Guan, K. L. Cell detachment activates the Hippo pathway via cytoskeleton reorganization to induce anoikis. *Genes Dev,* 26, 54-68 (2012).

Zhao, H., Liang, Y., Xu, Z., Wang, L., Zhou, F., Li, Z., Jin, J., Yang, Y., Fang, Z., Hu, Y*., et al.* N-glycosylation affects the adhesive function of E-Cadherin through modifying the composition of adherens junctions (AJs) in human breast carcinoma cell line MDA-MB-435. *J Cell Biochem,* 104, 162-75 (2008).

Zhao, X., and Guan, J. L. Focal adhesion kinase and its signaling pathways in cell migration and angiogenesis. *Adv Drug Deliv Rev,* 63, 610-5 (2011).

Zilberman, Y., Ballestrem, C., Carramusa, L., Mazitschek, R., Khochbin, S., and Bershadsky, A. Regulation of microtubule dynamics by inhibition of the tubulin deacetylase HDAC6. *J Cell Sci,* 122, 3531-41 (2009).

Zuco, V., De Cesare, M., Cincinelli, R., Nannei, R., Pisano, C., Zaffaroni, N., and Zunino, F. Synergistic antitumor effects of novel HDAC inhibitors and paclitaxel in vitro and in vivo. *PLoS One,* 6, e29085 (2011).